Part Programming to Realize Chatter Free and Efficient High Speed Milling

THÈSE N^{O} 5549 (2012)

PRÉSENTÉE LE 25 OCTOBRE 2012

À LA FACULTÉ DES SCIENCES ET TECHNIQUES DE L'INGÉNIEUR
LABORATOIRE DES OUTILS INFORMATIQUES POUR LA CONCEPTION ET LA PRODUCTION
PROGRAMME DOCTORAL EN SYSTÈMES DE PRODUCTION ET ROBOTIQUE

ÉCOLE POLYTECHNIQUE FÉDÉRALE DE LAUSANNE

POUR L'OBTENTION DU GRADE DE DOCTEUR ÈS SCIENCES

PAR

Saurabh AGGARWAL

acceptée sur proposition du jury:

Prof. H. Bleuler, président du jury
Prof. P. Xirouchakis, Dr I. A. Stroud, directeurs de thèse
Dr I. O. Avram, rapporteur
Prof. G. Bissacco, rapporteur
Dr E. Boillat, rapporteur

ÉCOLE POLYTECHNIQUE
FÉDÉRALE DE LAUSANNE
Suisse
2012

Acknowledgements

It gives me an immense pleasure to acknowledge the help and support of numerous individuals during the course of this research work.

I would like to start by extending my sincere thanks to my thesis director Prof. Paul Xirouchakis for offering me the opportunity to work at Laboratory of Computer-Aided Design and Production (LICP) and for his constant encouragement and support during my PhD work.

I thank my thesis co-director Dr. Ian Anthony Stroud for his suggestions and careful corrections of my thesis. I would like to thank Prof. Hannes Bleuler of EPFL for his acceptance to be the jury president for my PhD oral exam and making the exam process comfortable for me. I am thankful to Prof. Giuliano Bissacco of Denmark Technical University, Dr. Eric Boillat of EPFL and Dr. Oliver Avram of Dixi Polytool SA for accepting to spend their precious time in reviewing my thesis and giving their valuable suggestions.

I wish to thank Prof. Yusuf Altintas of University of British Columbia for his valuable suggestions during the advanced training of milling process modeling and simulations.

I am greatly thankful to Dr. Jitender Rai, Dr. Sandeep Dhanik and Dr. Nenad Nešić for their collaboration, suggestions and motivation. I must thank to Dr. Oliver Avram and Mr. Karim Collomb for their support during experiments.

My thanks go to Dr. Ahmed Bufardi and Mr. Olcay Akten in translating the abstract into French. I also thank to Dr. Rahul Mulik for his suggestions for thesis. My special thanks to Anna, Soumaya, Drazen, Olcay, Bogdan Predrag, Ahmed, Arif for their valuable suggestions for the oral exam presentation.

I owe special thanks to our industrial partners Mr. David Schranz and Mr. Jean-Philippe Besuchet of Mikron Agie Charmilles AG and Mr. Ole Köser of Calcom ESI for their collaboration and constructive criticism on parts of this research work. I thank Mr. Mohit Goel of EPFL and Mr. Jérémie Monnin of ETHZ for their suggestions for signal processing. Special thanks to Dr. André Catana of Technology Transfer Office of EPFL for his constant support for our patent filing.

I am thankful to all colleagues/friends at EPFL from past (Young Seok, Jong-Ho, Ali, Aristeidis, Sandeep, Oliver and Kiran) and present (Apostolos, Olcay, Soumaya, Ahmed, Gajanan, Arif, and Rahul) for sharing nice talks during coffee/lunch breaks. I had also a pleasure to share the office with wonderful officemates Andreas and Jong-Ho. Special thanks to Sylvia and Carol for their assistance in administrative stuff. I would also like to thank mentors of various

courses/trainings for PhD programs, DIT, library, language center and human resources.

I would also like to thank WorldMUN team members for sharing the amazing experience at various model united nation conferences and social activities.

I would not have been able to maintain the healthy state-of-mind necessary to finish the thesis without a constant support from my friends in Switzerland. My heartiest regards to Adil Rasheed, Sandeep Dhanik, Sandy Herzlieb, Nandita Aggarwal and Debabrata Dash for their encouragement, suggestions, love and care. I cannot forget the support from Shravan during my first days in Lausanne. Thanks to Saurabh, Wilson, Nirav and Paman and Sriniketh for their enjoyable company at EPFL. I must thank Felix, Maria, Nathalie, Olga, Yann, Christophe, Patrick, Jairo, Jagdeep, Aristeidis, Camille, Sebastian, Dipanjan, Laura, my wonderful neighbors and all my loving International/Indian/Punjabi friends who made my stay in Switzerland a memorable one.

I owe my loving gratitude to my mother for her love and encouragement. Without her support this work would not have been possible. My special gratitude to my sister, jija ji and sweetest niece for their lovely support. Finally, I would like to dedicate this thesis to my father who is always a source of inspiration for me. Daddy you will always remain in our hearts.

Above all, I want to express my humble and whole hearted prostration before God for sprinkling his unprecedented favor upon me.

Abstract

High speed milling (HSM) is the most known machining process due to its application in various industries. In milling, a rotating cutting tool removes a large amount of material along a predefined toolpath to manufacture the final part with a desired shape. Milling of prismatic parts[1] is very important in automotive, aerospace, mold and die industries. Even complicated parts are machined from a blank first by 2.5D roughing followed by 3D-5D finishing.

Modern production floors have adopted high speed CNC[2] machine tools to execute part programs, developed by CAD/CAM[3] systems, to manufacture the final workpiece. The overall productivity of the milling process depends on the choice of cutting conditions and the toolpath. Current CAD/CAM systems do not provide any guidance to select cutting conditions due to the unavailability of models of the complex physical and dynamic interaction of machine tool and workpiece systems. Moreover, toolpath generation by CAD/CAM packages is purely geometric in nature and results in engagement angle variation along the toolpath.

The selection of cutting conditions and toolpath rely solely on the part programmer's experience, CAD/CAM systems, handbook guidelines or specifications provided in the catalogues of cutting tools and machine tools. Their poor selection often causes chatter, high fluctuation of cutting forces, and/or violation of the available limits of power and torque of the machine tool. These phenomena result in poor surface finish, workpiece damage, high cutting tool wear, violation of tolerance limits, additional cost, unwanted waste and significant reduction in machine tool working life. In order to avoid these problems, part programs need to be verified iteratively using trial and error experiments and often conservative cutting conditions are selected. These practices lead to long preparation time of part programs and lower machining performance, which in a nutshell significantly lower overall productivity. Moreover, machine tool capabilities are not fully utilized due to the conservative selection of cutting conditions.

In order to address these challenges, a genetic algorithm (GA) based optimal milling (OptMill) system is developed for optimal selection of cutting conditions and/or toolpath for a given set of inputs of machine tool/spindle/tool holder/cutting tool and workpiece system. Operational constraints of the machine tool, such as spindle speed and feed limits, available spindle power and torque, chatter vibration[4] limits due to the dynamic interaction between cutting tool

[1] Geometry consists of features that represent 2D contours extruded in a perpendicular direction
[2] Computerized Numerical Control
[3] Computer-Aided Design and Manufacturing
[4] Amplitude of the cutting tool tip vibrations due to the regenerative effect

and workpiece, permissible limits of bending stress and deflection of the cutting tool and clamping load limits of the workpiece system are embedded. The developed system is applied to different industrial use cases: (i) Minimization of pocket milling time considering one-way toolpath (ii) minimization of machining time for multi-feature prismatic parts with the implementation of pre-processing modules: extraction of toolpath and workpiece boundary from APT[5] and STEP[6] files respectively and calculation of engagement angle along the toolpath (iii) optimal selection of cutting conditions and corresponding smooth and constant engagement toolpath for pocket milling. The selected cutting conditions and/or toolpath are also validated using dedicated experiments conducted during the course of the research work. The present research work is inspired from an ongoing CTI project[7].

Following enhanced methodologies the identification of important inputs to mathematical models for prediction of cutting forces and chatter free limits have also been developed to expand the scope of the developed OptMill system.

- Tangential force coefficients, an important input for prediction of cutting forces and chatter free limits, are identified experimentally with the use of a cutting force dynamometer. This experimental setup is quite costly and not practical for industrial implementation. An enhanced methodology is presented for the indirect identification of tangential force coefficients from the spindle motor current. The methodology includes the development of an empirical model for cutting torque prediction from spindle motor current with the implementation of a spindle power model that accounts for all mechanical and electrical power losses. The cutting torque predicted by the developed model is then used for tangential force coefficient identification, and is also validated experimentally with direct measurement using a cutting torque dynamometer.

- Dynamic response of each variant of machine tool/spindle/tool holder/cutting tool, in terms of FRF[8], is required to predict chatter free limits accurately. FRF is often measured with hammer testing experiments. In order to avoid these tedious tests, an enhanced procedure using the receptance coupling technique is implemented to predict the FRF of a machine tool/spindle/tool holder/cutting tool system for different cutting tools. The predicted FRFs via numerical simulation are also validated with experimental measurement.

Though the existing mathematical models predict accurately the chatter free limits, their use in small production floors has not yet been achieved due to the absence of technical expertise and experimental resources. Moreover, even modern machine tools do not provide any guidance to the machine operator regarding the occurrence of chatter during machining. To meet industrial requirements, a computationally fast, easy to use and practical system is developed that detects chatter automatically during milling and thereafter proposes a control

[5] Automatically Programmed Tool

[6] STandard for the Exchange of Product model data

[7] ChatFree: Part programming to realize chatter-free and efficient pocket milling (CTI-Project No.10008.1 PFES-ES)

[8] Frequency Response Function

strategy to the machine operator. The developed online chatter detection and control system is also validated experimentally with an industrial end-user partner.

Apart from the many challenges and the developments discussed above, milling of thin-walled workpieces is also a concern due to changing dynamics during machining. Thus, an enhanced numerical procedure is developed for the selection of chatter free cutting conditions while considering the change in workpiece dynamics along the toolpath using finite element analysis.

In order to realize the developed system, MATLAB is used as a programming language. Geometrical modeling and part programming of prismatic parts is done with CATIA. The data acquisition platform for the experimental validation is designed in LABVIEW. Finite element modeling and analysis is implemented with the ANSYS parametric design language (APDL). The developed system is very appealing for industrial application by direct integration with existing CAD/CAM systems and/or modern machine tools. Increase in overall productivity is ensured by optimal selection of cutting conditions and/or toolpath and simultaneous avoidance of repercussions due to their wrong selection.

Keywords: Computer-Aided Design and Manufacturing, Prismatic Parts, Pocket Milling, High Speed Milling Optimization, Genetic Algorithm, Machine Tool Dynamics, Finite Element Modeling, Online Chatter Detection and Control

Résumé

Le fraisage à grande vitesse (FGV) est le processus d'usinage le plus connu en raison de son application dans diverses industries. Dans le fraisage, un outil de coupe rotatif supprime une grande quantité de matériau le long d'un parcours d'outil prédéfini pour fabriquer la pièce finale avec une forme souhaitée. Le fraisage de pièces prismatiques[9] est très important dans les secteurs de l'automobile, de l'aérospatiale et des moules et des matrices. Même les pièces compliquées sont usinés à partir d'une pièce brute par une ébauche 2.5D suivie par une finition 3D-5D.

Les centres de production modernes ont adopté les machines-outils CNC[10] à grande vitesse pour exécuter les programmes de commande, développés par des systèmes CAO/FAO, pour fabriquer la pièce finale. La productivité globale du processus de fraisage dépend duchoix des conditions de coupe et du parcours d'outil. Les systèmes actuels de CAO/FAO ne fournissent aucune indication pour sélectionner les conditions de coupe en raison de l'indisponibilité des modèles d'interaction physique et dynamique complexes de la machine-outil et la pièce à usiner. En outre, la génération des parcours d'outil par les modules CAO/FAO est purement géométrique et induit des variations de l'angle d'engagement le long du parcours d'outil.

La sélection des conditions de coupe et du parcours d'outil compte uniquement sur l'expérience d'un programmeur du programme de commande, les systèmes CAO/FAO[11], les directives dans le manuel d'utilisateur ou sur les spécifications prévues dans les catalogues des outils de coupe et des machines-outils. Leur mauvaise sélection provoque souvent broutage, de la fluctuation élevée des forces de coupe et/ou de la violation des limites de la puissance disponible et du couple de la machine-outil. Ces phénomènes se traduisent par un mauvais état de la surface, un endommagement de la pièce, une usure élevée de l'outil de coupe, une violation des limites de tolérance, un coût supplémentaire, des déchets indésirables et une réduction significative de la vie de la machine-outil. Afin d'éviter ces problèmes, les programmes de commande doivent être vérifiés de manière itérative à l'aide des expériences d'essai et d'erreur et souvent des conditions de coupe conservatrices sont sélectionnées. Ces pratiques augmentent le temps de préparation pour les programmes de commande et diminuent la performance d'usinage, qui en gros diminuent la productivité totale. En plus, les capacités des machines-outils ne sont pas utilisées complètement en raison de la sélection des conditions

[9] Géométrie comprend des caractéristiques qui représentent des contours 2D extrudés dans la direction perpendiculaire

[10] Contrôle numérique

[11] Conception et production assistée par ordinateur

de coupe conservatrices.

Afin de relever ces défis, un système “optimal milling (OptMill)” basé sur un algorithme génétique (AG) est développé pour une sélection optimale des conditions de coupe et/ou des parcours d'outil pour un ensemble de données de la machine-outil/broche/porte-outil/outil de coupe et du système pièce. Les contraintes opérationnelles de la machine-outil, comme la vitesse de la broche et la vitesse d'avance, la puissance et le couple disponible de la broche, les limites des broutage[12] en raison de l'interaction dynamique entre l'outil de coupe et la pièce, les limites admissibles de la contrainte de flexion et de la déflexion de l'outil de coupe et les limites du force de serrage de la pièce à usiner, sont incorporées. Le système développé est appliqué à différents cas industriels : (i) la minimisation du temps de fraisage d'une poche compte tenu d'un parcours d'outil simple (ii) la minimisation du temps d'usinage pour un multitraitement des pièces prismatiques avec l'initiation des préparations : l'extraction du parcours d'outil et les bords de la pièce à usiner à partir des fichiers APT[13] et STEP[14] respectivement, et du calcul de l'angle d'engagement le long du parcours d'outil (iii) la sélection optimale des conditions de coupe et du parcours de l'engagement correspondant régulier et constant de l'outil pour le fraisage de poche. Les conditions de coupe et/ou du parcours de l'outil sélectionnées sont également validées par des expériences réalisées au cours du travail de recherche. Le travail de recherche actuel est inspiré du projet CTI[15] en cours.

Les méthodes améliorées suivants, pour l'indentification des inputs importants pour les modelés mathématiques de prédiction des forces de coupe et des conditions de coupe sans broutage, sont également développées pour étendre le domaine du systéme OptMill développé.

- Les coefficients de force tangentielle, les inputs importants pour la prédiction des forces de coupe et des limites des conditions de coupe sans broutage, sont identifiés expérimentalement avec l'utilisation d'un dynamométre pour la force de coupe. Ce dispositif expérimental est très coûteux et pas pratique pour l'implémentation dans l'industrie. Une méthode améliorée est présentée pour l'identification indirecte des coefficients de force tangentielle à partir du courant dans la broche moteur. La méthode comprend l'élaboration d'un modéle empirique pour prédire le couple de coupe à partir du courant dans la broche moteur avec l'introduction d'un modéle de puissance de la broche qui considére toutes les pertes de puissance mécaniques et électriques. Le couple de coupe prédit par le modéle développé est utilisé ensuite pour l'identification des coefficients de force tangentielle, et est également validé expérimentalement avec des mesures directes en utilisant un dynamométre pour le couple de coupe.
- Le temps de réponse dynamique de chaque variante de la machine-outil/broche /porte-outil/outil de coupe, en termes de FRF[16], est nécessaire pour prévoir les limites des

[12] Amplitude des vibrations de la pointe de l'outil de coupe en raison de l'effet régénératif.
[13] Outil programmé automatique
[14] STandard pour l'échange de données du modèle du produit
[15] ChatFree : Programmation du programme de commande pour réaliser le fraisage de poche sans broutage et efficace (CTI-Projet No.10008.1 PFES-ES)
[16] Réponse en fréquence

conditions de coupe sans broutage avec précision. FRF est souvent mesuré à l'aide d'expériences utilisant le marteau. Afin d'éviter ces tests fastidieuses, une procédure améliorée à l'aide de la technique de couplage réceptance est implémentée pour prédire la FRF d'une machine-outil / broche / porte-outil / système d'outil de coupe pour différentes outils de coupe. Les FRF prédites par la simulation numérique sont également validées par des expérimentaux.

Bien que les modéles mathématiques existants prédisent des limites des conditions de coupe sans broutage avec précision, leur utilisation dans les petits ateliers n'a pas encore été atteinte en raison de l'absence d'expertise technique et des moyens expérimentaux. Par ailleurs, même les machines-outils modernes ne fournissent aucune indication à l'opérateur concernant l'apparition de broutage en cours d'usinage. Pour répondre aux besoins industriels, un systéme de calcul rapide, facile à utiliser et pratique est développé qui détecte automatiquement le broutage pendant le fraisage et propose par la suite une stratégie de contôle à l'opérateur. Le système online de détection et de contrôle de broutage est également validé expérimentalement avec le partenaire industriel.

A part les nombreux défis et développements discutés ci-dessus, le fraisage des pièces avec des parois minces est également un sujet de préoccupation en raison de sa dynamique instable pendant l'usinage. Ainsi, une procédure améliorée numérique est développée pour le choix des conditions de coupe sans broutage tout en tenant compte du changement de la dynamique de la pièce le long du parcours d'outil en utilisant l'analyse par éléments finis.

Afin de réaliser le système développé, MATLAB est utilisé comme le langage de programmation. La modélisation géométrique et la programmation des programmes de commande prismatiques est faite avec CATIA. La plate-forme d'acquisition de données pour la validation expérimentale est conçue dans LabVIEW. La modélisation et l'analyse par éléments finis est faite avec la conception paramétrique d'ANSYS (APDL). Le système développé est très attrayant pour les applications industrielles par une intégration directe dans les systèmes existants CAO/FAO et/ou dans les machines-outils modernes. L'augmentation de la productivité globale est assurée par la sélection optimale des conditions de coupe et/ou des parcours de l'outil et l'évitement simultané des répercussions de leur mauvaise sélection.

Mots-clés : conception et production assistée par ordinateur, pièces prismatiques, fraisage de poche, optimisation de fraisage à grande vitesse, algorithme génétique, dynamique de machines-outils, modélisation par éléments finis, détection et contrôle online de broutage

Contents

List of Figures

List of Tables

List of Abbrevations

$\overline{F}_x$	Average cutting force in feed direction
$\overline{F}_y$	Average cutting force in normal to feed direction
$\overline{F}_z$	Average cutting force in axial direction
ω_m	Angular speed of spindle
ϕ	Immersion angle
ϕ_{ex}	Exit angle from the cutting zone
ϕ_{st}	Start angle in the cutting zone
A_e	Radial depth of cut in mm
A_p	Axial depth of cut in mm
D	Diameter of the end mill in mm
D_p	Depth of the pocket in mm
F_a	Axial cutting force in N
F_r	Radial cutting force in N
F_t	Tangential cutting force in N
f_t	Feed rate in *mm/rev-flute*
F_x	Cutting force in feed direction in N
F_y	Cutting force in normal to feed direction in N
F_z	Cutting force in axial direction in N
I	Spindle motor current in A
K_{ac}	Cutting force coefficient in axial direction N/mm^2
K_{ae}	Edge force coefficient in axial direction N/mm

k_{lm}	Load meter constant
K_{rc}	Cutting force coefficient in radial direction N/mm^2
K_{re}	Edge force coefficient in radial direction N/mm
K_{tc}	Cutting force coefficient in tangential direction N/mm^2
K_{te}	Edge force coefficient in tangential direction N/mm
L_p	Length of the pocket in mm
N	Number of flutes of the cutting tool
n	Spindle speed in rpm
P_{ACeff}	Effective power in W
U	Spindle motor voltage
W_p	Width of the pocket in mm
AE	Acoustic Emission
APT	Automatically Programmed Tool
CAD	Computer-Aided Design
CAM	Computer-Aided Manufacturing
ChatFree	Chatter Free
CL	Cutter Location
CNC	Computerized Numerical Control
DFT	Discrete Fourier Transform
FEA	Finite Element Analysis
FFT	Fast Fourier Transform
FRF	Frequency Response Function
FT	Fourier Transform
HSM	High Speed Milling/Machining
IRC	Inverse Receptance Coupling
LDV	Laser Doppler Vibrometer
MDOF	Multi-Degree-of-Freedom

NC	Numerical Control
noap	Number of Axial Passes
nop	Number of Passes
norp	Number of Radial Passes
RC	Receptance Coupling
RCSA	Receptance Coupling Substructure Analysis
SF	Spindle Frequency in *Hz*
SLD	Stability Lobe Diagram
STEP	STandard for the Exchange of Product model data
TPF	Tooth Passing Frequency in *Hz*

1 Introduction

1.1 Background

The desired shapes of most mechanical parts are accomplished by various machining operations. Material removal processes are still the most widely used machining processes to manufacture the final product though there is a significant development in the manufacturing domain (Quintana, 2009). A blank is converted into the final product by removing extra material by turning, drilling and milling followed by special operations such as boring, broaching and grinding (Altintas, 2000). Among different types of material removal processes, milling holds a dominant position in the manufacturing practices due to its wide range of industrial applications (Held, 1991b). In milling, a rotating cylindrical cutting tool removes the material along a predefined toolpath to achieve the desired shape of final workpiece. Often large amounts of material are removed from the blank during milling operations (Faassen, 2007).

In the manufacturing of automotive and aerospace parts, mold and die, 2.5D (or 2.5-axis) milling is very important (Hatna et al., 1998; Tekeli and Budak, 2005). Often in industrial practice even complicated parts are machined from a blank first by 2.5D rough milling followed by 3D-5D finishing operations (Lee and Chang, 1995). 2.5D milling is able to perform point-to-point, contouring and pocketing operations. More than 80% of all mechanical parts to be machined can be manufactured by only pocket milling: the removal of material within a defined boundary (Held, 1991a; Lambregts et al., 1996). Most modern production floors are equipped with high speed CNC (computer numeric control) machine tools and advanced CAD/CAM (computer-aided design/manufacturing) software to enhance the speed and accuracy of the overall machining process.

1.1.1 High Speed Milling

High speed milling (HSM) is able to achieve high material removal rates at higher spindle speeds and feed rates. HSM has become an indispensable process in modern manufacturing

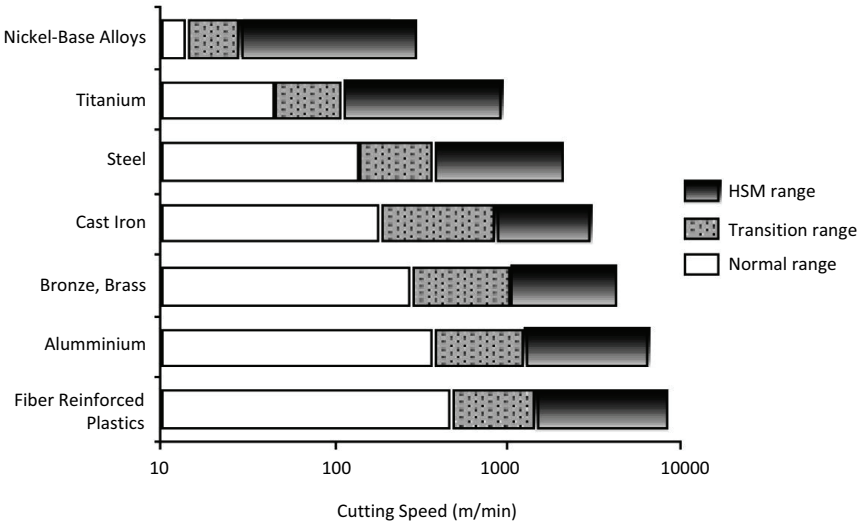

Figure 1.1: Definition of high speed milling (Schulz and Moriwaki, 1992)

industry due to its high productivity and reliability. Even though HSM has been known for a long time, authors have not established its clear and concise definition. A comprehensive summary of these definitions is given by (Agba et al., 1999; Quintana, 2009). The few definitions, which are mainly encountered in the literature, are highlighted below:

- Spindle designers define HSM as spindles with DN numbers of 500,000 to 1,500,000. The DN number is the product of the spindle diameter in mm with spindle speed in rpm.
- Based on the peripheral speed of the cutting tool, cutting speeds of 1500ft/min (~7.6m/s) or more are considered as high speed machining.
- High speed milling generally refers to end milling or ball nose end milling at high rotational speeds (10,000-1,00,000rpm) (Urbanski et al., 2000).
- The term “high speed milling” is generally used to describe end milling with small diameter cutting tools ($\leq$ 10mm) at high rotational speeds ($\geq 10,000$rpm) (Toh, 2005).
- High speed milling is defined based on the workpiece material and corresponding cutting speed as shown in Figure 1.1 (Schulz and Moriwaki, 1992).
- Smith and Tlusty defined HSM based on spindle and cutting tool dynamics (Smith and Tlusty, 1997). HSM occurs whenever the tooth passing frequency (TPF) can approach a substantial fraction of the dominant (most flexible) natural frequency of the machine tool system. TPF is defined as:

$$\text{TPF} = \frac{Nn}{60} \tag{1.1}$$

Here, N is the number of flutes of the cutting tool and n is the spindle speed in rpm

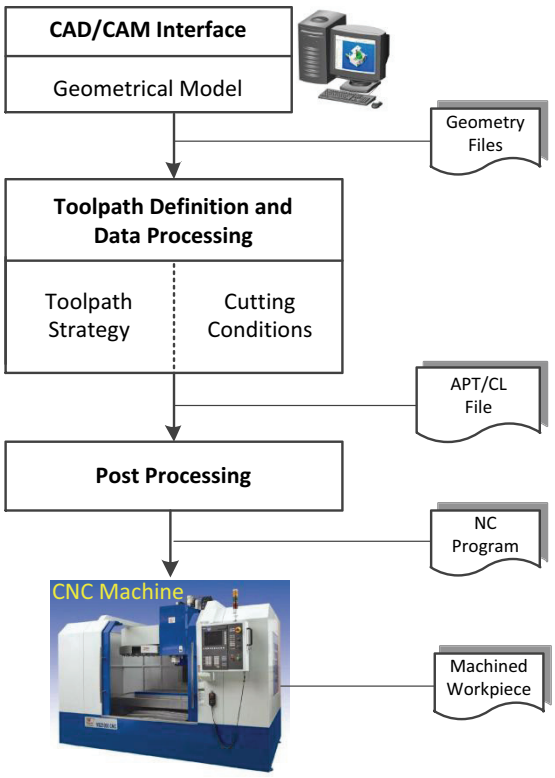

Figure 1.2: Steps involved in part programming

1.1.2 NC Part Programming

Modern CAM systems facilitate the generation of part programs from geometrical models created in a CAD environment. Part programs are sets of numerical commands to guide the CNC machine tools to follow a predefined sequence of machining operations at predetermined speeds necessary to produce a workpiece of desired shape and dimensions. Several CAD/CAM systems are available in the modern manufacturing industry. The main steps involved in NC part programming, as presented in Figure 1.2, are summarized below:

(i) The part programmer[1] can create the geometrical model of the desired part in the CAM package or directly import it from CAD system.

(ii) After the geometric modeling, the machine datum, part boundaries, cutting tool, approach/retract planes and other operational parameters are defined. The CAM system requires geometrical parameters namely axial and radial depth of cut to compute the toolpath trajectory. Spindle speed and feed rate are also needed to define the movement

[1] In industrial practice, toolpath trajectory and cutting conditions are selected by the user. Depending upon the size of the manufacturing unit, user can be a part programmer or a machine operator. In large manufacturing units often the NC part programs are prepared by a part programmer and the actual machining is performed by a machine operator. In small production floors the same person acts both as a part programmer and a machine operator.

of a cutting tool along the toolpath trajectory. The cutting conditions, namely spindle speed, feed rate, axial depth of cut and radial depth of cut, are represented in Figure 1.3.

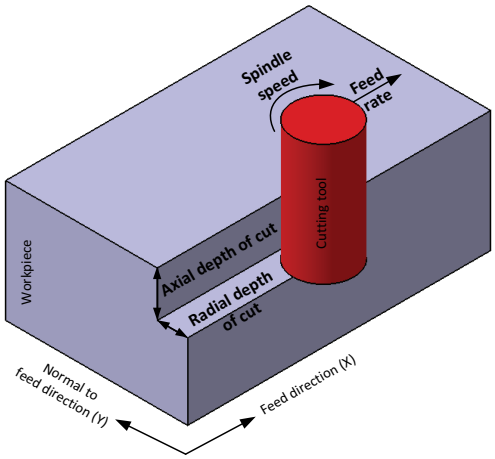

Figure 1.3: Definition of cutting conditions: spindle speed (n), feed rate (f_t), radial depth of cut (A_e) and axial depth of cut (A_p)

(iii) The computer will process the input data to generate the toolpaths and corresponding APT (automatically programmed tool) or CL (cutter location) file.

(iv) Post processing is required to convert the general instructions from APT file to machine specific NC codes. A post processor is computer software which converts the cutting tool movement into a format which the machine controller can interpret correctly. These NC part programs are then transferred to a CNC machine tool for actual machining.

The performance of the developed NC part program, which is directly dependent on the selection of cutting conditions and toolpath, is the driving factor for the overall productivity of the complete milling process.

1.2 Motivation

In spite of many advances in CNC machine tools and CAD/CAM software, an industrial part programmer must adhere to the procedure (as shown in Figure 1.4) to finalize the part program to manufacture the final workpiece.

For a given machine tool/spindle/tool holder/cutting tool and workpiece system, the physical phenomena that occur due to the interaction between machine tool and workpiece system during the milling process depend significantly on the choice of cutting conditions. Cutting conditions have complex non-linear relationships with different physical phenomena (Balachandran, 2001; Wiercigroch and Budak, 2001; Altintas and Weck, 2004). Current CAD/CAM

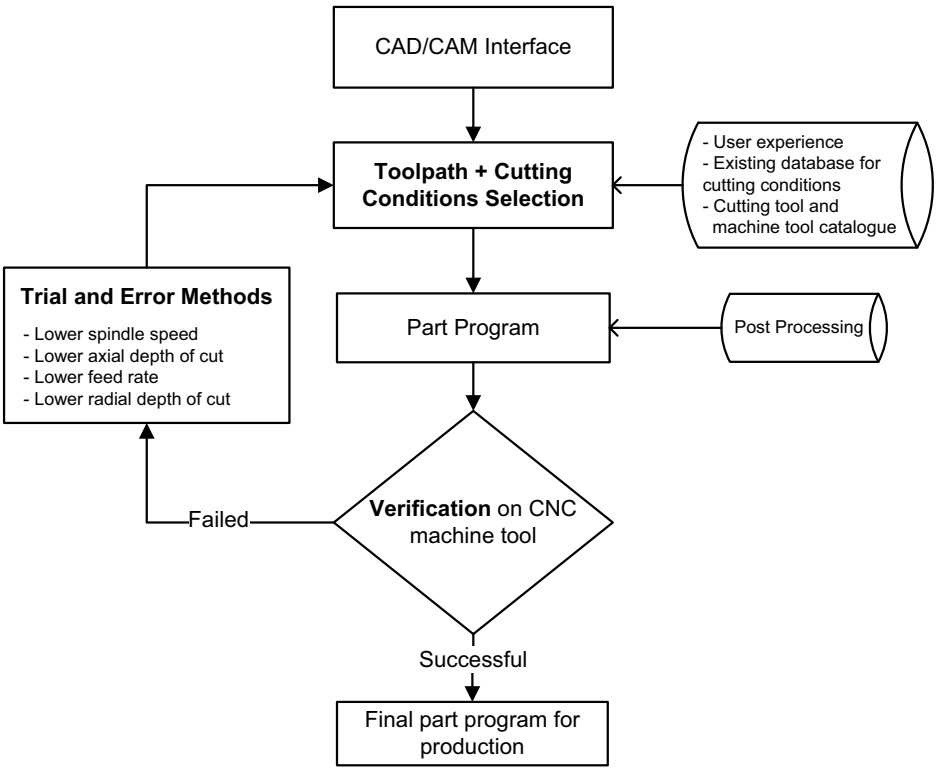

Figure 1.4: Industrial development of part programs

packages do not provide any guidance for selection of cutting conditions due to the unavailability of milling process modeling and corresponding input parameters. The selection of cutting conditions relies solely on part programmer experience, handbook guidelines or specifications provided in catalogues of cutting tools and machine tools (Rai, 2008; Shunmugam et al., 2000). Even the experienced user cannot ensure the right selection of cutting conditions as physical phenomena change significantly with every new variant of machine tool/spindle/-tool holder/cutting tool and workpiece system. Moreover, toolpath generation by current CAD/CAM packages is purely geometric in nature and results in changes in radial depth of cut along the toolpath (Kramer, 1992). Poor selection of cutting conditions and toolpath at the part programming stage leads to the following problems during actual machining:

- Machine tool and workpiece system vibrations, also known as chatter vibrations, are encountered frequently. Chatter vibrations occur due to the dynamic interaction of the machine tool system and workpiece (Altintas and Budak, 1995; Quintana, 2009). Chatter is the most undesirable and complex phenomenon which leads to unavoidable consequences during any machining process. During rough milling the dynamics of the machine tool system are more dominant but in the milling of thin-walled parts, workpiece system dynamics become significant (Bravo et al., 2005; Davies and Balachandran, 2000).

- Wrong selection of cutting conditions leads to high magnitude of cutting forces. Moreover, the variation of radial depth of cut along the generated toolpath causes high fluctuations of cutting forces along the toolpath (Tandon et al., 2002; Dhanik, 2009).
- Selected cutting conditions often violate the available limits of cutting power,cutting torque or feed rate of the machine tool (Altintas, 2000).
- Excessive wear and/or breakage of the cutting tool (Byrne et al., 1995).

These problems lead to poor surface finish, workpiece damage, violation of tolerance limits, additional cost, unwanted waste and reduction in the machine tool spindle working life. In order to overcome these problems, part program needs to be verified iteratively using trial and error experiments and often conservative cutting conditions are selected. This procedure leads to long preparation time of part programs and lower machining performance which thus lowers significantly overall productivity (Hatna et al., 1998). Moreover, machine tool capabilities are not fully utilized due to the selection of conservative cutting conditions.

The competitive economic environment has brought new challenges to the manufacturing industry. Significant reduction in machining time and production cost, and improvement in overall productivity have become an ultimate requirement. For a given machine tool/spindle/-tool holder/cutting tool and workpiece system, the main objective of the part programmer is to select chatter free cutting conditions with lower cutting forces while respecting the power and torque limits of machine tools and other practical constraints of milling system. Therefore, right and optimal selection of cutting conditions is of great concern for manufacturing industry (Wang et al., 2004; Rai et al., 2009). Smooth toolpaths with minimum variation of radial depth of cut along the cutting path have apparent improvements over the toolpaths generated by current CAD/CAM systems for high speed milling (Dhanik, 2009). In order to satisfy the pressing need of modern manufacturing, a system must be developed to ensure the optimal selection of cutting conditions and toolpath while respecting the limits of various physical phenomena occurring during high speed milling.

The goal of achieving high material removal rates is often hampered by chatter vibration and high cutting forces. Chatter and high cutting forces affect significantly the surface quality, permissible tolerance limits and working life of spindle and cutting tools. Several authors have developed mathematical models to predict accurately the chatter free cutting conditions and cutting forces. The following barriers are often encountered for their complete implementation at production floors:

(1) For prediction of chatter free cutting conditions by mathematical modeling, dynamic characteristics of machine tool/spindle/tool holder/cutting tool combination are required (Altintas and Budak, 1995; Solis et al., 2004). The dynamic characteristics, in terms of frequency response functions (FRF), are identified experimentally for every new variant of machine tool/spindle/tool holder/cutting tool system. To avoid a large number of exper-

iments, an enhanced modeling procedure can be implemented to predict the dynamic characteristics of different variants (Schmitz and Burns, 2003; Park et al., 2003).

(2) Force coefficients are an important input for mathematical models to predict cutting forces and chatter free cutting conditions (Budak et al., 1996; Altintas and Budak, 1995). These force coefficients are identified experimentally (with the use of cutting force dynamometer) for a given cutting tool geometry and workpiece material (Budak and Altintas, 1994). This experimental setup is quite costly and even not practical for implementation in industrial environments. Development of a simple and enhanced methodology is thus required to facilitate the identification of force coefficients on production floors.

Chatter is the most complex and widely studied topic in machining research. Many studies have been executed to understand, detect, avoid, prevent, reduce or suppress chatter vibration (Altintas and Weck, 2004; Budak, 2006b; Quintana and Ciurana, 2011). These research studies require costly experimental setups, complex mathematical modeling or prior knowledge of dynamic characteristics to target chatter vibration. Mathematical modeling to predict chatter free cutting conditions is a complex task due to the multi-degree-of-freedom (MDOF) system, multiple cutting flutes, variable cutting forces and chip load directions (Balachandran, 2001). Though developed mathematical models predict accurately the chatter free cutting conditions their implementation in production floors has not yet been achieved due to absence of technical expertise and experimental resources. There is still a practical need to bring to the production floors an inexpensive, easy to use and computationally fast system that can automatically detect chatter vibration during milling and thereafter propose a control strategy to the machine operator. This will be a considerable step towards achieving the goal of smart machining.

Apart from many challenges discussed above, milling of thin-walled workpiece is also a concern due to its changing dynamics along a toolpath which further makes the selection of chatter free cutting conditions a difficult task (Thevenot et al., 2006a; Davies and Balachandran, 2000). Change in workpiece dynamics can be studied with experimental modal analysis or using numerical tools like finite element analysis (FEA). FEA facilitates investigation of the workpiece dynamic behavior even at the part programming stage when the actual workpiece does not exist. The development of an enhanced procedure using FEA will surely guide the part programmer to select chatter free cutting conditions for milling of thin-walled workpieces.

1.3 Research Objectives

In order to address the challenges and requirements stated in the previous section, the following main objectives are defined for this research work:

1. To develop a genetic algorithm (GA) based optimization system for the optimal selection of cutting conditions and/or toolpath at the part programming stage while respecting

the practical constraints of the machine tool and workpiece system. Implementation of the developed optimization system for the different use cases:

(i) For a given pocket dimensions and material, and machine tool/spindle/tool holder/cutting tool system, minimization of pocketing time with one-way toolpaths by optimal selection of cutting conditions. Implementation and experimental validation of this use case of milling systems.

(ii) For a given multi-feature prismatic part general toolpaths, minimization of machining time by optimal selection of cutting conditions. Implementation and experimental validation of this use case of milling systems.

(iii) For a given pocket, minimization of pocket milling time by optimal selection of cutting conditions and corresponding smooth and constant stepover toolpath. Implementation and experimental validation of this use case of milling systems.

2. Development of a procedure for prediction of machine tool system FRFs for different end mills. Implementation and experimental validation of predicted FRFs.

3. To develop an enhanced methodology for the indirect identification of tangential force coefficients from the spindle motor current. Implementation and experimental validation of the proposed methodology.

4. Development of an online chatter detection and control system in order to detect automatically the existence of chatter vibrations and propose a control strategy. Implementation and experimental validation of the developed system.

1.4 System Architecture

The overall architecture of the developed system[2] with various inputs, developments and corresponding outputs for the research work is presented in Figure 1.5. Different developed subsystems, with their corresponding inputs, are combined to achieve different objectives of 2.5D high speed milling. The overall architecture is explained briefly in a generalized way with various developments and their inputs and corresponding outputs:

- The workpiece geometrical and part programming information is pre-processed from the corresponding inputs with the following developments:
  - Feature boundary and depth is extracted from the STEP file of a geometrical model created in the CAD system. Feature boundary and depth for the simple shaped features can also be entered manually.
  - The part programming information, in terms of toolpath trajectory with linear and circular segments, is extracted from the APT file generated from a CAM system.

[2] It is termed OptMill (Optimal Milling)

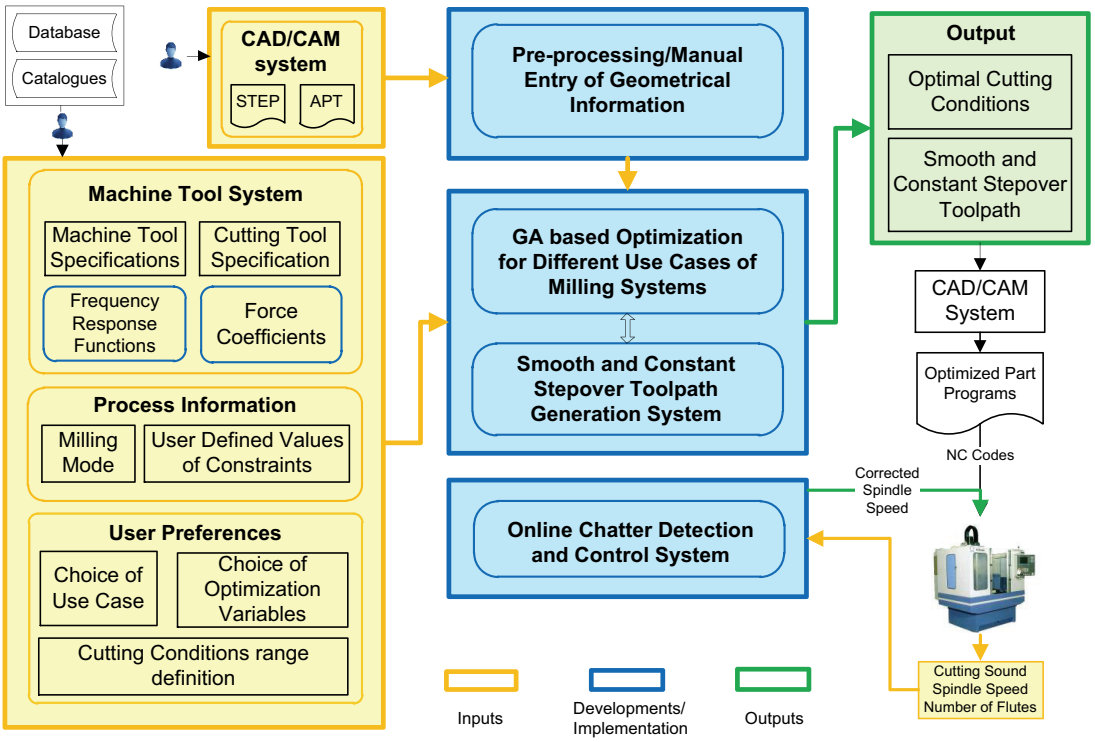

Figure 1.5: System architecture of OptMill system

  - The pre-processed geometrical and part programming information is used for the calculation of engagement angles along the toolpath.

  The geometrical and part programming information of the workpiece is used as an input to the developed system for different use cases of milling system.

- A GA based optimization system (Chapter 3) is developed for selection of cutting conditions and/or toolpaths for high speed milling. The system includes inputs from the machine tool and workpiece system, process related information and user preferences. Operational constraints of the machine tool, such as available cutting power and torque, chatter vibration limits due to the dynamic interaction between cutting tool and workpiece, acceptable limits of bending stress and deflection of the cutting tool and clamping load limits of the workpiece system are embedded in the optimization system (Section 3.2). Various submodules of the GA based optimization are developed in a generic way. The following three different use cases are targeted with the developed optimization system:

  - For given pocket dimensions, pocketing time with one-way toolpaths is minimized by optimal selection of spindle speed, feed rate, axial and radial depths of cut. The user has also the possibility of fixing one of the optimization variables based on the requirements and application (Section 3.3).
  - For a given set of APT and STEP files of a multi-feature prismatic part, machining

time for each feature is minimized by optimal selection of spindle speed, feed rate and axial depth of cut. During this use case, radial depth of cut is kept constant (Section 3.4).

- For given pocket dimensions and other set of inputs, pocketing time is minimized by optimal selection of all the cutting conditions and corresponding smooth and constant stepover toolpath (Section 3.5).

The developed optimization system is implemented for the optimal selection of cutting conditions and/or toolpath for different workpieces and is also verified experimentally (Chapter 4).

- In order to increase the scope of the overall system, the following enhanced methods and procedures are developed to identify the important inputs for the OptMill system:
  - An enhanced methodology is presented for the indirect identification of tangential force coefficients from the spindle motor current. The methodology includes the development of an empirical model for cutting torque prediction from spindle motor current with the implementation of spindle power model that accounts for all mechanical and electrical power losses (Chapter 5).
  - Dynamic characteristics of each variant of machine tool/spindle/tool holder/end mill, in terms of FRF, is required to predict chatter free limits accurately. FRFs are often measured with hammer testing experiments. In order to avoid the tedious tests, an enhanced procedure using the receptance coupling technique is implemented to predict the FRF of a machine tool/spindle/tool holder/cutting tool system for different cutting tools (Chapter 6).
- An online chatter detection and control system is developed. The system is able to detect the existence of chatter vibration in the case of unstable milling and proposes an alternative spindle speed to realize stable milling. The developed system can also be used as an independent system on production floors (Chapter 7).
- Apart from the many developments discussed above, an enhanced numerical procedure is developed for the selection of chatter free cutting conditions while considering the change in workpiece dynamics using finite element analysis (Appendix G).

2 State-of-the-Art

2.1 Cutting Force during Milling

Cutting force during milling is one the most significant process parameters. High cutting forces cause cutting tool and workpiece deflections which may result in violation of permissible tolerances (Budak, 2006a). Moreover, high cutting forces have an adverse effect on the working life of cutting tools and thus affect significantly the overall productivity of the milling process. Accurate prediction of cutting forces helps to calculate the required cutting power and torque from the machine tool, to control tolerance limits and to improve the working life of the cutting tool. In this section a brief introduction to the geometry of the cutting tool and cutting force modeling is presented.

A milling process consists of an end mill (or cutting tool) that has multiple cutting flutes on both its periphery and its tip which allows end cutting and peripheral cutting. The envelop or outer geometry of the general cutting tool is defined by seven geometrical parameters $(D, R, R_r, R_r, \alpha, \beta, h)$ as presented in Figure 2.1a. Shapes of the different end mills used in industry can be realized from the geometrical parameters as shown in Figure 2.1b. Simple cylindrical helical end mills are used in the milling of prismatic parts, bull nosed end mills produce parts with bottom floors with fillets, tapered helical end mills are used in five axis machining of jet engine compressors, and form cutting tools are used to mill complex profiles such as turbine blade carrier rings. A helical cutting edge is wrapped around the outer geometry of the end mill as shown in Figure 2.1c. Cutting point (P) along the cutting edge trajectory for different helical end mills is shown in Figure 2.1d. The accurate identification of the coordinates of cutting point (P) along the cutting edge plays a vital role in the mechanics of cutting (Engin and Altintas, 2001).

For the prediction of cutting forces, the cutting edge is assumed to be a sequence of infinitesimal single point cutting edge segments. The differential tangential (dF_t), radial (dF_r) and axial (dF_a) cutting forces (as shown in Figure 2.1c) are computed for every cutting edge segment along the cutting edge to account for total cutting forces. The differential cutting forces acting

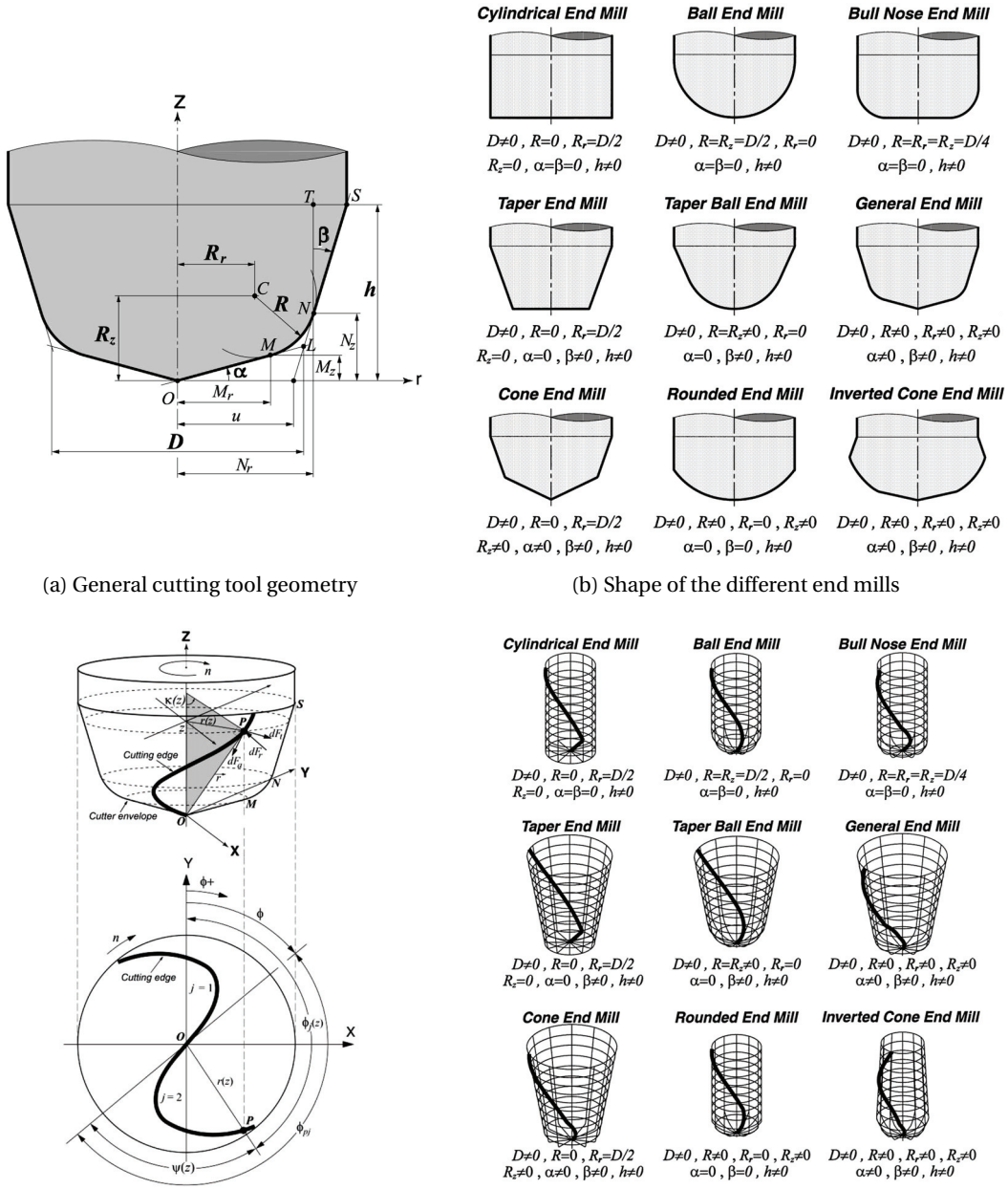

(a) General cutting tool geometry

(b) Shape of the different end mills

(c) Cutting edge of the general end mill

(d) Helical cutting edge of different end mills

Figure 2.1: Geometry of different end mills (Engin and Altintas, 2001)

on the infinitesimal cutting edge segment are given by:

$$\begin{aligned} dF_t(\phi) &= \left[K_{tc}h(\phi) + K_{te}\right] dz \\ dF_r(\phi) &= \left[K_{rc}h(\phi) + K_{re}\right] dz \\ dF_a(\phi) &= \left[K_{ac}h(\phi) + K_{ae}\right] dz \end{aligned} \tag{2.1}$$

where, K_{tc}, K_{rc} and K_{ac} are the cutting force coefficients contributed by shearing action and K_{te}, K_{re} and K_{ae} are the edge force coefficients in tangential, radial and axial directions respectively. Force coefficients are the parameters which represent the combined property of the cutting tool geometry and workpiece material. dz is the edge contact length. $h(\phi)$ is the uncut chip thickness normal to the cutting edge which varies with the position of cutting point (P) and the immersion angle (as shown in Figure 2.2). Chip thickness is expressed as:

$$h(\phi) = f_t \sin\phi \tag{2.2}$$

where, f_t is the feed rate in mm/rev-flute and ϕ is the time varying immersion angle. Cutting forces in feed (dF_x), normal to feed (dF_y) and axial (dF_z) directions are presented in the form of differential cutting forces (Equation 2.1) as (Altintas, 2000):

$$\begin{aligned} dF_x(\phi) &= -dF_t \cos\phi - dF_r \sin\phi \\ dF_y(\phi) &= dF_t \sin\phi - dF_r \cos\phi \\ dF_z(\phi) &= dF_a \end{aligned} \tag{2.3}$$

Cutting forces are modeled for given cutting tool geometry, cutting conditions and workpiece

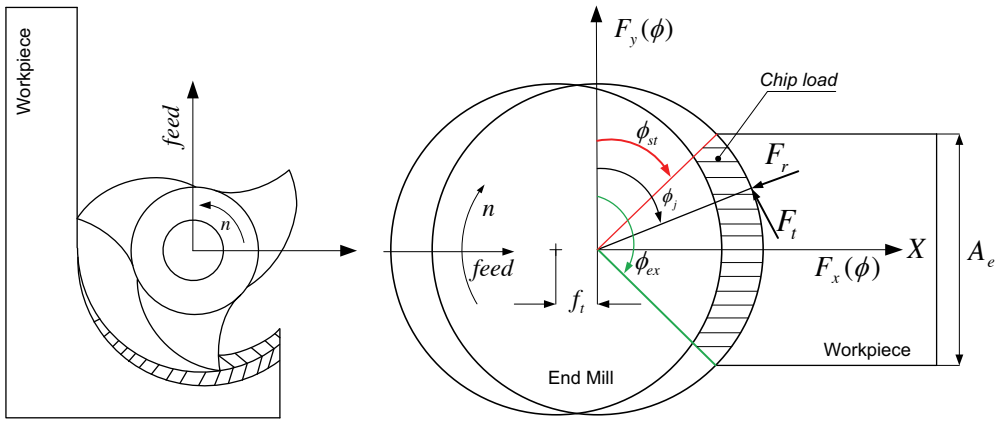

Figure 2.2: Geometrical representation of the milling process, redrawn from (Altintas, 2000)

material. There are two different force analysis models: mechanics of cutting model and mechanistic models. These models are differentiated based on the identification of force coefficients.

2.1.1 Mechanics of Cutting Model

In the mechanics of cutting approach, force coefficients are determined from analytical models of oblique cutting with the following procedure:

- Shear angle (ϕ_c), average friction angle (β_a) and shear yield stress (τ_s) are evaluated

experimentally from orthogonal cutting experiments (turning tests). During the orthogonal cutting experiments, chip thickness and tangential and feed forces are measured. Chip thickness is measured with a micrometer and cutting forces are measured with a cutting force dynamometer.

- The following assumptions are made: the orthogonal shear angle is equal to the normal shear angle in oblique cutting ($\phi_c \equiv \phi_n$); normal rake angle in oblique cutting is equal to the rake angle in orthogonal cutting ($\alpha_r \equiv \alpha_n$); the chip flow angle is equal to the oblique angle ($\eta \equiv i$); the friction coefficient (β_a) and shear yield stress (τ_s) are the same in both orthogonal and oblique cutting operations for a given speed, chip load and cutting tool-workpiece material combination.
- Cutting force coefficients are expressed as (Budak et al., 1996):

$$\begin{aligned} K_{tc} &= \frac{\tau_s}{\sin\phi_n} \frac{\cos(\beta_n - \alpha_n) + \tan i \tan\eta \sin\beta_n}{\sqrt{\cos^2(\phi_n + \beta_n - \alpha_n) + \tan^2\eta \sin^2\beta_n}} \\ K_{rc} &= \frac{\tau_s}{\sin\phi_n \cos i} \frac{\sin(\beta_n - \alpha_n)}{\sqrt{\cos^2(\phi_n + \beta_n - \alpha_n) + \tan^2\eta \sin^2\beta_n}} \\ K_{ac} &= \frac{\tau_s}{\sin\phi_n} \frac{\cos(\beta_n - \alpha_n) \tan i - \tan\eta \sin\beta_n}{\sqrt{\cos^2(\phi_n + \beta_n - \alpha_n) + \tan^2\eta \sin^2\beta_n}} \end{aligned} \tag{2.4}$$

Mostly, orthogonal cutting experiments are repeated for a range of cutting speed, rake angle and uncut chip thickness to prepare a database for certain cutting tools and workpiece materials. The values of shear angle, average friction angle and shear yield stress are further used to determine force coefficients using the oblique cutting model presented by Equation 2.4. Oblique cutting transformation using basic orthogonal parameters can predict the force coefficients before the cutting tool is manufactured.

2.1.2 Mechanistic Model

The identification of force coefficients from time consuming orthogonal cutting tests is not a feasible and practical approach. In such cases, a mechanistic approach is used for quick calibration of cutting tools. For a given cutting tool and workpiece material, the mechanistic approach for force coefficient identification has the following steps:

- A set of slot cutting (full immersion) experiments are conducted at different feed rates. Spindle speed and axial depth of cut are kept constant during the experiments.
- The cutting forces in feed, normal to feed and axial directions are measured with a cutting force dynamometer. The total force per spindle revolution is collected and divided by the number of flutes of the cutting tool to avoid the influence of run out in the machine tool.

- Force coefficients are then identified by equating the experimentally evaluated average cutting forces to analytically derived average milling force expressions for slot milling. The average cutting forces per tooth period are presented as (Altintas, 2000):

$$\begin{aligned}\overline{F}_x &= -\frac{NA_p}{4}K_{rc}f_t - \frac{NA_p}{\pi}K_{re}\\ \overline{F}_y &= +\frac{NA_p}{4}K_{tc}f_t + \frac{NA_p}{\pi}K_{te}\\ \overline{F}_z &= +\frac{NA_p}{\pi}K_{ac}f_t + \frac{NA_p}{2}K_{ae}\end{aligned} \tag{2.5}$$

  here, $\overline{F}_x$, $\overline{F}_y$ and $\overline{F}_z$ are the average cutting forces per tooth period in feed, normal to feed and axial directions respectively. f_t is the feed rate and A_p is the selected axial depth of cut.

- The average cutting forces can be expressed by a linear function of feed rate as:

$$\overline{F}_q = \overline{F}_{qc}f_t + \overline{F}_{qe} \quad (q = x, y, z) \tag{2.6}$$

  The average cutting forces at each feed rate are measured and cutting components ($\overline{F}_{qc}$ and $\overline{F}_{qe}$) are estimated by linear regression of the data. Using Equation 2.5 and Equation 2.6 cutting force coefficients are evaluated by:

$$\begin{aligned}K_{tc} &= +\frac{4\overline{F}_{yc}}{NA_p} \quad \text{and} \quad K_{te} = +\frac{\pi\overline{F}_{ye}}{NA_p}\\ K_{rc} &= -\frac{4\overline{F}_{xc}}{NA_p} \quad \text{and} \quad K_{re} = -\frac{\pi\overline{F}_{xe}}{NA_p}\\ K_{ac} &= +\frac{\pi\overline{F}_{zc}}{NA_p} \quad \text{and} \quad K_{ae} = +\frac{2\overline{F}_{ze}}{NA_p}\end{aligned} \tag{2.7}$$

This procedure is repeated for each combination of cutting tool geometry and workpiece material. Force coefficients are directly calibrated for an existing cutting tool with the mechanistic model.

2.2 Vibrations in the Milling Process

Mechanical vibrations during milling arise due to the lack of dynamic stiffness of one or several components of the machining system composed of machine tool, spindle, tool holder, cutting tool and workpiece. These vibrations can be categorized into three different types: free vibrations, forced vibrations and self-excited vibrations

(i) Free vibrations occur when the machining system, which is displaced from its equilibrium state, is allowed to vibrate freely. For example, due to rapid reversal of reciprocating

masses such as machining tables, or due to the initial engagement of cutting tool and workpiece.

(ii) Forced vibrations result from periodic forces within the system such as unbalanced rotating masses or the intermittent engagement of a cutting tool.

(iii) Self-excited vibrations extract energy to begin and grow themselves from the interaction between cutting tool and workpiece during machining.

Researchers have successfully developed methodologies to avoid, reduce or even eliminate the occurrence of free and forced vibrations. On the other hand, self-excited vibrations create instability during any machining process and are the most undesirable, complex and the least controllable phenomenon .

The aim of achieving high material removal rates during high speed milling is often hampered by chatter vibrations. Chatter is a self-excited vibration that can occur during any machining process. Chatter vibrations are characterized by high fluctuations of cutting forces and chaotic relative motion between cutting tool and workpiece. As a consequence, chatter lowers the surface quality of the workpiece, reduces spindle and cutting tool working life and thus affects significantly the overall productivity of the machining process. For this reason, chatter has been a noted topic for academic and industrial research.

Physical mechanisms causing chatter can be divided into two main categories:

(i) **Primary Chatter**
Primary chatter is caused by the physical mechanisms of the cutting process such as friction at the contact area between cutting tool and workpiece, thermo-mechanical effects on chip formation or by the stress distribution on the normal rake face. Primary chatter typically occurs at lower spindle speeds.

(ii) **Secondary Chatter**
Secondary chatter is caused by the regenerative effect which is a function of chip thickness variation that occurs due to vibrations of machine tool system, workpiece system, or the interaction of both systems.

Secondary chatter is the most common form of self-excited vibrations and the most important cause of instability during high speed milling (Faassen et al., 2003; Totis, 2009). For this reason it is been meant by authors that “chatter” refers only to regenerative chatter.

2.2.1 Regenerative Effect

Several studies have been performed since the late 1950s concerning the stability of machining processes. The theory of chatter in metal cutting was first established by (Tobias and Fishwick,

1958; Tlusty and Polacek, 1963). Later, a study from (Merritt, 1965) presented a foundational understanding of regenerative chatter or self-excited vibrations.

A complete milling system is comprised of machine tool system and workpiece system as shown in Figure 2.3. The machine tool system consists of machine tool, spindle, tool holder and cutting tool whereas workpiece system is mainly composed of the workpiece.

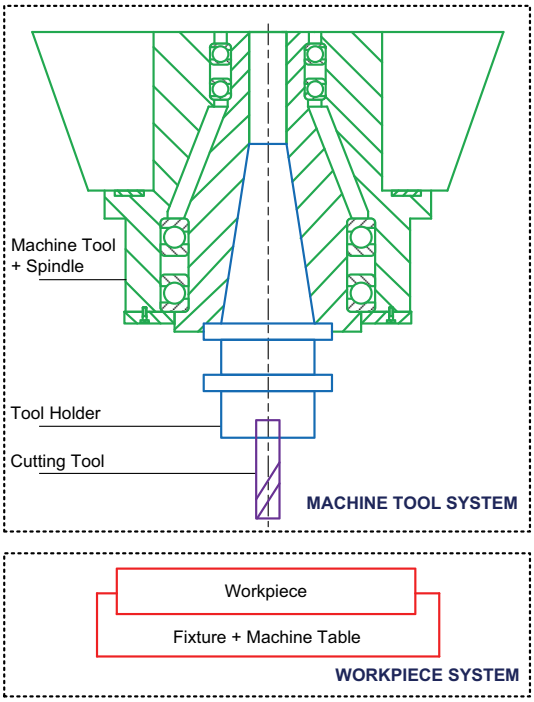

Figure 2.3: Complete milling system

A flexible machine tool system and rigid workpiece system (as shown in Figure 2.4) is considered to explain briefly the regenerative process. The machine tool system vibrates under the action of cutting forces. These vibration are imprinted on the surface of the machined workpiece by the flute of the cutting tool. The next flute on the rotating cutting tool overcuts the wavy surface generated by the previous flute. This wavy surface varies the instantaneous chip thickness which modulates the cutting force and cutting tool vibrations (i.e., a feedback mechanism is produced that leads to self-excited vibrations). The variation of chip thickness strongly depends on the phase difference between the wavy surface left by previous flute and current cutting tool vibration. This phenomenon is illustrated in Figure 2.5. If the relative phase $\varphi = 0°$, the dynamic chip thickness is zero and leads to stable cutting cutting. When the relative phase $\varphi = 180°$, the resulting forces and vibrations grow very large and lead to high chatter vibrations.

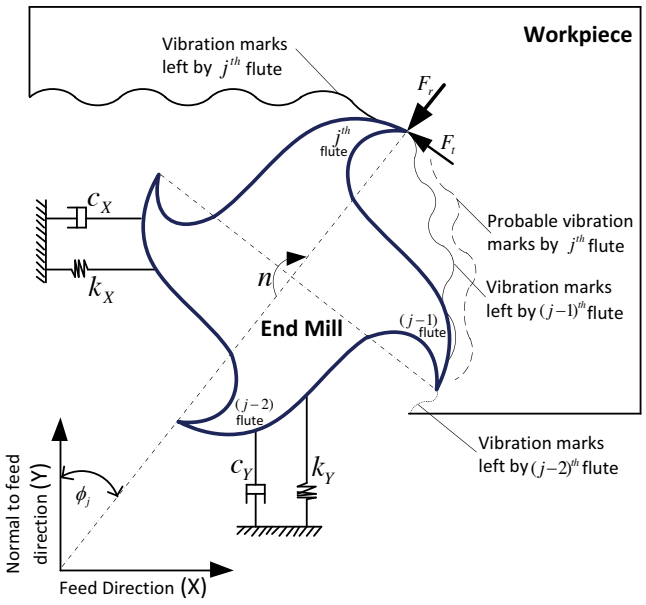

Figure 2.4: Flexible machine tool system, redrawn from (Altintas and Budak, 1995)

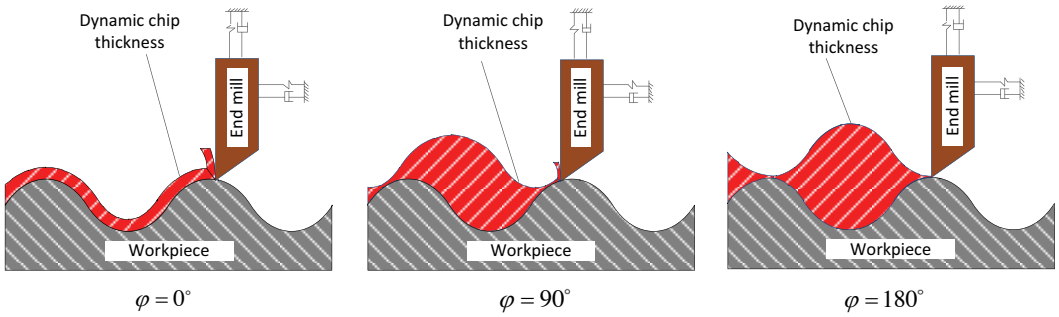

Figure 2.5: Effect of phase difference on the chip thickness

2.3 Chatter Vibrations

Various studies have been conducted for prediction, detection, avoidance, control or suppression of chatter vibrations. Four principal research lines to target chatter vibrations are presented in Figure 2.6:

(I) **Offline Strategies**: This research line focuses on avoidance of the chatter phenomenon without modifying the dynamic characteristics of the system composed of machine tool, spindle, tool holder, cutting tool and workpiece. In these strategies, stable (or chatter free) limits of milling processes are predicted from the dynamic response of the existing system by using mathematical modeling. No actual cutting is required during the implementation of offline strategies.

(II) **Online Strategies**: This research line focuses on detecting or recognizing chatter dur-

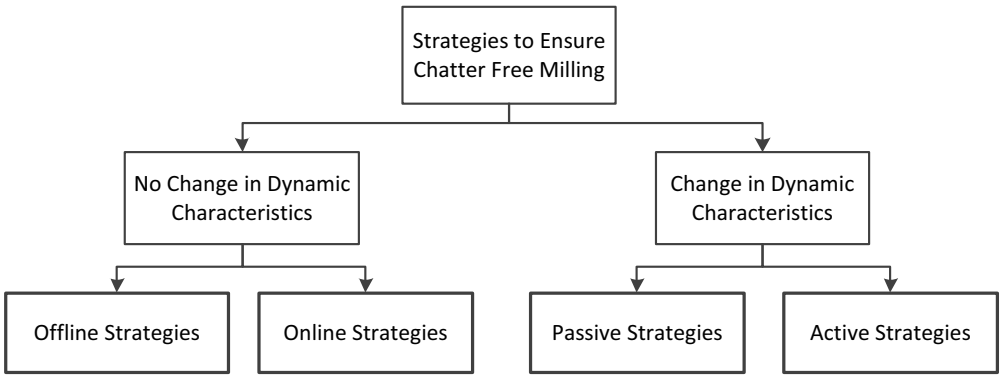

Figure 2.6: Principal research lines for chatter, redrawn from (Quintana and Ciurana, 2011)

ing actual cutting with the use of sensor technologies, process monitoring and signal processing techniques. Researchers have developed systems for chatter detection by monitoring and/or processing individual/combination of signals such as vibration, sound, cutting power, cutting forces measured with different sensors. These strategies do not modify the dynamic characteristics of the existing system.

(III) **Passive Strategies**: The main aim of this research line is to ensure stable machining by using passive strategies to damp, reduce and control the self-excited vibrations. Passive strategies are based on improving the design of the machine tool system to change its performance against chatter or in the use of additional instruments that can absorb the extra energy or disrupt the regenerative effects.

(IV) **Active Strategies**: Active strategies are focused on the use of elements, devices or actuators that actively modify the system behavior to suppress the chatter as soon as it occurs. Active systems have the ability to monitor the dynamic state of the machine tool system, diagnose certain occurrences and actively execute the decisions, if necessary, that change the system to a more adequate state. Active vibration reduction systems are generally composed of monitoring, diagnose and execution elements.

Offline and online strategies ensure the stability of milling processes without modifying the existing milling system. In subsequent sections, only offline (Section 2.4) and online (Section 2.5) strategies are presented and their use for chatter prediction is detailed.

2.4 Offline Strategies

In offline strategies, the stability limits are predicted from the dynamic response of the system and other input parameters. The border between stable and unstable cuts can be described in terms of a chart called stability lobe diagram (SLD) as shown in Figure 2.7. The area below the curve is a stable region (chatter free) and the area above is an unstable region (chatter). In HSM, the milling process is more prone to chatter due to the absence of the process damping effect.

Process damping usually occurs at low spindle speeds and provides stability due to the short undulations left on the workpiece surface by high frequency vibrations. These surface waves interfere with the cutting tool flank and dampen the resulting vibrations. Process damping allows achievement of higher axial depth of cut but with significant reduction in cutting tool working life. It is possible to select a combination of cutting conditions by taking advantage of the lobbing effect which results in the higher chatter free material removal rate as shown in Figure 2.7 (Faassen, 2007).

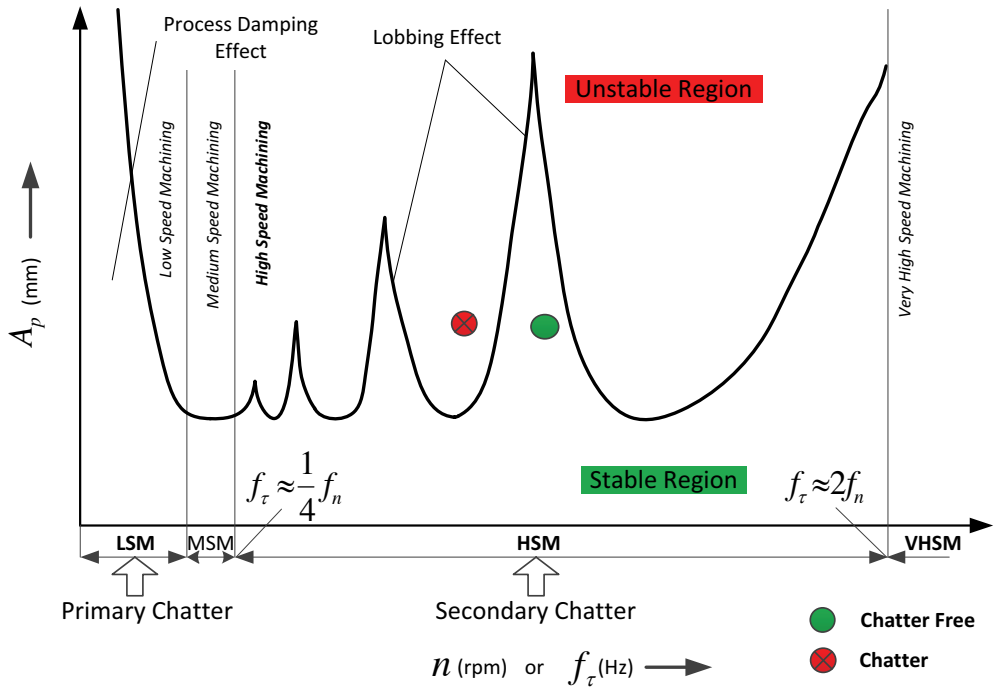

Figure 2.7: Stability lobe diagram, here f_n is the natural frequency of the dominant mode and f_τ is the tooth passing frequency

Mathematical modeling to develop stability lobe diagrams is a complex task due to the multi-degree-of-freedom (MDOF) system, multiple cutting flutes, variable cutting forces and chip load directions. (Balachandran, 2001) has investigated the dynamic stability of milling operations with cylindrical end mills. The study reviewed mechanics based models which allow for both regenerative effects and loss of contact effects for the application of partial immersion, high immersion and slotting operations. Detailed modeling and experimental investigations of the cutting process mechanics and different chatter mechanisms are provided by (Wiercigroch and Budak, 2001). They outlined the perception of non-linear dynamics to capture the major phenomena causing chatter in machining operations. (Altintas and Weck, 2004) reviewed fundamental modeling of chatter vibrations in turning, boring, drilling, milling and grinding processes. The dynamic modeling and chatter stability of milling processes is presented in their study. Various stability models and approaches are compared with experimentally validated time domain simulation results. A recent study from (Quintana and Ciurana, 2011)

reviewed various studies for prediction, detection, avoidance, control and suppression of chatter. All the above mentioned studies have concluded that work from (Altintas and Budak, 1995) is an indispensable reference for the stability limit prediction. Their study presented stability analysis using a zeroth order Fourier term to approximate the cutting force variation and achieved reasonably accurate stability lobe diagrams.

The stability lobe diagram prediction model requires dynamic characteristics of the system (in terms of FRFs), force coefficients (as presented in Section 2.1), radial depth of cut, milling mode, and diameter and number of flutes of the cutting tool.

Dynamic characteristics of the system is an important input for SLD prediction. In the subsequent paragraphs, the procedure for FRF measurement is reviewed.

FRF Measurement

Dynamic characteristics, in terms of frequency response functions (FRF), are identified at the contact point between the machine tool system and the workpiece. FRF is a transfer function expressed in the frequency domain which is composed of complex functions with real and imaginary parts. The FRF represents the response of the system to the applied force as a function of excitation frequency. The response of the system can be given in terms of displacement, velocity or acceleration. For a given machine tool system, FRF is often measured by experimental modal analysis. Experimental set up for FRF measurement is quite simple although there exist different variants in terms of specific items used. A general experimental setup for FRF measurement is presented in Figure 2.8. There are two integral parts to any FRF measurement system: (i) excitation mechanism and (ii) transduction system.

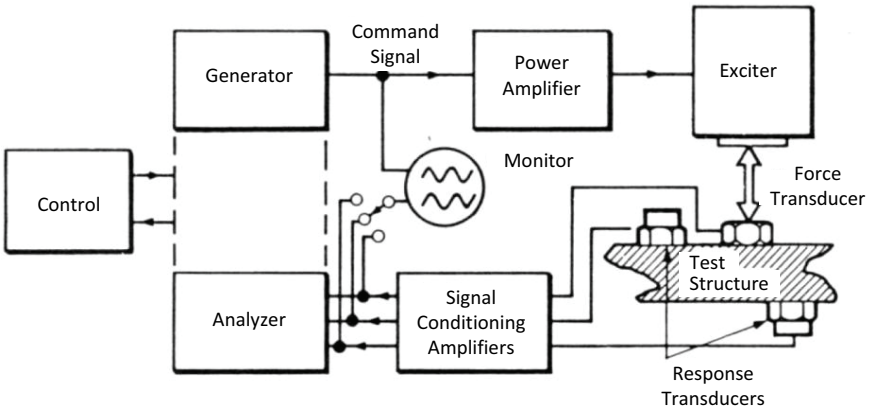

Figure 2.8: General layout of FRF measurement system (Ewins, 1999)

- ***An Excitation Mechanism***

  The excitation mechanism is composed of an excitation function and excitation system. Various excitation functions (steady state, periodic or transient)

are applied with different excitation systems (impactors, shakers or vibrators). Generally, the choice of excitation function dictates the choice of excitation system. Shakers (mechanical, electromagnetic or electro-hydraulic) are used for heavy test systems and generate a predefined force at a variable frequency. Shakers are attached type excitation system and can be even applied for rotating test systems. The main disadvantage of shakers is their costly, complex and unpractical experimental setup for industrial implementation. On the other hand, impact testing[1] has simple experimental setup and shorter measurement time which makes it the most widely used excitation system. The hammer is the most common impact testing device. The equipment consists of an impactor, usually with a set of different tips and heads which serve to extend the frequency and force level ranges depending upon the application. The impact force provided by the hammer has short duration and can be analyzed as a narrow pulse with a flat frequency spectrum. Thus it excites a wide frequency range, which contains the natural modes of the milling system.

- ***A Transduction System***
  The response (displacement, velocity or acceleration) of the test system under the action of excitation generated by the excitation system is captured by a transducer system. A piezoelectric type of transducer, attached to the test system, is an electromechanical sensor that generates an electrical output when subjected to vibration. Three types of piezoelectric transducers are mostly available for response measurement: force gauge, accelerometer and impedance head. The accelerometer is the mostly used due to its high sensitivity, wide frequency range and light weight. When the accelerometer vibrates, an internal mass in the assembly applies a force to the crystal element which is proportional to the acceleration. There is an increasing use of laser transducers which have an advantage of being non-intrusive in their operation but they are costly and complex measurement setup is a major drawback for industrial implementation.

The great insight on FRF measurement is detailed in (Ewins, 1999). For FRF measurement of machine tool system, it is concluded that hammer and accelerometer are most suitable. Impact testing can also be used for FRF measurement of workpiece systems. FRFs of the workpiece system can also be computed by finite element analysis of geometrical models of workpiece. At the part programming stage, due to the non-existence of the workpiece, numerical methods are more reasonable then their experimental counterparts.

The offline strategies can be divided in three main research lines (as shown in Figure 2.9) based on their target system: machine tool system approach, workpiece system approach and

[1] also called hammer testing or tap testing

coupled approach. These approaches are briefly explained in the following subsections.

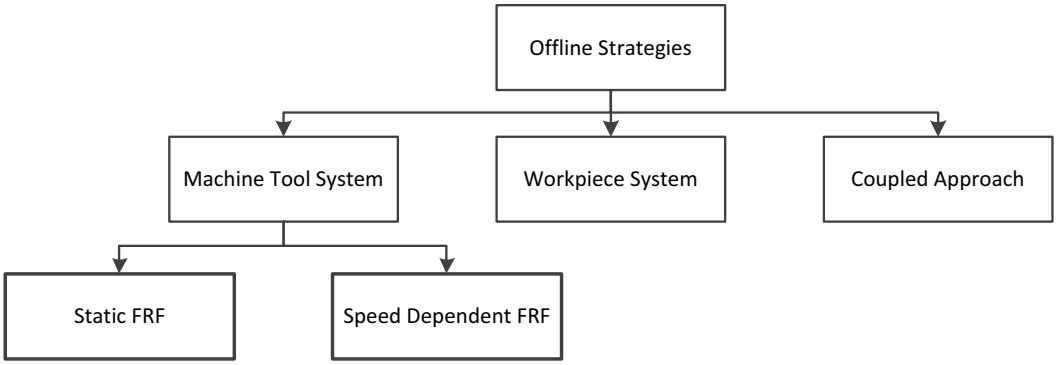

Figure 2.9: Offline strategies for chatter

2.4.1 Machine Tool System Approach

In this approach stability analysis is performed by considering only the dynamic characteristics of the machine tool system. During rough milling operations a large amount of material is removed with flat end mills with the risk of chatter vibrations. In this case, the dynamic characteristics of the machine tool system are more dominant than the workpiece dynamics (Bravo et al., 2005; Davies and Balachandran, 2000). For a given machine tool/spindle/tool holder/cutting tool system, FRFs are identified at the cutting tool tip which is the contact point between machine tool and workpiece systems. After identification of the FRF, a frequency domain analysis is done for stability lobe diagram development (Altintas and Budak, 1995). The machine tool system approach can be further decomposed in two different types: (i) speed independent FRF and (ii) speed dependent FRF.

(i) Speed Independent FRF

In this approach, FRFs are obtained at the cutting tool tip from a non-rotating spindle. Hammer testing is widely used in research as well as in industry due to its compactness, accuracy, flat frequency and practicality of use . In this experimental technique, the system is excited with an impact hammer instrumented with a piezoelectric force transducer and the resulting response is measured with an accelerometer. A recent study from (Solis et al., 2004) has combined the chatter analytical prediction model with experimental multi-degree-of-freedom modal analysis to develop stability lobe diagram. The setup is shown in Figure 2.10.

In order to avoid chatter, few software packages help production floors to generate stability lobe diagrams for a given set of inputs (CutPro, 2008; MetalMax, 2008). Their experimental kits include hammer testing instruments for FRF measurement along with software packages.

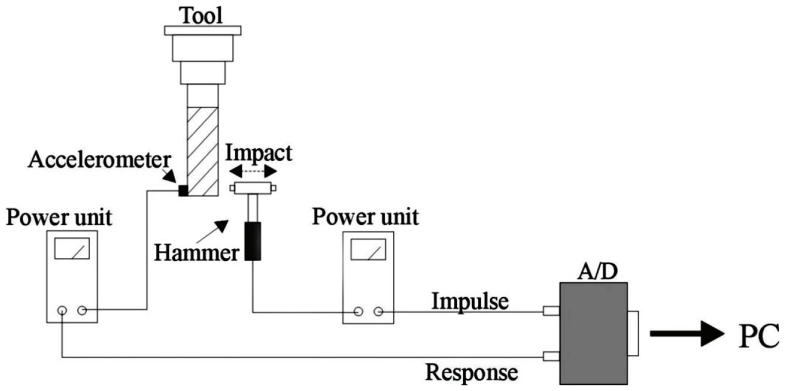

Figure 2.10: FRF measurement by hammer testing (Solis et al., 2004)

(ii) Speed Dependent FRF

Some studies have investigated the change in machine tool system dynamics at high spindle speeds by considering the effect of gyroscopic moments and centrifugal forces (Faassen et al., 2003; Schmitz et al., 2004; Gagnol et al., 2007). Response of rotating machine tool system due to the excitation force at different spindle speeds is measured by contact free laser transducer. Experimental setup (with laser sensor) for measurement of speed dependent FRF is presented in Figure 2.11. A study from Schmitz (Schmitz et al., 2004) compared the stability lobe diagrams developed from speed dependent FRF and speed independent FRF as presented in Figure 2.12. The study has revealed that even deeper axial depths of cut can be achieved due to the increased dynamic stiffness at higher spindle speeds.

The speed dependent FRF measurement setup is complex and costly for industrial implementation and moreover, the location of excitation force and response measurement point is not properly defined. A recent study from (Gagnol et al., 2007) developed numerical models to predict spindle/tool holder/cutting tool dynamics at high spindle speeds from detailed knowledge about the geometry and construction of the spindle, which in general is not available to part programmers in a manufacturing environment.

2.4.2 Receptance Coupling

FRF of the machine tool system is one of the important inputs required for the development of stability lobe diagrams with frequency domain analysis. These FRFs are measured at the cutting tool tip with hammer impacts and measurement of the response with an accelerometer (as presented in Section 2.4.1). Each variant of machine tool/spindle/tool holder/cutting tool combination results in different dynamic characteristics. In order to avoid the tedious testing procedure for every new variant, studies from (Schmitz, 2000; Schmitz et al., 2001; Schmitz and Burns, 2003) has introduced receptance coupling substructure analysis (RCSA). In RCSA, the machine tool system is divided in different subsystems. The dynamic characteristics of each subsystem are identified separately and then combined to obtain the machine tool/spindle/-

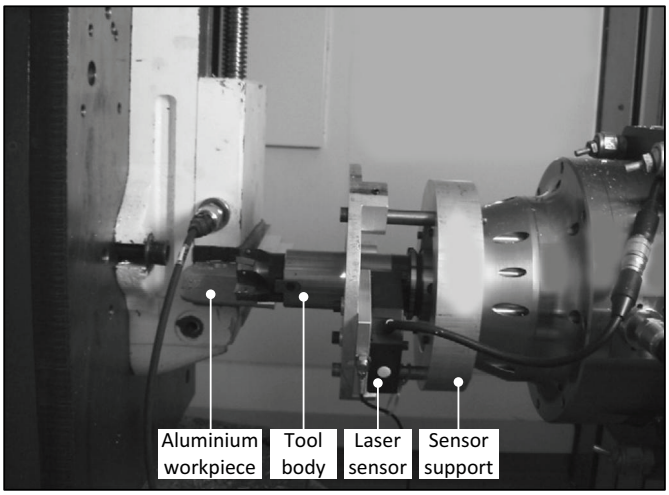

Figure 2.11: Experimental setup for measurement of speed dependent FRF (Gagnol et al., 2007)

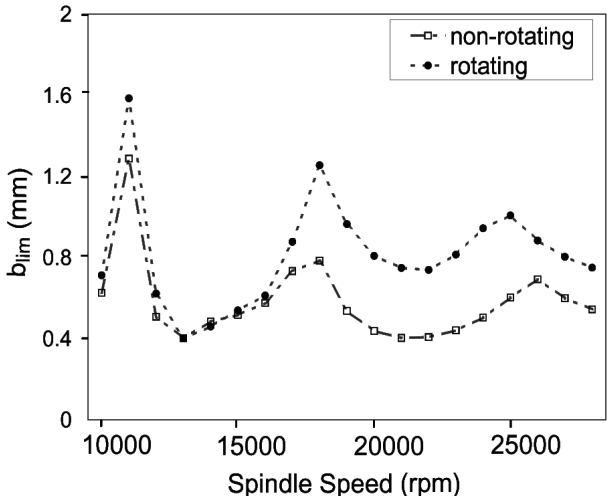

Figure 2.12: SLD with speed dependent FRF (Schmitz et al., 2004), here b_{lim} is the limiting value of axial depth of cut

tool holder/cutting tool system FRF at the cutting tool tip. The accuracy of the RCSA depends on the FRF of each subsystem and the joint dynamics of the subsystems at the joint location.

The machine tool/spindle/tool holder/cutting tool system can be divided into three subsystems: machine tool/spindle, tool holder and cutting tool (Cheng, 2007; Schmitz and Duncan, 2005; Zhang et al., 2011). In this technique, the experimental FRF of machine tool/spindle are coupled with the numerically predicted FRFs of tool holder and cutting tool. Dynamic modeling of the tool holder is a difficult task due to its complex geometry and contact surfaces. Accuracy of the modeling results depends upon case to case analysis and its industrial implementation is quite difficult where there exist different types of tool holder. Moreover,

detailed knowledge of the design parameters of the tool holder are not available to the part programmer.

Some studies have decomposed the machine tool system into two subsystems which are as follows:

- Subsystem A: End mill (cutting tool)
- Subsystem B: Machine tool/spindle/tool holder

These two subsystems are connected with connection parameters (springs and dampers) to predict the system's FRF. A study from (Park et al., 2003) has demonstrated that the machine tool system can be modeled accurately by using translational and rotational springs and dampers as shown in Figure 2.13. The study has compared the results with a previous study by (Schmitz, 2000) which considered only translational degrees of freedom.

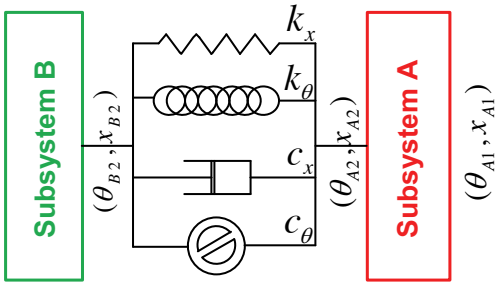

Figure 2.13: System with translational and rotational springs, and dampers

Experimental or analytical FRFs of the individual subsystems are used to predict the system's dynamic response at any spatial coordinates selected for subsystem measurements. Identified FRFs of individual subsystems can be combined with the study from (Park et al., 2003) in order to predict the FRFs at the cutting tip for every new end mill.

2.4.3 Workpiece System Approach

In this offline approach, stability limits are analyzed from the dynamic characteristics of flexible workpiece while considering the machine tool system as rigid. This approach is applied for the peripheral milling of thin-walled workpieces (Bravo et al., 2005; Adetoro et al., 2010). FRFs of the flexible workpiece system are determined with experimental techniques or numerical models. At the part programming stage, due to the non-existence of the final workpiece, finite element approaches are more relevant. A review study of finite element analysis and simulations of machining is presented by (Mackerle, 1998; Mackerle, 2003). The dynamic characteristics of the workpiece system are different at different cutting points of cutting tool and workpiece. Moreover, they change significantly due to material removal

during milling of the workpiece. The effect of workpiece dynamics on the stability limits has been investigated by various authors (Thevenot et al., 2006b; Thevenot et al., 2006a; Davies and Balachandran, 2000). They developed the three dimensional stability lobe diagram as presented in Figure 2.14.

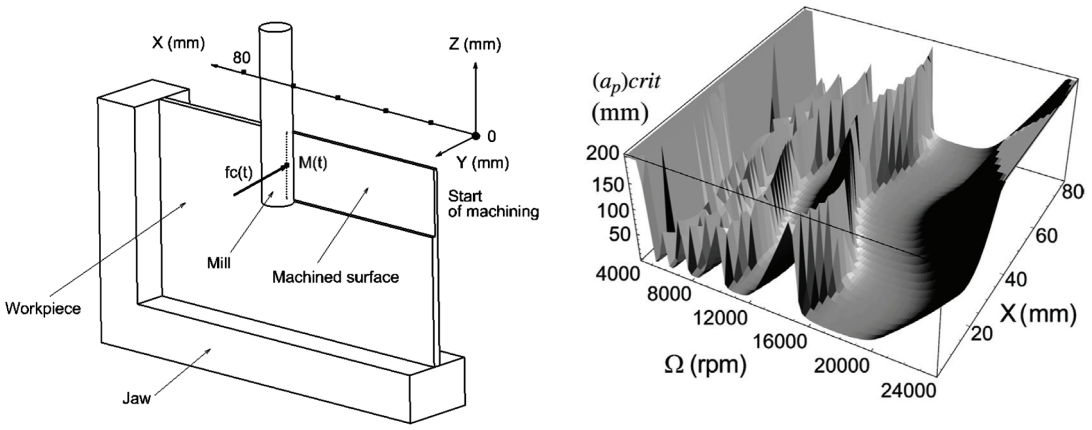

(a) Flexible workpiece

(b) 3D stability lobe diagram

Figure 2.14: Stability analysis of flexible workpiece dynamic (Thevenot et al., 2006b)

2.4.4 Coupled Approach

A few recent studies have been performed to conduct stability analysis by coupling the dynamic behavior of machine tool and workpiece systems (Bravo et al., 2005; Le Lan et al., 2007; Mane et al., 2008). A methodology is developed to predict coupled FRF by presenting the relationship of cutting tool/thin-wall interaction, in up and down milling, as shown in Figure 2.15. In the coupled system, the relative displacement between cutting tool and workpiece is due to the sum of their individual displacements. A 3D stability lobe diagram has been developed based on the relative movement of both systems. It is concluded that the proposed 3D SLD is different and more exact than the one generated from the mere superposition of individual SLDs of machine tool and workpiece systems (Bravo et al., 2005). (Mane et al., 2008) implemented the same methodology to predict 3D SLD by coupling the FRFs of the workpiece with speed dependent FRFs of the machine tool system.

2.5 Online Strategies

During part programming stage, chatter free cutting conditions can be selected from stability lobe diagrams developed by mathematical modeling. However, this approach requires complete knowledge of the dynamic characteristics of the machine tool system and the physical phenomenon occurring at the cutting zone, which is difficult for industrial users to realize in practice. Moreover, complex and varying dynamics of the MDOF system makes accurate

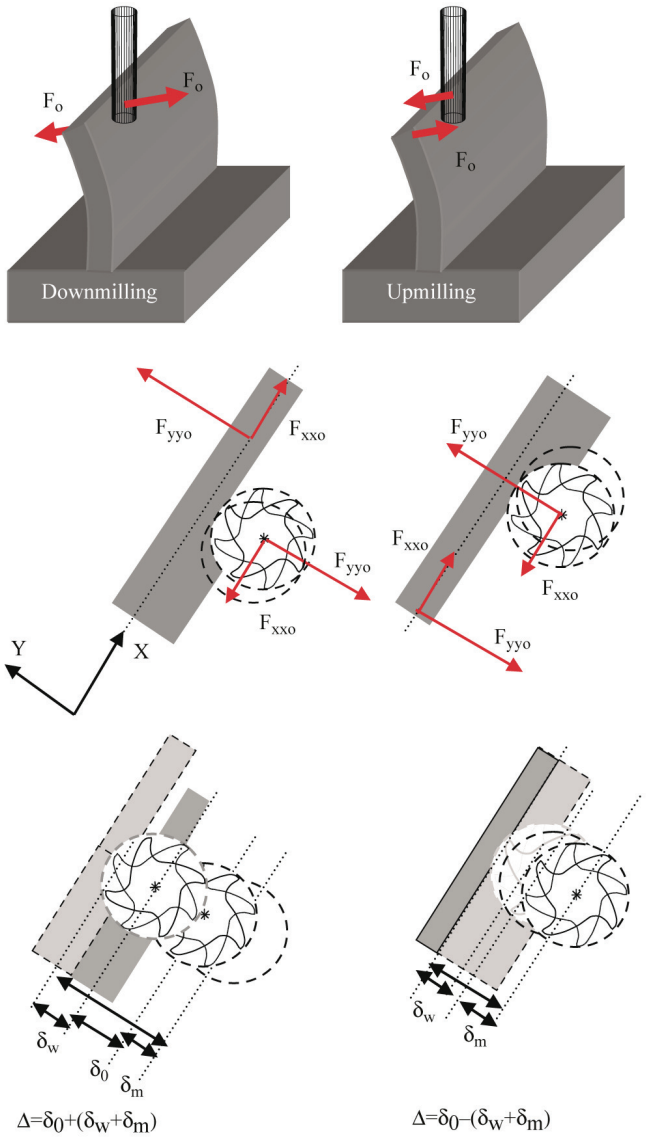

Figure 2.15: Dynamic coupling of machine tool system and workpiece (Bravo et al., 2005)

prediction of SLDs a difficult task. In online strategies, chatter is detected during the actual milling process. Chatter vibrations may typically range in frequencies from 100Hz, due to vibrations from machine table or machine structure, to as high as 5000Hz, for cutting tool or flexible thin-walled workpiece (Delio et al., 1992). Researchers have developed methods consisting of online chatter detection, by monitoring a certain signal which is measured by a corresponding sensor. Chatter can also be identified by a machine operator by simply listening to cutting noise and observing the surface quality. In this section, a brief literature review is presented for different sensors and their application for chatter detection.

2.5.1 Different Sensors and Scope for Chatter Detection

Various studies have been performed for the chatter detection with different sensors and signal processing techniques. (Tlusty and Andrews, 1983) presented a review study of various sensors and their capabilities for unmanned machining. They classified cutting forces and spindle motor sensors as the primary sensors necessary for chatter detection and control. (Byrne et al., 1995) reviewed the state-of-the-art studies for cutting tool monitoring, chatter detection and prevention in the milling process. (Altintas and Chan, 1992) have implemented various sensors (dynamometer for cutting forces, proximity sensor for displacements and microphone for sound signals) for detection and suppression of chatter in milling. (Tarng and Chen, 1994) developed a real-time sensor chatter detection system that analyzes the cutting forces in end milling operations. (Soliman and Ismail, 1996) presented a detailed comparison of the cutting force signal measured with dynamometer, vibration signal measured by accelerometer, sound signal using a microphone and current signal of spindle drive for chatter detection in the milling process. (Soliman and Ismail, 1997) developed a system to detect chatter with spindle drive current signal of vertical milling machine. (Kuljanic et al., 2008) presented a multisensory approach for online chatter detection in face milling operations. Comparison of various sensors (rotating dynamometer, accelerometer, acoustic emission and electric power sensors) is demonstrated along with various signal processing techniques for chatter detection. They concluded that axial cutting force, cutting torque and accelerations signals can be applied successfully for chatter detection in face milling operations at lower spindle speed. (Kuljanic et al., 2009) developed an intelligent chatter detection system consisting of accelerometer and axial force sensors and with implementation of advanced signal processing techniques. (Faassen, 2007; Dijk et al., 2010) presented an in-process chatter detection technique which detects chatter in the premature stage from the acceleration signal in the time domain. The use of laser Doppler vibrometery (LDV) for chatter detection is used by (Tatar and Gren, 2008). The main advantage of LDV is the possibility of performing non-contact measurement on a rotating cutting tool. LDV can be used to detect chatter vibrations at high frequencies.

Studies have concluded that the narrow bandwidth of the current sensors imposes a serious restriction on their implementation for chatter detection in the milling process which usually develops at high frequencies (Soliman and Ismail, 1996). An electric power sensor is not useful for chatter recognition as the frequency spectrum of power signal is poor and is limited to very low frequencies (less than 100Hz). The electric power sensor may only be applied for very low spindle speeds (Kuljanic et al., 2008). Chatter identification with acoustic emission (AE) signal is less reliable as its signal characteristics do not change during unstable milling. The force dynamometer has maximum frequency range of 1kHz under ideal conditions. The force dynamometer has its own natural mode (below 1000Hz) which makes chatter detection difficult (Riviére et al., 2006; Delio et al., 1992). Moreover, the costly and unpractical experimental setup also limits its industrial implementation. Though signals from transducers (accelerometers, displacement, and velocity transducers) provide wider frequency spectra (about 5 kHz) their use is also restricted. Accurate detection of chatter with an accelerometer lies in the proper selection of its mounting location which requires prior knowledge of dynamic behavior over

the expected range of machine operation. Different attachments and cutting tools, varying geometry of workpiece produce numerous chatter mode shapes and frequencies, this makes the placement of accelerometer or other transducers a difficult task (Delio et al., 1992). Non-contact displacement sensors, like LDV is not practical at all for industrial implementation due to their special and costly experimental setup (Tatar and Gren, 2008).

Microphone as Chatter Detection Sensor

(Smith, 1987) studied that the acoustic pressure emitted during machining process is proportional to the displacement of cutting tool. The cutting sound during interaction of machine tool system and workpiece system can be used for chatter detection. (Dijk et al., 2010) presented a detailed comparison of microphone and accelerometer for chatter detection in high speed machining. With the help of dedicated experiments, the microphone has been shown to be the best sensor to detect chatter in high speed milling applications. Various studies have been performed to compare the available sensors for chatter detection and it is concluded that microphone is an excellent sensor as compared to other available sensors (Delio et al., 1992; Soliman and Ismail, 1996; Hendriks, 2005; Riviére et al., 2006; Quintana and Ciurana, 2011; Zhang and Li, 2012). Many case studies related to chatter prediction models are verified experimentally with successful use of microphone (Schmitz et al., 2002; Schmitz and Burns, 2003; Weingaertner et al., 2006; Quintana et al., 2009; Quintana et al., 2008; Tsai et al., 2009; Tsai et al., 2010).

Various advantages of a microphone for chatter detection during milling processes are as follows:

- Microphone provides high and flat frequency bandwidth (up to 10000Hz) which is far greater than other sensors. Microphone can be used for the complete working range of spindle speeds.

- Microphone detects chatter vibrations originating from any natural mode of machine tool system and workpiece system. No prior knowledge of the dynamics of the milling system is required for chatter detection system.

- Microphone can be located remotely without any serious effects to sensor performance.

- Microphone can even detect chatter vibrations during low-immersion milling.

- Microphone is cheap, reliable and practical for use in industrial applications.

2.5.2 Chatter Recognition Techniques

Sensor signal can be expressed as the sum of periodic and aperiodic components (Kuljanic et al., 2008):

$$S(t) = S_p(t) + S_a(t) \tag{2.8}$$

where $S_p(t)$ is the τ-periodic component and $S_a(t)$ is the aperiodic component. τ is the spindle revolution period. The periodic component of the signal contains the harmonics of the spindle frequency (SF), while all the other components are treated in the aperiodic term. During stable milling processes, only periodic component are present in the signal whereas during unstable milling, there is a significant presence of aperiodic components in the measured signal along with periodic components.

There are some studies in the literature which demonstrate the signal processing technique which can help to recognize chatter.

- In the threshold level technique the chatter phenomenon is detected by comparing the magnitude of a sensor signal in the time domain. If the magnitude of the measured sensor signal exceeds the predefined threshold value, chatter case is considered.
- In the statistical detection technique, the variance of a signal measured at one sample per revolution is compared against a predefined threshold value of variance. If the measured variance exceeds the predefined value, the chatter case is detected.
- In frequency domain analysis, the time domain signal is converted into a frequency domain with a discrete Fourier transform. During stable cutting, the frequency spectrum is composed of only spindle frequency, tooth passing frequency and their harmonics but in the case of unstable milling there is the presence of chatter peaks.

More detailed literature on various sensors for chatter detection and their scope, different techniques for chatter recognition and chatter control is presented in Appendix F.2.

2.5.3 Online Strategies for SLD Generation

Online strategies are also used to develop the stability lobe diagram (SLD) for a given machine tool/spindle/tool holder/cutting tool and workpiece material system. In this approach, cutting tests are performed at different combinations of spindle speed and axial depth of cut. During each cutting test, chatter is detected with a chatter detection system or simply by observation. From the marking of results of each cutting test on a chart with spindle speed vs axial depth of cut, stable and unstable regions are defined. This approach requires a large number of cutting tests. For example (Quintana et al., 2009) executed 600 experiments (mesh of 20 axial depth of cut per 30 spindle speeds) for generation of stability lobe diagram. In order to reduce the number of cutting tests, (Quintana et al., 2008) proposed an experimental method to generate

the SLD directly on a workpiece which permits a gradual increase of the axial depth of cut along the feed direction. The proposed methodology and workpiece is presented in Figure 2.16 and the corresponding SLD on the workpiece is shown in Figure 2.17.

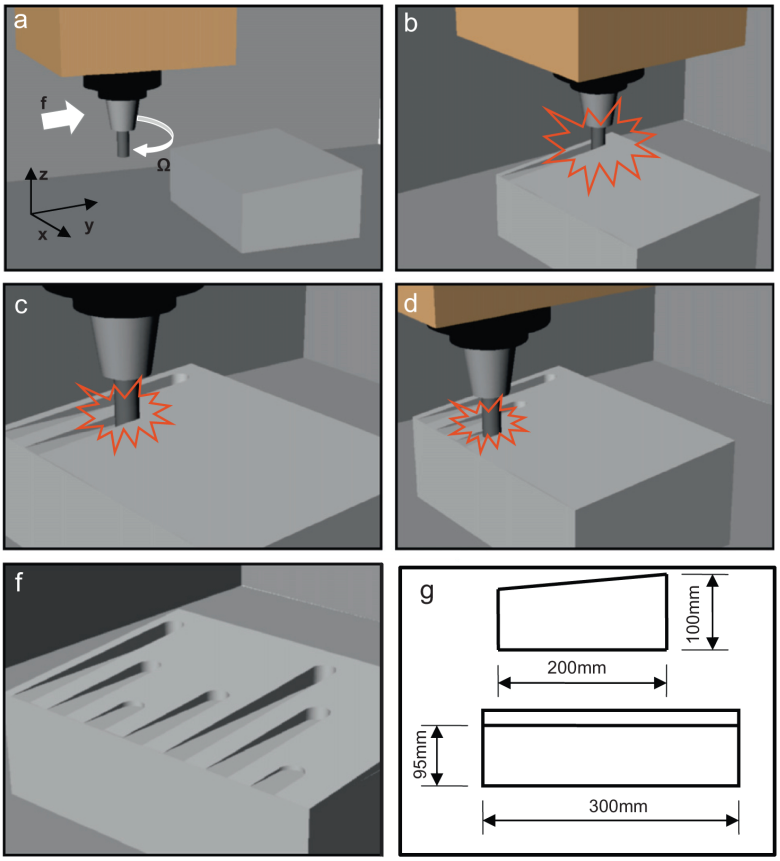

Figure 2.16: Concept of experimental generation of SLD. (a,b) Axial depth of cut increases in feed direction until chatter occurs. (c,d) Increase in spindle speed for different cutting passes. (f) SLD is physically marked on the workpiece. (g) Workpiece dimensions (Quintana et al., 2008)

Experimental generation of SLD is applicable for very small production floors which have no technical knowledge and sophisticated resources. Every new variant of machine tool/spindle/-tool holder/cutting tool and workpiece material combination require generation of a new SLD. Experimental Identification of SLD for each variant is not a feasible solution.

2.6 Optimization of Milling Process

For a given machine tool/spindle/tool holder/cutting tool/workpiece material system and required shape of the workpiece, both the cutting conditions and the toolpath affect significantly the overall productivity of the milling process. On modern production floors, the cutting

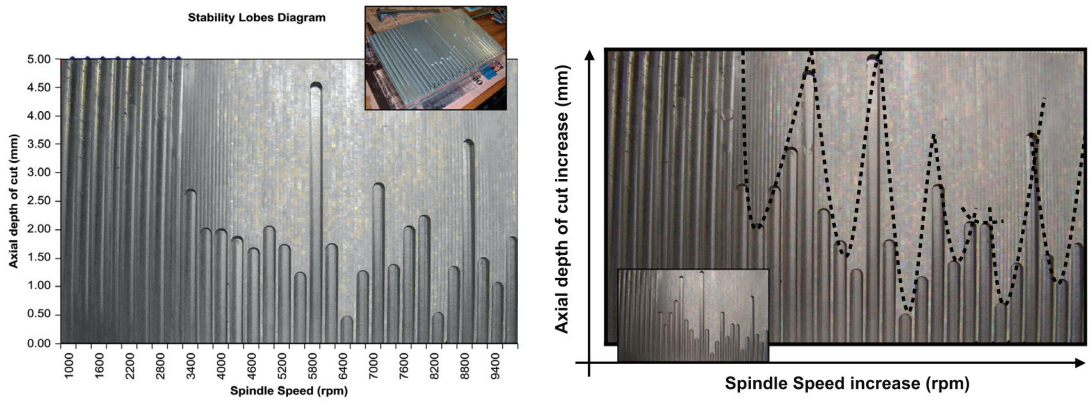

(a) Results of cutting passes

(b) SLD marked on the workpiece surface

Figure 2.17: Experimentally developed SLD on the workpiece (Quintana et al., 2008)

conditions are selected by a part programmer and are chosen based on his/her experience, guidelines provided in cutting tool and machine tool catalogues, or an existing database of cutting conditions. Cutting toolpaths and corresponding NC codes are generated with the aid of CAD/CAM software. The right selection of cutting conditions and toolpaths is not always guaranteed due to the dynamic behavior of flexible machine tool systems, rigid body kinematics of machine tool systems at higher speeds, complex physical interactions between the cutting tool and workpiece, high variation of radial depth of cut along the toolpath. Wrong selection of cutting conditions leads to chatter vibrations, high cutting forces, high fluctuation of cutting forces along the toolpath, cutting tool wear, poor surface finish, violation of available cutting power and torque and even reduction in spindle working life. Moreover, current part programs to machine prismatic parts are generated with a long overall preparation time and with rather “slow” machining time performance in terms of fully exploiting the capabilities of modern high speed machine tools. Various developed models/procedures by different researchers can be useful to avoid the individual problems mentioned above. Selection of cutting conditions and toolpaths in this way does not ensure the optimal solution for a given machine tool/spindle/tool holder/cutting tool/workpiece material system and required shape of the workpiece.

The overall productivity of the milling system can be improved by the right and optimal selection of either cutting conditions or toolpaths. In the following subsections literature is reviewed about the aspects mentioned for optimization.

2.6.1 Selection of Cutting Conditions

In milling operations, cutting conditions have a non-linear relationship affecting the physical limits of machine tool, cutting tool and workpiece system. Broad working ranges of cutting conditions due to the high capabilities of modern machine tools and cutting tools make the search space of the optimization problem huge. Different techniques have been developed to

find optimal solutions in milling processes. Minimization of machine time or maximization of material removal rate are the most targeted problems which are solved with help of various optimization techniques. Some optimization methods produce accurate optimal solutions by rigorous computations but they are not computationally economical. Other methods develop solutions closer to the optimum value with better computational efficiency. Therefore, a compromise between the high accuracy of a rigorous solution and lower accuracy of a computationally efficient method has to be made.

With the use of genetic algorithms (GA), the impact and power of artificial intelligence techniques have been reflected on the overall performance of optimization system. A genetic algorithm (GA) is a computerized search and optimization algorithm based on the mechanics of natural genetics and selection. A GA is a computationally fast algorithm to find the near or exact global optimal solution within the entire search space. A GA operates on the optimization problem with a defined objective function without solving any mathematical equation but only by working on many possible solutions within the entire search space that are not just optimal. Reproducing new and better solutions from previous ones with the help of various GA operators, the GA is capable of finding solutions that are near to the global optimal solutions. It is possible to get multiple solutions close to the optimal solution with a single simulation. To get multiple solutions, traditional methods need to be applied a number of times each starting from different initial conditions and hoping to achieve a different solution each time.

A number of research studies have been conducted to determine the optimal cutting conditions for the milling process. (Rai et al., 2009) used the genetic algorithm approach to maximize the material removal rate for multi-tool milling operations. (Dereli et al., 2001) optimized cutting conditions for milling operations by minimizing the unit cost of the final part. (Tandon et al., 2002) developed an evolutionary computation based method to minimize the machining time by optimizing spindle speed and feed rate. (Shunmugam et al., 2000) presented a method for optimal cutting condition selection in multi-pass face milling. (Wang et al., 2004) demonstrated a method to optimize the production time for multi-pass milling.

None of the above mentioned studies considered the most important technological constraint, stability during high speed milling, in their developed optimization models. Moreover, these studies are also lacking in the number of optimization variables[2] considered while respecting few or even less important constraints of the machine tool, cutting tool and workpiece system.

(Tekeli and Budak, 2005) presented a procedure for selection of chatter free axial and radial depths of cut to reduce the number of cutting passes for pocket milling as shown in Figure 2.18a. Axial and radial depths of cut are chosen from the stability chart (axial depth of cut vs radial depth of cut) developed for a fixed spindle speed as shown in Figure 2.18b. The

[2] cutting conditions in the optimization model are called design variables/decision variables/optimization variables

number of passes (nop) required to mill the pocket is given by:

$$nop = ceil\left(\frac{d_p}{A_p}\right) ceil\left(\frac{l_p}{A_e}\right) \tag{2.9}$$

here, l_p and d_p are the length and depth of pocket respectively. A_p and A_e are the stable axial and radial depths of cut. $ceil$ is the round-up function.

To minimize the machining time spindle speed and feed rate must also be optimized along with the number of cutting passes. It is obvious that real optimization cannot be achieved without considering all cutting conditions: spindle speed, axial depth of cut, radial depth of cut and feed rate, and important constraints simultaneously (Palanisamy et al., 2007).

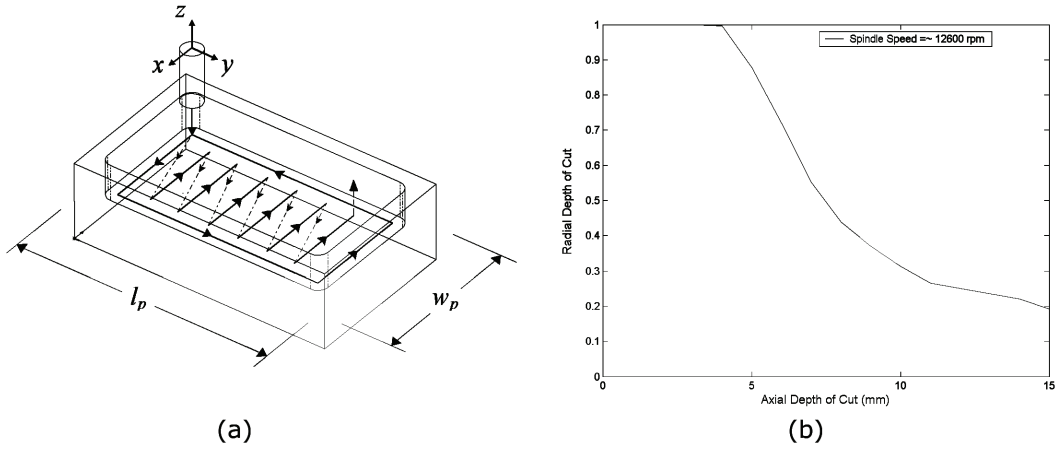

Figure 2.18: Minimization of number of cutting passes (a) Pocket geometry (b) Stability lobe diagram at fixed spindle speed, radial depth of cut axis values is divide by diameter of cutting tool (Tekeli and Budak, 2005)

2.6.2 Selection of Toolpath

More than 80% of all mechanical parts to be machined can be manufactured by pocket milling. A pocket is generated by sweeping a cylindrical end mill inside the desired boundary. The rotating end mill removes the material in the feed direction along a predefined path containing a set of lines, arcs and splines, which is termed “toolpath” (Held, 1991a; Lambregts et al., 1996). Current CAD/CAM software provide two different types of toolpath trajectory for pocket milling: (i) direction parallel toolpath and (ii) contour parallel toolpath (Kim and Choi, 2002).

(i) One-way and zig-zag toolpaths are the most common form of direction parallel toolpaths. One-way toolpaths, as shown in Figure 2.19a, are unidirectional toolpaths which maintain consistent milling mode (up or down milling) and constant radial depth of cut along the toolpath. However, a considerable amount of time is wasted on unproductive

connecting paths between the start of a new path and end of the previous path. On the other hand, zig-zag toolpaths, as shown in Figure 2.19b, are bidirectional toolpaths which provide continuous cutting. The mode of milling changes after every linear cut in the case of zig-zag toolpaths.

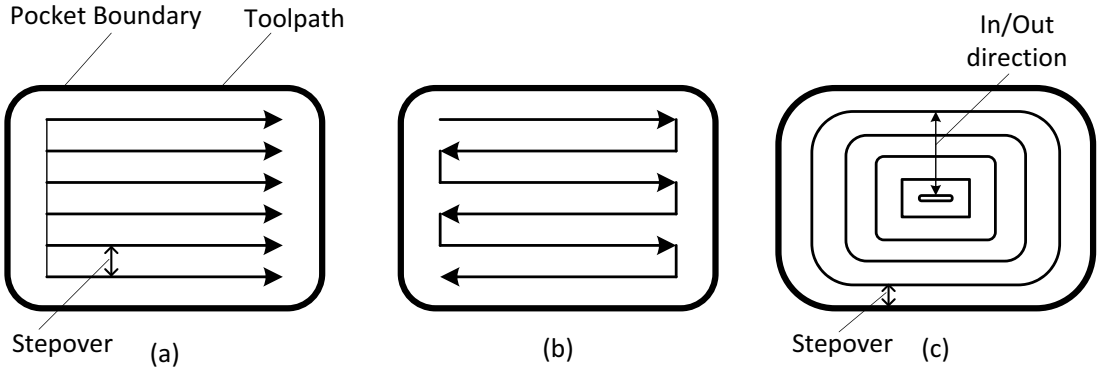

Figure 2.19: Toolpath routines for pocket milling (a) One-way toolpath (b) Zig-zag toolpath (c) Contour parallel toolpath

(ii) Contour parallel toolpaths, as shown in Figure 2.19c, are based on the offsetting of the boundary by a stepover value which is the same as the spacing in direction parallel toolpaths. Contour parallel toolpaths have the advantage of maintaining the same milling mode along the toolpath. Moreover, idle machining time is reduced significantly.

Overall productivity of the milling process is directly proportional to the machining time. The theoretical machining time is obtained by summation of divisions of length of each path segment by its corresponding feed rate. This theoretical time calculation ignores the effect of kinematics (acceleration and deceleration) of CNC machines during actual machining. Due to the kinematic limitations of machine tools, the machine has to slow down at sharp corners or high curvature portions of the toolpath (Dhanik, 2009). In toolpath consisting of many small path segments, the machining time is drastically increased because of the frequent acceleration/deceleration of the cutting tool along toolpath. (Kim and Choi, 2002) presented one of the very first models of milling time based on the kinematic capability (acceleration and deceleration) of the machine tool. They concluded that the effect of acceleration and deceleration on the total machining time is even more significant at higher spindle speeds and feed rates.

In contour parallel toolpath, idle time spent in lifting, positioning and plunging is reduced as the cutting tool is always in contact with workpiece. Moreover, the effect of kinematics of the machine tool has lesser effect as compared to directional parallel toolpaths. However, it is difficult to maintain the same radial depth of cut along the toolpath. In the corner sections, the engagement angle (or radial depth of cut) increases significantly compared to the straight sections as presented in Figure 2.20. This change in radial depth cut results in significant

fluctuation in cutting forces and may also lead to chatter vibrations (Ko and Shaw, 2009; Kramer, 1992).

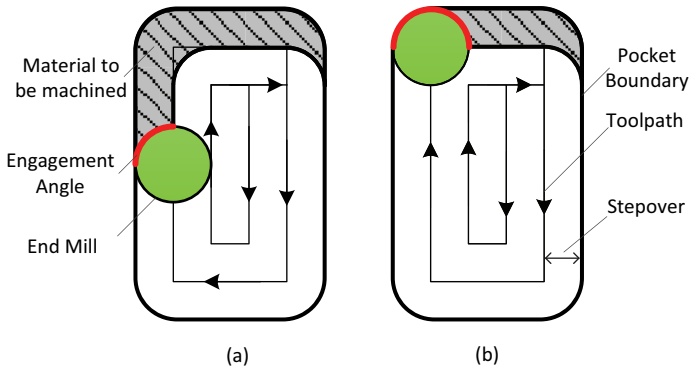

Figure 2.20: Different engagement conditions (a) Straight section (b) Corner section

The above mentioned problems are reduced significantly by selection of a toolpath that minimizes radial depth of cut variations as well as curvature change variations while avoiding leftover material at the corners (Dhanik, 2009).

2.7 Tangential Force Coefficients Identification

Identification of force coefficients is necessary for accurate prediction of cutting forces and chatter free regions. Force coefficients must be experimentally determined for a given combination of cutting tool geometry and workpiece material as presented in Section 2.1.2. In the standard procedure, the cutting force coefficients are identified from average values of cutting force components measured experimentally by a cutting force dynamometer with slot cutting experiments at different feed rates (Wang et al., 2012; Budak and Altintas, 1994). This experimental set up is impractical in modern shop floors due to its high cost and complex hardware setup. Therefore, there is a constant need in industry for simple and efficient procedures for identification of force coefficients. Tangential cutting force coefficients affect significantly the magnitude of cutting forces and limiting values of stable depths of cut. The higher the tangential cutting force coefficient, the higher are the cutting forces and the lower are the allowable values of stable depths of cut (Altintas, 2000).

(Dunwoody, 2010) has proposed a procedure for indirect identification of tangential force coefficients (K_{tc} and K_{te}) from cutting torque. Instead of being measured directly, the cutting torque is obtained from the difference between spindle power consumption in material cutting and air cutting. The spindle motor current, measured by a built-in load meter, is proportional to the total power spent by the spindle, which is expressed as:

$$I = K_{lm} P_{ACeff} \tag{2.10}$$

here: I is the spindle current proportional to the total spindle power (useful power spent in cutting plus losses measured by a built-in load meter and obtained from the controller), K_{lm} is the load meter constant and P_{ACeff} is the effective power from the electrical network.

The total power spent by the spindle is calculated as the product of spindle angular speed (ω_m) and the sum of the torques that spindle has to overcome during machining:

$$I = K_{lm}\omega_m(T_{cut} + b\omega_m + T_{cf}) \tag{2.11}$$

here: T_{cut} is the cutting torque, $b\omega_m$ is the torque needed to overcome viscous friction and T_{cf} is the torque needed to overcome Coulomb friction.

For air cutting ($T_{cut} = 0$), the measured spindle motor current accounts only for power losses which is expressed as:

$$I_f = K_{lm} b\omega_M^2 + K_{lm} T_{cf} \omega_M \tag{2.12}$$

here: I_f is the spindle current proportional to the power losses in spindle. By estimating the parameters (K_{lm}, b and T_{cf}) in Equation 2.11, the cutting torque (T_{cut}) can be identified.

Slot cutting tests at different feed rates are performed and the cutting torque is identified from spindle current measured from machine controller. The average cutting torque is related to the tangential force coefficients which is given by:

$$\overline{T}_c = \frac{RNA_pK_{tc}}{\pi} f_t + \frac{RNA_pK_{te}}{2} \tag{2.13}$$

here, R is the radius of the cutting tool, A_p is the axial depth of cut during slot cutting experiments, N is the number of flutes of the cutting tool, f_t is the feed rate. Tangential cutting and edge components $\left(\frac{RNA_pK_{tc}}{\pi}, \frac{RNA_pK_{te}}{2}\right)$ are estimated by linear regression of the cutting torque values.

The spindle power model developed by Dunwoody is simple and efficient, but does not take into account the dependency of Coulomb friction losses on spindle speed, which is especially important in the case of high speed machining (Cao and Altintas, 2004). Furthermore, this model does not include the electric losses in the spindle motor. A more detailed model for total spindle power estimation is required which includes all mechanical and electrical sources of power loss in the spindle drive.

2.8 Summary of the State-of-the-Art

The overall productivity of the milling process depends on the performance of part programs which is directly related to the selection of cutting conditions and toolpath. Their wrong

selection often causes chatter vibrations, high fluctuation of cutting forces, and/or violation of available limits of power and torque of a machine tool. The problems can be avoided by the selection of cutting conditions based on mathematical models and enhanced methodologies developed by various researchers. Milling software (CutPro, 2008; MetalMax, 2008) developed by research groups suggest cutting conditions to avoid the above mentioned problems but does not ensure their optimal selection for a given machine tool and workpiece system.

Different research studies which have been performed for the optimal selection of cutting conditions have the following shortcomings:

- Most of the studies (Shunmugam et al., 2000; Dereli et al., 2001; Tandon et al., 2002; Rai et al., 2009) do not consider the most important constraint, the stability of the milling process, in their developed optimization systems.
- Studies which, though they consider stability, are limited in the number of optimized cutting conditions, other practical constraints of machine tool and workpiece system, and toolpath geometry. (Tekeli and Budak, 2005; Palanisamy et al., 2007).
- The study from (Heo et al., 2010) presented an optimization system for the optimal selection of cutting conditions for pocket milling but the study is limited to contour parallel toolpaths and, moreover, does not take into account change in the engagement angle along the toolpath.
- The studies do not consider the optimal selection of cutting conditions for CATIA generated or user defined toolpath along different machine tool axes for multi-feature prismatic parts.
- The toolpath generated by current CAM systems (CATIA V5, 2010) are purely geometric in nature. They result in change in engagement angle along the toolpath. Moreover they do not consider the effect of kinematics of high speed milling tools during toolpath generation.
- For overall improvement in productivity part programs must be optimized by simultaneous consideration of cutting conditions and toolpath geometry for high speed milling. There is no such study available which consider the optimal selection of cutting conditions and corresponding smooth and constant engagement toolpath for pocket milling.

Force coefficients are important inputs for the prediction of cutting forces and stable limits. For the present objectives, a mechanistic model can be used for the identification of force coefficients. (Dunwoody, 2010) developed an approach for the indirect identification of these force coefficients from spindle motor current. The spindle power model developed by Dunwoody is simple and efficient but does not take into account the dependency of Coulomb friction losses on spindle speed, which is especially important in the case of high speed machining.

It is concluded that chatter during milling can be avoided by selecting cutting conditions based on the stability lobe diagrams. The stability lobe diagrams are generated accurately with offline strategies. The frequency response functions (FRF) are an important input for the generation of stability lobe diagrams. The FRFs of the machine tool system are measured accurately with hammer testing experiments at the cutting tool tip. Researchers (Schmitz et al., 2001; Park et al., 2003) have developed the receptance coupling technique for prediction of these FRFs for different end mills.

Online strategies are used for chatter detection and control during actual cutting. The following remarks are made from the reviewed literature:

- A microphone is an excellent sensor as compared to other available sensors due to its high frequency range and practicality (Delio et al., 1992; Riviére et al., 2006; Quintana and Ciurana, 2011). Frequency domain analysis of cutting sound signals is an appropriate chatter recognition technique for the present work.
- The approach presented by (Smith, 1987; Harmonizer, 2008) is limited for selected cutting conditions. Chatter is detected with the defined threshold value of the dominant peak based on prior experiments.
- (Dijk et al., 2010) presented an approach for chatter control but their chatter detection system lacks in accuracy and automatic detection of chatter at different spindle speeds and other cutting conditions.

2.9 Detailed Formulation of the Research Objectives

Significant improvements in overall productivity of milling systems are ensured by targeting the challenges and research gaps mentioned in the previous section.

Optimization System for Milling

Development of a genetic algorithm (GA) based milling optimization system for the optimal selection of cutting conditions while respecting the practical constraints of the machine tool and workpiece system.

Consideration of operational constraints of the machine tool, such as spindle speed and feed limits, available spindle power and torque, chatter vibration limits due to the dynamic interaction between cutting tool and workpiece, acceptable limits of bending stress and deflection of the cutting tool and clamping load limits of the workpiece in the developed optimization system.

Development of different modules in a generic way that overall optimization system can satisfy the following use cases for high speed milling of prismatic parts:

1. Minimization of pocket milling time considering one-way toolpaths for a given dimensions and material, and machine tool/spindle/tool holder/cutting tool system with the following developments:

    - Optimal selection of all cutting conditions: spindle speed, feed rate, axial depth of cut and radial depth of cut.
    - Development of subsystems to keep one of the cutting conditions constant depending upon user requirements and consideration of corresponding constraints.

2. Minimization of machining time for a given multi-feature prismatic part and machine tool/spindle/tool holder/cutting tool system with the following developments:

    - Development of a pre-processor to extract multiple features (pocket, contouring, facing) and their corresponding toolpaths (along different machine axes containing linear and circular segments) from the APT file. Extraction of feature boundaries from STEP files.
    - Implementation of an engagement angle detection algorithm to find the maximum value of radial depth of cut encountered along the toolpath.
    - Optimal selection of spindle speed, axial depth of cut and feed rate while keeping the limiting value of the radial depth of cut constant.
    - Consideration of stability constraints by taking the effect of different dynamic characteristics of the machine tool axes.

3. Minimization of pocket milling time for given pocket dimensions and material, and machine tool/spindle/tool holder/cutting tool system with the following developments:

    - Extraction of pocket boundary depth from the STEP file.
    - Consolidation of the developed module for generation of smooth and constant engagement toolpaths which minimize the radial depth of cut variations.
    - Optimal selection of all the cutting conditions (spindle speed, feed rate, radial depth of cut and axial depth of cut) and corresponding smooth and constant engagement toolpath for high speed pocket milling

Implementation and Experimental Validation of the Optimization System

- Implementation of the developed optimization system for different use cases for the optimal selection of cutting conditions and/or toolpath for different prismatic parts.
- Experimental validation of the optimal cutting conditions and/or smooth and constant engagement toolpath (selected based on simulations) with various measured signals during actual machining.

Indirect Identification of Force Coefficients

Development of an enhanced methodology for the identification of tangential force coefficients from spindle motor current with the following developments:

- Implementation of a spindle power model which accounts for all mechanical and electrical power losses for high speed machining.
- Development of an empirical model for cutting torque prediction from the spindle motor current.
- Experimental validation of the developed cutting torque prediction model and its industrial implementation for tangential force coefficients identification.

FRF Prediction by Receptance Coupling

Development of a procedure using receptance coupling technique to predict FRFs of machine tool systems at the cutting tool tip for different end mills. Validation of the predicted FRFs via numerical simulations with direct experimental measurement of FRFs via hammer testing.

Online Chatter Detection and Control

Development of an online chatter detection and control system with the following developments:

- Development of an accurate and automatic chatter detection system for all possible ranges of spindle speed and other cutting conditions.
- Implementation of a chatter control approach in the case of existence of chatter.
- Experimental validation of the developed chatter detection and control system for different machine tool systems and different cutting conditions.

Stability Analysis of Flexible Workpieces

Development of a procedure for the selection of stable cutting conditions for milling of thin-walled workpieces:

- Finite element analysis of thin-walled workpieces to study the change in dynamic characteristics along the toolpath.
- Prediction of chatter free cutting conditions for thin-walled workpieces taking into consideration changing dynamics.

3 Optimization System for 2.5D Milling

3.1 Genetic Algorithm based Optimization

In high speed milling, there is a large range of choices for cutting conditions due to the enhanced capabilities of modern machine tools and cutting tools. This large range of choices of cutting conditions makes the practical search space huge. The non-linear and non-smooth relationship of cutting conditions with various physical phenomena encountered during milling make the optimization problem a complex task. These kind of difficult optimization problems are solved accurately and efficiently using genetic algorithm (GA). A genetic algorithm is a computerized search and optimization technique based on the mechanics of natural genetics and selection. A GA is a computationally fast algorithm to find near or exact global optimal solution within a large and complex feasible search space. In this section, GA implementation and its enhanced capabilities for the developed system are presented in a more generalized way. The developed modules of the GA based optimization system, along with pre-processed inputs, will be applied for different different use cases of the milling system.

3.1.1 GA Initialization

Definition of Search Space

From the given set of inputs of machine tool/spindle/tool holder/cutting tool and workpiece system, the practical search space of cutting conditions/optimization variables for the optimization problem is defined in Equation 3.1.

$$\begin{aligned} n_{lowerbound} \leq n \leq n_{upperbound} \\ f_{t_{lowerbound}} \leq f_t \leq f_{t_{upperbound}} \\ A_{p_{lowerbound}} \leq A_p \leq A_{p_{upperbound}} \\ A_{e_{lowerbound}} \leq A_e \leq A_{e_{upperbound}} \end{aligned} \tag{3.1}$$

- The upper bound of the spindle speed is selected from the machine tool specifications. The lower bound is fixed as 5000rpm in order to avoid low speed machining.
- Bounds of the feed rate are defined from machine tool feed limits or from from permissible values from cutting tool catalogues.
- Axial depth of cut lies between 0 to minimum of (cutting tool length and depth of the feature).
- The bounds of the radial depth of cut lie between 0 to the cutting tool diameter.

These bounds can also be defined directly by the user depending upon the application and requirements.

Encoding of Optimization Variables

From lower and upper bounds, the values of optimization variables (X_i's) are encoded with a binary-coded string, composed of zeros(0) and ones (1), which is called a chromosome (Rai, 2008). For the present case, the optimization variables (X_i's) are: spindle speed (n), axial depth of cut (A_p), radial depth of cut (A_e) and feed rate (f_t). A segment of each optimization variable is assigned with bits (also called genes). The length of each segment is selected based on the accuracy required for the solution. A chromosome with 6-bits per optimization variable (also called "bitsize") is illustrated in Figure 3.1. Each cutting condition is a quarter segment of a coded binary string and represents a percentage value of the range of the cutting conditions which is given by:

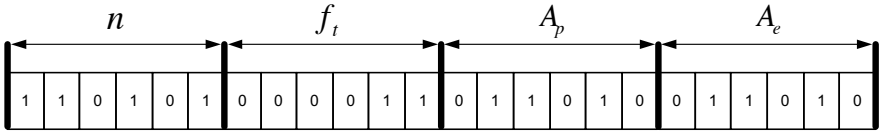

Figure 3.1: Binary-coded string (chromosome structure)

$$X_i = \left(\frac{X_{i_{upperbound}} - X_{i_{lowerbound}}}{max(\text{binary} \rightarrow \text{decimal})} \right) Y_i + X_{i_{lowerbound}} \tag{3.2}$$

Here, $X_{i_{upperbound}}$ and $X_{i_{lowerbound}}$ are the upper and lower bounds of the cutting conditions respectively. The Y_i are the decoded values (decimal values) of the binary segments of the chromosome corresponding to each cutting condition . The X_i are the mapped values of the cutting conditions. For example, let us assume that the spindle speed range is 10000–20000rpm. For the chromosome illustrated in Figure 3.1, the maximum decimal value of the 6-bit binary segment is 63, $[(111111)_2 = 63]$. The decoded value (Y) of the binary segment corresponding to spindle speed is 53, $[(110101)_2 = 53]$. The mapped value of the spindle speed, n, will be 18412rpm. The same procedure is adopted to map the values of other cutting conditions.

There are the following flexibilities for the chromosome structure in order to implement the optimization system for different use cases and user requirements:

- The bitsize of the chromosome can be changed depending upon the application. Accuracy of the optimization variables is directly proportional to the chosen bitsize of the chromosome.
- One of the optimization variables for the optimization problem can be kept constant depending on the user requirements or use case with the developed optimizations system.
- The developed program will encode the chromosome with defined bitsize and corresponding number of optimization variables.

Initial Population

The initial population is created by randomly generating the chromosomes. The steps involved in generating the initial population for GA initiation are presented in Fig. 3.2. The feasibility of each chromosome is checked with various constraints presented in Section 3.2. It is important to mention that the operational limits for spindle speed and feed rate for the machine tool are already taken into account during the selection of their bounds during GA initialization. For better GA performance only the practical limits of axial and radial depth of cut are used during the selection of their ranges. Feasible chromosomes (chromosomes which respect all the constraints) are solutions to the optimization problem which may or may not be optimal. The optimization problem can be defined as maximization of material removal rate or minimization of machining time. The calculated value of the objective function (machining time or material removal rate) for each feasible chromosome is presented in the terms of fitness value (f).

3.1.2 GA Operators

After creating the initial population, the next generation (new population) is produced using various GA operators namely reproduction, crossover and mutation. The steps of the algorithm for creating the new population are presented in Figure 3.3. The GA operators used in the developed system are explained in the following paragraphs:

Reproduction

Reproduction selects the above average chromosomes (chromosomes with higher fitness values) from the current population and makes the mating pool in a probabilistic manner. The i^{th} chromosome in the population is selected with a probability proportional to its fitness

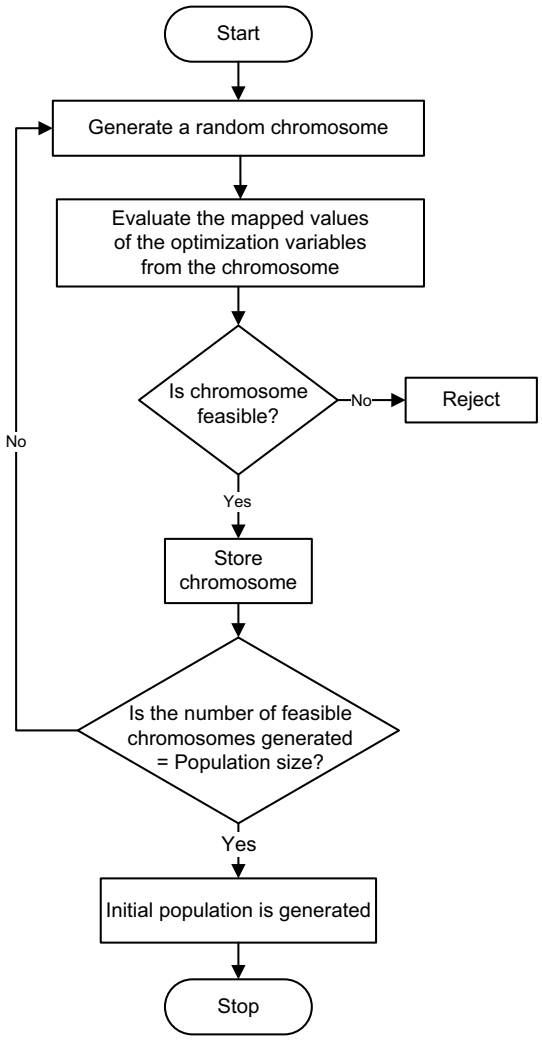

Figure 3.2: Algorithm to generate the initial population

value, f_i. The probability p_i for selecting the i^{th} chromosome is given by Equation 3.3.

$$p_i = \frac{f_i}{\sum_{j=1}^{P_{size}} f_j} \tag{3.3}$$

Here P_{size} is the number of chromosomes in the population (also called population size). A roulette wheel selection method is used as a reproduction operator. A roulette wheel is created and divided into slots equal to the population size. The width of the slot is proportional to the fitness value of the chromosome. For example, a roulette wheel for five chromosomes is given in Figure 3.4. A slot width for the first chromosome is calculated as $\frac{25}{25+5+40+10+20}$. It is obvious from the roulette wheel selection that chromosomes with higher fitness values have a greater chance of being selected for the mating pool than the chromosomes with a lesser fitness value. In order to ensure that better chromosomes from the previous population are

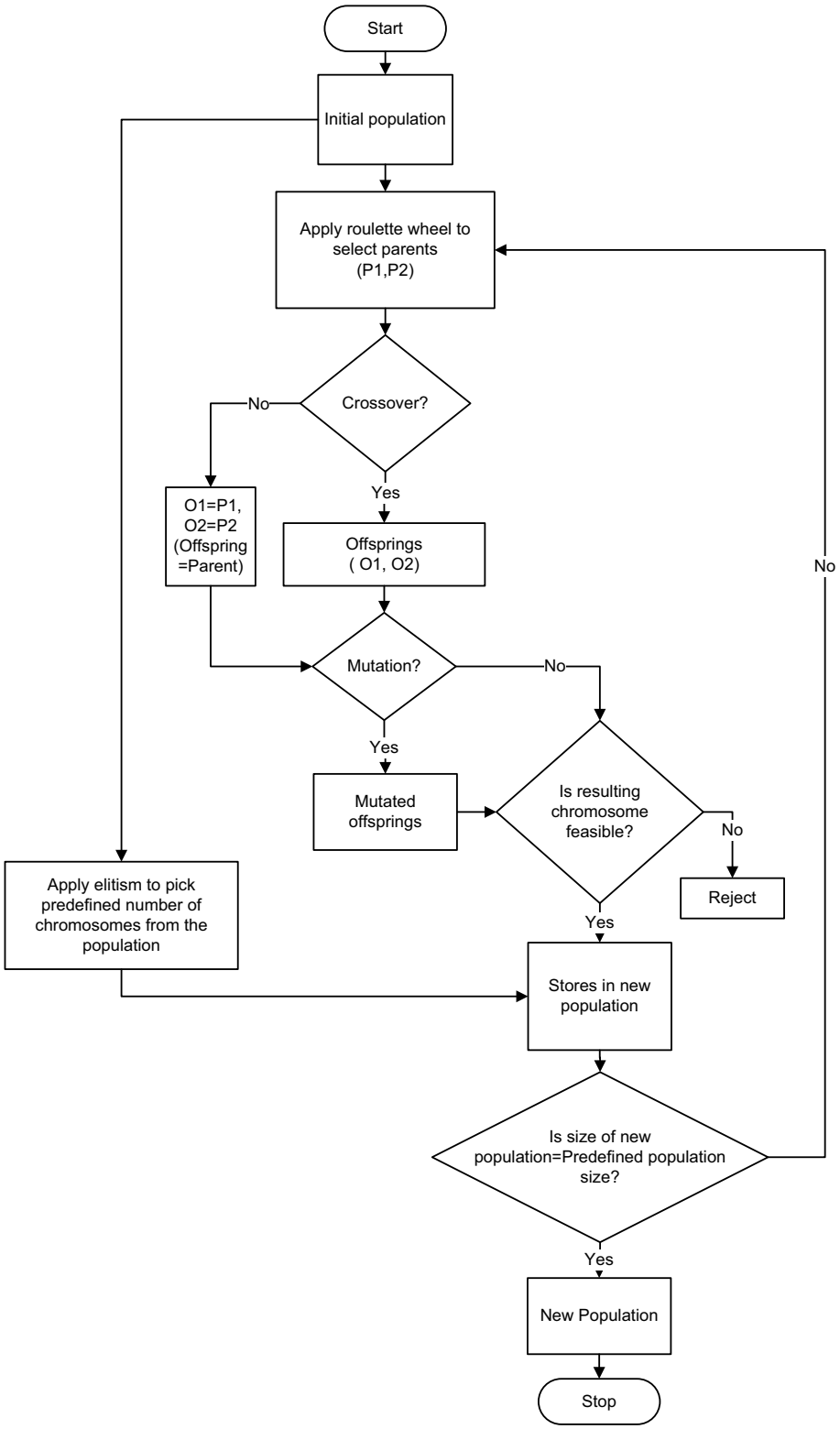

Figure 3.3: Algorithm to generate new population from the previous population

not lost during reproduction, elitism is also used. In elitism, a fixed number of chromosomes (with better fitness value) are taken from the previous population and transferred directly to the new population.

Chromosome	Fitness
1	25
2	5
3	40
4	10
5	20

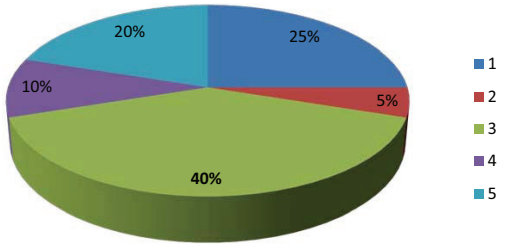

Figure 3.4: Roulette wheel as reproduction operator

Crossover

Two different chromosomes (now called parents) are selected from the roulette wheel to generate two offspring (also called children). The multi-point crossover operator is applied in the present work. A predefined crossover probability (C_{prob}) is set (usually a high value, 60–100%). Parents P1 and P2 are selected for crossover and the crossover site is chosen by generating a random number. As an example, a multi-point crossover operator with random crossover site "3" is shown in Figure 3.5. P1 and P2 are interchanged with their alleles (0 and 1) between crossover sites to give birth to offsprings, O1 and O2.

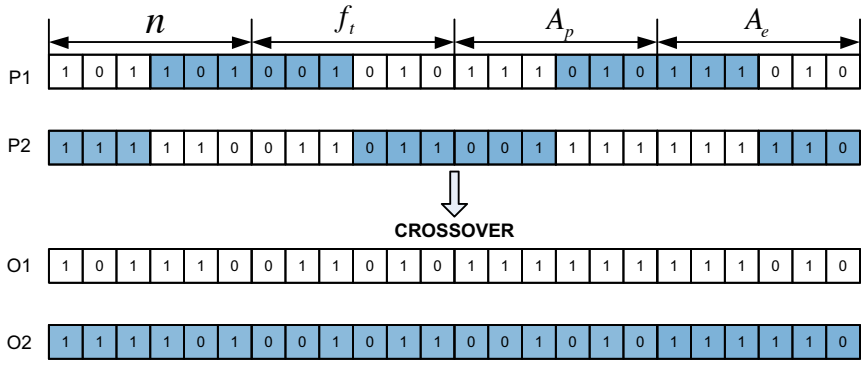

Figure 3.5: Crossover operator

Mutation

As the optimization problem is highly nonlinear, a mutation operator is used to prevent the GA solution falling into a local minima/maxima. A predefined mutation probability (M_{prob}) is set for GA analysis (usually a small value, 1–5%). During mutation the allele of the gene is interchanged; zero(0) is changed with one(1) and vice versa. In the present work, for a given

chromosome, each gene has an independent chance, with predefined mutation probability, to mutate. The mutation operator used for the developed system is shown in Figure 3.6. In this example, '3' and '20' are the mutation sites. Only feasible mutated offspring, defined as feasible chromosomes, are taken in the next generation.

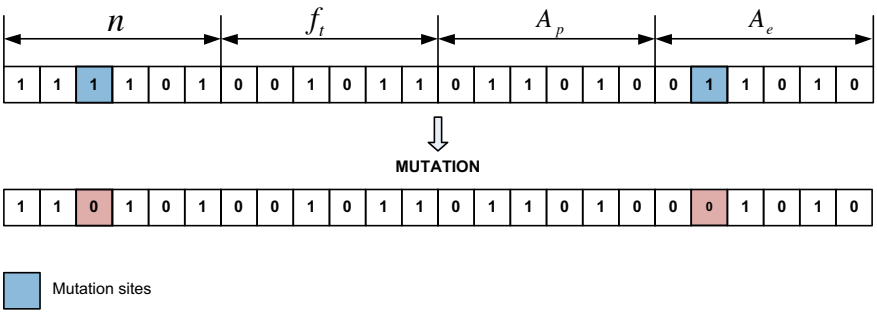

Figure 3.6: Mutation operator

3.1.3 GA Iteration Loop

Using the above defined GA operators, the next generation (new population) is produced. The GA is an iterative loop and will continue until the predefined generation size (G_{size}) is reached. The steps involved are presented in Figure 3.7.

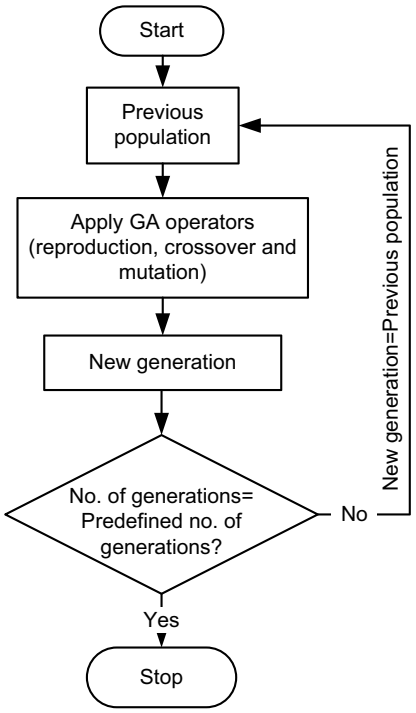

Figure 3.7: Algorithm for iteration loop for GA analysis

3.2 Modeling of Embedded Constraints

For a given machine tool/spindle/tool holder/cutting tool and workpiece system, the physical phenomena which happen during cutting due to the interaction between cutting tool and workpiece are significantly affected by the choice of cutting conditions. In the present work, the optimal selection of cutting conditions is achieved while respecting the various operational, technological and dynamic constraints which are detailed in the following subsections.

3.2.1 Cutting Force, Power and Torque

Cutting forces are generated during the milling process due to the interaction of cutting tool and workpiece. High cutting forces cause cutting tool and workpiece deflections which may result in the violation of permissible tolerances (Budak, 2006a). High cutting forces have an adverse effect on the working life of the cutting tool and lead to high power and torque requirements from the machine tool. The cutting forces depend on the cutting tool geometry, workpiece material and cutting conditions. In the present work, cutting tool and workpiece material are available as inputs to the system. The combined property of cutting edge geometry and workpiece material is identified in the term of force coefficients. A mechanistic model[1] is used for the identification of force coefficients. Once the force coefficients are known, cutting forces can be predicted for different cutting conditions by using analytical models (Budak and Altintas, 1994; Altintas, 2000). The module to predict the cutting forces, power and torque is presented in Figure 3.8. The inputs to the cutting force analytical model are: specifications of cutting tool, force coefficients, cutting conditions, milling mode. The geometry of helical end

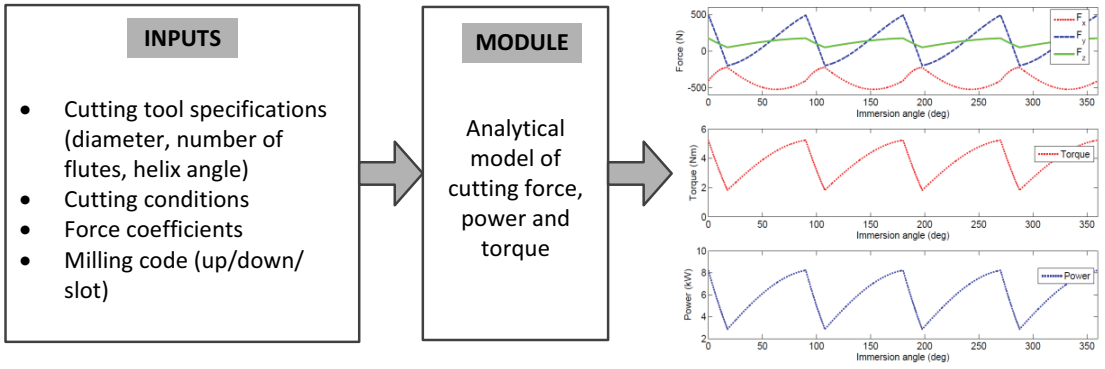

Figure 3.8: Module for analytical cutting force modeling

mill[2] with multiple flutes is shown in Fig. 3.9.

The geometry of chip formation at the cutting zone between cutting tool and workpiece

[1] presented in Appendix 2.1.2
[2] end mills are used as cutting tool in the milling operations

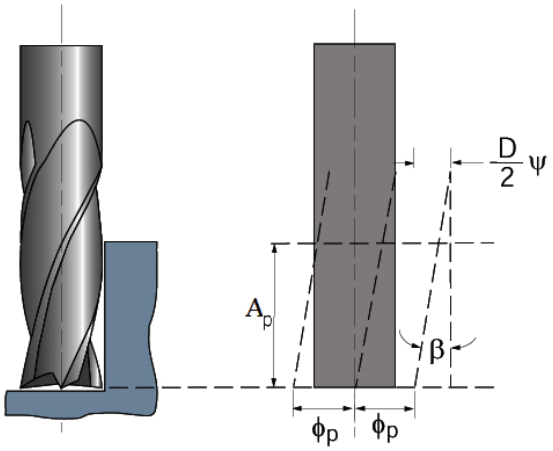

Figure 3.9: Geometry of a helical end mill (Altintas, 2000), here D denotes the diameter, β is the helix angle and ϕ_p is the pitch angle

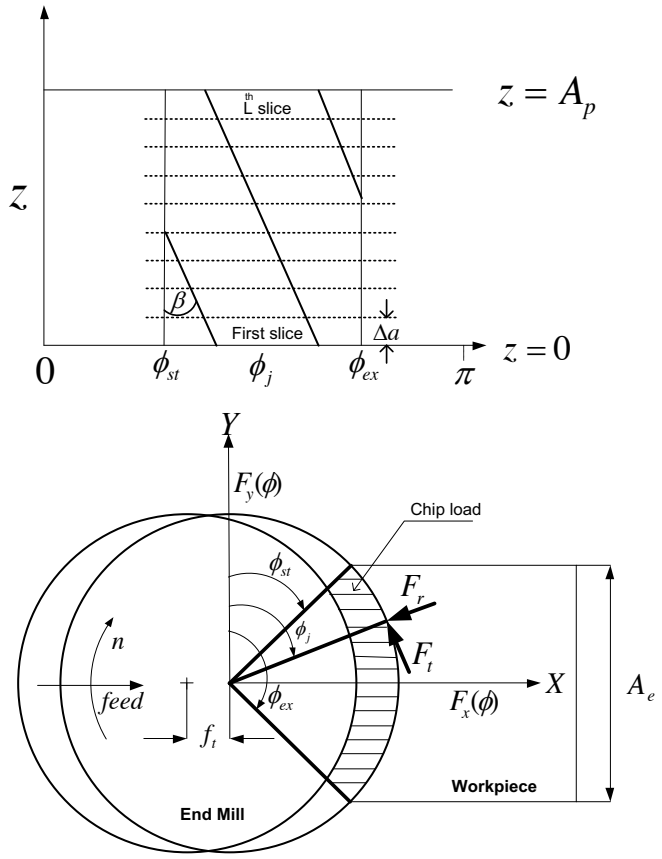

Figure 3.10: Chip formation phenomenon in milling operation

material is shown in Fig. 3.10. The instantaneous chip thickness by the j^{th} flute is given by:

$$h_j(\phi, z) = f_t \sin\phi_j(z) \tag{3.4}$$

where f_t denotes the feed rate in mm/rev-flute and ϕ_j denotes the instantaneous immersion angle. The immersion angle for the j^{th} flute at axial depth of cut z is presented by

$$\phi_j(z) = \phi + j\phi_p - \psi \tag{3.5}$$

here, ϕ is the reference immersion angle designated from the bottom end of one flute. ψ is the lag angle at axial depth of cut z and is presented by

$$\psi = \frac{2tan\beta}{D} z \tag{3.6}$$

Tangential ($dF_{t,j}$), radial ($dF_{r,j}$) and axial ($dF_{a,j}$) cutting forces acting on the differential element along the cutting edge with height Δa and uncut chip area ($\Delta a h_j(\phi_j(z))$) are expressed as:

$$\begin{aligned} dF_{t,j}(\phi,z) &= [K_{tc}h_j(\phi_j(z)) + K_{te}]\Delta a \\ dF_{r,j}(\phi,z) &= [K_{rc}h_j(\phi_j(z)) + K_{re}]\Delta a \\ dF_{a,j}(\phi,z) &= [K_{ac}h_j(\phi_j(z)) + K_{ae}]\Delta a \end{aligned} \tag{3.7}$$

Where K_{tc}, K_{rc} and K_{ac} are the cutting force coefficients contributed by the shearing action and K_{te}, K_{re} and K_{ae} are the edge force coefficients in the tangential, radial and axial directions respectively. The elemental cutting forces in the feed (X), normal to feed (Y) and axial (Z) directions are presented as:

$$\begin{aligned} dF_{x,j}(\phi_j(z)) &= -dF_{t,j}\cos\phi_j(z) - dF_{r,j}\sin\phi_j(z) \\ dF_{y,j}(\phi_j(z)) &= +dF_{t,j}\sin\phi_j(z) - dF_{r,j}\cos\phi_j(z) \\ dF_{z,j}(\phi_j(z)) &= +dF_{a,j} \end{aligned} \tag{3.8}$$

The elemental cutting forces contributed by all flutes in the cutting zone are calculated and summed to obtain the total instantaneous forces on the cutting tool at an immersion angle ϕ. The cutting forces are produced only when the cutting tool is in the cutting zone.

$$F_x(\phi), F_y(\phi), F_z(\phi) > 0 \quad \phi_{st} \le \phi \le \phi_{ex} \tag{3.9}$$

here, ϕ_{st} and ϕ_{ex} are respectively the start and exit angles in the cutting zone. These angles depend on the milling mode, radial depth of cut and diameter of the cutting tool as shown in Figure 3.11.

The resultant cutting forces acting on the cutting tool are expressed as:

$$F(\phi) = \sqrt{F_x(\phi)^2 + F_y(\phi)^2 + F_z(\phi)^2} \tag{3.10}$$

The cutting torque (T_c) and cutting power (P_c) are calculated from the tangential cutting

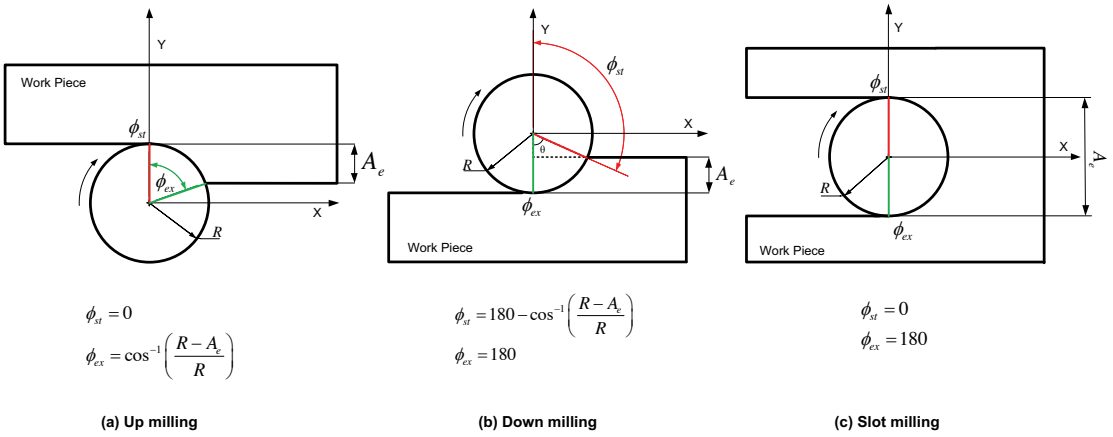

Figure 3.11: Different milling modes

forces as:

$$T_c(\phi) = \frac{DF_t(\phi)}{2000} \tag{3.11}$$

$$P_c(\phi) = \frac{2\pi n T_c(\phi)}{60000} \tag{3.12}$$

Here T_c is the torque overcome for material cutting in Nm, P_c is the cutting power in kW. Cutting power and cutting torque for selected cutting conditions should not exceed the available limits of the machine tool spindle power and spindle torque. The mean values of cutting power and torque per cutting tool revolution are used during the optimization analysis. Complete modeling and validation of prediction of cutting forces is presented in Appendix A

3.2.2 Stability of the Milling Process

Wrong selection of cutting conditions during process planning may lead to unstable milling (chatter vibrations). During the part programming stage, in order to realize chatter free cutting conditions, their selection must be done from the stability lobe diagram. In the present work, the stability of the milling process is ensured by using offline strategies (as explained in Section 2.4). In order to develop the stability lobe diagram for a given machine tool system, the zeroth order frequency domain solution developed (Altintas and Budak, 1995) is embedded in the developed optimization system.

Different inputs from the machine tool system and workpiece system are used for the prediction of chatter free limits during high speed milling. Various inputs required for the development of SLD are presented as following:

- The dynamic characteristics, in terms of frequency response functions of the machine

tool/ spindle/ tool holder/ cutting tool at the cutting tool tip, in the feed X and normal to feed direction Y are assigned in two ways:

- Speed independent FRFs are measured directly with hammer testing.
- FRFs can be defined from dynamic parameters with following equations:

$$\begin{aligned} \Phi_{\mathrm{xx}} &= \frac{\omega_{nx}^2}{k_x}\left(\frac{1}{\omega_{nx}^2-\omega_c^2+i2\omega\omega_{nx}\zeta_y}\right) \\ \Phi_{\mathrm{yy}} &= \frac{\omega_{ny}^2}{k_y}\left(\frac{1}{\omega_{ny}^2-\omega_c^2+i2\omega\omega_{ny}\zeta_y}\right) \end{aligned} \tag{3.13}$$

  Here ω_{nx} and ω_{ny} are the natural frequencies of the dominant modes in the feed X and normal to feed Y directions respectively. k_x and k_y are the stiffness values in the feed and normal to feed directions respectively. ζ_x and ζ_y are the damping ratios.

- Tangential and radial cutting force coefficients (K_{tc} and K_{rc})
- Diameter and number of flutes of the cutting tool
- Pre-defined values of the constant cutting conditions ($A_p/A_e/n$) during the frequency domain solution.
- Milling mode (up/down)

For a given set of inputs, the limiting value of axial depth of cut is calculated by (Altintas and Budak, 1995):

$$A_{plim} = -\frac{2\pi\Lambda_R}{NK_{tc}}\left(1+\kappa^2\right) \tag{3.14}$$

here, K_{tc} is the tangential cutting force coefficient, N is the number of flutes of the cutting tool. $\kappa = \dfrac{\Lambda_I}{\Lambda_R}$, Λ_R and Λ_I are respectively the real and imaginary parts of the eigenvalue solution which is given by:

$$\Lambda = -\frac{1}{2a_0}\left(a_1 \pm \sqrt{a_1^2-4a_0}\right) \tag{3.15}$$

and

$$\begin{aligned} a_0 &= \Phi_{\mathrm{xx}}(\omega)\Phi_{\mathrm{yy}}(\omega)(\alpha_{xx}\alpha_{yy}-\alpha_{xy}\alpha_{yx}) \\ a_1 &= \alpha_{xx}\Phi_{\mathrm{xx}}(\omega)+\alpha_{yy}\Phi_{\mathrm{yy}}(\omega) \end{aligned} \tag{3.16}$$

Φ_{xx} and Φ_{yy} are the frequency response functions in feed and normal to feed directions respectively. The α terms are the directional milling coefficients which depend on radial depth

of cut and radial cutting force coefficient, are presented as:

$$\begin{aligned}
\alpha_{xx} &= \frac{1}{2}\left[\cos 2\phi - 2K_{\mathrm{r}}\phi + K_{\mathrm{r}}\sin 2\phi\right]_{\phi_{st}}^{\phi_{ex}} \\
\alpha_{xy} &= \frac{1}{2}\left[-\sin 2\phi - 2\phi + K_{\mathrm{r}}\cos 2\phi\right]_{\phi_{st}}^{\phi_{ex}} \\
\alpha_{yx} &= \frac{1}{2}\left[-\sin 2\phi + 2\phi + K_{\mathrm{r}}\cos 2\phi\right]_{\phi_{st}}^{\phi_{ex}} \\
\alpha_{yy} &= \frac{1}{2}\left[-\cos 2\phi - 2K_{\mathrm{r}}\phi - K_{\mathrm{r}}\sin 2\phi\right]_{\phi_{st}}^{\phi_{ex}}
\end{aligned} \tag{3.17}$$

Spindle speed is given by:

$$n = \frac{60\omega_c}{N(\pi - 2\tan^{-1}\kappa + 2s\pi)} \tag{3.18}$$

ω_c is the chatter frequency and s is the number of waves generated between the tooth periods as presented in Figure 3.12. Further details of the stability limit prediction theory are presented in Appendix D.

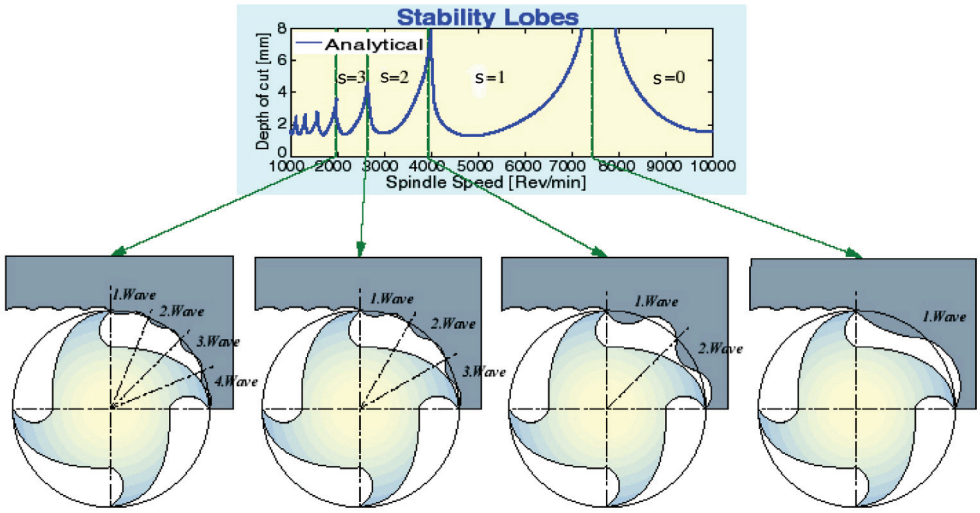

Figure 3.12: Stability peaks corresponds to integer number of waves between tooth periods in milling (Altintas and Weck, 2004)

The stability lobe diagram is unique for a given machine tool/spindle/tool holder/cutting tool and workpiece material system. The effect of feed rate on the stability limit is minimal at high speed milling (Tekeli and Budak, 2005). SLD can be presented in three different ways based on the constant cutting conditions during the frequency domain analysis. These different SLD algorithms are embedded in the optimization system as stability constraints and will be simulated based on applications and requirements. The different types of SLD and their development are detailed in the following subsections:

Axial depth of cut (A_p) *vs* spindle speed (n) at fixed radial depth of cut (A_e)

This SLD represents limiting values of axial depths of cut versus different spindle speeds at a fixed value of radial depth of cut. This SLD is commonly generated in the literature to identify chatter free regions. For the development of this SLD, the frequency domain solution developed by Altintas and Budak (Altintas and Budak, 1995) is used. The algorithm for SLD development is briefly explained as following:

- Calculate the direction coefficients for a given A_e, radial depth of cut value or given ϕ_{st} and ϕ_{ex}, from Equation 3.17.
- Select a chatter frequency from the frequency response function around a dominant machine tool system mode.
- Solve for the eigenvalues with Equation 3.15. This will give two possible solutions.
- Calculate the value of limiting axial depth of cut (A_{plim}) from Equation 3.14. The two eigenvalues will give two possible values of A_{plim}. Only the positive real values of A_{plim} will be accepted for further analysis.
- The spindle speed is calculated from Equation 3.18 for each lobe value (full vibration waves), $s = 0, 1, 2, \ldots$

  At this point, at a given chatter frequency (ω_c), the points (corresponding to different s values) indicated in Figure 3.13 are obtained.

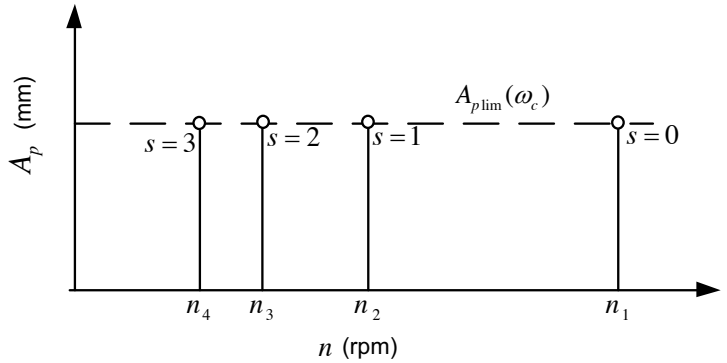

Figure 3.13: Presentation of different spindle speed at different lobe numbers

- The same procedure is repeated by scanning all the chatter frequencies around all the dominant machine tool modes from the frequency response function of the milling tool system.

For validation purposes, the input data, as presented in Table 3.1, are taken from a recent study (Tekeli and Budak, 2005). The stability lobe diagram (A_p vs n) at a fixed A_e value is generated for given set of inputs by the above mentioned algorithm. It is clear from the results

Table 3.1: Inputs for validation of SLD (A_p and n) (Tekeli and Budak, 2005)

D	N	K_{tc}	K_r	ω_{nx}	ω_{ny}	k_x	k_y	ζ_x	ζ_y	A_e
mm		MPa		Hz	Hz	kN/m	kN/m			mm
16	3	600	0.07	600	650	5600	5600	0.035	0.035	10.72

(Figure 3.14) that the developed SLD matchs exactly with the SLD from (Tekeli and Budak, 2005).

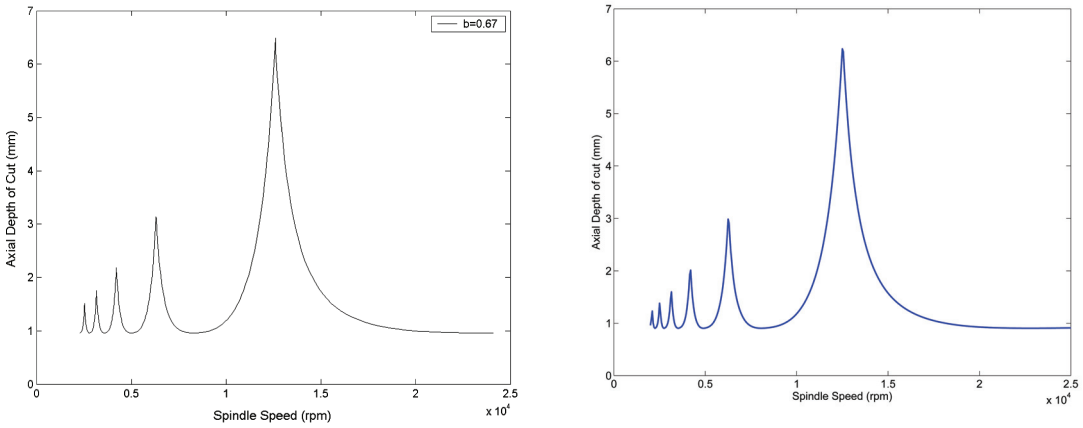

(a) SLD (A_p and n) results from (Tekeli and Budak, 2005), b is the radial depth (percentage of cutting tool diameter)

(b) Modeled SLD (A_p and n)

Figure 3.14: SLD (A_p and n) validation

This developed algorithm is implemented in the optimization system for the following requirements and optimization use cases:

1. When all the cutting conditions are chosen as optimization variables, the limiting value of the axial depth of cut at selected spindle speed (mapped value from the chromosome) is identified from the developed SLD at a given radial depth of cut (mapped value of the chromosome). For every new chromosome the SLD algorithm at fixed A_e (mapped values from the chromosome) is simulated to check its feasibility against the stability constraints.

2. When the optimization analysis is performed at constant value of the radial depth of cut, SLD at fixed A_e is simulated once for the entire optimization to develop the SLD (A_p vs n). Stable combinations of A_p and n are identified from the developed SLD. These combinations remain the same for a given optimization problem, so these combinations are used to check the feasibility of all the chromosomes generated during the complete optimization simulation.

Radial depth of cut (A_e) *vs* spindle speed (n) at fixed axial depth of cut (A_p)

(Tekeli and Budak, 2005) have extended the theory from (Altintas and Budak, 1995) to identify the stable radial depths of cut at different spindle speeds at a fixed value of axial depth of cut. The following steps explain the algorithm for development of this SLD:

- Select a chatter frequency range. Generally chatter vibrations occur at frequencies which are close to the natural frequencies of the machine tool/spindle/tool holder/cutting tool system. For a given chatter frequency:
  - Scan the full range (0° to 180°) of exit angles in the case of up milling or start angles in the case of down milling. Calculate the directional coefficients (α_{xx}, α_{xy}, α_{yy} and α_{yx}) from Equation 3.17 and constants (a_0 and a_1) from Equation 3.16. The directional coefficients are calculated for all scanned values of the exit angles (up milling) or start angles (down milling) values; the right exit/start angle is found two steps ahead.
  - Solve for the eigenvalues (Equation 3.15) and calculate the values of A_{plim} from Equation 3.14.
  - Determine the values of ϕ_{ex} or ϕ_{st} for which the calculated value of A_{plim} matches the A_p values.
  - Depending upon the exit or start angles values, calculate A_{elim} from the following equations:

$$\begin{aligned} A_{elim} &= \frac{D}{2}\big(1-\cos(\phi_{ex})\big) \qquad \text{upmilling} \\ A_{elim} &= \frac{D}{2}\big(1+\cos(\phi_{st})\big) \qquad \text{downmilling} \end{aligned} \tag{3.19}$$

- Calculate the spindle speeds corresponding to the chatter frequency using Equation 3.18 for each lobe value (full vibration waves) $s = 0, 1, 2, \ldots$
- The same procedure is repeated by scanning all the chatter frequencies around all dominant machine tool modes from the transfer function of the milling system.

For validation purposes the input data, presented in Table 3.2, is taken from (Tekeli and Budak, 2005). The corresponding SLDs are shown in Figure 3.15.

Table 3.2: Inputs for validation of SLD (A_e and n) (Tekeli and Budak, 2005)

D	N	K_{tc}	K_r	ω_{nx}	ω_{ny}	k_x	k_y	ζ_x	ζ_y	A_p
mm		MPa		Hz	Hz	kN/m	kN/m			mm
16	3	600	0.07	600	650	5600	5600	0.035	0.035	1.5

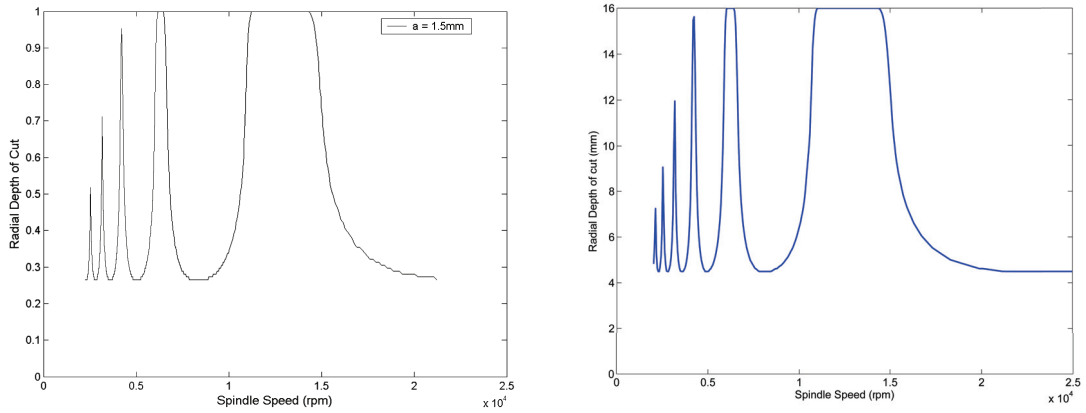

(a) SLD (A_e and n) results from (Tekeli and Budak, 2005), radial depth of cut is presented in $\frac{A_e}{D}$ and a is the axial depth of cut

(b) Modeled SLD (A_e and n)

Figure 3.15: SLD (A_e and n) validation

This developed algorithm is implemented in the optimization system for the following requirement:

1. This SLD algorithm is used when the optimization analysis is performed at a fixed value of axial depth of cut. The SLD at fixed A_p (defined value from the user) is simulated once for the entire optimization simulation to compute chatter free combinations of A_e and n from the SLD. These combinations are used to check the feasibility of each chromosome during the complete optimization simulation.

Axial depth of cut (A_p) *vs* radial depth of cut (A_e) at fixed spindle speed (n)

The SLD represents the combination of chatter free axial depth of cut versus radial depth of cut at a fixed value of spindle speed. In the development of this SLD, radial depth of cut values are varied from $(0-D)$. At each radial depth of cut value, A_{plim}, the limiting value of axial depth of cut is calculated at a desired value of spindle speed. For validation purposes the input data, presented in Table 3.3, is taken from (Tekeli and Budak, 2005). Developed and reference SLD are shown in Figure 3.16.

Table 3.3: Inputs for validation of SLD (A_e and A_p) (Tekeli and Budak, 2005)

D	N	K_{tc}	K_r	ω_{nx}	ω_{ny}	k_x	k_y	ζ_x	ζ_y	n
mm		MPa		Hz	Hz	kN/m	kN/m			rpm
16	3	600	0.07	600	650	5600	5600	0.035	0.035	12600

This developed algorithm is implemented in the optimization system for the following cases:

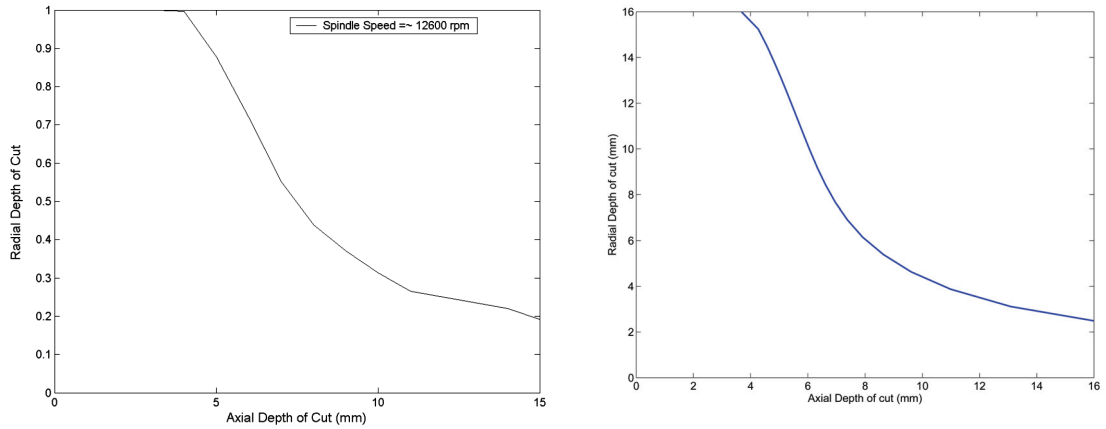

(a) SLD (A_e and A_p) results from (Tekeli and Budak, 2005), radial depth of cut is presented in $\frac{A_e}{D}$

(b) Modeled SLD (A_e and A_p)

Figure 3.16: SLD (A_e and A_p) validation

1. When the optimization is performed at fixed spindle speed (defined value from the user), the SLD at fixed n is simulated once for the entire optimization to identify the combinations of stable A_e and A_p. This same SLD information will be used to check the feasibility of each chromosome during the complete optimization simulation.

All the above mentioned algorithms are implemented in the developed optimization system. Depending on user requirements and optimization use cases, the corresponding stability algorithms are simulated to check the stability constraint for every chromosome.

SLDs in Different Feed Directions

Although the main objective of the designer of a machine tool is to achieve the same dynamic characteristics of the machine x and y axes there are always some differences. In the case of one-way toolpaths, the feed direction of the cutting tool is consistent but in the case of contour parallel toolpaths, the cutting tool has different feed directions with reference to the machine tool axes. If the difference of dynamic characteristics in the machine tool axes (x and y) is large, the limiting values of stable depths of cut along the machine axes can be different (Weck et al., 1994). This effect is presented as an example in Figure 3.17. It can be concluded from Figure 3.17 that there is a significant difference in the values of stable depths of cut in machine tool x and y directions. In the present work, stability lobe diagrams are generated while considering different machine axes (x and y) as feed direction in stability analysis. Minimum values of stable depths of cut are then identified from the generated stability lobe diagrams. It is assumed that the dynamics in feed and negative feed directions are same.

Dynamic Characteristics (Machine x)	Dynamic Characteristics (Machine y)
$\omega_{nx} = 600$ Hz $k_x = 5600$ kN/m $\xi_x = 0.035$	$\omega_{ny} = 660$ Hz $k_y = 5600$ kN/m $\xi_y = 0.035$

(x,y)→ machine coordinate system

(X,Y)→ feed and normal to feed directions

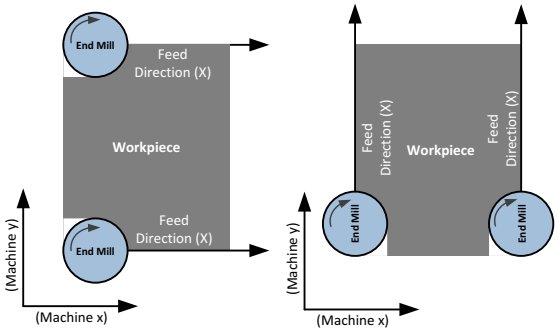

(a) Dynamic characteristics of machine tool system in different machine axes

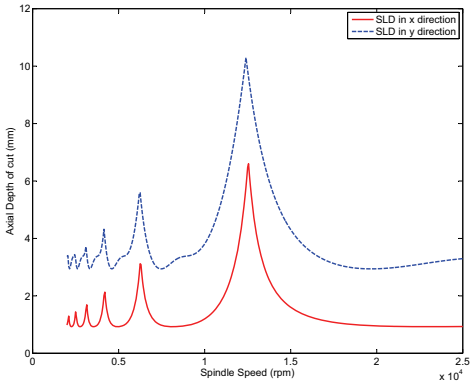

(b) SLD at fixed A_e with up milling 50% immersion

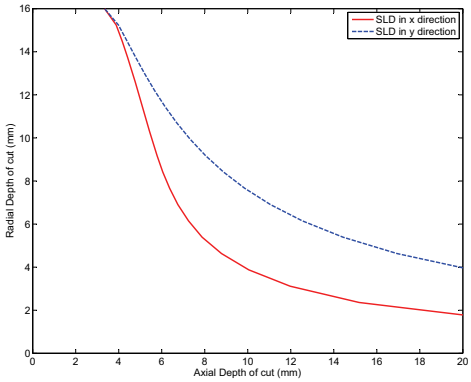

(c) SLD at fixed n=12600rpm and up milling

Figure 3.17: Chatter free limits for different machine axes

3.2.3 Cutting Tool Bending Stress

The bending stress is produced in the cutting tool due to the action of cutting forces during the milling process. This phenomenon is presented in Figure 3.18. The bending moment generated due to the cutting forces is given by Equation 3.20 (Rai, 2008).

$$M = F\left(L - \frac{A_p}{3}\right) \tag{3.20}$$

Here L is the overhang length of the cutting tool and is given by:

$$L = L_{tool} - L_{fix} \tag{3.21}$$

L_{fix} is the length of the portion of the cutting tool inside the toolholder. The bending stress developed in the cutting tool due to the bending moment is given by:

$$\sigma_b = \frac{MD_c}{2I} \tag{3.22}$$

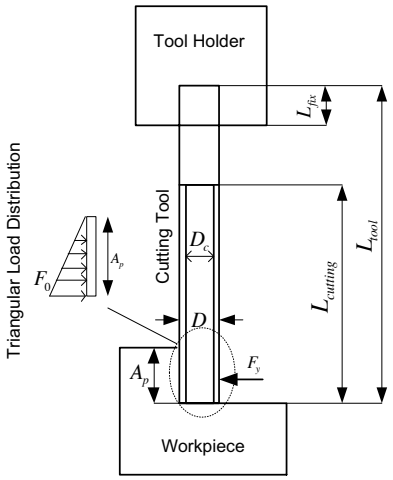

Figure 3.18: Bending moment acting on the cutting tool

Here I and D_c are the area moment of inertia of the tool cross-section and equivalent cutting tool diameter respectively and are calculated by the following equations (Rai, 2008):

$$D_c = 0.8D \tag{3.23}$$

$$I = \frac{\pi D_c^4}{64} \tag{3.24}$$

D is the diameter of the cutting tool. The developed bending stress for selected cutting conditions (mapped values from the chromosome) should not exceed the yield stress limit of the cutting tool material. This avoids breakage of the cutting tool and avoids unnecessary delay during the machining process.

3.2.4 Deflection of Cutting Tool

The cutting tool is deflected under the action of cutting forces developed during milling. Excessive static deflection due to high cutting forces may lead to poor part quality, violation of tolerance limits, reduction in the cutting tool working life and the overall productivity. It is important to control cutting tool deflections within the allowed tolerance limits by appropriate selection of cutting conditions. Using a cantilever beam model, the cutting tool deflection is computed by Equation 3.25 (Budak, 2006a; Rai et al., 2009).

$$\delta = \frac{1}{EI}\left[\frac{F_0 A_p (L - \frac{A_p}{3})L^2}{4} - \frac{F_0 A_p L^3}{12} + \frac{F_0 {A_p}^4}{120}\right] \tag{3.25}$$

Here E is Young's Modulus, F_0 is the cutting load per unit length and is calculated by:

$$F_0 = \frac{2F_{ymax}}{A_p} \tag{3.26}$$

F_{ymax} is the maximum value of the cutting force in the normal to feed direction. Cutting tool deflections developed for selected cutting conditions (mapped values from the chromosome) must be within allowed tolerance limits.

3.2.5 Clamping Load Limits

On production floors, the clamping load is decided based on the stiffness of the workpiece in order to avoid unnecessary workpiece deformations during milling. Higher cutting forces encountered during milling cause workpiece displacement if the clamping forces are not sufficient. The resulting cutting forces generated for selected cutting conditions must be less than the applied clamping load to avoid workpiece rigid body displacements.

3.3 Use Case 1: Optimization System for Pocket Milling with One-Way Toolpath

The objective of the part programmer is to choose the cutting conditions which produce minimum machining time while respecting the important constraints of the machine tool and workpiece system. One-way toolpaths are one of the most common routines in CAM systems. These toolpaths have the advantage of maintaining constant radial depth of cut, the same feed direction and consistent milling mode along the toolpath. The pocket dimensions and corresponding one-way toolpaths are presented in Figure 3.19. The first slot pass in inevitable.

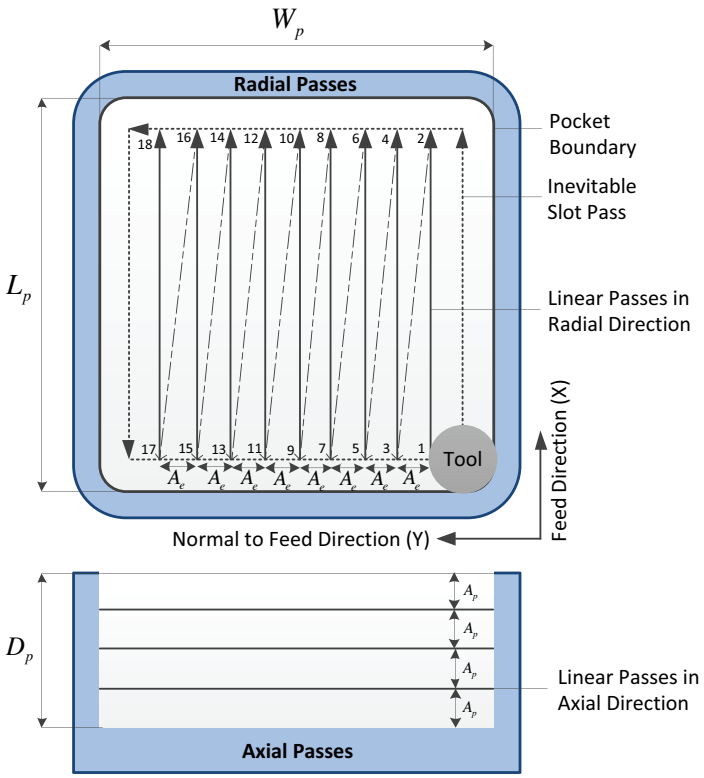

Figure 3.19: Pocket with one-way toolpaths

Radial and axial depths of cut are required for the geometrical definition of the toolpaths. The total number of linear passes (nop) required to mill the complete pocket, which depends on the number of radial passes (norp) for selected radial depth of cut and number of axial passes (noap) for selected axial depth of cut, is given by:

$$\text{nop} = \underbrace{ceil\left(\frac{W_p - 2D}{A_e}\right)}_{norp} \underbrace{ceil\left(\frac{D_p}{A_p}\right)}_{noap} \tag{3.27}$$

Spindle speed and feed rate are used to define the movement of the cutting tool along the toolpath. The machining time for pocket milling is presented as:

$$T_{mac} = \frac{\text{nop}\left(L_p - 2D\right)60}{nf_tN} \tag{3.28}$$

here, L_p, W_p and D_p are the length, width and depth of the pocket in mm respectively. $ceil$ is the round-up function. A_e and A_p are the radial and axial depths of cut in mm respectively. n represents the spindle speed in rpm and f_t represents the commanded feed rate in mm/rev-flute. N is the number of flutes of the cutting tool. Acceleration/deceleration of the machine tool is not included in the formula for machining time as their effect on commanded feed rate is not a major concern in the present work.

For a given set of inputs of machine tool/spindle/tool holder/cutting tool system and pocket, machining time depends on the selection of all cutting conditions. A study from (Tekeli and Budak, 2005) presented a method to reduce machining time by minimizing the number of cutting passes for pocket milling by selecting chatter free axial and radial depths of cut. It is clear from Equation 3.28 that the machining time for pocket milling cannot be minimized without considering spindle speed and feed rate along with the number of passes.

The present optimization use case minimizes pocket milling time by considering all cutting conditions, spindle speed, feed rate, axial and radial depths of cut, and practical constraints of the machine tool and workpiece system.

Problem Definition

For a given set of inputs of machine tool/spindle/tool holder/cutting tool system and pocket dimensions, the pocket machining time is minimized by optimal selection of cutting conditions (spindle speed, feed rate, axial and radial depths of cut) while respecting the important constraints of the machine tool and workpiece system. The overall architecture of the developed system for minimization of machining time for pocket milling is presented in Figure 3.20.

Detailed steps of the development of this optimization use case are:

1. GA based optimization is initiated with definition of the bounds of all the optimization variables (cutting conditions: spindle speed, feed rate, axial and radial depths of cut) as presented in Section 3.1.1. It is important to mention that only a practical/feasible search space is defined.
2. For this optimization use case, the chromosome structure (as shown in Figure 3.1) consists of four optimization variables: spindle speed, feed rate, axial and radial depths of cut.
3. The initial population is created with randomly generated feasible chromosomes (the

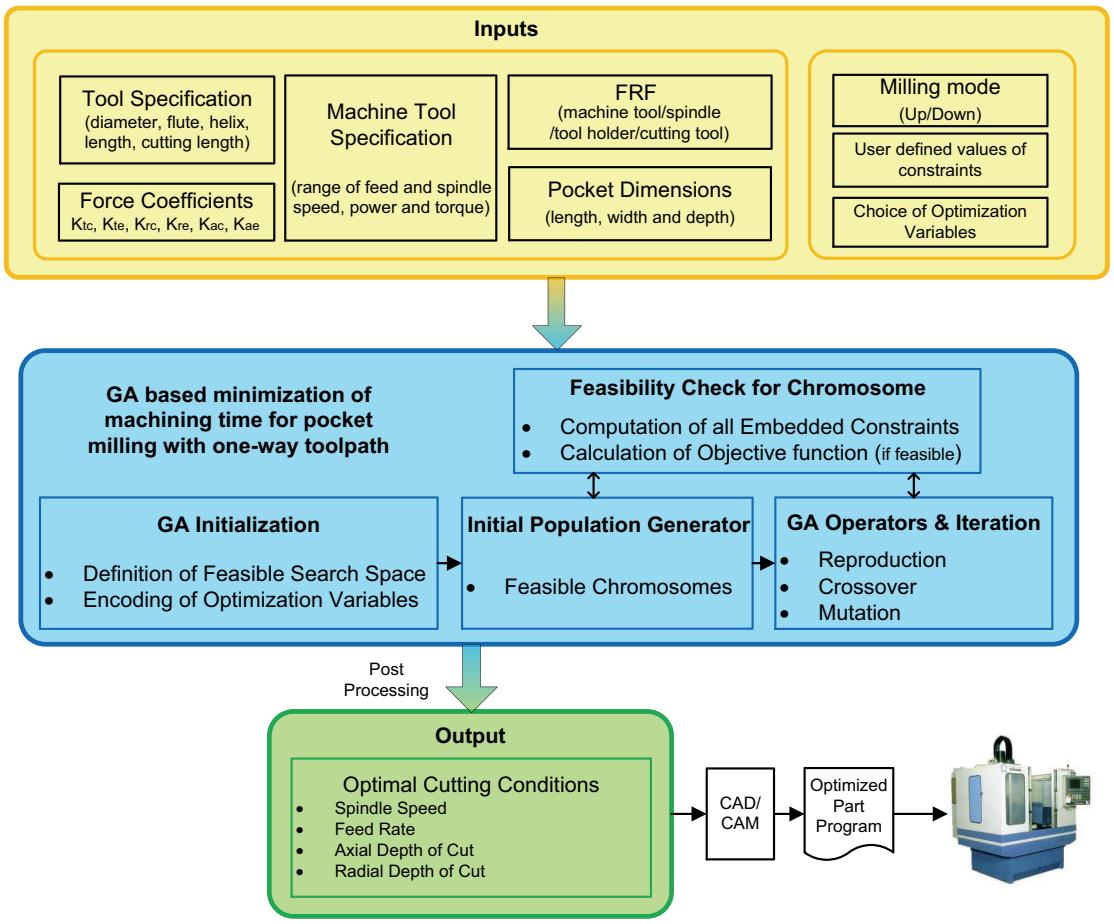

Figure 3.20: System architecture of pocket milling with one-way toolpath

algorithm is presented in Figure 3.2). Feasibility of each chromosome is checked against all the constraints defined in Section 3.2. For every chromosome, SLD in the feed direction is identified at fixed value of radial depth of cut (mapped value from the chromosome). At a selected spindle speed (mapped value from chromosome), the limiting value of the axial depth is compared with a selected value of axial depth of cut (mapped value from the chromosome).

4. For every feasible chromosome, the machining time is calculated using Equation 3.28. In the present work, minimization of pocket machining time is converted into a maximization problem. The fitness value of each feasible chromosome is given by:

$$f = \frac{1}{1 + T_{mac}} \tag{3.29}$$

5. The next generation (new population) from the current population is generated by using various GA operators (reproduction, crossover and mutation) as described in Section 3.1.2. The corresponding detailed algorithm is presented in Figure 3.3.

6. The iteration loop of the GA (as presented in Figure 3.7) will be simulated until the predefined number of generations (G_{size}) is met.

7. The result of simulation after predefined G_{size} is optimal values of spindle speed, feed rate, axial and radial depths of cut.

8. The optimal values of axial and radial depths of cut are post-processed to distribute them evenly by maintaining the same number of axial (noap) and radial (norp) cutting passes as:

$$\text{norp} = ceil\left(\frac{W_p - 2D}{A_e}\right) \quad \text{and} \quad \text{noap} = ceil\left(\frac{D_p}{A_p}\right) \tag{3.30}$$

   The adjusted axial and radial depth of cut are given by:

$$A_e^{'} = \frac{W_p - 2D}{\text{norp}} \quad \text{and} \quad A_p^{'} = \frac{D_p}{\text{noap}} \tag{3.31}$$

   It is important to mention that the pocket machining time remains the same as the value of 'nop' does not change with readjusted values of axial and radial depths of cut. The adjusted values of the axial and radial depths of cut are always smaller than or the same as their optimal counterparts.

9. One-way toolpaths are generated with optimal values of cutting conditions in the CAM system. Optimal part programs are post-processed to generate NC codes which are executed on CNC machine tool to realize the final workpiece.

The developed optimization use case (Aggarwal and Xirouchakis, 2012)[3] is implemented for optimal section of cutting conditions for different pockets (Section 4.1). The optimal values of cutting conditions are also verified experimentally (Section 4.5).

3.4 Use Case 2: Optimization System for Prismatic Part

Problem Definition

In industrial practice, the geometrical model of the prismatic feature (or workpiece) is realized in the CAD system. This geometrical information is saved in the STEP file format. The CAM system uses the geometrical model of the feature to generate the corresponding toolpaths. The toolpath information is stored in the APT file format. In this optimization use case, for a given set of inputs of machine tool/spindle/tool holder/cutting tool system and APT and STEP files, the pocket machining time is minimized for each prismatic feature by optimal selection of spindle speed, feed rate and axial depth of cut while respecting all the constraints presented

[3] Aggarwal, S. and Xirouchakis, P. (2012)., Selection of optimal cutting conditions for pocket milling using genetic algorithm. *The International Journal of Advanced Manufacturing Technology*, DOI: 10.1007/s00170-012-4472-x.

in Section 3.2. In this optimization use case, radial depth of cut is kept constant during optimization analysis. In the subsequent sections, the detailed steps of the development of this optimization use case are presented

3.4.1 Pre-Module for Geometrical Information

In this section, the extraction of toolpath information from the APT file and extraction of feature geometrical information from the STEP file are presented. The engagement angle (or radial depth of cut) is calculated along the toolpath. The steps involved in the pre-module for the extraction of geometrical information is presented in Figure 3.21. The pre-module has the following outputs which are used during the optimization analysis: (a) limiting value of radial depth of cut along the toolpath (b) depth of the feature (c) toolpath for one axial pass

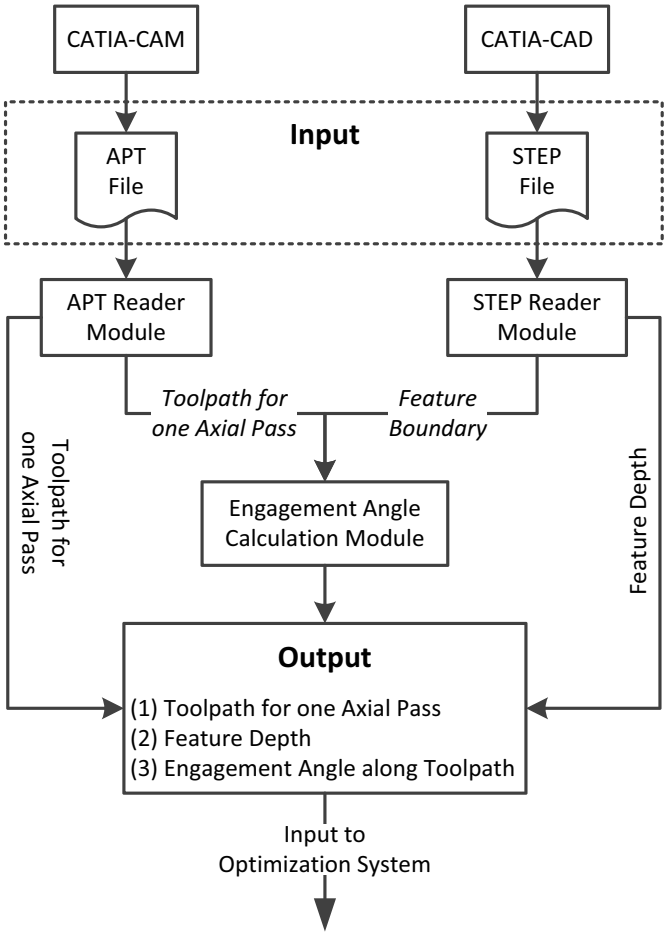

Figure 3.21: Pre-module for geometrical information extraction

APT Extraction

The CAM system generates the necessary toolpath of the feature from its geometrical model created in a CAD system. The cutting tool removes the material from the blank with defined feed rate and spindle speed along the defined toolpath to realize the final shape of the feature. This information is stored in APT file format. In the present work, the toolpath geometrical information is extracted from the APT file. The APT reader module is presented in Figure 3.22. The developed APT module has the following steps:

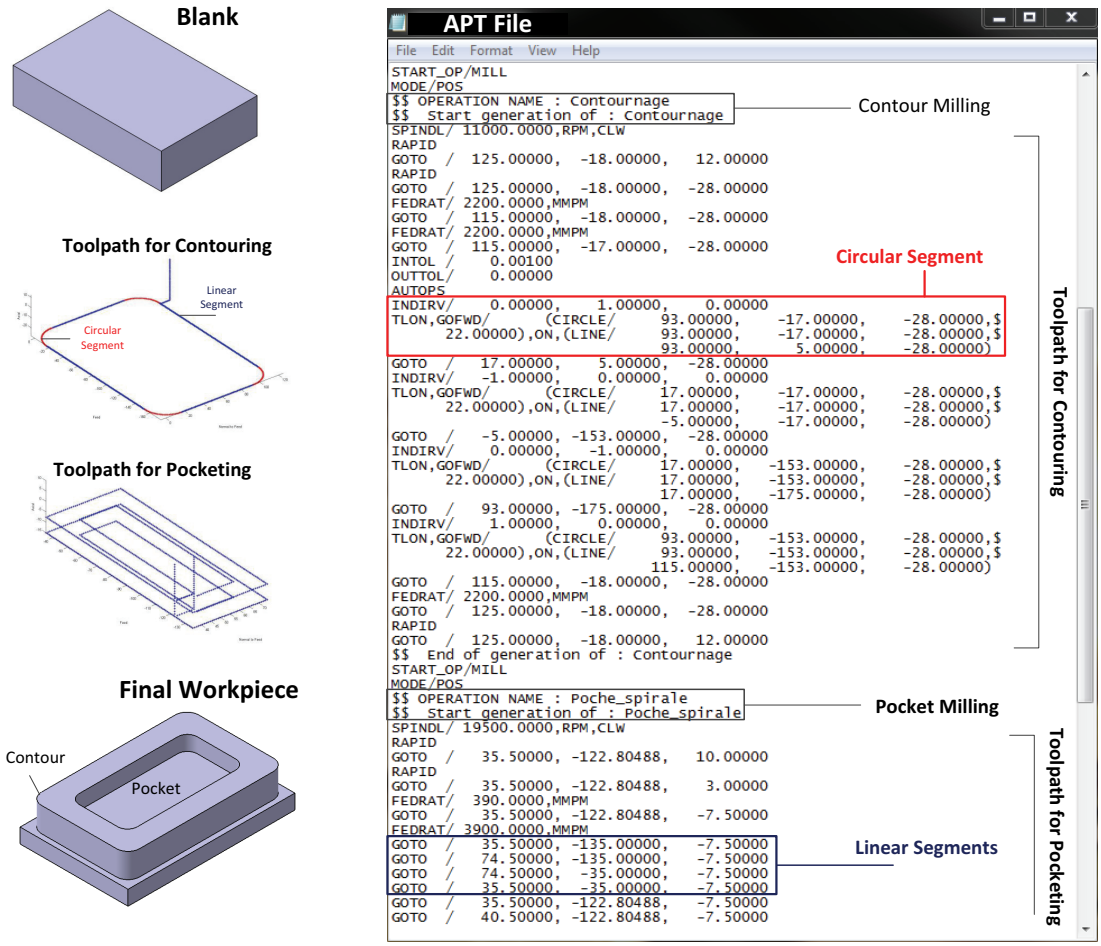

Figure 3.22: Toolpath extraction from the APT file

- Different prismatic features (facing, contouring and pocket) are extracted from a given APT file.
- For each feature, the corresponding geometrical information of the toolpath is extracted.
- All the linear and circular segments along the entire toolpath trajectory are identified.

- Toolpath for one axial pass are identified from the complete toolpaths with different axial passes.

The toolpath for one axial pass is used as one of the inputs for the engagement angle calculation module and also for the calculation of total machining time.

STEP Extraction

The geometrical information of the prismatic feature is saved in the STEP file format generated from a CAD system. In the present work, the STEP reader module developed by Stroud is implemented in the present work to extract the boundary and depth of prismatic feature. Further details of the STEP reader module are found in (Stroud, 2006; Stroud and Nagy, 2011). The extracted geometrical information of the desired feature is used in the following aspects:

1. Feature boundary and toolpath for one axial pass are used for the calculation of engagement angle along the toolpath.
2. Depth of the feature is used to define the range of axial depth of cut as an optimization variable and also used for the calculation of total machining time.
3. The feature boundary is converted into parametric form which is used as an input to generate constant stepover toolpaths (Section 3.5).

Engagement Angle Calculation

For a given feature boundary and toolpath for one axial pass, the engagement angle along the toolpath is calculated with the module developed by (Nešić, 2012). The overall system is presented in Figure 3.23. In this study the "exact" method is used for the calculation of the engagement angle. The exact method is based on the implementation of a stepwise algorithm for finding the Boolean interactions. This algorithm consists of four steps: (1) compute the interactions between two objects; (2) separate the objects boundaries at the interaction edges; (3) recombine the objects by joining elements from the two boundaries and (4) separate the bodies into shells and clean-up.

The calculation of the engagement angle has two stages. In the first stage the model of the material to be removed is subtracted from the current model to produce the results of machining. In the second stage, the model of the material to be removed is intersected with the same current model to give the shape of the material that is removed in the current step.

Toolpaths generated from CAM system result in change in radial depth of cut along the toolpath. With the engagement angle calculation module the change in the engagement angle (or radial depth of cut) along the toolpath can be identified accurately. From the engagement angle calculations, the limiting value of the radial depth of cut is chosen. This

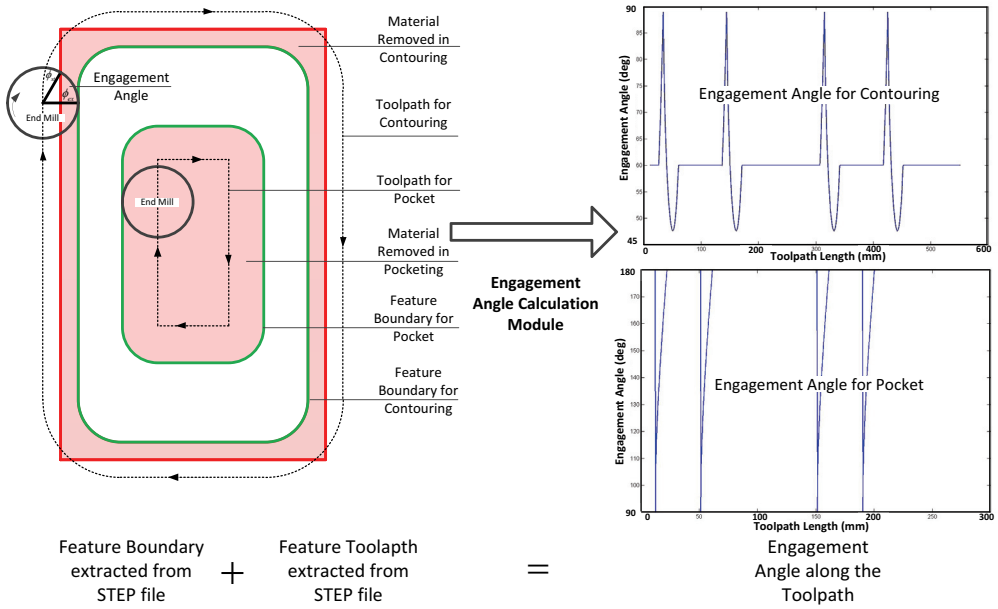

Figure 3.23: Engagement angle calculation

limiting value of radial depth of cut is kept constant and the remaining cutting conditions are used as optimization variables. In the case of contouring operations, the engagement angle calculation module is quite useful for determining the limiting value of radial depth of cut.

During pocket milling, often high radial depths of cut are chosen with toolpaths developed in CAM systems. Often slot cutting (full immersion) conditions are encountered along the toolpath. In these cases, the limiting value of radial depth of cut can be directly considered as full immersion without engagement calculations.

3.4.2 Detailed Steps of the Algorithm

In this section, the detailed steps of the development of this optimization use case are presented as:

- GA based optimization is initiated with definition of the bounds of the optimization variables (spindle speed, feed rate, axial depth of cut) as presented in Section 3.1.1. The range of axial depth of cut is defined from 0-min (cutting length of the cutting tool and feature depth). Depth of the feature is either extracted from the STEP file or defined manually.

- In this optimization use case, the radial depth of cut is kept constant during the complete optimization simulation. The constant value of A_e is either taken from engagement calculation or defined as user input. The genetic algorithm is initiated by creating the structure of the chromosome with three optimization variables: spindle speed, feed rate

and axial depth of cut.

- The initial population is created with randomly generated feasible chromosomes (the algorithm is presented in Figure 3.2). The feasibility of each chromosome is checked against all the constraints defined in Section 3.2. The stability limits in the feed and normal to feed directions are identified at a fixed value of radial depth of cut. The minimum value of stable axial depth of cut and spindle speed combinations is selected from feed and normal to feed direction SLDs. These stable combinations are used to check the feasibility against stability for each chromosome generated during the entire optimization analysis.

- For each feasible chromosome, the total machining time is calculated using the following equation:

$$T_{mac} = \frac{ceil\left(\frac{D_p}{A_p}\right)\left(L_{toolpath_{oneaxialpass}}\right)60}{nf_tN} \tag{3.32}$$

  Here, here, $L_{toolpath_{oneaxialpass}}$ is the length of the toolpath for one axial level which is extracted from the APT file. D_p is the depth of the feature. In this present optimization use case, the toolpath generated from the CAM system remains the same only the number of axial levels may change. The minimization of the machining time problem is converted into a maximization problem. The fitness value for each feasible chromosome is calculated as:

$$f = \frac{1}{1 + T_{mac}} \tag{3.33}$$

- The next generation (new population) from the current population is generated by using various GA operators (reproduction, crossover and mutation) as described in Section 3.1.2. The iteration loop for the GA will be simulated until the predefined number of generations (G_{size}) is met.

- The output of this optimization use case is optimal values of spindle speed, feed rate and axial depth of cut. The new part programs are generated in a CAD/CAM system with optimal cutting conditions while keeping the same toolpath trajectory. The optimal part programs will be post-processed and the corresponding NC codes will be sent to the CNC machine tool for manufacturing of the final workpiece.

3.5 Use Case 3: Optimization System for Pocket Milling with Smooth and Constant Engagement Toolpaths

Toolpaths generated by CAM systems result in change in radial depth of cut along the toolpath as presented in Section 2.6.2. The significant changes in radial depth of cut lead to high fluctua-

tions in cutting force and power, and often lead to chatter vibrations during milling. Moreover, sharp corners in the toolpath are detrimental for high speed machine tool kinematics. To target these problems, smooth and constant engagement toolpaths are consolidated in this present optimization use case.

Problem Definition

For a given set of inputs of machine tool/spindle/tool holder/cutting tool system and STEP file of convex pocket , the pocket machining time is minimized by optimal selection of spindle speed, feed rate axial and radial depths of cut and corresponding smooth and constant engagement toolpaths while respecting all the constraints presented in Section 3.2. The overall system architecture with different inputs and developments is presented in Figure 3.24

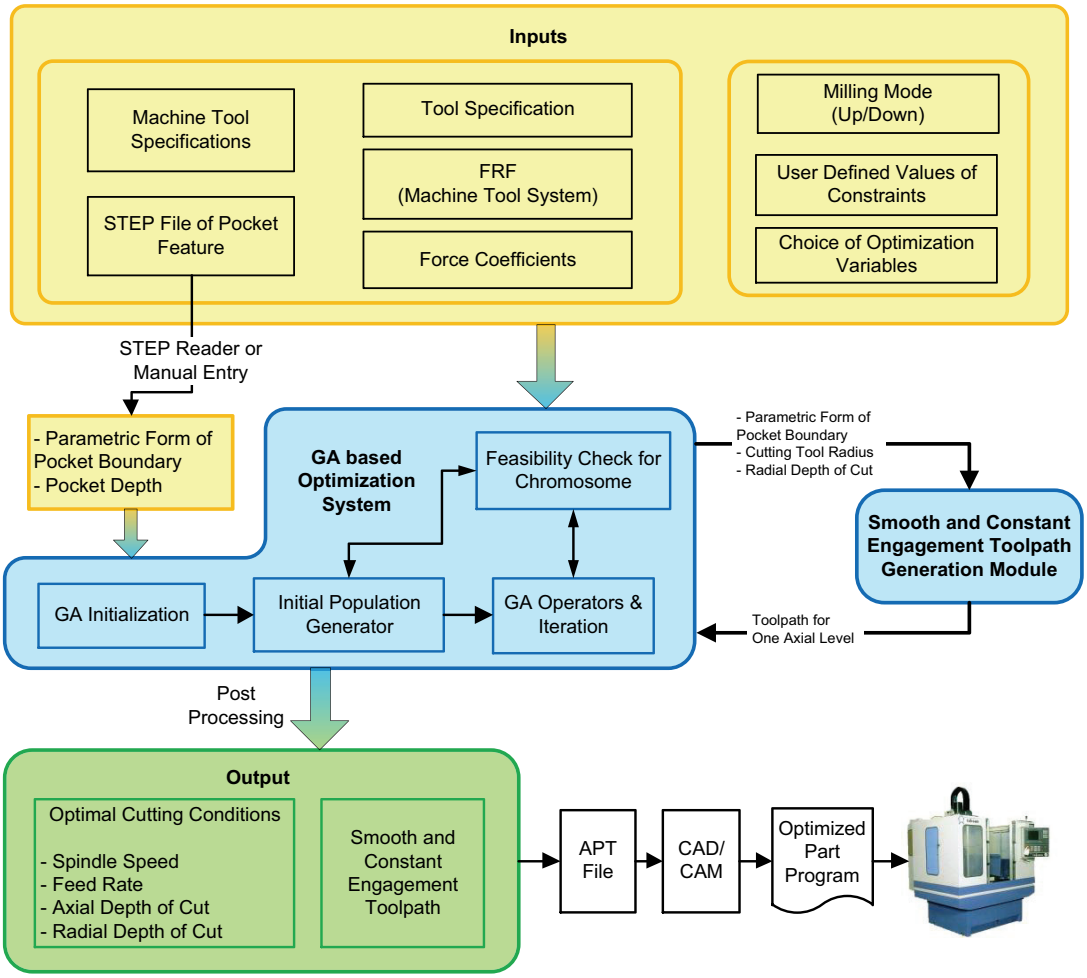

Figure 3.24: System architecture for pocket milling with smooth and constant engagement toolpaths

3.5.1 Smooth and Constant Engagement Toolpath Generation

The main steps involved in the generation of toolpaths are detailed below:

1. The main inputs to the toolpath generation module are: (a) parametric form of pocket boundary; (c) cutting tool radius; (b) step over value

2. For a given prismatic form of pocket boundary, the sign distance function is calculated using a fast marching method[4]. The region inside the pocket boundary is divided into rectangular grid points with predefined grid resolution. The sign distance function represents the distances of grid points from the pocket boundary. The sign distance function of a pocket boundary is stored in the form of a matrix named "[SignDist_Boundary]". This sign distance function is plotted in the form of a surface as shown in figure 3.25. A boundary conforming pass "(Boundary_Conforming_Pass)" is identified by finding the contour of "[SignDist_Boundary]" at cutting tool radius. "(Boundary_Conforming_Pass)" is the final pass which must be executed to achieve the desired shape of the pocket.

3. The first slot pass "(First_Slot_Pass)", which is a first pass for pocketing, is identified from "[SignDist_Boundary]". The sign distance function of "(First_Slot_Pass)" is then calculated using a fast marching method. This sign distance function is stored in the form of a matrix named "[SignDist_Slot]" and is also presented in Figure 3.25. "(First_Slot_Pass)" is the first cutting pass of the modified toolpath "(Modified_Toolpath)".

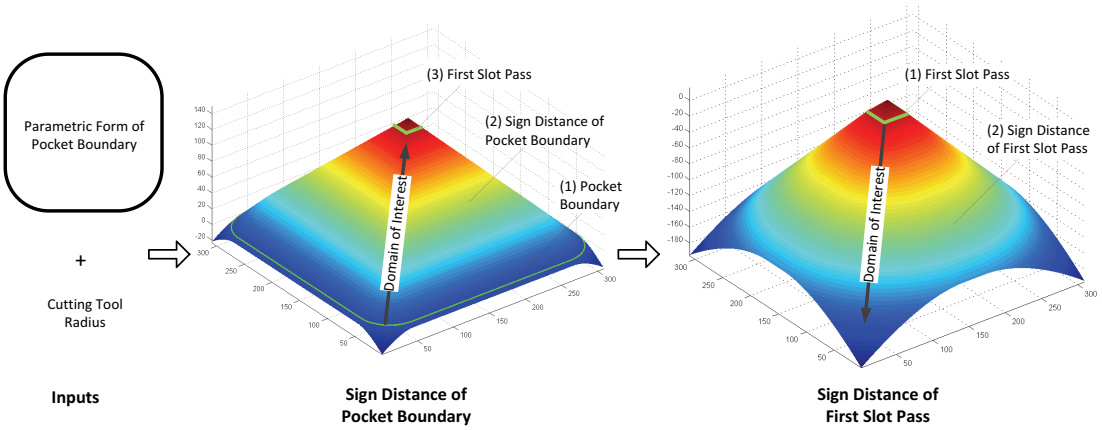

Figure 3.25: Presentation of sign distance functions

- The material boundary generated by "(First_Slot_Pass)" is identified from the contour of "[SignDist_Slot]" at cutting tool radius. The next cutting pass of the modified toolpath "(Modified_Toolpath)" is identified from the resulting material boundary generated by "(First_Slot_Pass)". This concept is presented in Figure 3.26.

[4]Details can be found in (Dhanik, 2009)

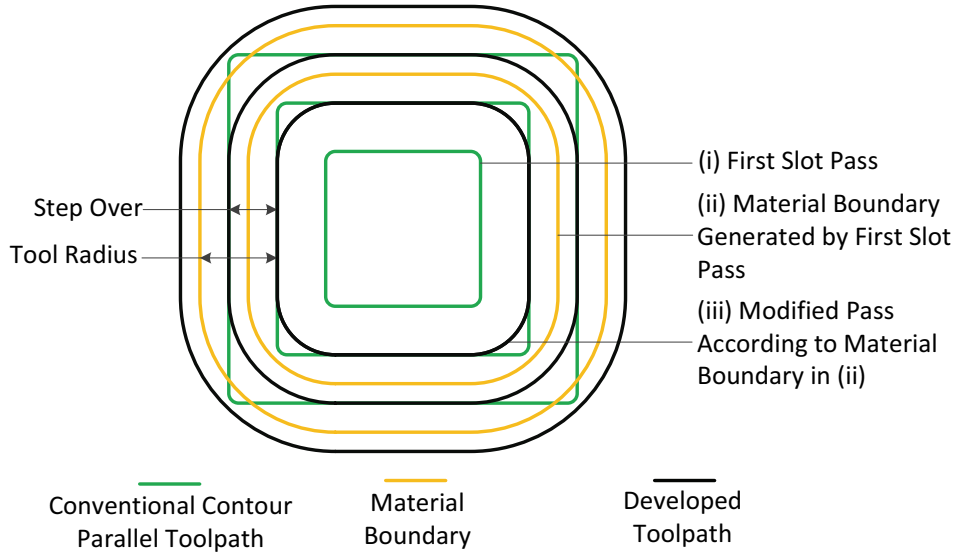

Figure 3.26: Concept of constant engagement toolpath generation, redrawn from (Dhanik, 2009)

4. An iterative loop is started to generate the successive cutting passes by extracting the contours of "[SignDist_Slot]" at a defined step over value. Every new extracted contour is termed "(Current_Pass)" and the condition in step 5 is checked everytime.

5. Intersection condition of two cutting passes: "(Boundary_Conforming_Pass)" and "(Current_Pass)". The intersection condition specifies whether "(Current_Pass)" exceeds the pocket boundary. This concept is presented in Figure 3.27. Different cases of intersection conditions implemented in the toolpath module are presented in Appendix E. If the intersection condition is met, corner looping is initiated.

   (a) From the intersection of the "(Boundary_Conforming_Pass)" and "(Current_Pass)", different corner points are identified. An array is initialized to store the ordered list of coordinates of the corner points (Points A1,B1 ... H1 as shown in Figure 3.28).

   (b) At a given corner, the coordinates of the intersecting points at different levels (A1B1 at level1, A2B2 at level2 ...) are identified. The intersecting points at different levels are identified from the intersection of "(Boundary_Conforming_Pass)" and "(Current_Pass)". At every different level, "(Current_Pass)" is modified with the next contour of "[SignDist_Slot]" at step over value. It is important to mention that depending on the shape of the pocket, there can be different numbers of corners and corresponding different numbers of levels.

   (c) Each corner loop consists of material removal passes (green lines) and returning passes (dotted lines).

6. The complete toolpath consists of all the constant step over passes and corner passes

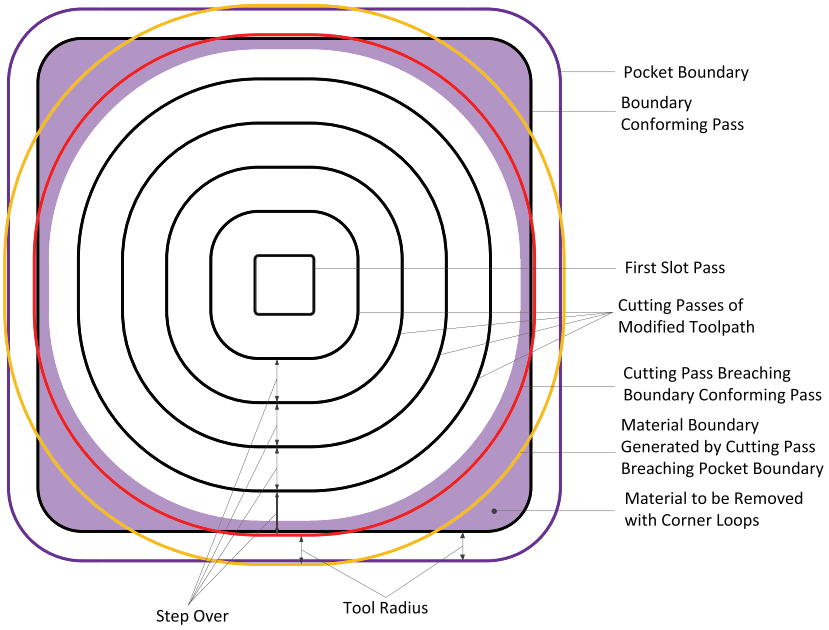

Figure 3.27: Smooth and constant engagement toolpaths, redrawn from (Dhanik, 2009)

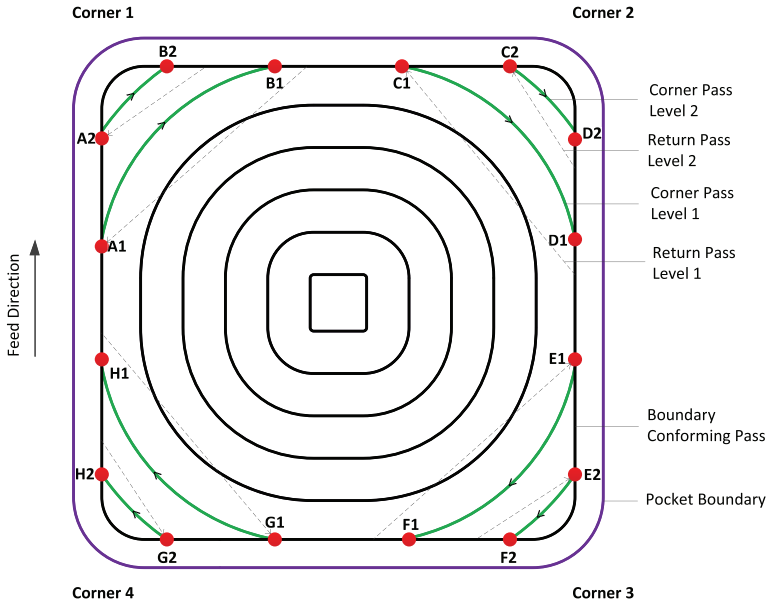

Figure 3.28: Concept of corner looping

with required linking between different passes.

The detailed algorithm for the generation of smooth and constant engagement toolpath can be found in (Dhanik, 2009).

3.5.2 Optimal Selection of Cutting Conditions and Toolpaths

In this section, the detailed steps of the development of this optimization use case are presented as:

1. The pocket boundary, extracted from a STEP file, is converted into parametric form. Pocket boundaries for simple shapes can also be defined manually. The sign distance functions of pocket boundary and first slot pass are calculated. These sign distance functions will be used to generate toolpaths (one axial level) at different radial depths of cut during the optimization analysis.

2. The GA based optimization is initiated with definition of the bounds of the optimization variables (spindle speed, feed rate, axial depth of cut) as presented in Section 3.1.1. Radial depth of cut is defined from $0.1D - D$. Here D is the diameter of the cutting tool.

3. The chromosome structure (as shown in Figure 3.1) consists of four optimization variables: spindle speed, feed rate, radial depth of cut and axial depth of cut.

4. The initial population is created with randomly generated feasible chromosomes (the algorithm is presented in Figure 3.2). The feasibility of each chromosome is checked against all the constraints defined in Section 3.2. For every chromosome, the SLDs in feed and normal to feed directions are identified at fixed value of radial depth of cut (mapped value from the chromosome). The minimum value of stable axial depth of cut and spindle speed combinations are identified from the generated SLDs in feed and normal to feed direction. At a given spindle speed (mapped value from chromosome), the limiting value of the axial depth is compared with selected axial depth of cut (mapped value from the chromosome).

5. For each feasible chromosome, a smooth and constant engagement toolpath for one axial level is generated at the selected radial depth of cut (mapped value from the chromosome). The machining time to mill the complete pocket is defined as:

$$T_{mac} = \frac{ceil\left(\frac{D_p}{A_p}\right)\left(L_{toolpath_{oneaxialpass}}\right)60}{nf_tN} \tag{3.34}$$

   Here, $L_{toolpath_{oneaxialpass}}$ is the length of the constant step over toolpaths for one axial level. The complete toolpath consists of the same toolpath at different axial passes. D_p is the depth of the pocket. The minimization of machining time problem is converted into a maximization problem. The fitness value for each feasible chromosome is calculated as:

$$f = \frac{1}{1 + T_{mac}} \tag{3.35}$$

6. The next generation (new population) from the current population is generated by using various GA operators (reproduction, crossover and mutation) as described in Section 3.1.2. The iteration loop for the GA will be run until the predefined number of generations (G_{size}) is met.

7. The output of the optimization system is optimal values of cutting conditions: spindle speed, feed rate, axial and radial depths of cut and corresponding toolpaths for the complete pocket.

8. The optimal value of the axial depth of cut is readjusted for even distribution by maintaining the same number of axial passes (noap) and is computed by:

$$A_p^{'} = \left(\frac{D_p}{\text{noap}}\right) \quad \text{where} \quad \text{noap} = ceil\left(\frac{D_p}{A_p}\right) \tag{3.36}$$

9. The complete toolpaths (generated with optimal value of radial depth of cut and number of axial levels) and optimal value of spindle speed and feed rate are written in APT format. This APT file is imported into the CAM system to generate the NC codes. These NC codes are then executed on a CNC machine to machine the required pocket.

The developed optimization use case is published as an international patent application under Patent Cooperation Treaty (PCT) (Aggarwal et al., 2012a)[5].

3.6 Conclusion

The overall productivity of the milling process is related to the performance of part programs which is directly proportional to the selection of cutting conditions and toolpath.

A genetic algorithm based optimization system, OptMill (Optimal Mill), is developed for the optimal selection of cutting conditions and/or toolpath at the part programming stage. Operational constraints of the machine tool, such as available cutting power and torque, chatter vibration limits due to the dynamic interaction between cutting tool and workpiece, acceptable limits of bending stress and deflection of the cutting tool and clamping load limits of the workpiece system are embedded in the optimization model. The developed system is a significant step toward narrowing the gap between virtual machining on CAD/CAM system and actual machining on CNC machine tools.

The enhanced capabilities of the developed optimization system in terms of definition of practical search space, encoded GA optimization variables and operators, targeted cutting conditions and embedded constraints are demonstrated with the development of three different optimization use cases. The different modules of the optimization system are developed

[5]Aggarwal, S., Dhanik, S. and Xirouchakis, P., High speed pocket milling optimisation, WO Patent 2012/107594 A1

in a generic way so that the overall system can satisfy different optimization use cases and user requirements.

Use Case 1: Optimization System for Pocket Milling with One-Way Toolpath: For given pocket dimensions, material and machine tool/spindle/tool holder/cutting tool system, pocket milling time is minimized for a one-way toolpath with the optimal selection of spindle speed, feed rate, axial and radial depth of cut while respecting various constraints.

The developed optimization use case is compared with other studies available in the literature ((Shunmugam et al., 2000; Dereli et al., 2001; Tandon et al., 2002; Tekeli and Budak, 2005)), and it demonstrates significant contributions in terms of targeted cutting conditions (optimization variables) and important practical constraint considered in the developed optimization model.

Use Case 2: Optimization System for Prismatic Part: For a given multi-feature prismatic part and machine tool/spindle/tool holder/cutting tool system, machining time is minimized by optimal selection of spindle speed, feed rate and axial depth of cut while respecting various constraints.

The developed optimization use case contributes as compared to (Heo et al., 2010; Rai et al., 2009) by considering the limiting values of radial depth of cut due to variation of engagement angle along the toolpath and important constraints. Moreover, the developed optimization system takes into account the toolpath geometry generated from the CAD/CAM system. The effect of change in stable depths of cut along different machine tool axes due to different dynamics characteristics is also modeled in the developed optimization model.

Use Case 3: Optimization System for Pocket Milling with Smooth and Constant Engagement Toolpaths: For a given machine tool/spindle/tool holder/cutting tool system and a convex pocket, the pocket milling time is minimized by optimal selection of all cutting conditions (spindle speed, feed rate, axial depth of cut and radial depth of cut) and corresponding smooth and constant engagement toolpath while respecting all embedded constraints. There is no such study available which considers the optimal selection of cutting conditions and corresponding smooth and constant engagement toolpath for pocket milling.

This novel approach is a significant contribution towards achieving the highest overall productivity for pocket milling.

4 Implementation and Experimental Validation of the Optimization System

4.1 Implementation of Optimization Use Case 1

The developed optimization use case1 is implemented to identify optimal cutting conditions for different pocket sizes. Details of the implementation are presented in the following subsections:

4.1.1 Definition of Various Inputs

All the input data for this optimization use case are presented as:

- A 6-axis vertical machine tool C.B.Ferrari A152 (shown in Figure 4.16) was used for the experiments. The machine tool is capable of rotational speeds up to 30000rpm, axis acceleration up to $5 m/s^2$ and feed speeds up to 50m/min. The rated power of the spindle is 12kW (constant power curve in the desired range of spindle speed).
- The specifications of the end mill used for machining are presented in Table 4.1.

Table 4.1: Specifications of the cutting tool (16mm end mill)

D	β	N	L_{tool}	$L_{cutting}$
(mm)	(deg)		(mm)	(mm)
16	40	2	92	26

- The material of the workpiece was Al-7075.
- Force coefficients for the given cutting tool and workpiece material combination are presented in Table 4.2. Force coefficients are experimentally identified by performing slot cutting tests at different feed rate values. For every slot cutting test, cutting forces in feed, normal to feed and axial directions are measured with a force dynamometer. Details of the identification of force coefficients are presented in Appendix B.

Table 4.2: Cutting force coefficients

K_{tc}	K_{rc}	K_{ac}	K_{te}	K_{re}	K_{ae}
(N/mm^2)	(N/mm^2)	(N/mm^2)	(N/mm)	(N/mm)	(N/mm)
681	86	218	12	19	2

- Frequency response functions of the specified machine tool/spindle/tool holder/cutting tool system are measured at the cutting tool tip with hammer impacts. FRFs are measured in feed and normal to feed directions. Details of the FRF measurement is explained in Appendix C. Measured FRFs in feed and normal to feed directions are presented in Fig. 4.1.

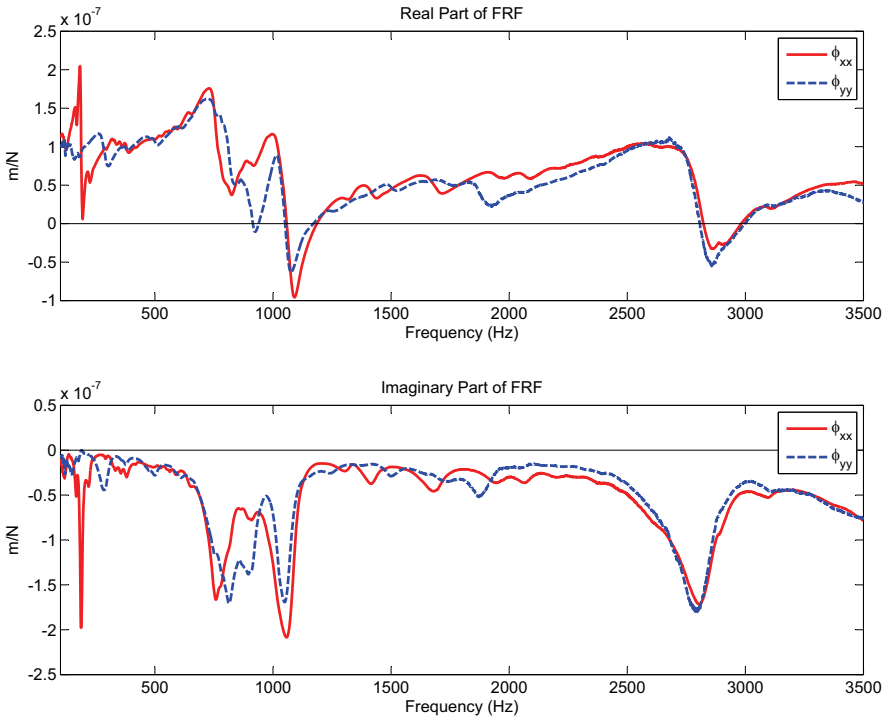

Figure 4.1: Experimentally measured frequency response function

- The clamping load limit is defined as 1500N, allowable cutting tool deflection is fixed as 0.15mm and permissible bending stress is taken as 2683MPa.

- The preferred milling mode is selected as up-milling.

- By choice, all cutting conditions were selected as optimization variables.

4.1.2 Tuning of the Optimization System

The bounds of cutting conditions, spindle speed is 10000–30000rpm, feed rate is 0.05–0.2mm/rev-flute, radial depth of cut is 0–16mm and axial depth of cut is 0–25mm, were selected for GA initialization.

The various GA parameters (population size (P_{size}), crossover probability (C_{prob}), mutation probability (M_{prob}) and generation size (G_{size})) are tuned by investigating their influence on pocket machining time. Convergence analysis for different GA parameters were performed for pocket size (150x150x25). Simulations were run by varying each GA parameter and keeping the others constant. For each variation, two simulations were run and the average milling time was calculated.

The convergence results for different values of generation size and population size are presented in Figure 4.2(a) and Figure 4.2(b) respectively. Based on convergence results, a generation size (G_{size}) of 100 and population size (P_{size}) of 20 was selected. It is important to mention that increasing the values of G_{size} and P_{size} significantly increases the computational time so their proper selection is necessary. Crossover probability was set to 90% and the results of the convergence are presented in Figure 4.2(d). Mutation probability has only a small influence on the optimal machining time as presented in Figure 4.2 (c) and its value is set to 4%. Elitism size of 2 is used during the optimization analysis.

4.1.3 Results of the Simulation

The optimization use case was implemented to identify the optimal cutting conditions for pockets of different sizes. The results are presented in Table 4.3. Predicted values of the constraints with each set of cutting conditions are also presented. This shows that identified cutting conditions respect the permissible limits of the constraints.

Convergence results of GA analysis for a pocket (150x150x25) are presented in Figure 4.3. Figure 4.3(a)(b)(c) and (d) present respectively the values of spindle speed, feed rate, axial depth of cut and radial depth of cut with increase in generations. The convergence results of fitness values and machining time are presented in Figure 4.3(e)(f).

The optimal cutting conditions selected from the developed optimization use case were also verified experimentally (Section 4.5).

Table 4.3: Optimal cutting conditions for different pockets

$L_p/W_p/D_p$	$n/f_t/A_p/A_e$	norp/noap/nop	$A_p^{'}/A_e^{'}$	T_{mac}	P_c	T_c	σ_b	δ	A_{plim}	F_{clamp}
150/150/25	23986/0.1548/5/14.98	8/5/40	5/14.75	38.14	11.67	4.6	174.7	0.07	11.1	621.8
100/160/60	13175/0.1190/22.66/8.63	15/3/45	20/8.53	58.53	11.2	8.1	256	0.06	24.8	997
170/100/20	16667/0.1667/6.67/14.73	5/3/15	6.67/ 13.60	22.36	11.47	6.57	242.1	0.09	22.5	870.8
140/140/38	12858/0.1810/22.29/6.10	8/5/40	19/6	50.13	11.15	8.26	270.2	0.05	33.2	1045.7

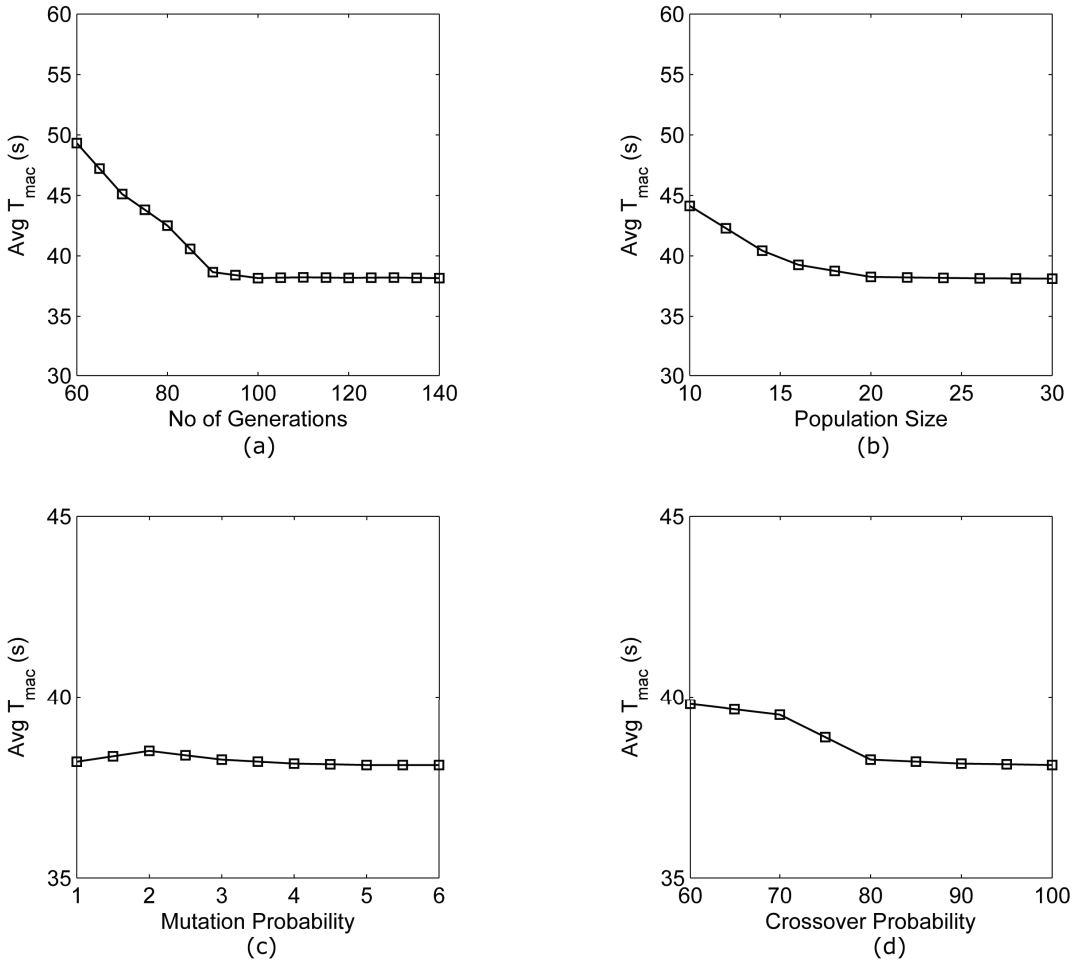

Figure 4.2: Effect of GA parameters on machining time

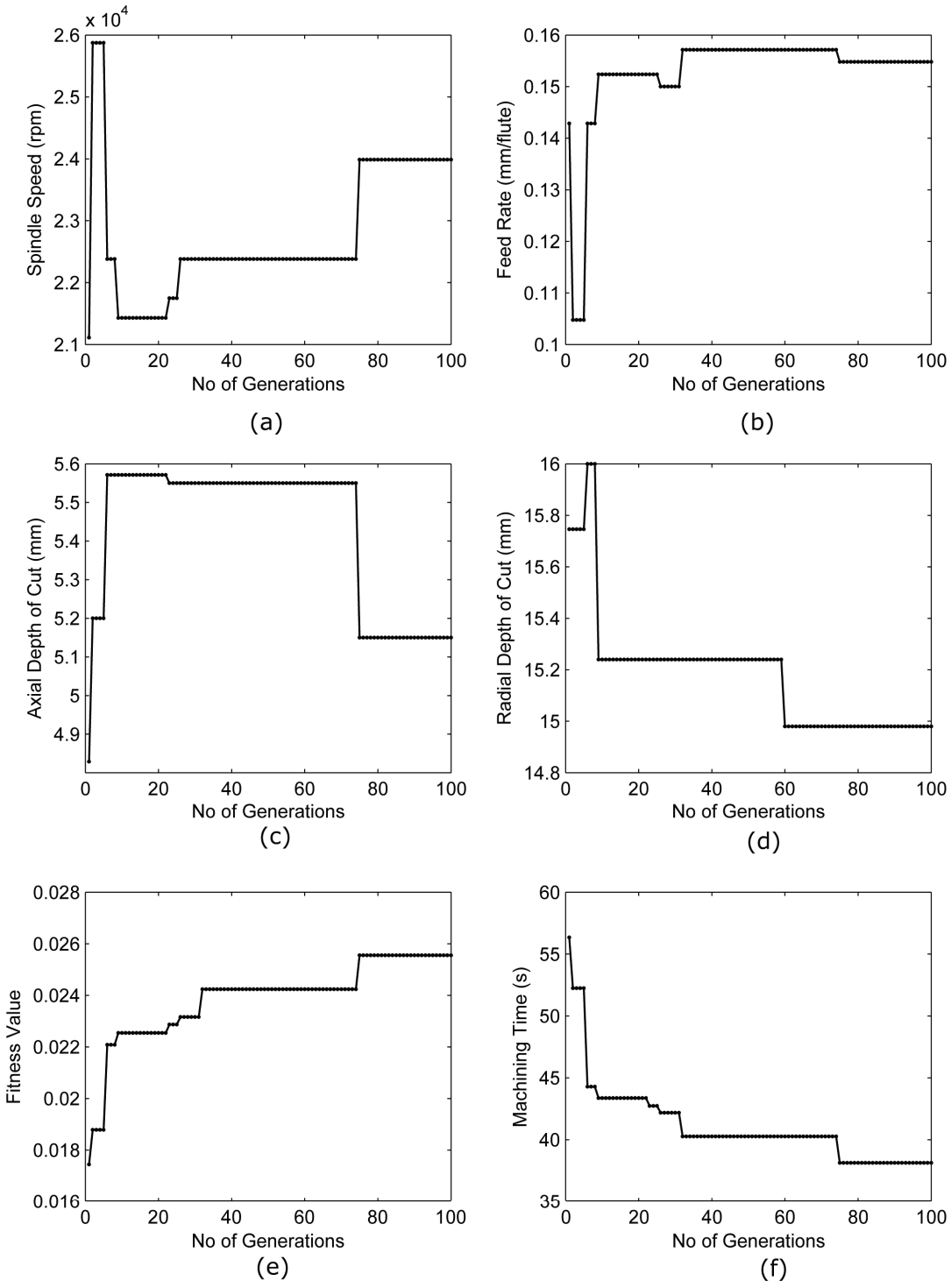

Figure 4.3: Convergence of cutting conditions

4.2 Implementation of Optimization Use Case 2

4.2.1 Definition of Various Inputs

- A 6-axis vertical machine tool C.B.Ferrari A152 was used for the experiments.
- The specifications of the end mill used are presented in Table 4.4.

Table 4.4: Specifications of the cutting tool (20mm end mill)

D	β	N	L_{tool}	$L_{cutting}$
(mm)	(deg)		(mm)	(mm)
20	40	2	104	32

- The dimensions of the prismatic part are presented in Figure 4.4a. The prismatic part is chosen from (Avram, 2010). In that study, the right selection (chatter free) of cutting conditions were made under the scope of present work. The prismatic part consists of two manufacturing features: pocket and contour. The feature depth for the pocket and contour are 15mm and 25mm respectively. The geometrical information of the prismatic part is extracted from APT and STEP files. The extracted toolpath for one axial level for pocketing and contouring are presented in Figure 4.4b and Figure 4.4c .

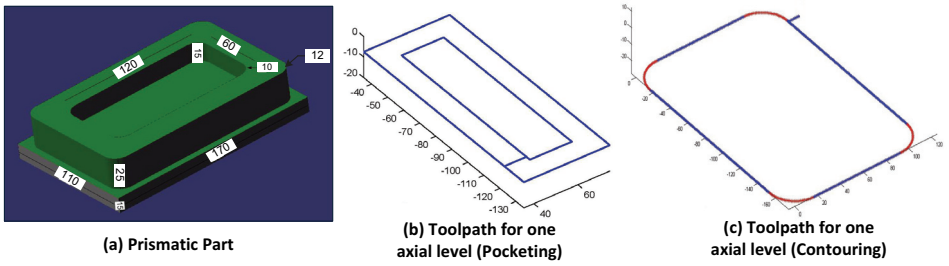

Figure 4.4: Toolpath for pocket milling

The length of the toolpath for one axial level for pocket is computed as 496mm. The calculated engagement angle along the toolpath for the pocket is shown in Figure 4.5. The radial depth of cut for optimization analysis for pocket is kept fixed as full immersion (20mm).

- The length of the toolpath for one axial level for feature is computed as 571mm. The calculated engagement angle along the toolpath for contour is shown in Figure 4.6. The maximum value of the engagement angle along the contouring toolpath is ~89.2deg. Radial depth of cut for optimization analysis for contouring is kept fixed as half immersion (9.8mm).
- The material of the workpiece was Certal (AlZnMgCu0.5/EN AW-7072).

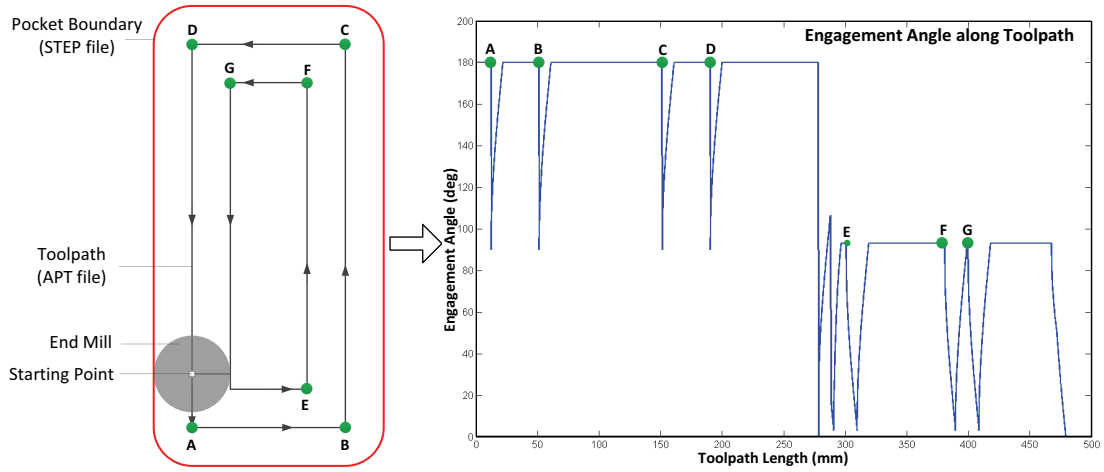

Figure 4.5: Engagement angle for pocket

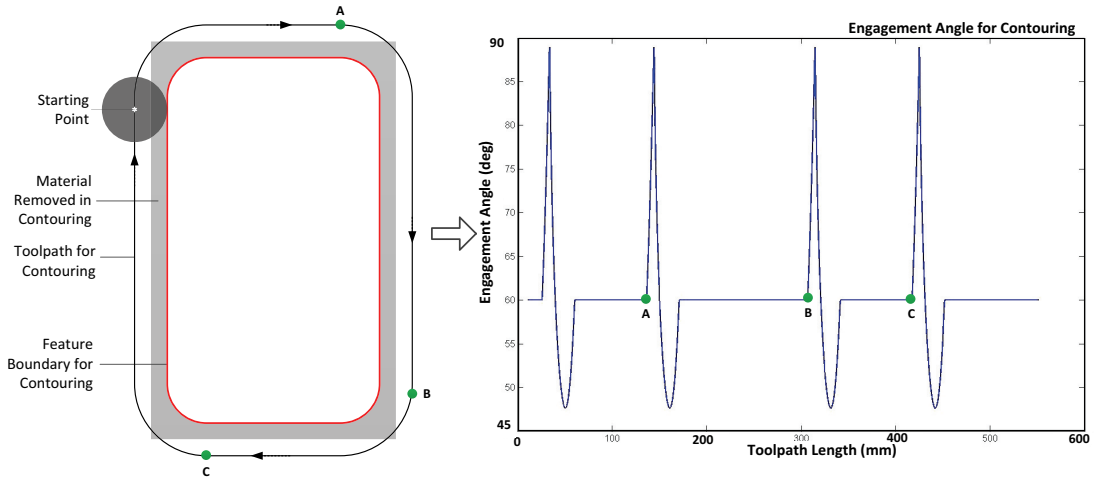

Figure 4.6: Engagement angle for contouring

Table 4.5: Cutting force coefficients

K_{tc}	K_{rc}	K_{ac}	K_{te}	K_{re}	K_{ae}
(N/mm^2)	(N/mm^2)	(N/mm^2)	(N/mm)	(N/mm)	(N/mm)
796	168	222	27	30	2

- Force coefficients for the given cutting tool and workpiece material combination are presented in Table 4.5.
- Measured FRFs of the used spindle/tool holder/end mill system in the feed and normal to feed directions are presented in Figure 4.7.
- The clamping load limit is defined as 1500N, allowable cutting tool deflection is fixed as 0.15mm and permissible bending stress is taken as 2683MPa.

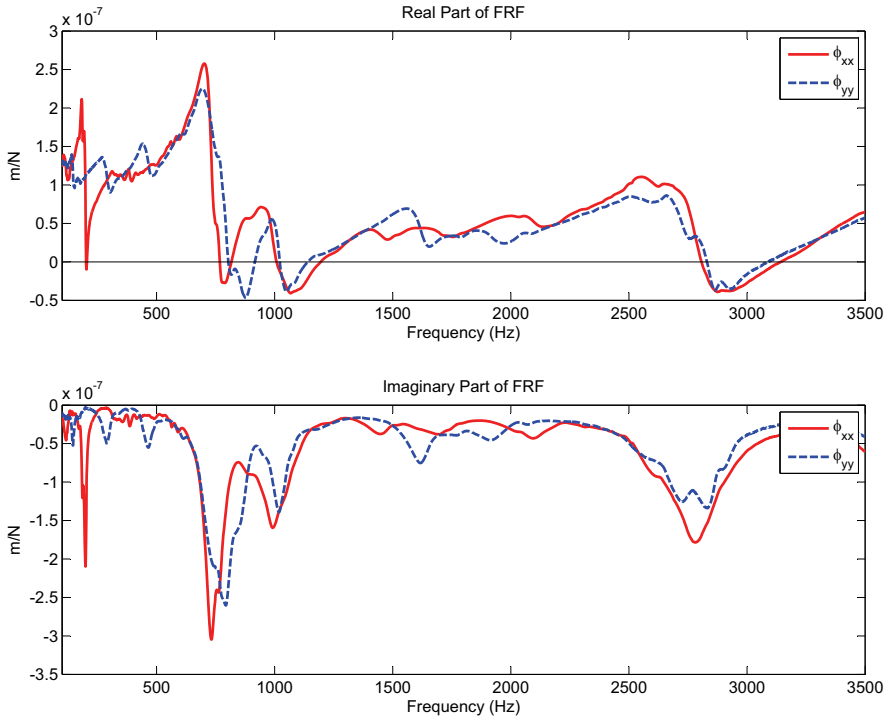

Figure 4.7: Experimentally measured frequency response function

4.2.2 Results of the Simulation

Simulations of the optimization analysis for pocket and contouring are performed at fixed value of the radial depth of cut at 20mm and 10mm respectively. Spindle speed, feed rate and axial depth of cut are the optimization variables. The range of spindle speed and feed rate are defined as 10000–20000rpm and 0.05–0.15mm/rev-flute respectively. The range of axial depth of cut for pocketing and contouring are chosen as 0–15mm and 0–25mm respectively. Generation size (G_{size})of 70 and a population size (P_{size}) of 20 is selected. Crossover and mutation probability are set as 90% and 4% respectively. Elitism size of 2 is used during the optimization analysis. The convergence result of machining time and corresponding values of spindle speed, feed rate, axial depth of cut for pocket are presented in Figure 4.8. The corresponding cutting conditions for contour milling are identified as spindle speed=19524rpm, feed rate=0.1022mm/flute, Axial depth of cut=12.7mm. The readjusted value of axial depth of cut for the same number of axial passes is selected as 12.5mm.

4.2.3 Reduction in Machining Time

Cutting conditions for pocket milling are also selected by a machine user on the production floor based on his/her experience and guidance from a cutting tool catalogue. The chosen values of cutting conditions by the machine user and selected values of cutting conditions with the developed optimization system are compared in Table 4.6. The toolpath geometry for

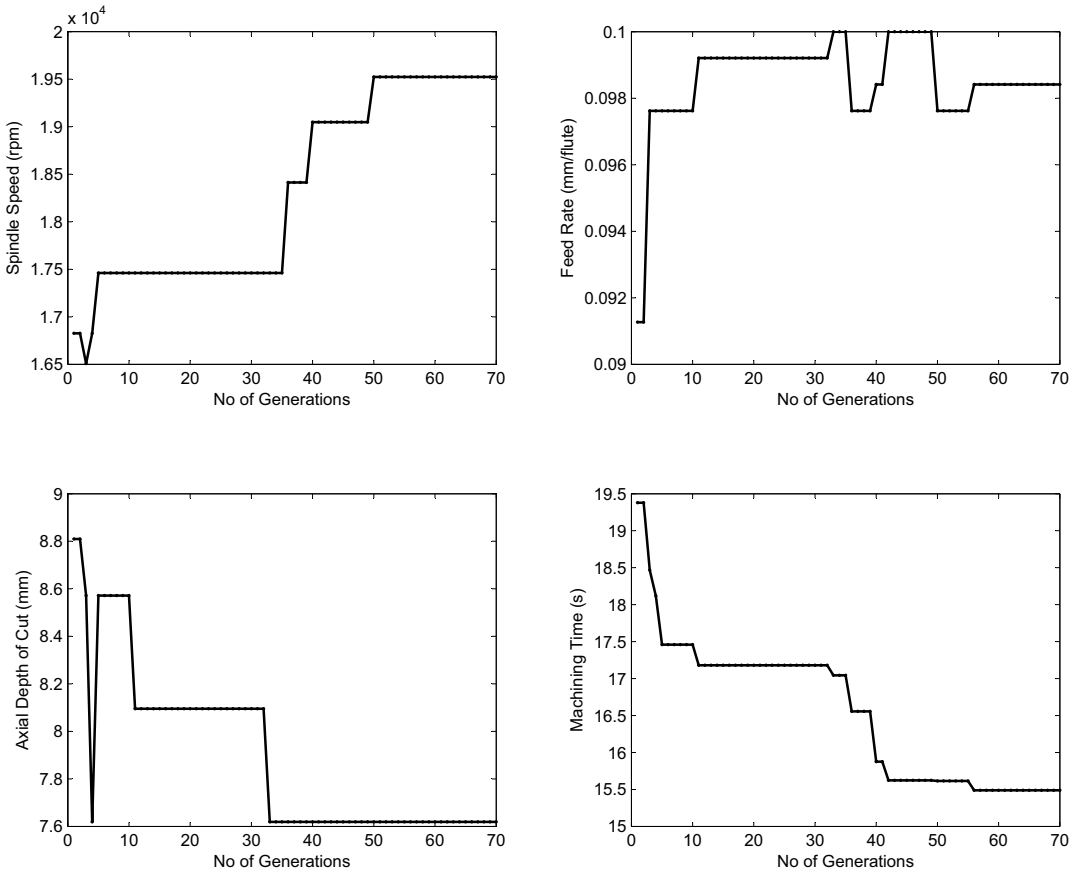

Figure 4.8: Convergence of cutting conditions for pocket

one axial level is the same for both cases. The machining time for complete toolpaths (with corresponding cutting conditions) for both cases is identified from a CATIA simulation. It is concluded that significant reduction in machining time is achieved.

Table 4.6: Reduction in machine time

Cutting Conditions (Production Floor)				Cutting Conditions (Optimization System)				Reduction
n	A_p	noap	T_{mac}	n	A_p	noap	T_{mac}	%
rpm	mm		s	rpm	mm		s	
14000	5	3	38.6	19524	7.5	2	20.2	**47.6**

'noap' is number of axial passes, f_t is 0.1mm/rev-flute

The optimal cutting conditions selected from the developed optimization use case are also verified experimentally (Section 4.6).

4.3 Implementation of Optimization Use Case 3

4.3.1 Definition of Various Inputs

- The dimensions of the pocket are presented in Figure 4.9. Parametric form is calculated from the extracted pocket boundary from STEP file.

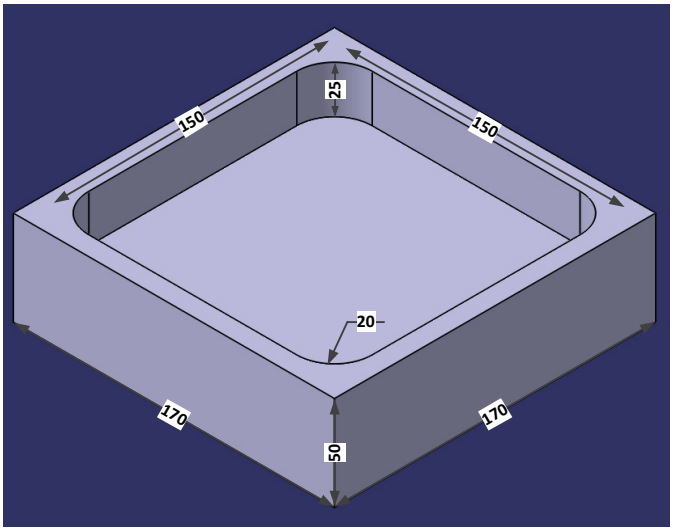

Figure 4.9: Dimensions of the pocket used for validation

- A 6-axis vertical machine tool C.B.Ferrari A152 (as shown in Figure 4.16) was used for experiments.
- The specifications of the end mill used for machining are presented in Table 4.1.
- The material of the workpiece was Al-7075.
- Force coefficients for the given cutting tool and workpiece material combination are presented in Table 4.2.
- Measured FRFs in feed and normal to feed directions are presented in Fig. 4.1.

4.3.2 Results of the Simulation

During the optimization simulation, the toolpath at one axial level is generated at given radial depth of cut (mapped value from the chromosome) for every feasible chromosome. There are large number of feasible chromosomes generated during the optimization analysis. Generation of toolpath for every feasible chromosome is not an efficient approach as the toolpath generation algorithm is computationally expensive.

To achieve better computational efficiency, the toolpath for one axial level is generated at different stepover values (1mm to 16mm with an increment of 0.5mm). Toolpaths at different

step over values, generated using the smooth and constant engagement toolpath generation module, are presented in Figure 4.10. The toolpath lengths at different stepover values are also identified. The toolpath length against different values of stepover and corresponding computational time is presented in Figure 4.11. During the optimization simulation, at different radial depth of cut (mapped value from the chromosome), the toolpath length for one axial level is calculated by interpolation from the data presented in Figure 4.11.

Simulation of the optimization use case is performed with generation size (G_{size})of 100 and a population size (P_{size}) of 20, crossover and mutation probability as 90% and 4% respectively. Elitism size of 2 is used during the optimization analysis. The convergence result of machining time and corresponding values of spindle speed, feed rate, axial and radial depths of cut are presented in Figure 4.12. The optimal value of spindle speed is 24290rpm, feed rate is 0.15mm/flute, axial depth of cut is 5.2mm and radial depth of cut is 12.5mm. The post processed value of axial depth of cut is 5mm. The number of axial levels is 5.

The toolpath for one axial level is used to create the toolpath for entire pocket. The output from the optimization analysis is optimal cutting conditions and corresponding toolpaths for the entire pocket milling. The complete toolpath for pocket milling are shown in Figure 4.13 This output is written in APT format. NC codes are generated from this APT file with some post processing in a CAM system.

The optimal cutting conditions selected from the developed optimization use case are also verified experimentally (Section 4.7).

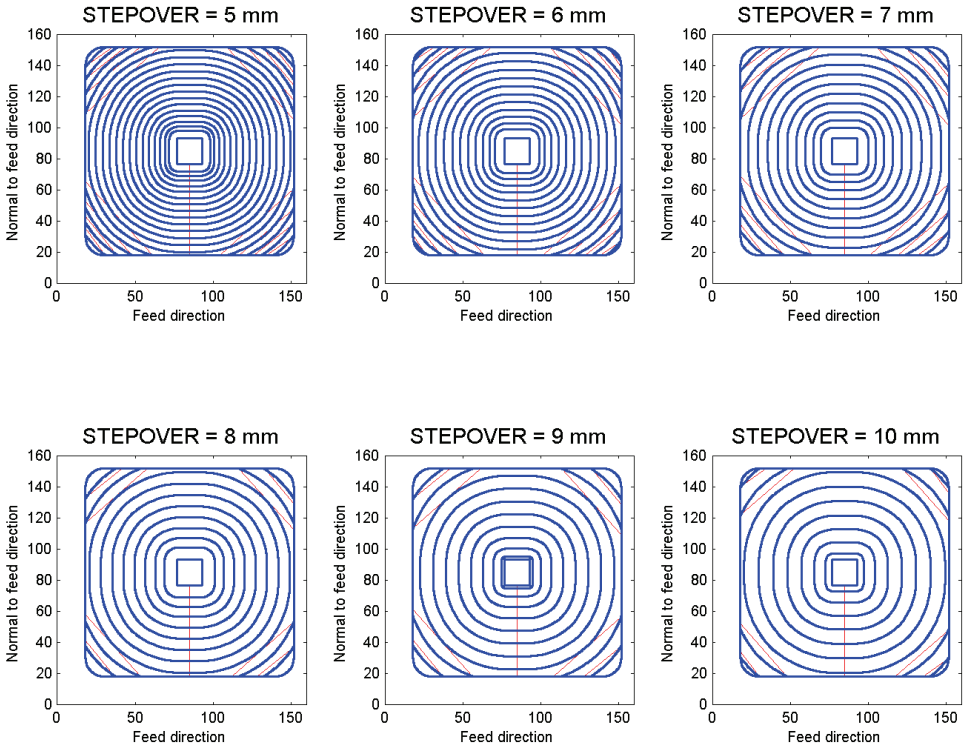

(a) Toolpath at different stepover values (5–10mm)

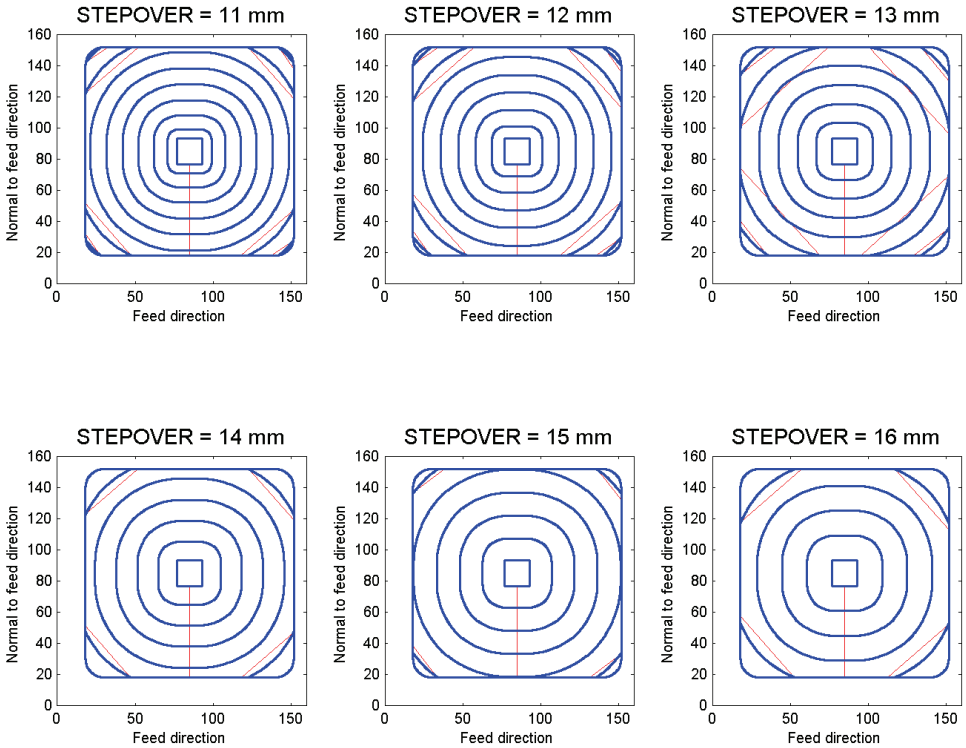

(b) Toolpath at different stepover values (11–16mm)

Figure 4.10: Toolpath at different stepover values

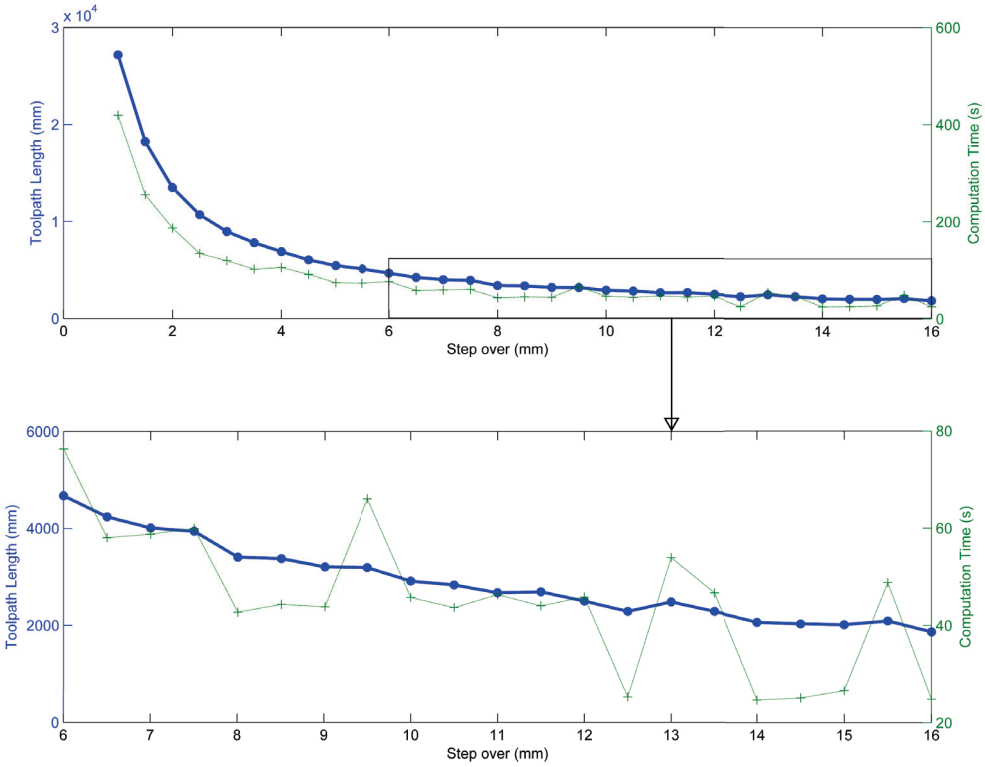

Figure 4.11: Toolpath length and computation time at different stepover

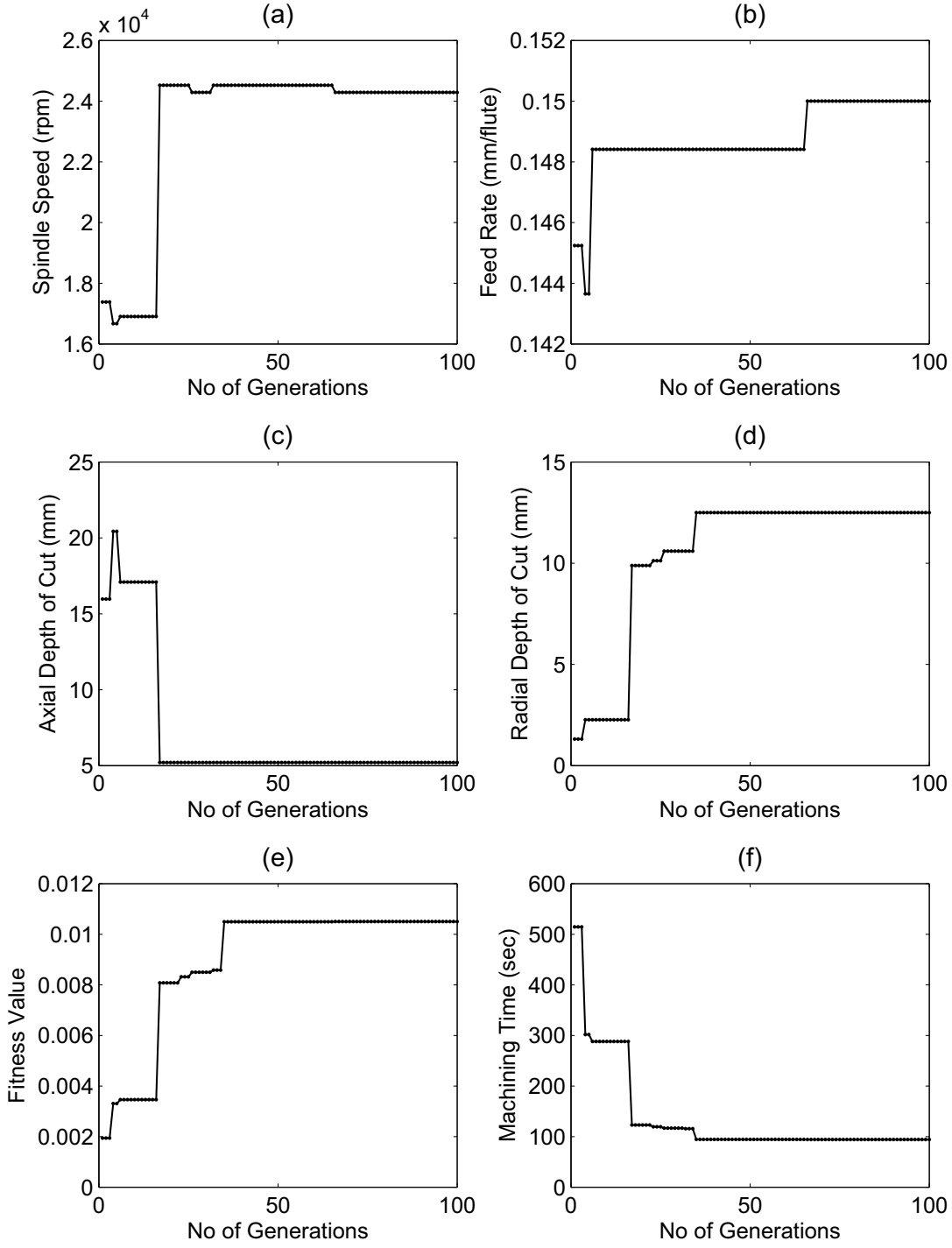

Figure 4.12: Convergence of cutting conditions for pocket milling

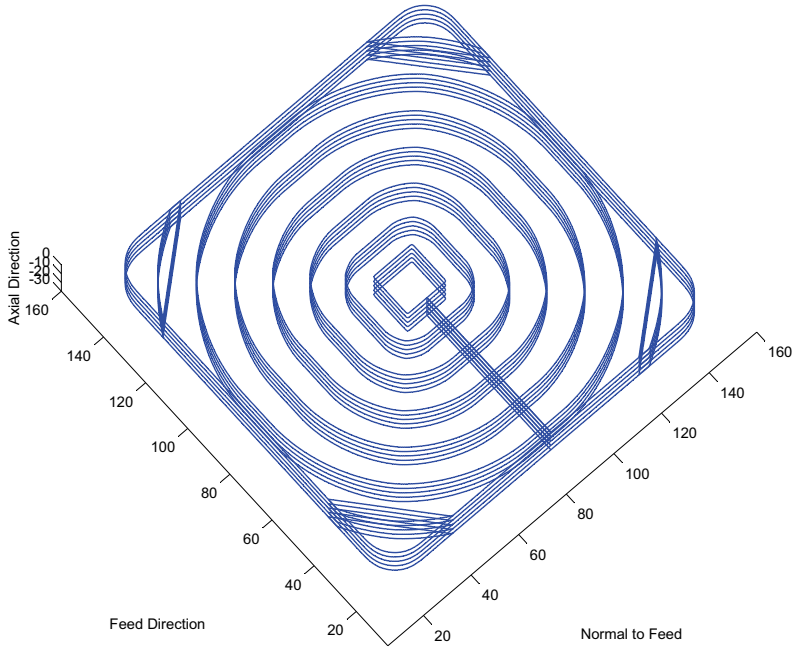

Figure 4.13: Complete constant engagement and smooth toolpath for pocket milling

4.4 Experiment Setup

Optimal values of cutting conditions selected from the developed optimization system are also validated experimentally. The experimental setup consists of the following subsystems and corresponding measurements:

- FRF measurement with impact hammer (Kistler 9722A500) and accelerometer (Kistler 8776A50)
- Measurement of cutting forces with cutting force dynamometer (Kistler 9255B) and amplifier (Kistler5070A10100)
- Recording of cutting sound with microphone (Shure PG81)
- Measurement of total power consumption with power sensor (Power Cell PPC-3)

The data acquisition platform is developed in LabVIEW 2010. FRF measurement is performed with (CutPro, 2008). Analysis of the measured signals is performed in (MATLAB, 2011). The overall experimental setup is presented in Figure 4.14.

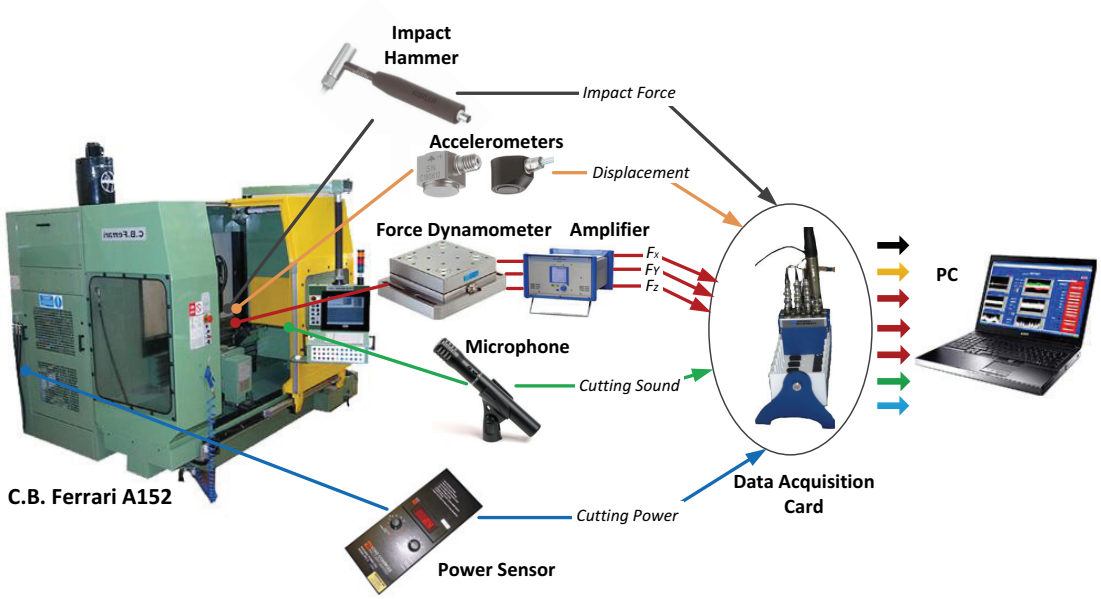

Figure 4.14: Overall experimental setup for validation of optimization system

Mounting of different sensors and the data acquisition system for the validation is presented in Figure 4.15.

In the following subsections the details of various subsystems are presented.

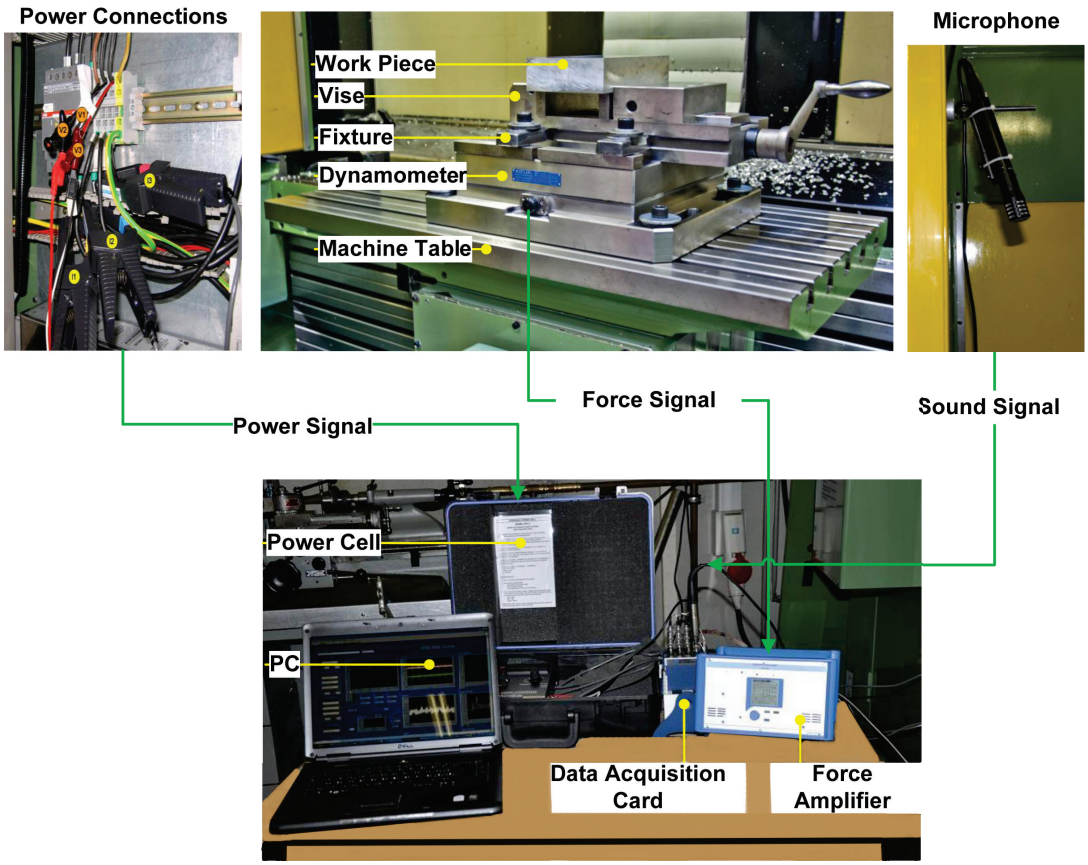

Figure 4.15: Experimental setup: mounting of sensors and data acquisition system

4.4.1 Machine Tool System

Cutting tests were performed on a 6-axis vertical machine tool C.B.Ferrari A152 as shown in Figure 4.16. The machine tool is capable of rotational speeds up to 30000rpm, axis acceleration up to $5m/s^2$ and feed speeds up to 50m/min. The rated power of the spindle is 12kW (constant power curve). The machine tool is equipped with numerical controller Elexa E580.

4.4.2 FRF Measurement

FRFs of the machine tool/spindle/tool holder/ cutting tool system at the cutting tool tip are measured using hammer testing. The corresponding experimental setup is presented in Figure 4.17. The experimental setup includes the impact hammer, an accelerometer and data acquisition system. The system is excited at the cutting tool tip by hammer impact and the corresponding response of the system is measured at the cutting tool tip by an accelerometer. The details of the experimental setup are presented in Appendix C.

Figure 4.16: C.B. Ferrari A152 machine tool

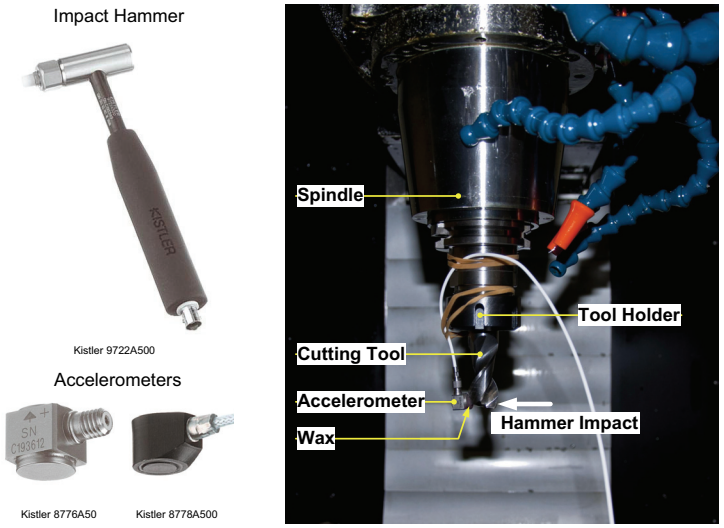

Figure 4.17: FRF measurement: hammer, accelerometer (Kistler, 2010) and their mounting

4.4.3 Cutting Sound Measurement

Optimally selected cutting conditions are validated against stability of the milling process for a given set of inputs. To detect the existence of chatter vibrations during milling of different workpieces, cutting sound signal is used as a chatter indicator. A shure microphone (PG81) is used to record the cutting sound during machining. The microphone has wide and uniform flat frequency response. The microphone is installed inside the machine tool casing and next to the cutting zone in order to reduce the effect of environmental noise. The microphone and its corresponding frequency response is shown in Figure 4.18.

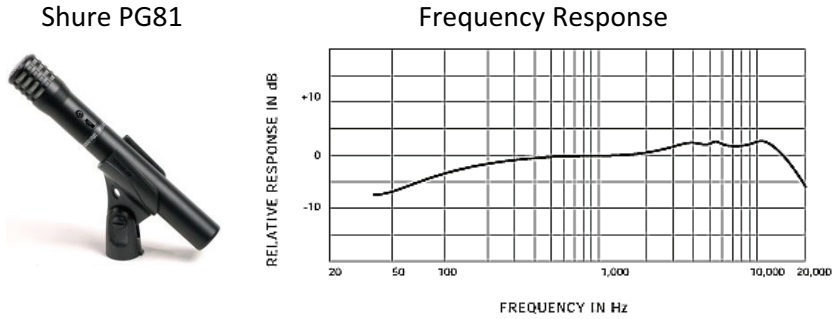

Figure 4.18: Shure microphone PG81 (Shure, 2010)

4.4.4 Cutting Force Measurement

Cutting forces in feed, normal to feed and axial directions are recorded with the help of cutting force dynamometer. The dynamometer system consists of a dynamometer, multi-channel charge amplifier and the connection cable. The dynamometer is clamped between the workpiece and table of the machine tool as shown in Figure 4.15. The dynamometer provides measurement of three orthogonal components of force acting from any direction on the top plate as presented in the detailed drawing of the dynamometer shown in Figure 4.19.

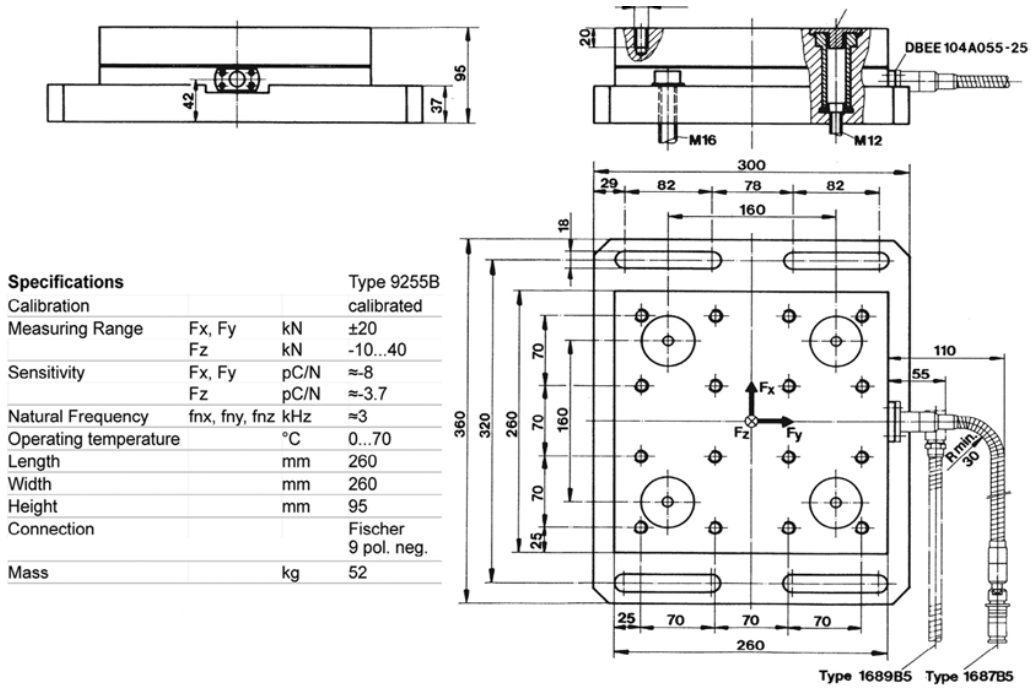

Specifications			Type 9255B
Calibration			calibrated
Measuring Range	Fx, Fy	kN	±20
	Fz	kN	-10...40
Sensitivity	Fx, Fy	pC/N	≈-8
	Fz	pC/N	≈-3.7
Natural Frequency	fnx, fny, fnz	kHz	≈3
Operating temperature		°C	0...70
Length		mm	260
Width		mm	260
Height		mm	95
Connection			Fischer 9 pol. neg.
Mass		kg	52

Figure 4.19: Multi-component piezoelectric dynamometer, Kistler 9255B (Kistler, 2010)

4.4.5 Cutting Power Measurement

Cutting power is measured during the cutting experiments by a power cell PPC-3 as presented in Figure 4.20. The installation of the different cables is presented in Figure 4.15. Due to the inaccessibility of the spindle motor, the power cell measures the total power consumed by the machine tool. For the present work, the power used for cutting is identified by subtracting the power used to run the spindle at given spindle speed from the total power measured by the power cell. A detailed description of the experimental setup can be found in (Avram, 2010).

Figure 4.20: Power cell PPC-3 (LoadControls, 2010)

4.5 Validation of Optimization Use Case 1

A rectangular pocket with dimensions 150mm x 150mm x 25mm with 8mm corner radius is milled to verify the optimal cutting conditions identified in Section 4.1. Spindle speed during the experiment is 24000rpm, feed rate is 0.1548mm/rev-flute, axial depth of cut is 5mm and radial depth of cut is 14.75mm.

Cutting sound, cutting forces in feed and normal to feed direction collected along one pass are shown in Figure 4.21(a)(b) and (c). The fast Fourier transform (FFT) of cutting sound and cutting force signals are also shown. Tooth passing frequency is 800Hz ($24000 * 2/60$) and spindle frequency is 400Hz ($24000/60$). It is evident that the cutting conditions are stable (chatter free) since there is no dominant frequency peak other than the spindle frequency, tooth passing frequency and their harmonics (Delio et al., 1992). Due to the high run out present in the machine tool, the spindle frequency is visible in the FFT plots of various signals. Higher values of the cutting forces are experienced than predicted which is due to the high run out in the machine tool.

The power consumed during cutting is found by subtracting the power spent to rotate the spindle at the selected spindle speed from the measured value of total power. Cutting power is

below the permissible limit of available power of 12kW as presented in Figure 4.21(d).

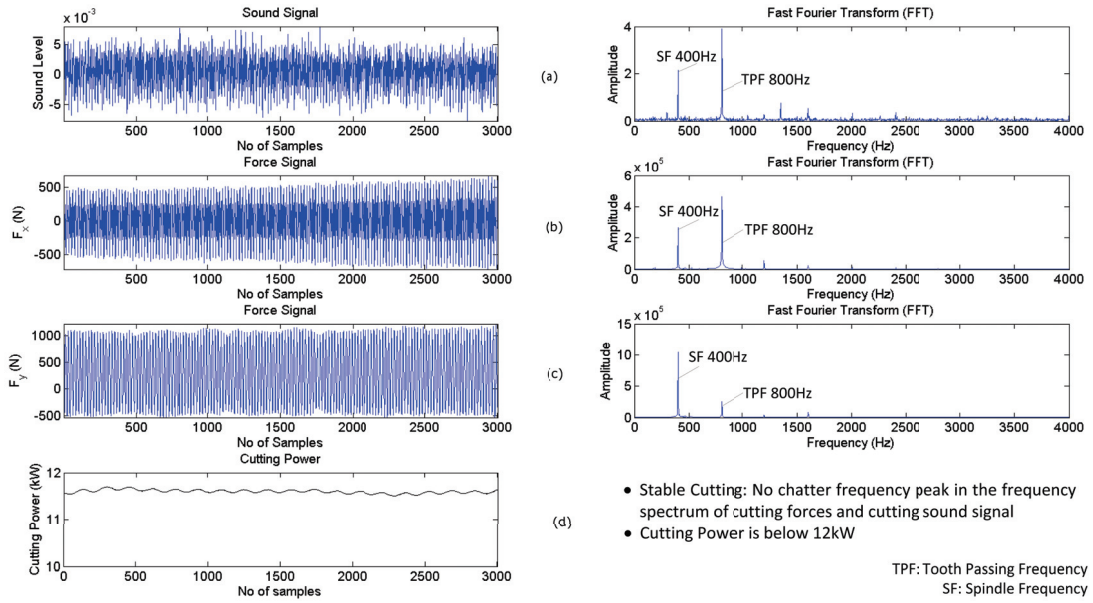

Figure 4.21: Verification of cutting conditions for optimization use case 1

4.6 Validation of Optimization Use Case 2

Optimal cutting conditions are selected for pocket milling as presented in Section 4.2. The optimal cutting conditions were also verified experimentally. The various signals were measured along the toolpath of pocket milling. The toolpath is the same for both axial levels. Measured signals are presented for the toolpath for one axial level in Figure 4.22.

Measured cutting forces in the x and y directions are measured for complete milling. Higher values of the cutting forces were experienced than predicted which is due to the high run out in the machine tool. The resultant of cutting forces is shown in Figure 4.22. The maximum magnitude of the resultant of cutting forces is below 720N.

The measured total power is presented in Figure 4.22. The variation in cutting power is due to the acceleration/deceleration of machine axes at corners and due to the variation in engagement angle along the toolpath. Power exceeds the limit of 12kW for a very short time at sharp corners which is due to the power spent for movement of the machine axes. If the total power from the spindle motor can be measured directly, these effects can be filtered from the power signal. The power spent for cutting is then computed by subtracting the power spent for rotation of the spindle at the selected spindle speed from the measured value of the total spindle power.

Figure 4.23 presents a fast Fourier transform of cutting forces and the sound signals measured

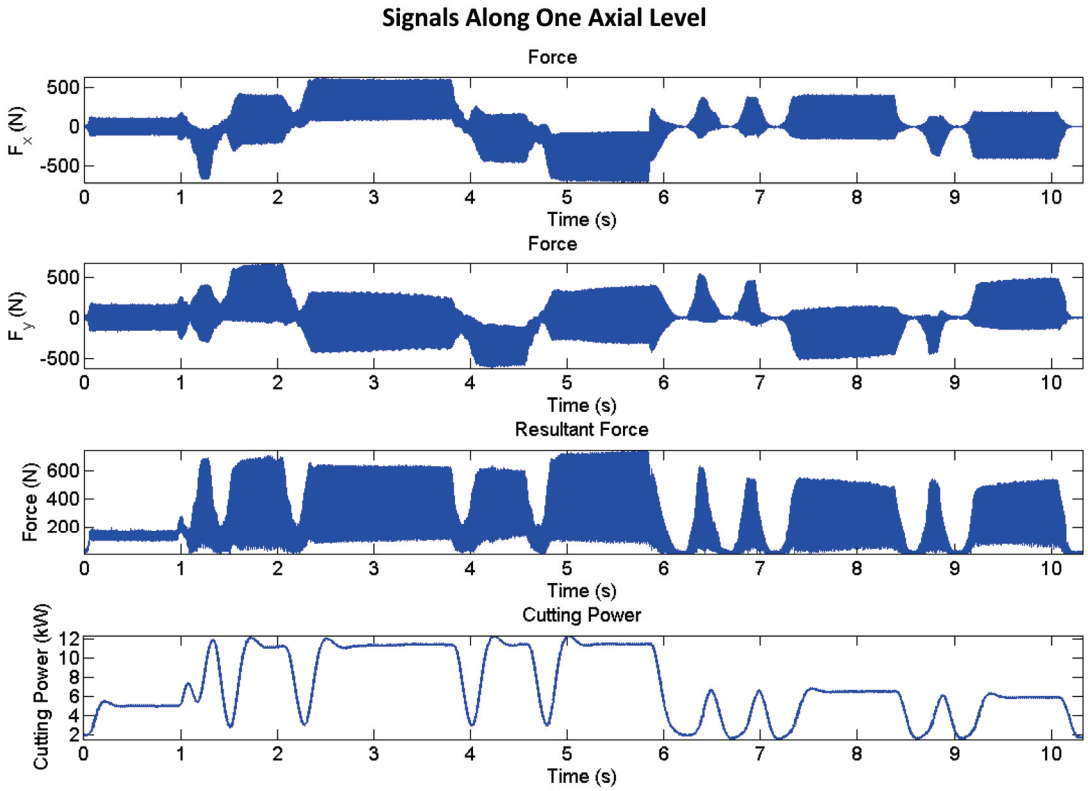

Figure 4.22: Signals collected during one axial level

during cutting. Tooth passing frequency is 650Hz ($19500*2/60$) and spindle frequency is 325Hz ($19500/60$). It is concluded that the cutting conditions are stable (chatter free) since there is no dominant frequency peak other than the spindle frequency, tooth passing frequency and their harmonics (Delio et al., 1992).

The power consumed during cutting is found by subtracting the power spent to rotate the spindle at the selected spindle speed from the measured value of total power. The cutting power is below the permissible limit of available power of 12kW as shown Figure 4.23(d).

Cutting conditions for contouring were also experimentally verified and also respect all the embedded constraints.

4.6.1 Energy Saving

A high value of cutting power is encountered with the use of optimal cutting conditions. In the present work, the objective is to minimize the machining time with the optimal selection of cutting conditions while respecting the constraints of the machine tool and workpiece system. Though the selected cutting conditions consume more cutting power their combined effect with minimum machining time leads to an overall energy saving. Moreover, during machining

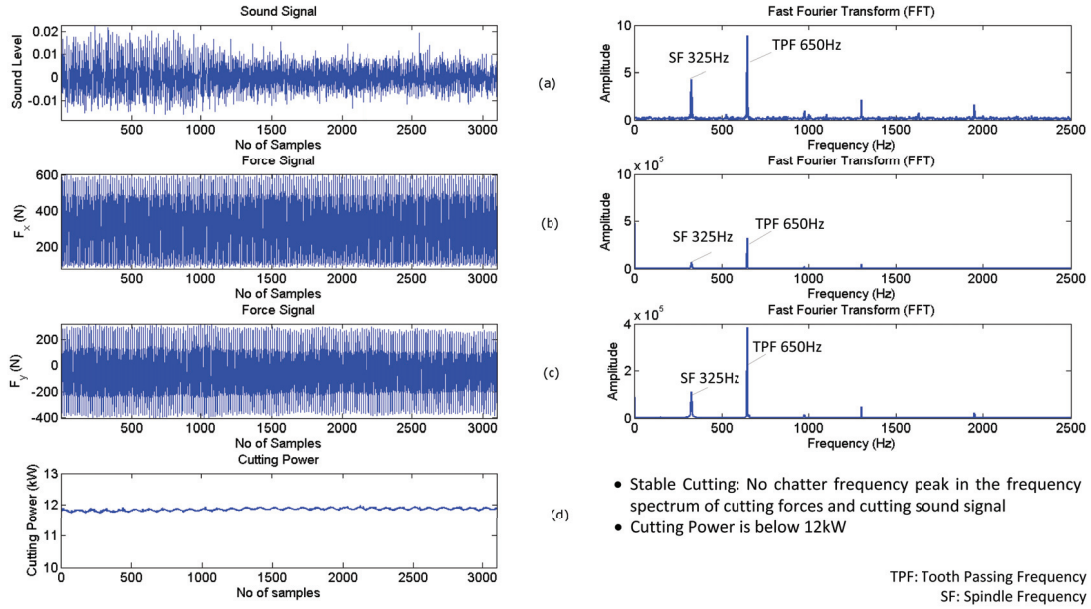

Figure 4.23: Verification of cutting conditions for optimization use case 2

operations, a significant amount of power is consumed for the movement of machine tool axes and other accessories like cooling pumps. This additional energy consumption during machining is also lowered due to reduction in machining time (Avram, 2010). Deep pockets are milled for comparison of the total energy consumed during machining. The details of the cutting tool, dimensions of the pocket, material are presented in Figure 4.24.

Pocket Dimensions
Length=160mm
Width=100mm
Depth=60mm

Workpiece Material
Al-7075

Cutting Tool Specifications
D=16mm, Helix=40deg
No of flutes=2
Total Length of tool=115mm
Cutting Length=17mm

Toolpath
Contour Parallel toolpath
(CATIA generated)

Figure 4.24: Details of deep pocket milling

Cutting conditions were selected by a machine user on the production floor based on the experience and guidance from cutting tool catalogue. Contour parallel toolpaths are generated using CATIA. For the same pocket and user defined toolpath (in CATIA), the cutting conditions were also selected with the developed optimization system. The chosen values of cutting conditions by the machine user and selected values of cutting conditions with developed optimization system are presented in Table 4.7. The toolpath geometry for each axial level is the same for both cases.

Table 4.7: Cutting conditions for deep pocket

Case-1: Cutting Conditions (Production Floor)				Case-2: Cutting Conditions (Optimization System)			
n	A_p	f_t	noap	n	A_p	f_t	noap
rpm	mm	mm/rev-flute		rpm	mm	mm/rev-flute	
11000	4	0.1364	15	24000	5	0.13	12

'noap' is number of axial passes

Total power is measured during complete pocket milling. The measured total power during complete pocket milling for both the cases is presented in Figure 4.25. There are 15 axial passes for user defined cutting conditions as compared to 12 for optimal cutting conditions. It is also important to mention that the optimal selected cutting conditions respect all the constraints embedded in the developed optimization system.

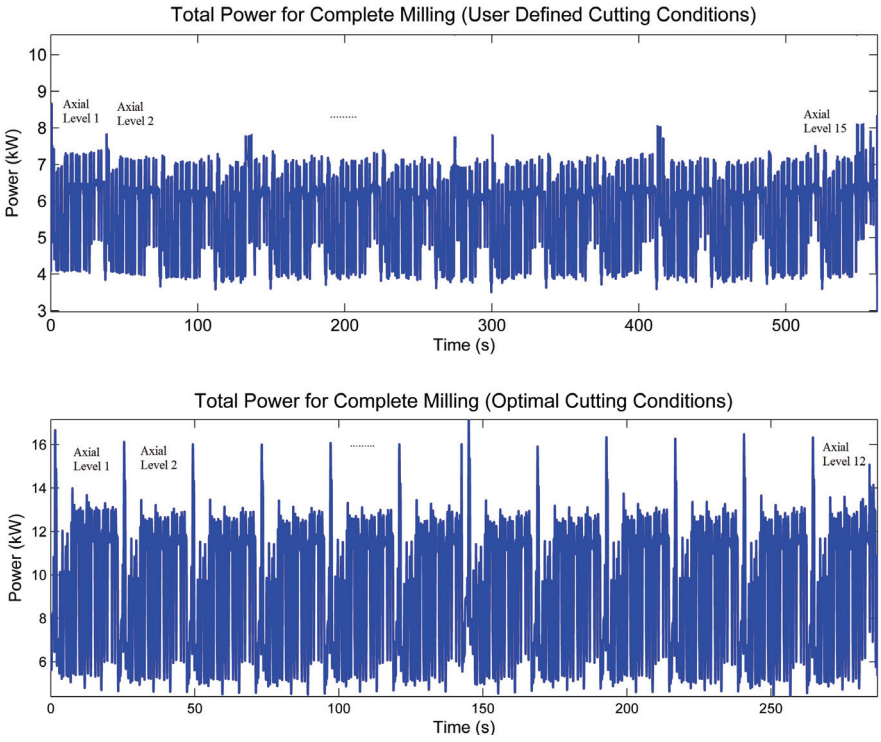

Figure 4.25: Measured total power during complete milling

The measured total power during for one axial pass for both cases is presented in Figure 4.26. The machining time for complete milling for both cases is measured during experiments. From the sampled data of total power and corresponding time steps, the total energy consumed during pocket milling is calculated. The machining time and energy consumed for both cases are compared in Table 4.8. It is concluded that there is a significant reduction in machining time and total energy with the developed optimization system.

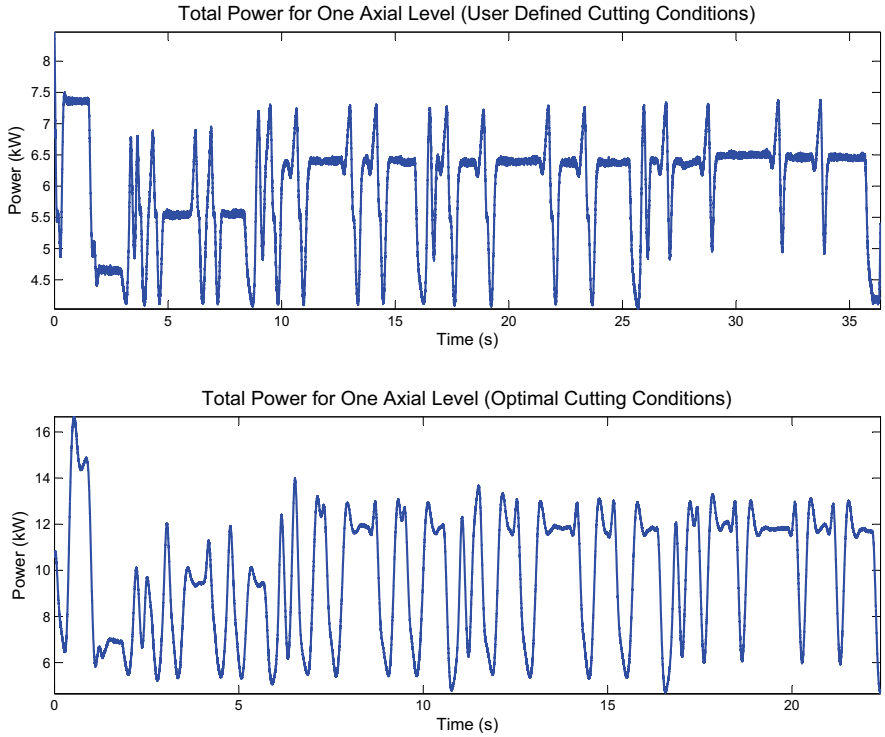

Figure 4.26: Measured total power during one axial pass

Table 4.8: Reduction in machining time and total energy

Case-1 (Production Floor)			Case-2 (Optimization System)			Reduction (%)	
$n/A_p/f_t$	T_{mac}	Energy	$n/A_p/f_t$	T_{mac}	Energy	T_{mac}	Energy
11000/4/0.1364	562.3s	3269.7KJ	24000/5/0.13	287s	2679.9KJ	**48.96**	**18.04**

4.7 Validation of Optimization Use Case 3

The optimal cutting conditions and corresponding toolpath for the desired pocket as presented in Section 4.3 were also verified experimentally. Figure 4.27 shows the measured cutting forces in the x and y directions, resultant of cutting forces and cutting power along toolpath for one axial level. The toolpath for one axial level contains the constant engagement contours along with corner loop passes. The magnitude of the resultant of cutting forces is below 1000N which is within the allowable limits. The measured cutting power is also shown in Figure 4.27. There is a variation in the power signal which is due to the power spent on the simultaneous movements of machine axes. The measured values of power are below 12kW which is the permissible limit.

Figure 4.28 presents the measured signals for one contour of the toolpath and their corresponding fast Fourier transform plots. Tooth passing frequency is 800Hz ($24000 * 2/60$) and spindle frequency is 400Hz ($24000/60$). Spindle frequency is quite visible in the FFT plot which

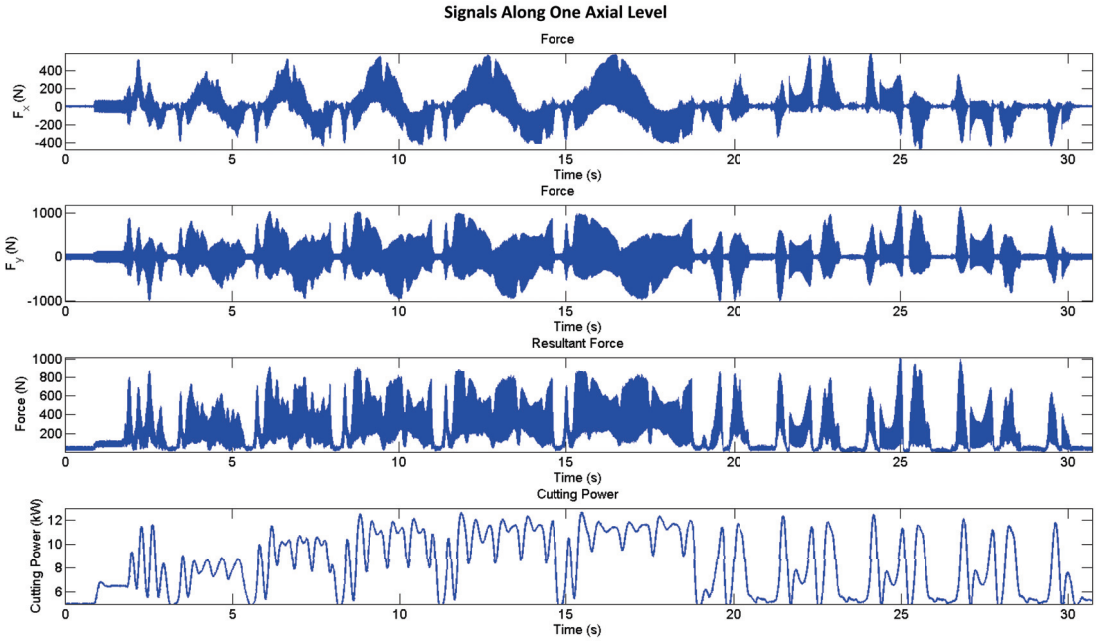

Figure 4.27: Signals collected during one axial level

is due to the high run out present in the machine tool. It is concluded that cutting conditions are stable (chatter free) since there is no dominant frequency peak other than the spindle frequency, tooth passing frequency and their harmonics (Delio et al., 1992).

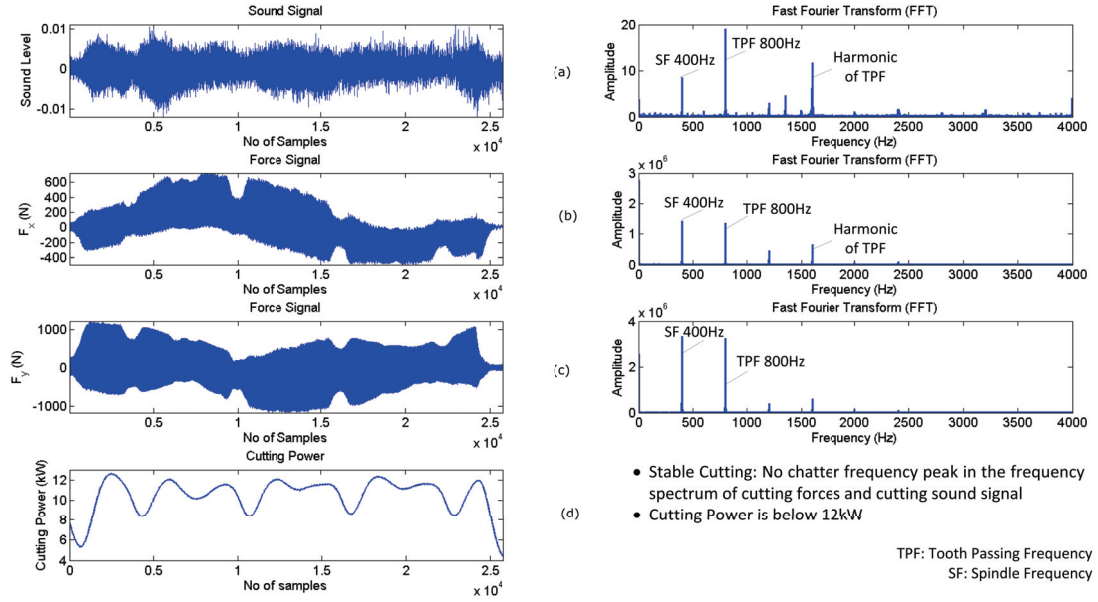

Figure 4.28: Verification of cutting conditions for optimization use case 3

4.7.1 Toolpath Verification

For a given pocket with length 150mm, width 90mm and corner radius 10mm, a constant engagement toolpath is generated with the smooth and constant engagement toolpath generation module presented in Section 3.5. End mill with 20mm in diameter is used for toolpath generation. The generated toolpath with 40% radial immersion is shown in Figure 4.29(a). A contour parallel toolpath with 40% radial immersion prepared with CATIA is shown in Figure 4.29(b).

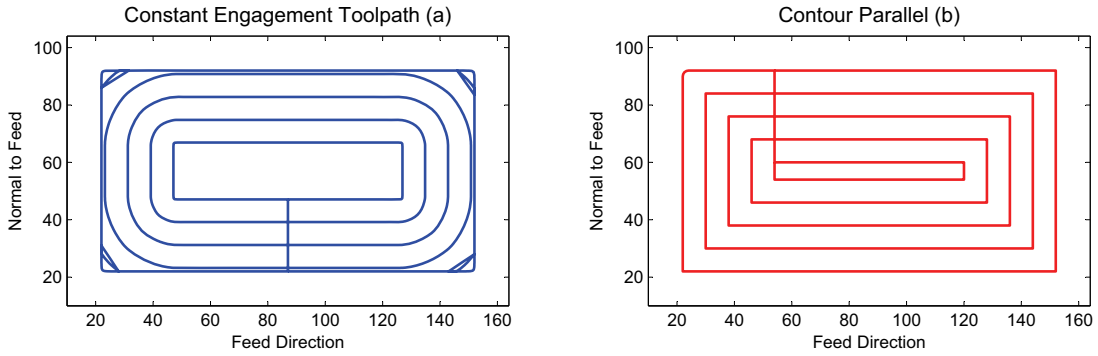

Figure 4.29: Contour parallel and constant engagement toolpath

These toolpaths are compared with experimentally measured cutting forces and power signals presented in Figure 4.30. Measured values are presented for one contour of the corresponding toolpaths. The cutting forces in the x and y directions are presented in Figure 4.30(a) and Figure 4.30(b). The resultant of cutting forces along the contours of the respective toolpaths are compared in Figure 4.30(c). It is clear from the plot that the constant engagement toolpath maintains consistent cutting force magnitude along the toolpath. The cutting tool remains in contact with the workpiece material during cutting tool movement. In the case of contour parallel toolpaths, the magnitude of the cutting forces varies along the toolpath. This variation in the cutting forces is due to the increased engagement angle in the corners and intermittent cutting. Figure 4.30(d) shows the cutting power signal measured along the toolpath. As the constant engagement toolpath also has smooth curvature, the variation in measured power along the toolpath is much smaller than for the contour parallel toolpaths. The high value of measured power in the case of the contour parallel toolpath is due to the increased engagement as well as due to the acceleration and deceleration of machine axes at sharp corners.

4.8 Conclusion

The developed optimization use cases 1 and 2 (Chapter 3) were implemented with real data of machine tool and workpiece systems for the optimal selection of cutting conditions for

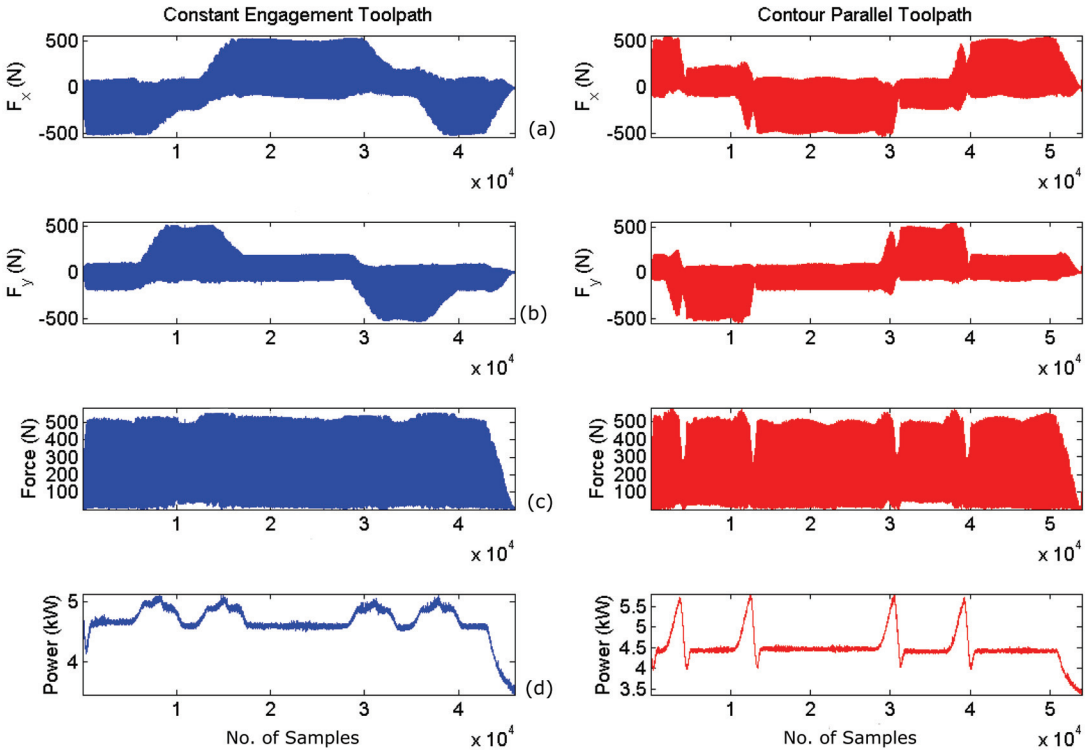

Figure 4.30: Experimental results for toolpath comparison

different workpieces.

For the case presented in Section 4.2, a **47.6%** reduction in machining time was achieved with the optimal cutting conditions selected with the developed optimization use case in comparison to the cutting conditions chosen by an experienced user based on catalogue guidelines. Similarly in the case of a deep pocket (Section 4.6.1), the optimal cutting conditions result in **48.96%** reduction in machining time and **18.04%** saving in total energy consumed during milling.

For optimization use case 3, optimal cutting conditions and corresponding smooth and constant engagement toolpaths were selected for a given convex pocket. The optimal values selected during different use cases were verified experimentally. The constant engagement toolpath was also compared with a conventional toolpath experimentally. FRFs of the machine tool system were measured by hammer testing. Cutting forces, total power and cutting sound signals were measured respectively with a cutting force dynamometer, power cell and microphone.

5 Indirect Identification of Tangential Force Coefficient

5.1 Introduction

Identification of force coefficients is necessary for accurate prediction of cutting forces (Section 3.2.1) and chatter free regions (Section 3.2.2) during milling. The force coefficients are identified from average values of cutting force components measured by a cutting force dynamometer with slot cutting experiments at different feed rates (as presented in Appendix B). This experimental set up is not practical on modern shop floors due to its high cost and complex hardware setup.

For the developed system (OptMill) the force coefficients are identified experimentally. In order to expand the scope of industrial implementation of the developed system, an enhanced procedure is presented for identification of force coefficients from spindle motor current.

Tangential cutting force coefficients affect significantly the magnitude of cutting forces and permissible values of stable depths of cut. The effect of K_{tc} and K_{rc} on stability lobes is presented in Figure 5.1. SLDs are drawn for an end mill with diameter 20mm, two flutes, full immersion and measured FRFs (as shown in Figure 4.7). It is concluded from Figure 5.1a that K_{tc} has a significant effect on the allowable stable depths of cut. The values of stable axial depths of cut at different spindle speeds are predicted at different K_{tc} values which are presented in Table 5.1. There is a significant difference in stable axial depths of cut at low and high values of K_{tc}. It is noted that the higher the tangential cutting force coefficient is, the lower are the allowable stable axial depths of cut. Whereas the effect of K_{rc} is comparatively negligible. There is only an insignificant horizontal shift of stability lobes as shown in Figure 5.1b with change in K_{rc}.

The effect of K_{tc} and K_{rc} on resultant of cutting forces and power is presented in Figure 5.2. An end mill (20mm, 2 flutes) with half immersion up milling is used for the plots. It is clear from Figure 5.2a and Figure 5.2c that magnitudes of the resultant of cutting forces and cutting power are affected significantly with the change in K_{tc}. There is an insignificant effect of K_{rc} on the resultant cutting force and it has no effect on the cutting power. It is noted that the

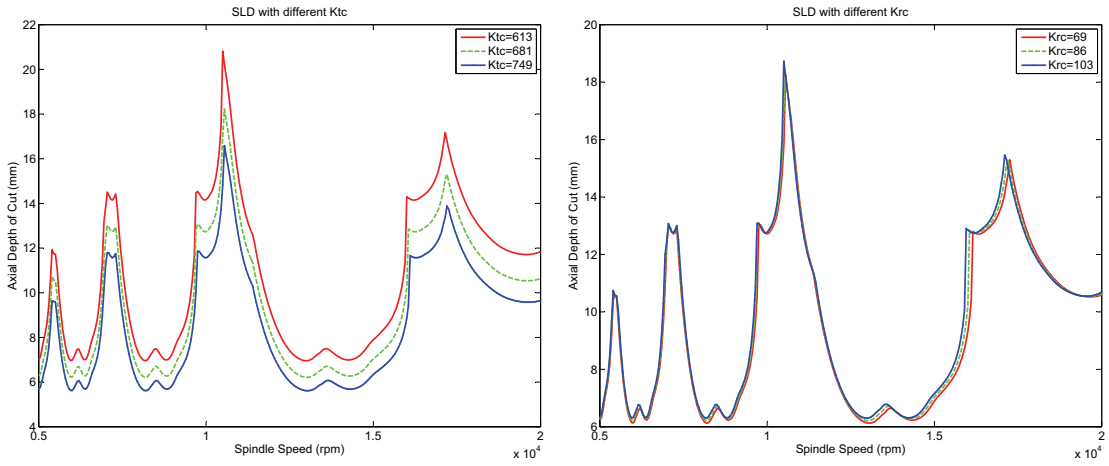

(a) Effect of K_{tc} on stability

(b) Effect of K_{rc} on on stability

Figure 5.1: Effect of K_{tc} and K_{rc} on stable limits

Table 5.1: Effect of tangential cutting force coefficients on stable limits

Spindle Speed rpm	A_{Plim} (mm) $K_{tc} = 613$	A_{Plim} (mm) $K_{tc} = 681$	A_{Plim} (mm) $K_{tc} = 749$	Max. Variation mm
10500	20.8	17	14.8	6
15000	7.9	7	6.3	1.6
19500	11.7	10.5	9.6	2.1

higher is the tangential cutting force coefficient, the higher are the resultant of cutting forces and power during milling.

As discussed in Section 2.7, (Dunwoody, 2010) has proposed a procedure for indirect identification of tangential force coefficients (K_{tc} and K_{te}) from cutting torque. Instead of being measured by direct experimentation, the cutting torque is obtained from the difference between spindle power consumption in material cutting and air cutting. The spindle motor current is proportional to the total power spent by the spindle, which is expressed as:

$$I = K_{lm} P_{ACeff} \tag{5.1}$$

where: I is the spindle current proportional to the total spindle power (useful power, spent on cutting plus losses measured by a built-in load meter and obtained from the controller), K_{lm} is the load meter constant and P_{ACeff} is the effective power from the electrical network. Spindle power model developed by Dunwoody is simple and efficient, but does not take into account the dependency of Coulomb friction losses on spindle speed, which is especially important in the case of high speed machining (Cao and Altintas, 2004). Furthermore, this model does not include the electric losses in the spindle motor. A more detailed model for total spindle power estimation is required which includes all mechanical and electrical sources of power loss in the spindle drive.

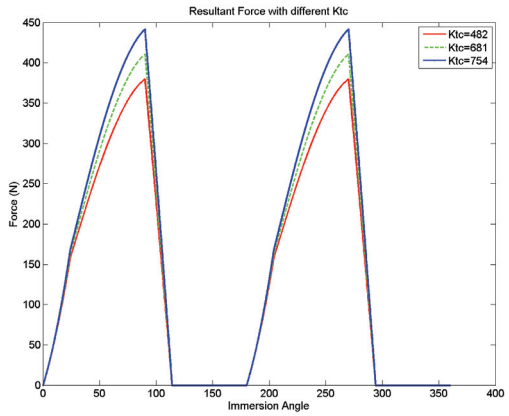

(a) Effect of K_{tc} on resultant force

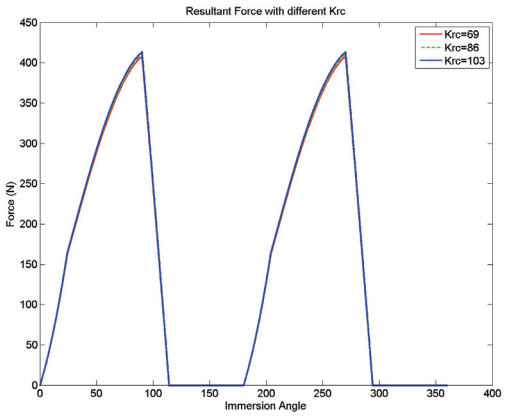

(b) Effect of K_{rc} on resultant force

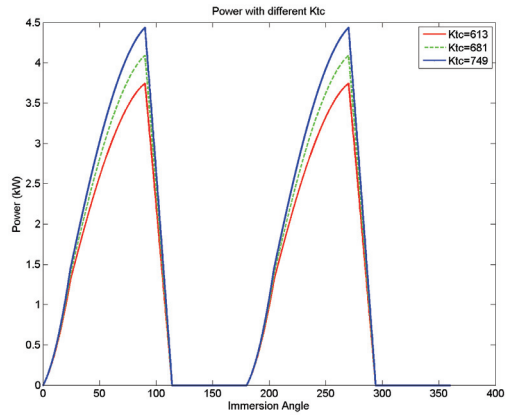

(c) Effect of K_{tc} on cutting power

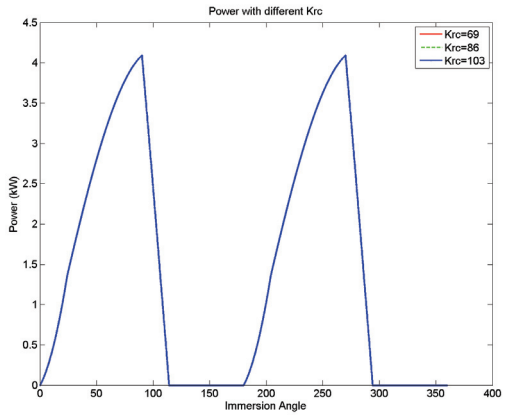

(d) Effect of K_{rc} on cutting power

Figure 5.2: Effect of K_{tc} and K_{rc} on resultant cutting force and power

In the present work, a holistic model for total spindle power calculation is implemented (Aggarwal et al., 2012b; Nešić, 2012). This model expresses all mechanical and electrical sources of power loss as a function of spindle angular speed and mechanical load on the spindle shaft, which allows for easy experimental validation and practical implementation. The enhanced procedure for cutting torque and tangential force coefficients identification from spindle motor current consists of four steps:

1. Development of a holistic theoretical model for total spindle power calculation, that includes the power loss due to the spin-related friction torque in the spindle bearings, the power loss due to the windage friction torque and electrical losses in the spindle motor

2. Air cutting tests at different spindle speeds (spindle motor current measurement) and slot cutting tests at different spindle speeds (spindle motor current and cutting torque measurement)

3. Development of an empirical model for cutting torque prediction, as a function of the spindle rotational speed and spindle current
4. Slot cutting tests at different feed rates for validation of the cutting torque prediction model and the identification of tangential force coefficients
    - spindle current measurement (for cutting torque prediction)
    - direct cutting torque measurement with a torque dynamometer (for comparison and validation of the procedure)

The developed procedure for cutting torque and tangential force coefficient identification from spindle motor current is published (Aggarwal et al., 2012b)[1]

5.2 Theoretical Model for Total Spindle Power Calculation

The total power (P_{AC}) drawn by a symmetrical three-phase induction motor from the electrical network is calculated as:

$$P_{AC} = \sqrt{3}UI \tag{5.2}$$

here: U is the voltage and I is the current. Only a portion of the total power, termed as effective electric input power P_{ACeff}, is actually used for overcoming mechanical losses or dissipated as heat which is expressed as:

$$P_{ACeff} = \sqrt{3}UI\left|\cos\varphi\right| \tag{5.3}$$

here: $\cos\varphi$ represents the power factor (φ is the phase angle between the vectors of voltage and the current). In modern electric motor designs automatic power factor correction units are implemented to achieve $\cos\varphi = 1$, thus reducing transmission losses and improving voltage regulation.

The total power used by a motorized spindle to overcome the mechanical load and compensate for mechanical and electrical losses in the system, is expressed by summing up the following components:

$$P_{ACeff} = P_{\text{cut}} + P_{\text{ml}} + P_{\text{el}} \tag{5.4}$$

here: $P_{\text{cut}} = T_{cut}\omega_M$ is the power providing the cutting torque T_{cut} , needed to overcome tangential cutting force in the cutting tool/workpiece contact at a spindle rotational speed ω_M. P_{ml} and P_{el} represent the total mechanical and electrical power losses respectively in the spindle drive system.

[1] Aggarwal, S., Nešić, N. and Xirouchakis, P., Cutting torque and tangential cutting force coefficient identification from spindle motor current. *The International Journal of Advanced Manufacturing Technology*, DOI: 10.1007/s00170-012-4152-x.

5.2.1 Mechanical Losses in a Motorized Spindle

Total mechanical losses in a motorized spindle are the consequence of the Coulomb and viscous friction phenomena in contact areas due to the relative motions of the members of kinematic pairs. The total torque required to overcome all sources of mechanical power loss in a motorized spindle is expressed as:

$$T_{ml} = \frac{P_{ml}}{\omega_M} = T_\mu + T_v \tag{5.5}$$

here: T_μ is the torque to overcome the Coulomb friction forces and T_v is the torque to overcome viscous friction forces. This equation is further decomposed according to the physical sources of friction loss into:

$$T_{ml} = T_{B\mu l} + T_{B\mu s} + T_{Bv} + T_{vw} \tag{5.6}$$

where: $T_{B\mu l}$ is the load-related friction torque in spindle bearings, $T_{B\mu s}$ is the spin-related friction torque in spindle bearings, T_{Bv} is the viscous friction torque in spindle bearings and T_{vw} is the windage friction torque in the air gap between the stator and the rotor.

5.2.2 Electrical Losses in a Motorized Spindle

The losses in electric motors originate from several motor components. They are due to very complex phenomena and are dependent on the type, characteristics and the application of an electric motor. Consequently, in spite of numerous research efforts resulting in various methodologies for analytical or experimental determination of these losses, they still represent a domain where many questions are left unanswered. According to their sources, electrical losses can be divided in four groups: copper losses in the stator P_{SCu}, copper losses in the rotor P_{RCu}, iron losses P_{MFe} and stray losses P_{stray}. Hence, the total losses due to electrical phenomena are calculated as:

$$P_{el} = P_{SCu} + P_{RCu} + P_{MFe} + P_{stray} \tag{5.7}$$

5.2.3 Model Synthesis

The modeling details of different component of power loss in spindle motor are explained in (Nešić, 2012; Aggarwal et al., 2012b). The analytical models of different power loss components are simplified and represented as polynomial functions of spindle speed. The various power loss components and their simplified empirical models are presented in Table 5.2. K_i^s are the experimentally determined constant parameters.

Table 5.2: Power loss components in a motorized spindle drive

Power loss component	Empirical Expression
Power needed to overcome the bearing friction torque due to applied load	$P_{B\mu l} = K_{B\mu l}\omega_M$
Power needed to overcome the spin-related friction torque	$P_{B\mu s} = K_{0B\mu s}\omega_M + K_{1B\mu s}\omega_M^3 + K_{2B\mu s}\omega_M^5$
Power needed to overcome the torque due to lubricant viscous friction	$P_{Bv} = K_{Bv}\omega_M^{\frac{5}{3}}$
Power loss due to windage friction torque	$P_{vw} = K_{vw}\omega_M^2$
Rotor copper loss	$P_{RCu} = K_{0RCu} + K_{1RCu}\omega_M^{-1} + K_{2RCu}\omega_M^{-2}$
Stator copper loss	$P_{SCu} = K_{0SCu} + K_{1SCu}\omega_M^{-1} + K_{2SCu}\omega_M^{-2}$
Iron loss	$P_{MFe} = K_{1MFe}\omega_M + K_{2MFe}\omega_M^2$
Stray losses	$P_{stray} = 0.012P_{cut}$

The total spindle power (Equation 5.4) is now expressed as:

$$\begin{aligned} & K_{B\mu l}\omega_M + K_{0B\mu s}\omega_M + K_{1B\mu s}\omega_M^3 + K_{2B\mu s}\omega_M^5 + K_{Bv}\omega_M^{\frac{5}{3}} + \\ P_{ACeff} \quad = \quad & K_{vw}\omega_M^2 + K_{0RCu} + K_{1RCu}\omega_M^{-1} + K_{2RCu}\omega_M^{-2} + K_{0SCu} + K_{1SCu}\omega_M^{-1} \\ & + K_{2SCu}\omega_M^{-2} + K_{1MFe}\omega_M + K_{2MFe}\omega_M^2 + 0.012P_{cut} + P_{cut} \end{aligned} \tag{5.8}$$

Spindle current proportional to the total spindle power, from Equation 5.1 and Equation 5.8, is given as:

$$\begin{aligned} & K_{lm}K_{2B\mu s}\omega_M^5 + K_{lm}K_{1B\mu s}\omega_M^3 + K_{lm}(K_{vw} + K_{2MFe})\omega_M^2 + K_{lm}K_{Bv}\omega_M^{\frac{5}{3}} \\ I \quad = \quad & + K_{lm}(K_{B\mu l} + K_{0B\mu s} + K_{1MFe})\omega_M + K_{lm}(K_{1RCu} + K_{1SCu})\omega_M^{-1} + \\ & K_{lm}(K_{2RCu} + K_{2SCu})\omega_M^{-2} + K_{lm}(K_{0RCu} + K_{0SCu}) + K_{lm}1.012T_{cut}\omega_M \end{aligned} \tag{5.9}$$

For air cutting ($T_{cut} = 0$), the measured spindle motor current accounts only for the losses in the spindle drive. Hence, Equation 5.9 becomes:

$$\begin{aligned} & K_{lm}K_{2B\mu s}\omega_M^5 + K_{lm}K_{1B\mu s}\omega_M^3 + K_{lm}(K_{vw} + K_{2MFe})\omega_M^2 + K_{lm}K_{Bv}\omega_M^{\frac{5}{3}} \\ I_f \quad = \quad & + K_{lm}(K_{B\mu l} + K_{0B\mu s} + K_{1MFe})\omega_M + K_{lm}(K_{1RCu} + K_{1SCu})\omega_M^{-1} + \\ & K_{lm}(K_{2RCu} + K_{2SCu})\omega_M^{-2} + K_{lm}(K_{0RCu} + K_{0SCu}) \end{aligned} \tag{5.10}$$

Different constants in Equation 5.10 are combined and the resulting expression is given by:

$$I_f = a_1\omega_M^5 + a_2\omega_M^3 + a_3\omega_M^2 + a_4\omega_M^{\frac{5}{3}} + a_5\omega_M + a_6\omega_M^{-1} + a_7\omega_M^{-2} + a_8 \tag{5.11}$$

Equation 5.9 is rewritten as:

$$I = I_f + K_{lm} 1.012 T_{cut} \omega_M \tag{5.12}$$

5.3 Development of an Empirical Model for Cutting Torque Prediction

The MIKRON HPM 600U, a 5-axis milling machine equipped with the controller iTNC530, was used for experiments. The experimental setup consists of following subsystems and corresponding measurements:

- Direct measurement of torque with cutting torque dynamometer (Kistler 9125A)
- Measurement of spindle motor current (with built-in current sensor) from machine tool controller
- Measurement of spindle power consumption with power sensor (only for monitoring purposes)

The data acquisition platform for spindle power and cutting torque signals was developed in LabVIEW 2010. The spindle motor current was collected with controller software (TNC-scopeNT). The overall experimental setup is presented in Figure 5.3.

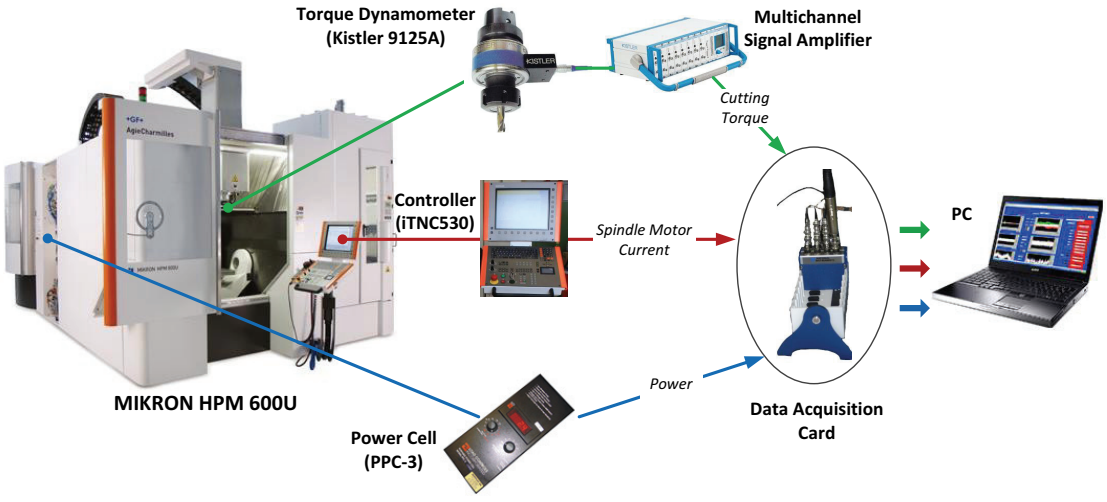

Figure 5.3: Overall experimental setup

A flat end mill diameter 20mm with 2 flutes was used as cutting tool. The material of the workpiece was Certal (AlZnMgCu 0.5). The mounting of the cutting torque dynamometer (Kistler 9125A) and the data acquisition platform are shown in Figure 5.4. The constants, ($i = 1, 2...8$), in Equation 5.11, are identified with air cutting experiments performed at different

spindle speeds. Spindle speed was varied from 500rpm to 20000rpm with an increment of 500rpm. Spindle motor current was acquired directly from the machine controller. By using MATLAB 2010a as programming environment, the developed model was fitted to the measured spindle motor current and the corresponding values of a_i were calculated.

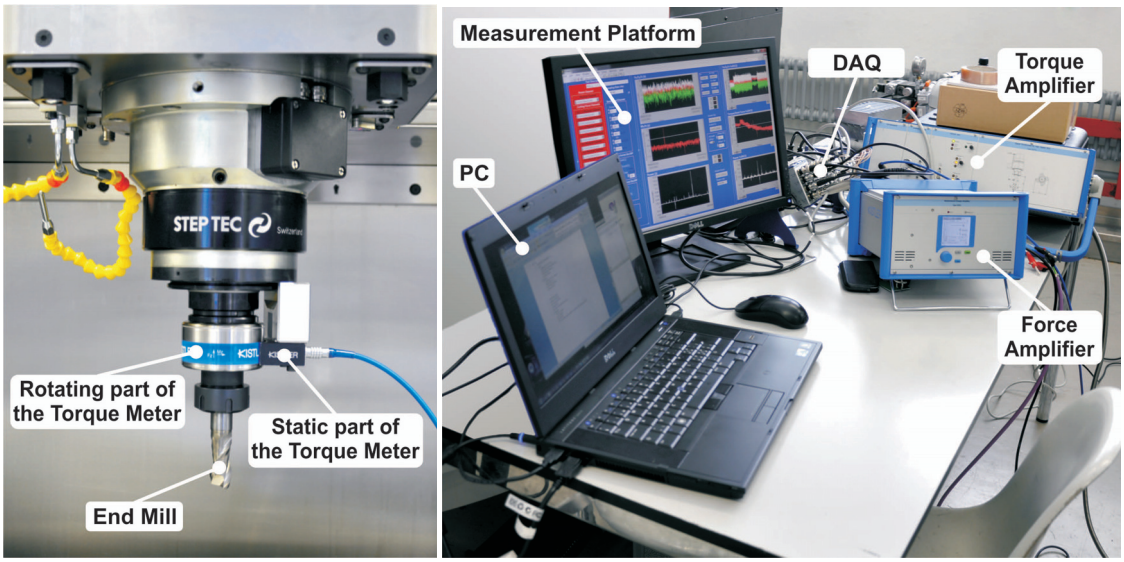

(a) Cutting torque dynamometer mounting (b) Data acquisition platform

Figure 5.4: Experimental setup

The obtained values of the constants corresponding to the model given in Equation 5.11, are:

$$\left.\begin{aligned} a_1 &= 4.98\cdot10^{-22}\left(\frac{\mathrm{A}}{\mathrm{rpm}^5}\right) & a_5 &= -1.21\cdot10^{-12}\left(\frac{\mathrm{A}}{\mathrm{rpm}}\right)\\ a_2 &= -1.73\cdot10^{-13}\left(\frac{\mathrm{A}}{\mathrm{rpm}^3}\right) & a_6 &= 2.76\cdot10^{-08}\left(\mathrm{A}\cdot\mathrm{rpm}\right)\\ a_3 &= 5.11\cdot10^{-9}\left(\frac{\mathrm{A}}{\mathrm{rpm}^2}\right) & a_7 &= -6.33\cdot10^{-05}\left(\mathrm{A}\cdot\mathrm{rpm}^2\right)\\ a_4 &= 3.25\cdot10^{-10}\left(\frac{\mathrm{A}}{\mathrm{rpm}^{5/3}}\right) & a_8 &= 0.1410 \end{aligned}\right\} \tag{5.13}$$

Although a_1 has a very small value its combined effect with ω_M at high spindle speed cannot be ignored. It helps to ensure accurate prediction of the developed model at higher spindle speeds.

After introducing the values of the constants , Equation 5.11 becomes:

$$\begin{aligned} I_f &= 4.98\cdot10^{-22}\omega_M^5 - 1.73\cdot10^{-13}\omega_M^3 + 5.11\cdot10^{-9}\omega_M^2 + 3.25\cdot10^{-10}\omega_M^{5/3} \\ &\quad -1.21\cdot10^{-12}\omega_M + 2.76\cdot10^{-8}\omega_M^{-1} - 6.33\cdot10^{-5}\omega_M^{-2} + 0.1410 \end{aligned} \tag{5.14}$$

A comparison of the results, presented in Figure 5.5, clearly shows better compliance of the developed model to the experimental data than Dunwoody's model (Equation 2.12).

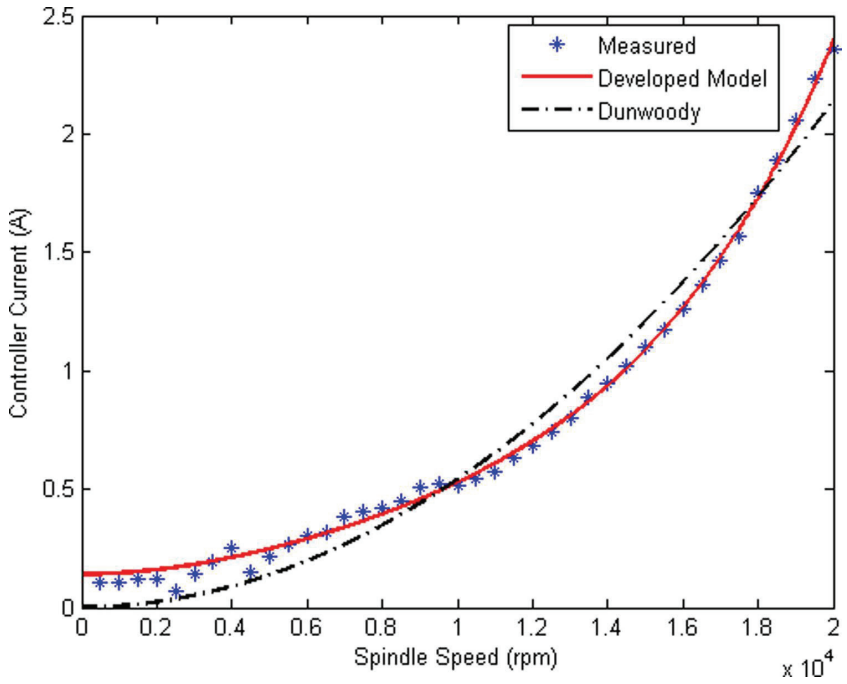

Figure 5.5: Air cutting experimental results

The load meter constant K_{lm} is identified with slot cutting experiments performed at different spindle speeds. Spindle speed is varied from 1000rpm to 20000rpm with an increment of 1000rpm. The stable axial depth of cut (=2mm) and feed (=0.1mm/rev-flute) are kept constant during the experiments. The cutting torque (T_{cut}) was measured with a cutting torque dynamometer while the spindle motor current corresponding to the total spindle power (I) was acquired directly from the machine controller. The spindle current proportional to the power loss (I_f) is calculated from Equation 5.14.

The measured values of the total spindle motor current (I_f) and the calculated spindle motor current corresponding to the power spent for cutting ($I - I_f$) are presented in Figure5.6a. The percentage of total losses, $\left(\frac{I_f \cdot 100}{I}\right)$, is presented in Figure 5.6b. The plots demonstrate that the total losses are quite significant, especially at high spindle speeds.

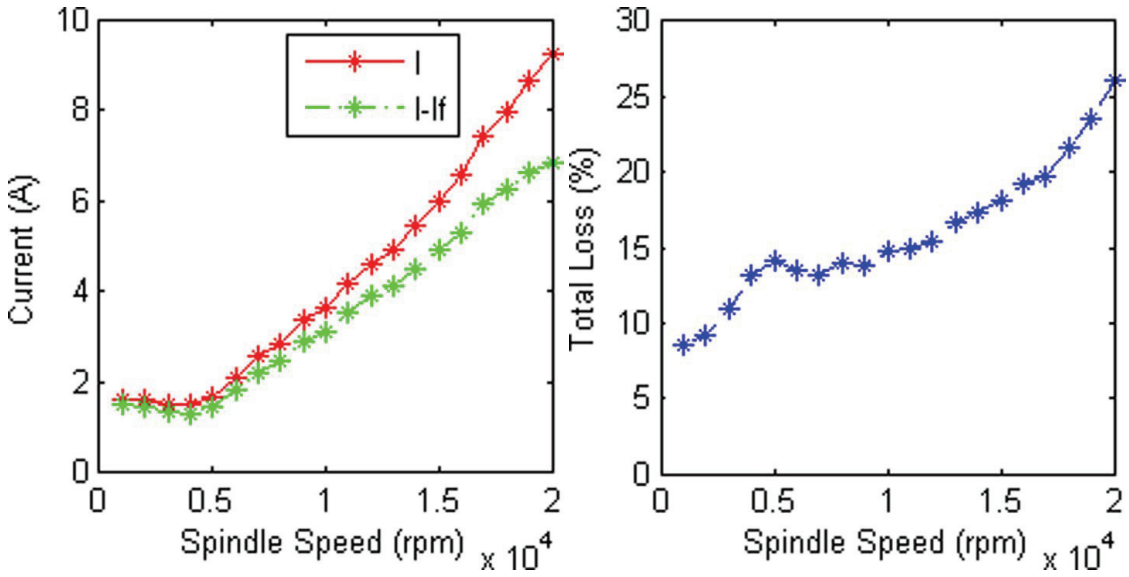

(a) Spindle speed vs current

(b) Spindle speed vs total losses

Figure 5.6: Illustration of the dependency of total power loss

Subsequently, from Equation 5.12, we get:

$$\frac{I - I_f}{1.012 T_{cut}} = K_{lm} \omega_M \tag{5.15}$$

The load meter constant K_{lm} is estimated by linear regression of the $\left(\frac{I - I_f}{1.012 T_{cut}}\right)$ values and the fitted line is presented as a solid line in Figure 5.7.

The values of the spindle motor current at lower spindle speeds are not reliable, as shown in Figure 5.6a, because they are too small to be measured accurately by the load meter. After excluding the data corresponding to spindle speeds smaller than 4000rpm (see Figure 5.7), the obtained value of K_{lm} is $1.9973 \cdot 10^{-4}$ A/W.

By rewriting the complete model Equation 5.9 as:

$$\begin{aligned} I \quad = \quad & 4.98 \cdot 10^{-22} \omega_M^5 - 1.73 \cdot 10^{-13} \omega_M^3 + 5.11 \cdot 10^{-9} \omega_M^2 \\ & + 3.25 \cdot 10^{-10} \omega_M^{5/3} - 1.21 \cdot 10^{-12} \omega_M + 2.76 \cdot 10^{-8} \omega_M^{-1} \\ & - 6.33 \cdot 10^{-5} \omega_M^{-2} + 0.1410 + 1.012 \cdot 1.9973 \cdot 10^{-4} T_{cut} \omega_M \end{aligned} \tag{5.16}$$

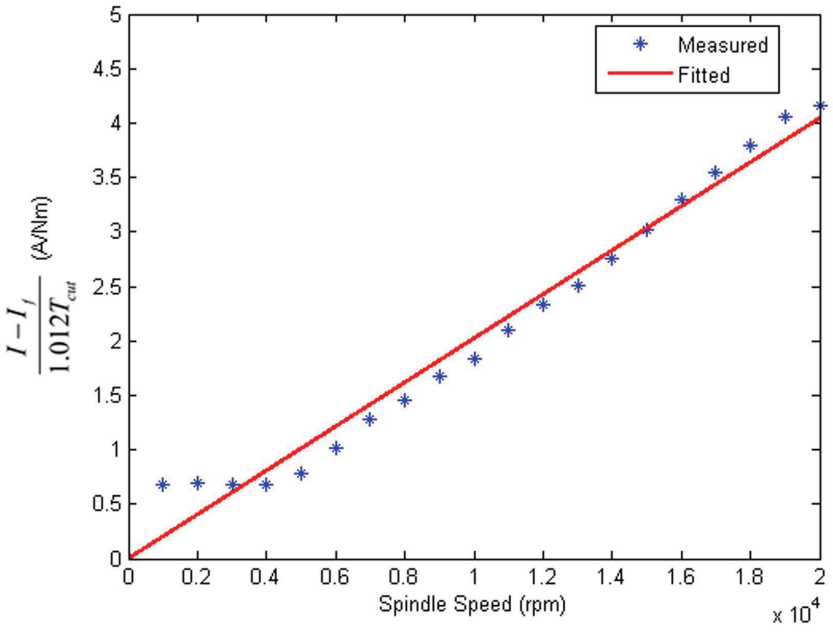

Figure 5.7: Slot cutting experimental results

From Equation 5.16, the developed model to estimate the cutting torque from the spindle motor current obtains its final expression as:

$$T_{cut} = \frac{I - 4.98\cdot10^{-22}\omega_M^5 + 1.73\cdot10^{-13}\omega_M^3 - 5.11\cdot10^{-9}\omega_M^2 - 3.25\cdot10^{-10}\omega_M^{5/3}}{1.012\cdot1.9973\cdot10^{-4}\omega_M} + \frac{1.21\cdot10^{-12}\omega_M - 2.76\cdot10^{-8}\omega_M^{-1} + 6.33\cdot10^{-5}\omega_M^{-2} - 0.1410}{1.012\cdot1.9973\cdot10^{-4}\omega_M} \quad (5.17)$$

Cutting torque (Equation 5.17) is defined as a function of spindle speed (rpm) and spindle motor current (A), which in turn is load dependent. The empirical model for cutting torque estimation is valid for the spindle speeds higher than 4000rpm.

It is probable that the load meter constant depends on the given combination of workpiece material and tool geometry. It is, however, still to be determined how significant this influence is.

5.4 Validation and Implementation of the Developed Cutting Torque Model

In the previous section it has been demonstrated that the developed model of the spindle power predicts the total power losses accurately. The next objective is to validate experimentally the developed cutting torque prediction model (Equation 5.17) and propose its implementation for tangential force coefficient identification.

Cutting force coefficients are identified by performing slot cutting experiments at different feed rates. Feed rate is varied from 0.04mm/rev-flute to 0.18mm/rev-flute with an increment of 0.02mm/rev-flute. Stable axial depth of cut (=4mm) and spindle speed (=7000rpm) are kept constant during the slot cutting experiments. Spindle motor current is acquired from the controller and then the cutting torque is estimated with the developed model (Equation 5.17).

For validation of the developed cutting torque prediction model, the cutting torque is also measured directly with the cutting torque dynamometer. The results presented in Figure 5.8 validate that the cutting torque predicted with the developed model is in good compliance with the measured cutting torque values. The same data will also be used to identify the tangential force coefficients.

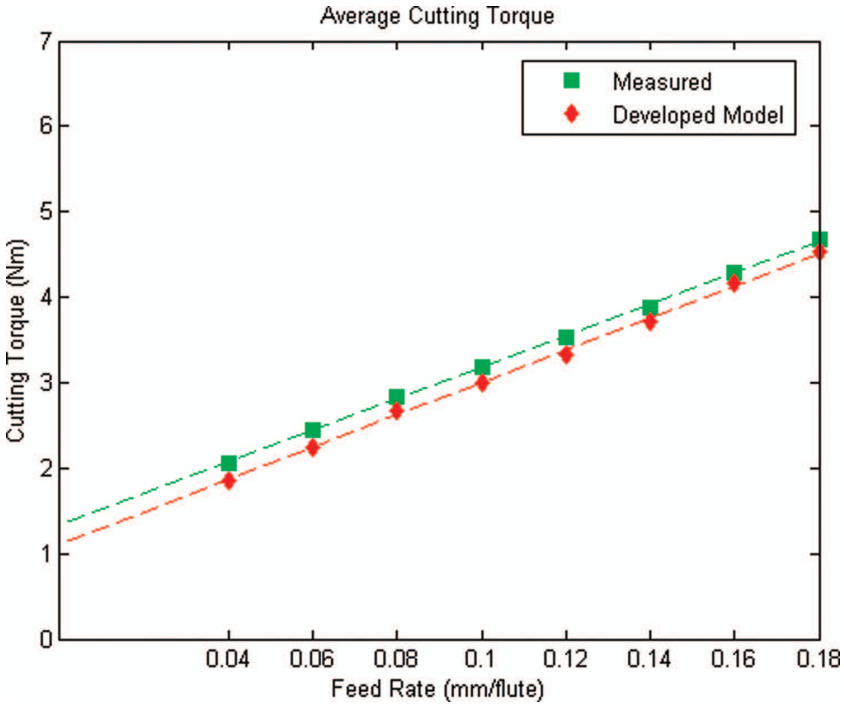

Figure 5.8: Average values of the cutting torque

The tangential cutting force per unit depth of cut along the cutting edge j of an end mill is given by (Altintas, 2000):

$$dF_{t,j}(\phi) = K_{tc}h(\phi) + K_{te} \tag{5.18}$$

Here (ϕ) is the immersion angle, K_{tc} is the tangential cutting force coefficient contributed by shearing action, K_{te} is the tangential edge force coefficient and $h(\phi)$ is the chip thickness which is given by:

$$h(\phi) = f_t \sin(\phi) \tag{5.19}$$

where f_t is the feed rate. The instantaneous cutting torque can be calculated as:

$$dT_{c,j}(\phi) = R\left(K_{tc}h(\phi) + K_{te}\right)g(\phi) \tag{5.20}$$

where: R is the radius of the milling tool, $g(\phi)$ is a function which is unity while the tooth is in the cutting zone and zero when the tooth is out of the cutting zone. The average torque per unit depth of cut is given by:

$$d\overline{T}_{c,j} = \frac{R}{2\pi}\int_0^{2\pi} g(\phi)\left[(K_{tc}f_t\sin(\phi) + K_{te})\right] \tag{5.21}$$

For slot cutting tests, the immersion angle is 180°

$$g(\phi) = \begin{cases} 1 & if \quad 0 \le \phi < \pi \\ 0 & if \quad \pi \le \phi < 2\pi \end{cases} \tag{5.22}$$

The average torque per unit depth of cut, for a single flute, is expressed as (Dunwoody, 2010):

$$d\overline{T}_{c,j} = \frac{RK_{tc}}{\pi}f_t + \frac{RK_{te}}{2} \tag{5.23}$$

and total average torque, for all cutting flutes and given depth of cut (A_p), is given by:

$$\overline{T}_c = \frac{RNA_pK_{tc}}{\pi}f_t + \frac{RNA_pK_{te}}{2} \tag{5.24}$$

The cutting and edge components $\left(\frac{RNA_pK_{tc}}{\pi}, \frac{RNA_pK_{te}}{2}\right)$ are estimated by linear regression of the cutting torque values as presented in Figure 5.8. Tangential force coefficients are identified from direct measurement of the cutting torque by a torque dynamometer and also from estimated values of cutting torque from the developed model. The comparison of the results is presented in Table 5.3. The edge force coefficient (K_{te}) has negligible effect on cutting

Table 5.3: Tangential force coefficients identified from the measured and the predicted cutting torque

Coefficient	Measured	Predicted	% Error
K_{tc} (N/mm^2)	726	743	2.34%
K_{te} (N/mm)	33.2	27.8	16.26%

forces and has no effect on chatter free region prediction (Altintas, 2000); therefore, 16.56% error in its determination is quite acceptable. On the other hand, precise identification of the tangential cutting coefficient K_{tc} is indispensable for accurate prediction of cutting forces and chatter free regions as concluded in Section 5.1. The difference between tangential cutting

coefficients identified from the predicted and experimentally measured cutting torque is only 2.34%, which represents another validation of the accuracy of the developed model for industrial application.

5.5 Conclusion

In this chapter, an enhanced procedure for tangential cutting force coefficient identification from the spindle motor current is presented. Spindle motor current, obtained from the integrated load meter, is proportional to the total spindle power. The cutting torque is obtained from the difference of spindle power consumption in material and air cutting by using a methodology that required the development of a mathematical spindle power model. Finally, the tangential cutting coefficients are identified from the obtained cutting torque. This procedure demonstrates several salient features compared to previous approaches.

The implemented model of spindle power considers all mechanical and electrical sources of power losses in the spindle motor. Mechanical losses (load-related friction in spindle bearings, spin-related friction, friction due to lubricant viscosity and windage friction) and electrical losses (rotor and stator copper loss, iron loss and stray losses) are all taken into account during the model development and expressed as a function of spindle rotational speed and load.

Further, an empirical model for cutting torque prediction has been developed from the results of air cutting and slot cutting experiments at different spindle speeds. It has been demonstrated that the developed model predicts the spindle power losses accurately. Predicted values of the cutting torque by using the developed empirical model are additionally validated by the simultaneous direct measurement of cutting torque from a cutting torque dynamometer. The results have demonstrated good compliance of the predicted cutting torque with the one obtained by direct measurement, thus proving the accurate identification of tangential cutting force coefficients.

6 FRF Prediction by Receptance Coupling

6.1 Introduction

The frequency response function (FRF) of the spindle/tool holder/end mill system is a necessary input for prediction of stable regions during milling. These FRFs are measured at the cutting tool tip by direct hammer testing. Each variant of spindle/tool holder/end mill system results in different dynamic characteristics which thus requires separate hammer tests.

For the developed system (OptMill), the FRFs are measured directly by hammer testing for each end mill. In order to expand the scope of industrial implementation of the developed system, an enhanced procedure is presented for the prediction of FRFs for different end mills for a given spindle/tool holder subsystem.

Studies from (Schmitz, 2000), (Schmitz et al., 2001) and (Schmitz and Burns, 2003) have introduced receptance coupling substructure analysis (RCSA). In RCSA, spindle/tool holder/cutting tool system is decomposed into different subsystems. The dynamic characteristics of each subsystem are identified individually and then combined with their joint dynamics to obtain the spindle/tool holder/cutting tool system FRF at the cutting tool tip. The accuracy of the RCSA depends on identification of the joint dynamics of the subsystems at the joint location and FRFs of each subsystem.

As the objective of the present work is to identify FRFs for different end mills, spindle/tool holder/cutting tool system is decomposed into the following two subsystems (as shown in Figure 6.1):

1. Subsystem A: end mill (cutting tool)
2. Subsystem B: spindle/tool holder

A study from Park (Park et al., 2003) has concluded that the milling system can be modeled accurately by using translational and rotational springs and dampers as connection parameters. This study shows the significance of rotational degrees of freedom in receptance coupling

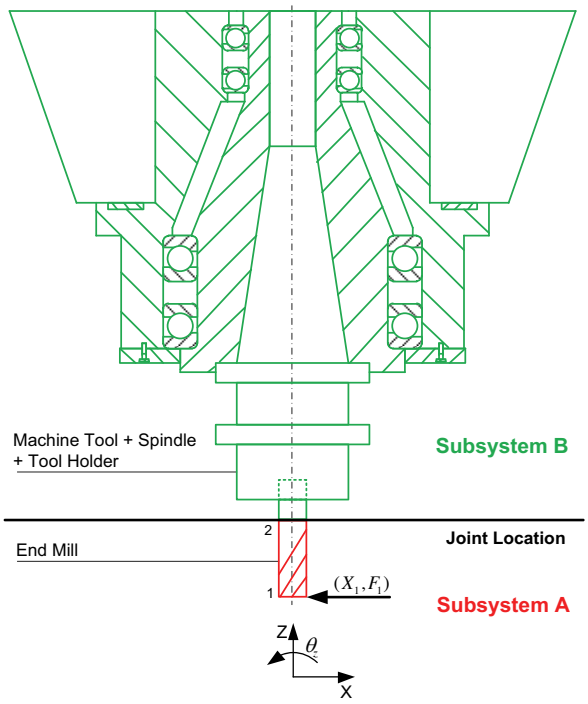

Figure 6.1: Spindle/tool holder/end mill system

as the previously mentioned studies from (Schmitz, 2000; Schmitz et al., 2001) only take the effect of translational degree of freedom.

A system's FRF can be predicted at any spatial co-ordinates ("joint location" in Figure 6.1) from the FRFs of individual subsystems. In Section 6.2, the general theory of receptance coupling is presented. The rotational degree of freedom FRFs of subsystem B are found by inverse receptance coupling as presented in Section 6.2.1. The FRFs of subsystem A are found by beam receptance modeling as presented in Section 6.3. The receptance coupling (RC) technique is based on force and displacement continuity between both subsystems.

6.2 Receptance Coupling with Joint Dynamics

In this section, the modeling details of receptance coupling with joint dynamics for subsystem A and subsystem B are presented (Park et al., 2003). The dynamic characteristics of subsystem A (beam with free-free ends, point 1 and point 2) are given by:

$$\begin{Bmatrix} X_1 \\ X_{A,2} \end{Bmatrix} = \begin{bmatrix} H_{A,11} & H_{A,12} \\ H_{A,21} & H_{A,22} \end{bmatrix} \begin{Bmatrix} F_1 \\ F_{A,2} \end{Bmatrix} \tag{6.1}$$

where X and F are the displacement and the force vectors applied on the system at point 1 and 2 respectively. $H_{A,ij}$ represents the FRFs between point i and j. The FRF of subsystem B

(spindle/tool holder) at its free end (point 2) is given by:

$$\{X_{B,2}\} = [H_{B,22}]\{F_{B,2}\} \tag{6.2}$$

The equilibrium and comparability conditions at the joint location (point 2) provide the following boundary conditions:

$$\begin{aligned} F_2 &= F_{A,2} + F_{B,2} \\ X_2 &= X_{A,2} = X_{B,2} \end{aligned} \tag{6.3}$$

The following equations are obtained by putting Equation 6.3 into Equation 6.1 and Equation 6.2.

$$\begin{aligned} X_2 &= H_{A,21}F_1 + H_{A,22}F_{A,2} \\ F_{B,2} &= (H_{A,22} + H_{B,22})^{-1}(H_{A,21}F_1 + H_{A,22}F_2) \end{aligned} \tag{6.4}$$

The displacements X_1 and X_2 can be expressed as a function of applied forces F_1 and F_2 as:

$$\begin{aligned} X_1 &= (H_{A,11} - H_{A,12}H_2^{-1}H_{A,21})F_1 + (H_{A,12} - H_{A,12}H_2^{-1}H_{A,22})F_2 \\ X_2 &= (H_{A,21} - H_{A,22}H_2^{-1}H_{A,21})F_1 + (H_{A,22} - H_{A,22}H_2^{-1}H_{A,22})F_2 \end{aligned} \tag{6.5}$$

The matrix form of Equation 6.5 is as follows:

$$\begin{Bmatrix} X_1 \\ X_2 \end{Bmatrix} = \begin{bmatrix} (H_{A,11} - H_{A,12}H_2^{-1}H_{A,21}) & (H_{A,12} - H_{A,12}H_2^{-1}H_{A,22}) \\ (H_{A,21} - H_{A,22}H_2^{-1}H_{A,21}) & (H_{A,22} - H_{A,22}H_2^{-1}H_{A,22}) \end{bmatrix} \begin{Bmatrix} F_1 \\ F_2 \end{Bmatrix} \tag{6.6}$$

Here, $H_2 = H_{A,22} + H_{B,22}$. Direct and cross transfer FRFs at the tool tip (point 1):

$$\begin{aligned} \frac{X_1}{F_1} &= [H_{A,11} - H_{A,12}(H_{A,22} + H_{B,22})^{-1}H_{A,21}] = H_{11} \\ \frac{X_1}{F_2} &= [H_{A,12} - H_{A,12}(H_{A,22} + H_{B,22})^{-1}H_{A,22}] = H_{12} \end{aligned} \tag{6.7}$$

The FRF at the cutting tool tip (point 1) is represented as a combination of FRFs related to: (i) end mill (ii) spindle/tool holder and (iii) joint parameters.

Both translational and rotational degrees of freedom are considered for accurate prediction of the machine tool system's FRF (Park et al., 2003). The translational and rotational degrees of freedom for subsystem A and subsystem B are shown in Figure 6.2a and Figure 6.2b respectively.

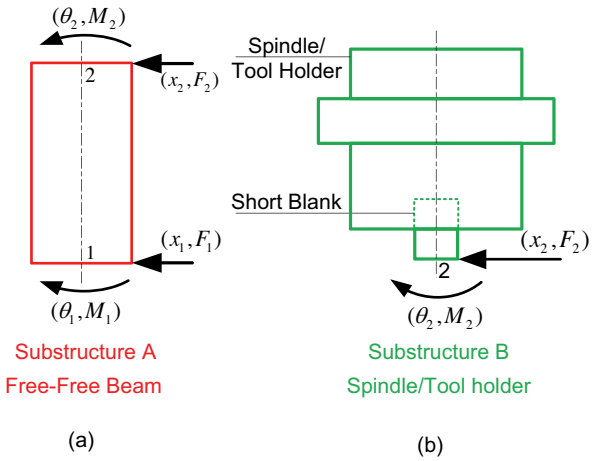

Figure 6.2: Degrees of freedom of end mill and spindle/tool holder

Equation 6.7 at the free end of the end mill is now expanded as:

$$\begin{Bmatrix} x_1 \\ \theta_1 \end{Bmatrix} = \begin{bmatrix} h_{11ff} & h_{11fM} \\ h_{11Mf} & h_{11MM} \end{bmatrix} \begin{Bmatrix} f_1 \\ M_1 \end{Bmatrix} \longrightarrow \{X_1\} = [H_{11}]\{F_1\}$$
$$\begin{Bmatrix} x_1 \\ \theta_1 \end{Bmatrix} = \begin{bmatrix} h_{12ff} & h_{12fM} \\ h_{12Mf} & h_{12MM} \end{bmatrix} \begin{Bmatrix} f_2 \\ M_2 \end{Bmatrix} \longrightarrow \{X_1\} = [H_{12}]\{F_2\} \tag{6.8}$$

Each element (h_{ij}) in the matrix is evaluated by including both translational (x) and rotational (θ) displacement due to lateral force (f) and moment (M). Direct and cross FRFs at the tool tip, which include both translational and rotational degrees of freedom, can be obtained by substituting Equation 6.8 into Equation 6.7:

$$\begin{aligned} [H_{11}] &= \begin{bmatrix} h_{A11ff} & h_{A11fM} \\ h_{A11Mf} & h_{A11MM} \end{bmatrix} - \begin{bmatrix} h_{A12ff} & h_{A12fM} \\ h_{A12Mf} & h_{A12MM} \end{bmatrix} [H_2]^{-1} \begin{bmatrix} h_{A21ff} & h_{A21fM} \\ h_{A21Mf} & h_{A21MM} \end{bmatrix} \\ [H_{12}] &= \begin{bmatrix} h_{A12ff} & h_{A12fM} \\ h_{A12Mf} & h_{A12MM} \end{bmatrix} - \begin{bmatrix} h_{A12ff} & h_{A12fM} \\ h_{A12Mf} & h_{A12MM} \end{bmatrix} [H_2]^{-1} \begin{bmatrix} h_{A22ff} & h_{A22fM} \\ h_{A22Mf} & h_{A22MM} \end{bmatrix} \end{aligned} \tag{6.9}$$

here

$$[H_2]^{-1} = \frac{1}{h_{2Mf}^2 - h_{2MM}h_{2ff}} \begin{bmatrix} -h_{2MM} & h_{2fM} \\ h_{2Mf} & -h_{2ff} \end{bmatrix} \tag{6.10}$$

and $h_{2ij} = h_{A22ij} + h_{B22ij}$ for each element $(i, j \longrightarrow f, M)$

Substituting $[H_2]^{-1}$ in Equation 6.9 and evaluating the first elements of $[H_{11}]$ and $[H_{12}]$ leads

to:

$$\begin{aligned} H_{11}(1,1) &= \frac{x_1}{f_1} = h_{A11ff} + \frac{1}{h_{2Mf}^2 - h_{2MM}h_{2ff}} \\ &\quad [h_{A21Mf}(-h_{2Mf}h_{A12ff} + h_{A12Mf}h_{2ff}) \\ &\quad + h_{A21ff}(-h_{2Mf}h_{A12Mf} + h_{2MM}h_{A12ff})] \end{aligned} \tag{6.11}$$

$$\begin{aligned} H_{12}(1,1) &= \frac{x_1}{f_2} = h_{A12ff} + \frac{1}{h_{2Mf}^2 - h_{2MM}h_{2ff}} \\ &\quad [h_{A22Mf}(-h_{2Mf}h_{A12ff} + h_{A12Mf}h_{2ff}) \\ &\quad + h_{A22ff}(-h_{2Mf}h_{A12Mf} + h_{2MM}h_{A12ff})] \end{aligned} \tag{6.12}$$

here

$$\begin{aligned} h_{2Mf} &= h_{A22Mf} + h_{B22Mf} \quad , \quad h_{2MM} = h_{A22MM} + h_{B22MM} \\ h_{2fM} &= h_{A22fM} + h_{B22fM} \quad , \quad h_{2ff} = h_{A22ff} + h_{B22ff} \end{aligned} \tag{6.13}$$

The objective is to find $H_{11}(1,1)$ for the spindle/tool holder/cutting tool system without performing impact testing for every new end mill. Equation 6.11 and Equation 6.12 will be used for the identification of rotational degrees of freedom FRFs by inverse receptance coupling.

6.2.1 Inverse Receptance Coupling

The transfer function matrix for subsystem A is:

$$\underline{H}^A = \begin{bmatrix} h_{A11ff} & h_{A11fM} & h_{A12ff} & h_{A12fM} \\ h_{A11Mf} & h_{A11MM} & h_{A12Mf} & h_{A12MM} \\ h_{A21ff} & h_{A21fM} & h_{A22ff} & h_{A22fM} \\ h_{A21Mf} & h_{A21MM} & h_{A22Mf} & h_{A22MM} \end{bmatrix} \tag{6.14}$$

The corresponding transfer function matrix for subsystem B is given by:

$$\underline{H}^B = \begin{bmatrix} h_{B22ff} & h_{B22fM} \\ h_{B22Mf} & h_{B22MM} \end{bmatrix} \tag{6.15}$$

Both $\underline{H}^A$ and $\underline{H}^B$ are symmetric matrices.

- Different FRFs of the transfer function matrix of subsystem A are computed by beam receptance modeling as presented in Section 6.3.
- For the spindle/tool holder transfer function matrix, h_{B22ff} is found by direct impact

testing (as shown in Figure 6.3) with a short blank tool which is a part of spindle/tool holder subsystem. FRFs h_{B22fM} and h_{B22Mf} are the same due to reciprocity. $h_{B22fM}(= h_{B22Mf})$ and h_{B22MM} cannot be measures directly as practical difficulties restrict the use of rotational accelerometers and moment excitation.

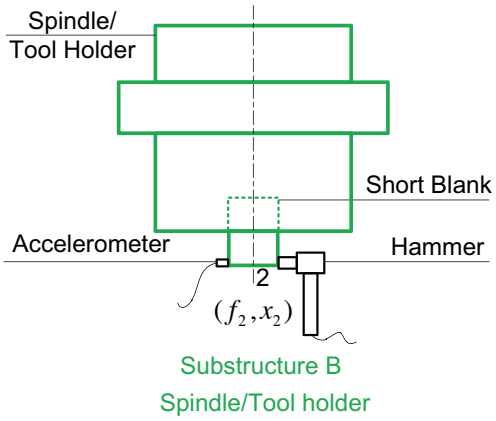

Figure 6.3: Experimental measurement of h_{B22ff}

The inverse receptance coupling technique is used to identify rotational degrees of freedom FRFs of the spindle/tool holder subsystem. In this technique, the direct transfer function, $H_{11}(1,1)$ and cross transfer function, $H_{12}(1,1)$ are measured with a long blank tool as shown in Figure 6.4. Transfer functions, $H_{11}(1,1)$ and $H_{12}(1,1)$, are measured by attaching the accelerometer at point 1 and applying impacts at point 1 and 2 respectively. The corresponding Transfer function matrix for the long blank (Equation 6.14) is calculated using beam receptance or finite element method which is discussed in Section 6.3. Please note that the length of the beam section used for beam theory or finite element method is L_{beam} as shown in Figure 6.4.

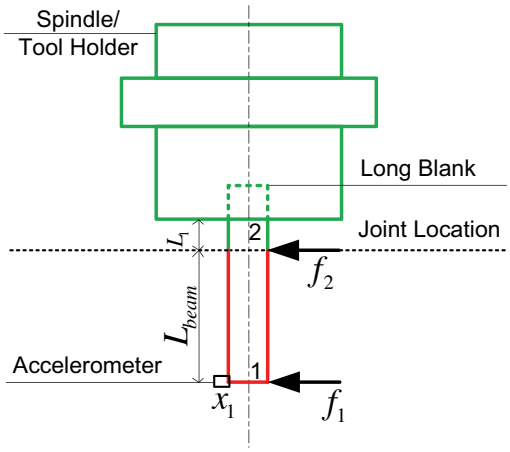

Figure 6.4: Inverse receptance coupling

By rewriting Equation 6.11 and Equation 6.12 as follows:

$$\begin{aligned} u &= a + \frac{f\left(-\beta b + ek\right) + c\left(-\beta e + \delta b\right)}{\beta^2 - \delta k} \\ v &= b + \frac{g(-\beta b + ek) + d(-\beta e + \delta b)}{\beta^2 - \delta k} \end{aligned} \tag{6.16}$$

where

$$\begin{array}{llll} H_{11}(1,1) = u & H_{12}(1,1) = v & h_{A11ff} = a & h_{A12ff} = b \\ h_{A21ff} = c & h_{A22ff} = d & h_{A12Mf} = e & h_{A21Mf} = f \\ h_{A22Mf} = g & h_{2ff} = k & h_{2Mf} = \beta & h_{2MM} = \delta \end{array} \tag{6.17}$$

The unknowns β and δ in Equation 6.16 can be expressed as:

$$\begin{aligned} \beta &= \frac{(-kug + kfv + kag - kfb + fdb - cbg)}{(ad - ud - cb + cv)} \\ \delta &= \frac{1}{(ab - ud - cb + cv)^2} \quad [kf^2v^2 + v(2kagf + bf^2d - 2kugf - ec^2g \\ &\quad + defc - 2bkf^2 - bfcg) - d^2efu + d^2efa + g^2ka^2 - decga + decgu \\ &\quad + g^2ku^2 + bdgfa - 2g^2kua + bec^2g - bdgfu - bdefc + 2bkugf + b^2kf^2 \\ &\quad - 2bkagf + bg^2cu + b^2fcg - b^2f^2d - bg^2ca] \end{aligned} \tag{6.18}$$

Rotational degrees of freedom FRFs for the spindle/tool holder subsystem are given by:

$$\begin{aligned} h_{B22Mf} &= \beta - h_{A22Mf} \\ h_{B22MM} &= \delta - h_{A22MM} \end{aligned} \tag{6.19}$$

$h_{B22fM}(= h_{B22Mf})$, h_{B22MM} and h_{B22ff} are the constant properties of the spindle/tool holder subsystem and can be stored in the constant database.

To predict the FRF of spindle/tool holder/end mill system, the FRFs of transfer function matrix of an end mill are identified by beam receptance or with finite element analysis while considering the effect of fluted portion. Please note that the length of the beam for the analysis should be taken from joint location to the end mill tip. Once the various FRFs for subsystem A and B are identified, Equation 6.11 is used to predict the cutting tip FRF.

6.3 Beam Receptance

As mentioned in Section 6.2.1, FRFs of the transfer function matrix (Equation 6.14) of the end mill/blank tool portion are required for RCSA. Dynamics of end mill/blank tool portion are identified by considering it as a free-free end beam. In this section Euler–Bernoulli and Timoshenko beam theories are used to predict beam dynamics. The program is written in MATLAB 2010a. The results are compared with the finite element model of 3D beam analyzed

with ANSYS 11.0. FRFs of the transfer function function matrix are identified for the beam specified in Table 6.1. The input data is taken from (Dijck, 2008).

Table 6.1: Properties of the beam section

D	L_{beam}	η	ρ	E	ν
mm	mm		kg/m^3	N/m^2	
10	42.5	0.01	14500	$5.9e^{11}$	0.22

D is the diameter of the circular beam, L_{beam} is the length of the beam, η is the solid damping value, ρ is the density of the material, E is the elastic modulus and ν is the poisson ratio.

6.3.1 Euler–Bernoulli Beam Theory

Euler–Bernoulli beam theory is a simplification of the linear theory of elasticity which provides a means of calculating the load-carrying and deflection characteristics of beams. For a uniform elastic beam subjected to lateral vibrations, the differential equation is written as to describe its lateral motion as a function of time, t, and position along the beam, x (Schmitz and Smith, 2009).

$$\frac{\partial^2 y}{\partial t^2} + \frac{EI}{\rho A}\frac{\partial^4 y}{\partial x^4} = 0 \tag{6.20}$$

I is the moment of inertia, and A is the cross-sectional area. For a free-free beam with translational and rotational degrees of freedom (Figure 6.2a), the transfer function matrix is given by:

$$\underline{H}^A = \begin{bmatrix} \frac{-c_1}{\lambda^3 c_7} & \frac{c_2}{\lambda^2 c_7} & \frac{c_3}{\lambda^3 c_7} & \frac{-c_4}{\lambda^2 c_7} \\ \frac{c_2}{\lambda^2 c_7} & \frac{c_5}{\lambda c_7} & \frac{c_4}{\lambda^2 c_7} & \frac{c_6}{\lambda c_7} \\ \frac{c_3}{\lambda^3 c_7} & \frac{c_4}{\lambda^2 c_7} & \frac{-c_1}{\lambda^3 c_7} & \frac{-c_2}{\lambda^2 c_7} \\ \frac{-c_4}{\lambda^2 c_7} & \frac{c_6}{\lambda c_7} & \frac{-c_2}{\lambda^2 c_7} & \frac{c_5}{\lambda c_7} \end{bmatrix} \tag{6.21}$$

here

$$\begin{aligned} c_1 &= \cos(\lambda l)\sinh(\lambda l) - \sin(\lambda l)\cosh(\lambda l) \\ c_2 &= \sin(\lambda l)\sinh(\lambda l) \\ c_3 &= \sin(\lambda l) - \sinh(\lambda l) \\ c_4 &= \cos(\lambda l) - \cosh(\lambda l) \\ c_5 &= \cos(\lambda l)\sinh(\lambda l) + \sin(\lambda l)\cosh(\lambda l) \\ c_6 &= \sin(\lambda l) + \sinh(\lambda l) \\ c_7 &= EI(\cos(\lambda l)\cosh(\lambda l) - 1) \end{aligned} \tag{6.22}$$

and

$$\lambda^4 = \omega^2 \frac{\rho A}{EI} \tag{6.23}$$

and

$$EI = EI(1 + i\eta) \tag{6.24}$$

l is the section length. The Euler–Bernoulli beam theory is validated for the beam presented in Table 6.1. The resulted FRFs are plotted in the form of Bode diagrams as shown in Figure 6.5a–Figure 6.5d and Figure 6.6a–Figure 6.6f.

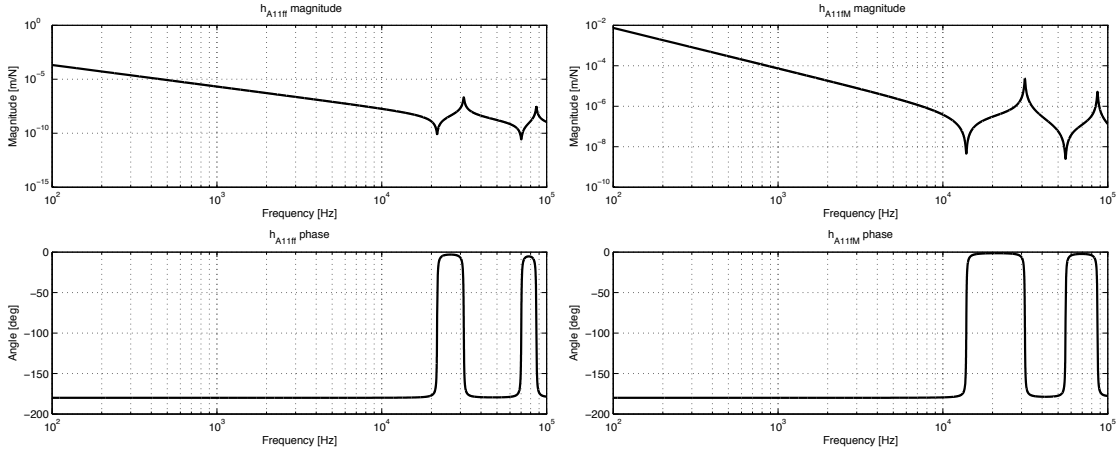

(a) Bode plot of h_{A11ff}

(b) Bode plot of h_{A11fM}

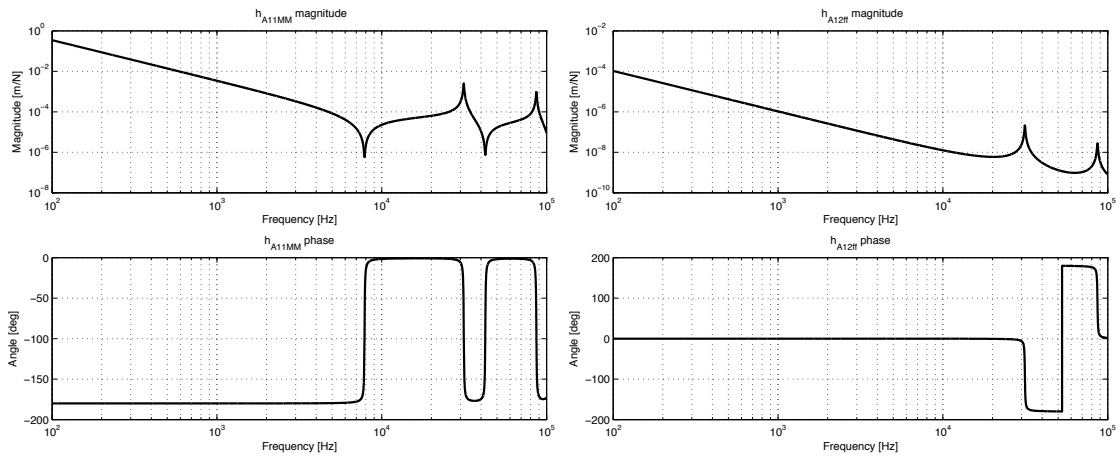

(c) Bode plot of h_{A11MM}

(d) Bode plot of h_{A12ff}

Figure 6.5: Bode plots using Euler–Bernoulli beam theory

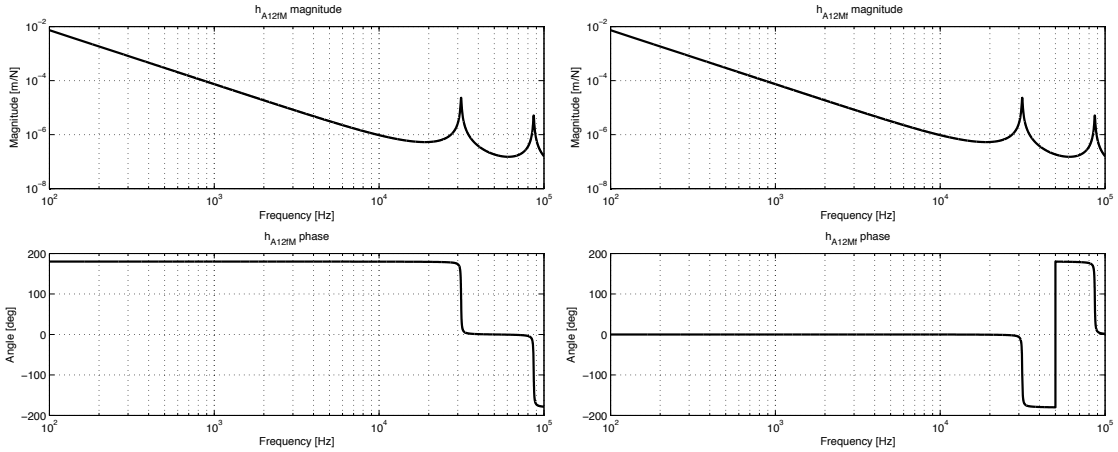

(a) Bode plot of h_{A12fM}

(b) Bode plot of h_{A12Mf}

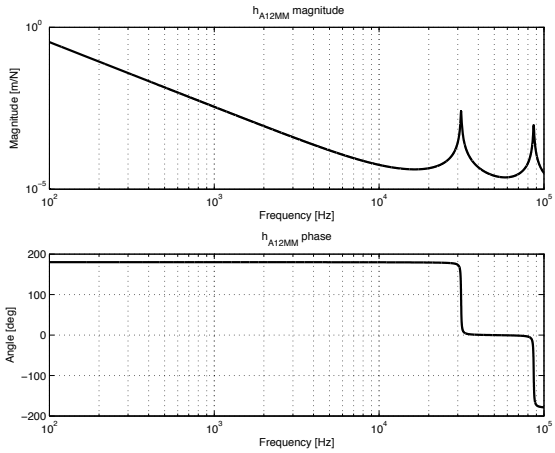

(c) Bode plot of h_{A12MM}

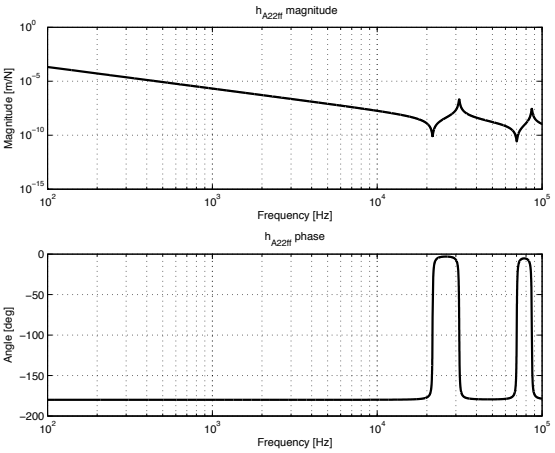

(d) Bode plot of h_{A22ff}

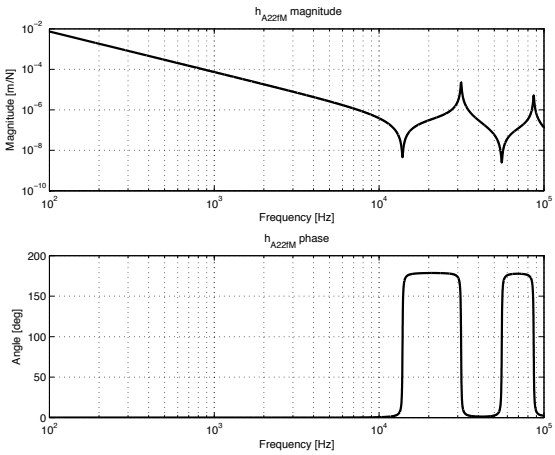

(e) Bode plot of h_{A22fM}

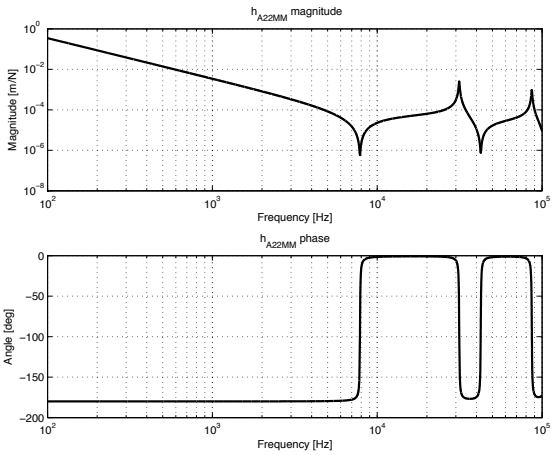

(f) Bode plot of h_{A22MM}

Figure 6.6: Bode plots using Euler–Bernoulli beam theory

6.3.2 Timoshenko Beam Theory

The Euler–Bernoulli beam theory leads to accurate results for beams which exhibit small cross-sectional area to length ratio (long slender beams). Generally for end mills/blank tools this condition does not hold and the Euler–Bernoulli theory does not lead to accurate predictions. For beams with high cross-sectional area to length ratio, shear effects become important. The Timoshenko beam model include rotary inertia and shear effects (Weaver et al., 1990). Each element has four degrees of freedom (rotation and translation at each end of the beam section). The corresponding differential equation is given by:

$$\left(\frac{\partial^2 y}{\partial t^2}+\frac{EI}{\rho A}\frac{\partial^4 y}{\partial x^4}\right)+\left(\frac{\rho I}{\hat{k}AG}\frac{\partial^4 y}{\partial t^4}+\frac{EI}{\hat{k}AG}\frac{\partial^4 y}{\partial x^2\partial t^2}\right)-\left(\frac{I}{A}\frac{\partial^4 y}{\partial x^2\partial t^2}\right)=0 \tag{6.25}$$

The mass matrix M and stiffness matrix K for a free-free beam section are given by (Yokoyama, 1990):

$$\begin{aligned} M \;=\; & \frac{\rho Al}{(1+\phi)^2}\begin{bmatrix} \frac{13}{15}+\frac{7\phi}{10}+\frac{\phi^2}{3} & \left(\frac{11}{210}+\frac{11\phi}{120}+\frac{\phi^2}{24}\right)l & \frac{9}{70}+\frac{3\phi}{10}+\frac{\phi^2}{6} & -\left(\frac{13}{420}+\frac{3\phi}{40}+\frac{\phi^2}{24}\right)l \\ & \left(\frac{1}{105}+\frac{\phi}{60}+\frac{\phi^2}{120}\right)l^2 & \left(\frac{13}{420}+\frac{3\phi}{40}+\frac{\phi^2}{24}\right)l & -\left(\frac{1}{140}+\frac{\phi}{60}+\frac{\phi^2}{120}\right)l^2 \\ & & \frac{13}{35}+\frac{7\phi}{10}+\frac{\phi^2}{3} & -\left(\frac{11}{210}+\frac{11\phi}{120}+\frac{\phi^2}{24}\right)l \\ Symmetric & & & \left(\frac{1}{105}+\frac{\phi}{60}+\frac{\phi^2}{120}\right)l^2 \end{bmatrix} \\ & +\frac{\rho Al}{(1+\phi)^2}\left(\frac{r_g}{l}\right)^2\begin{bmatrix} \frac{6}{5} & \left(\frac{1}{10}-\frac{\phi}{2}\right)l & -\frac{6}{5} & \left(\frac{1}{10}-\frac{\phi}{2}\right)l \\ & \left(\frac{2}{15}+\frac{\phi}{6}+\frac{\phi^2}{3}\right)l^2 & -\left(\frac{1}{10}-\frac{\phi}{2}\right)l & -\left(\frac{1}{30}+\frac{\phi}{6}+\frac{\phi^2}{6}\right)l^2 \\ & & \frac{6}{5} & -\left(\frac{1}{10}-\frac{\phi}{2}\right)l \\ Symmetric & & & \left(\frac{2}{15}+\frac{\phi}{6}+\frac{\phi^2}{3}\right)l^2 \end{bmatrix} \end{aligned} \tag{6.26}$$

Here, A is the area of cross-section, l is the element length, r_g is the radius of gyration and ϕ is the shear deformation parameter represented as:

$$\phi=\frac{12EI(1+\eta)}{\hat{k}GAl^2} \tag{6.27}$$

G is the shear modulus given by:

$$G=\frac{E}{2+2\nu} \tag{6.28}$$

ν is the poisson ratio, $\hat{k}$ is the shear coefficient which depends on the cross-section shape and

poisson ratio. For a circular section $\hat{k}$ can be given by (Hutchinson, 2001):

$$\hat{k} = \frac{6(1+\nu)^2}{7+12\nu+4\nu^2} \tag{6.29}$$

$$\begin{aligned} K \quad = \quad & \frac{EI(1+i\eta)}{l^3(1+\phi)^2}\begin{bmatrix} 12 & & 6l & -12 & 6l \\ & & (4+2\phi+\phi^2)l^2 & -6l & (2-2\phi-\phi^2)l^2 \\ & & & 12 & -6l \\ Symmetric & & & & (4+2\phi+\phi^2)l^2 \end{bmatrix} \\ & + \frac{\hat{k}AG\phi^2}{4l(1+\phi)^2}\begin{bmatrix} 4 & 2l & -4 & 2l \\ & l^2 & -2l & l^2 \\ & & 4 & -2l \\ Symmetric & & & l^2 \end{bmatrix} \end{aligned} \tag{6.30}$$

Mass and stiffness matrices also include the solid damping value. The element mass and stiffness matrices are assembled to form a global mass $\underline{M}$ and stiffness matrix $\underline{K}$. The equation of motion in the frequency domain is given for n elements:

$$[-\underline{M}\omega^2 + \underline{K}]\begin{bmatrix} x_1 \\ \theta_1 \\ x_2 \\ \theta_2 \\ . \\ . \\ . \\ x_{n+1} \\ \theta_{n+1} \end{bmatrix} = \begin{bmatrix} f_1 \\ m_1 \\ f_2 \\ m_2 \\ . \\ . \\ . \\ f_{n+1} \\ m_{n+1} \end{bmatrix} \tag{6.31}$$

The input data used for Timoshenko beam theory is presented in Table 6.1. The resulting FRFs are plotted in the form of Bode diagrams as shown in Figure 6.7a–Figure 6.7f and Figure 6.8a–Figure 6.8d.

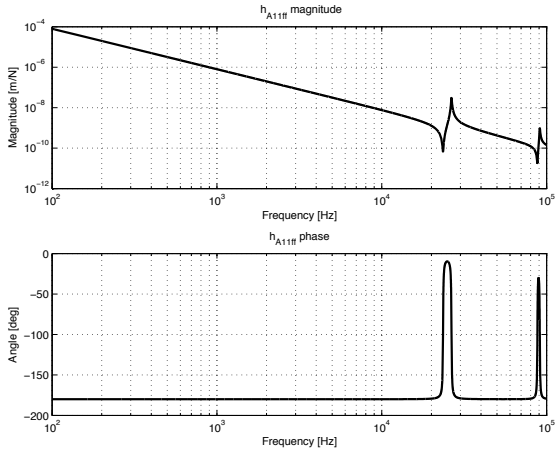

(a) Bode plot of h_{A11ff}

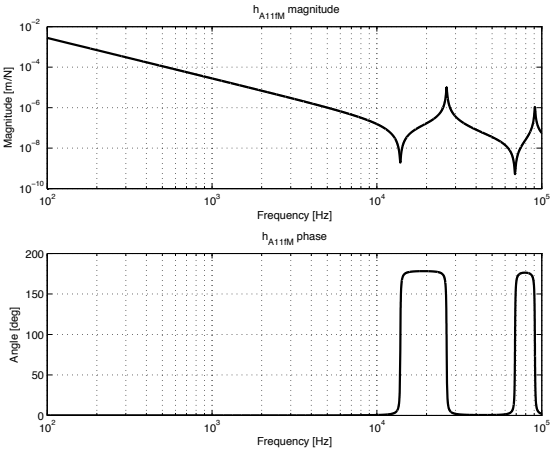

(b) Bode plot of h_{A11fM}

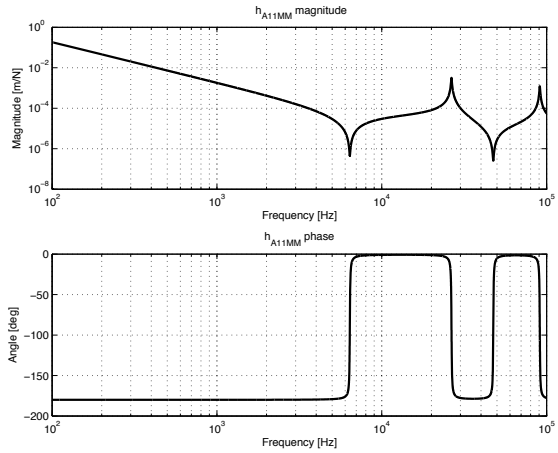

(c) Bode plot of h_{A11MM}

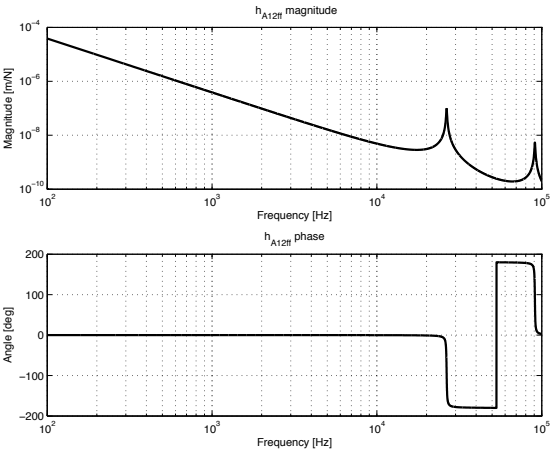

(d) Bode plot of h_{A12ff}

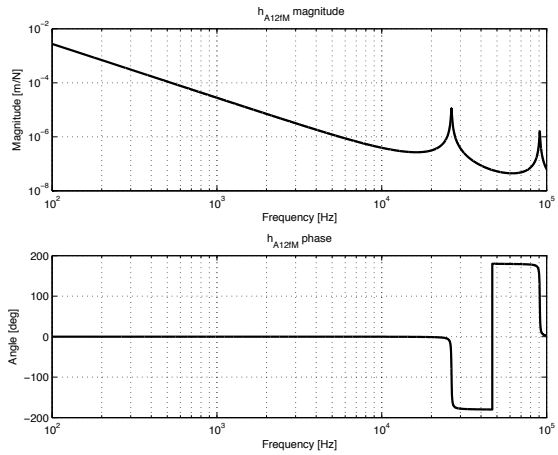

(e) Bode plot of h_{A12fM}

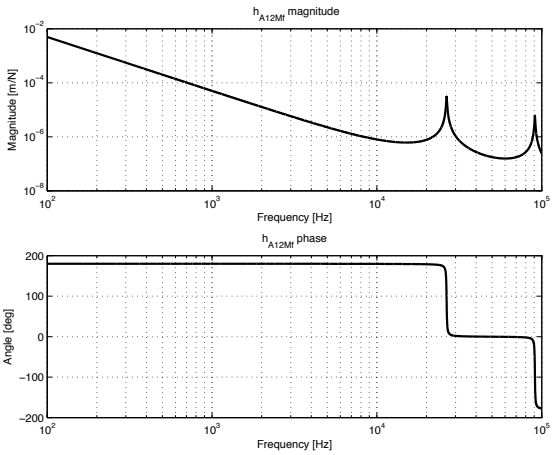

(f) Bode plot of h_{A12Mf}

Figure 6.7: Bode plots using Timoshenko beam theory

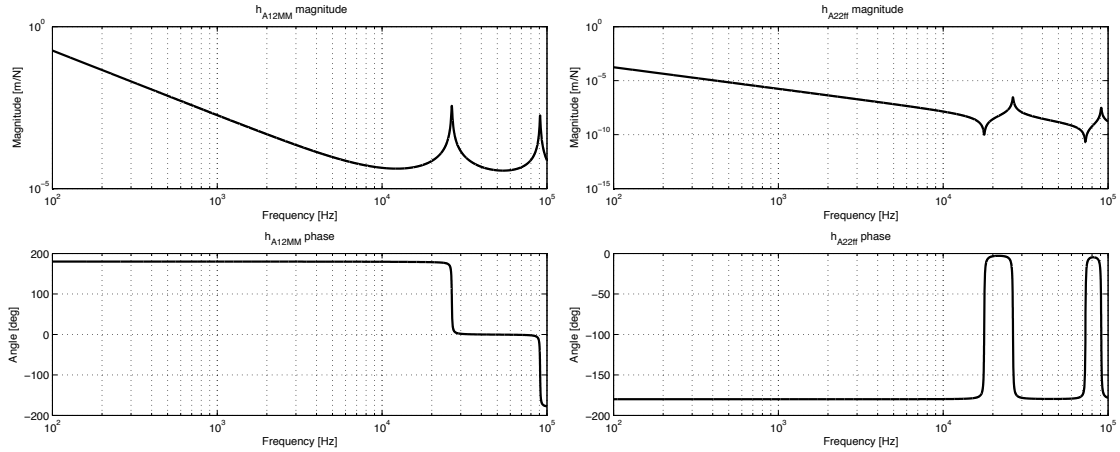

(a) Bode plot of h_{A12MM}

(b) Bode plot of h_{A22ff}

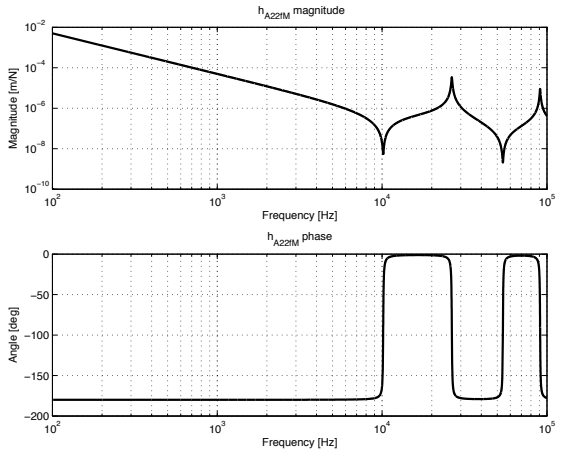

(c) Bode plot of h_{A22fM}

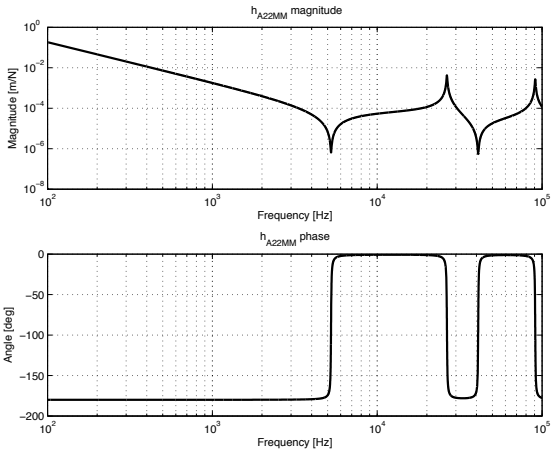

(d) Bode plot of h_{A22MM}

Figure 6.8: Bode plots using Timoshenko beam theory

6.3.3 Beam Modeling using FEM

In this subsection the dynamics characteristics of a beam (Equation 6.14) are predicted using finite element analysis of a 3D beam model. Finite element modeling and analysis is performed with ANSYS 11.0. In the preprocessing phase the 3D geometry of the blank tool is created. Material properties are defined in Table 6.1.

The element type used for this case is SOLID187. SOLID187 is a higher order 3D element with 10 nodes. SOLID187 has a quadratic displacement behavior and is well suited for modeling irregular meshes. The finite element model of the beam is shown in Figure 6.9. In the solution phase, modal analysis is performed with free boundary conditions. A subspace method is used for mode extraction. This method is suitable for evaluating the few modes and works well for well shaped solid elements. The beam section was meshed with element size of 6.

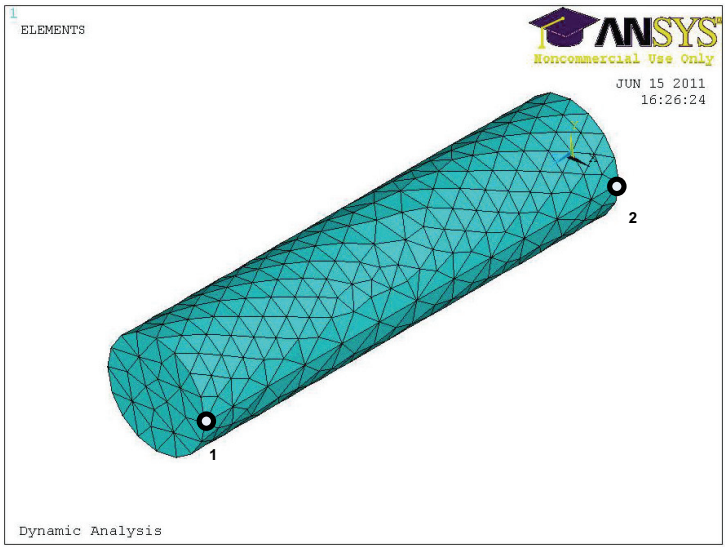

Figure 6.9: Finite element model of beam

The effect of mesh size on the natural frequency of the beam section is presented in Table 6.2. For the present work first 12 ($n = 12$) modes are evaluated. Natural frequencies of the first six modes occur at 0Hz.

Table 6.2: Effect of mesh size on the natural frequencies

meshsize	3	4	5	6	7
Mode 7	27668	27741	27788	27763	27691
Mode 8	27864	27861	27830	27768	27725
Mode 9	47650	47653	47603	47340	46913

In the post processing phase eigenvalues and eigenvectors of the first n modes at the points 1 and point 2 are retrieved in the form of "eig" files. A sample of an "eig" file for point 1 is shown in Figure 6.10. A MATLAB program is written to extract the corresponding eigenvalues and eigenvectors from the "eig" files. Eigenvalues represent the natural frequencies of the modes and eigenvectors represents the mode shapes. FRFs prediction using ANSYS is described using flowchart as shown in Figure 6.11. The transfer function matrix (Equation 6.14) for the blank tool is derived from eigenvalues and eigenvectors (U) for point 1 and point 2. Each FRF of the transfer function matrix being evaluated at frequency ω, excited at degree of freedom e and evaluated at degree of freedom d, can be calculated by the superposition of n modes as:

$$H(i\omega) = \sum_{k=1}^{n} \frac{U_{d,k} U_{e,k}}{\omega_{ok}^2 - \omega^2 + i2\omega\eta\omega_{ok}} \tag{6.32}$$

here

$$\omega_{ok} = (2\pi\omega_{nk})^2 \tag{6.33}$$

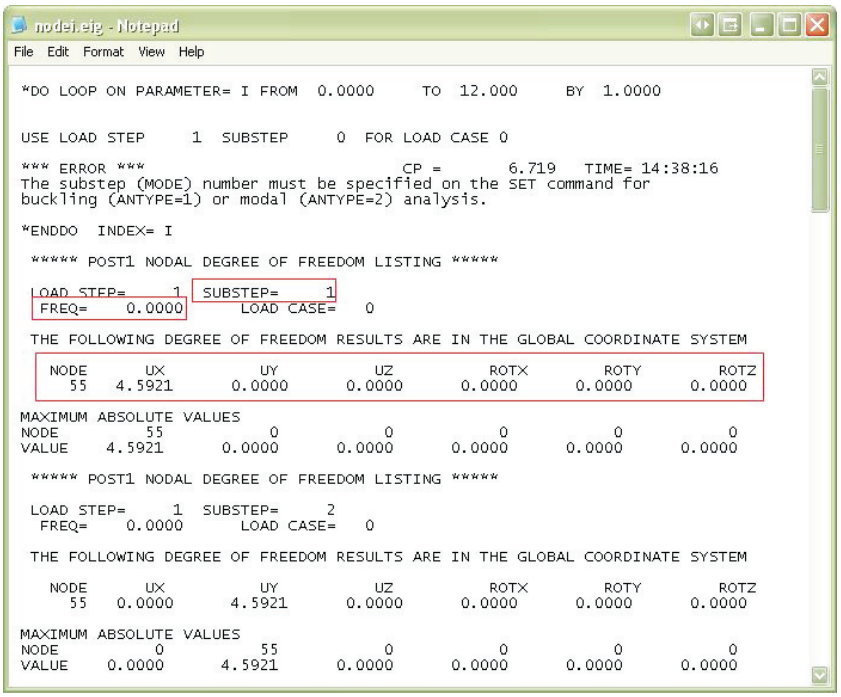

node1.eig - Notepad

File Edit Format View Help

```
*DO LOOP ON PARAMETER= I FROM  0.0000     TO  12.000     BY  1.0000


USE LOAD STEP     1  SUBSTEP     0  FOR LOAD CASE 0

*** ERROR ***                            CP =       6.719   TIME= 14:38:16
The substep (MODE) number must be specified on the SET command for
buckling (ANTYPE=1) or modal (ANTYPE=2) analysis.

*ENDDO  INDEX= I

 ***** POST1 NODAL DEGREE OF FREEDOM LISTING *****

 LOAD STEP=     1  SUBSTEP=     1
  FREQ=     0.0000       LOAD CASE=    0

 THE FOLLOWING DEGREE OF FREEDOM RESULTS ARE IN THE GLOBAL COORDINATE SYSTEM

   NODE      UX          UY          UZ          ROTX        ROTY        ROTZ
     55   4.5921      0.0000      0.0000      0.0000      0.0000      0.0000

MAXIMUM ABSOLUTE VALUES
NODE          55           0           0           0           0           0
VALUE     4.5921      0.0000      0.0000      0.0000      0.0000      0.0000

 ***** POST1 NODAL DEGREE OF FREEDOM LISTING *****

 LOAD STEP=     1  SUBSTEP=     2
  FREQ=     0.0000       LOAD CASE=    0

 THE FOLLOWING DEGREE OF FREEDOM RESULTS ARE IN THE GLOBAL COORDINATE SYSTEM

   NODE      UX          UY          UZ          ROTX        ROTY        ROTZ
     55   0.0000      4.5921      0.0000      0.0000      0.0000      0.0000

MAXIMUM ABSOLUTE VALUES
NODE           0          55           0           0           0           0
VALUE     0.0000      4.5921      0.0000      0.0000      0.0000      0.0000
```

Figure 6.10: Sample of “eig” file

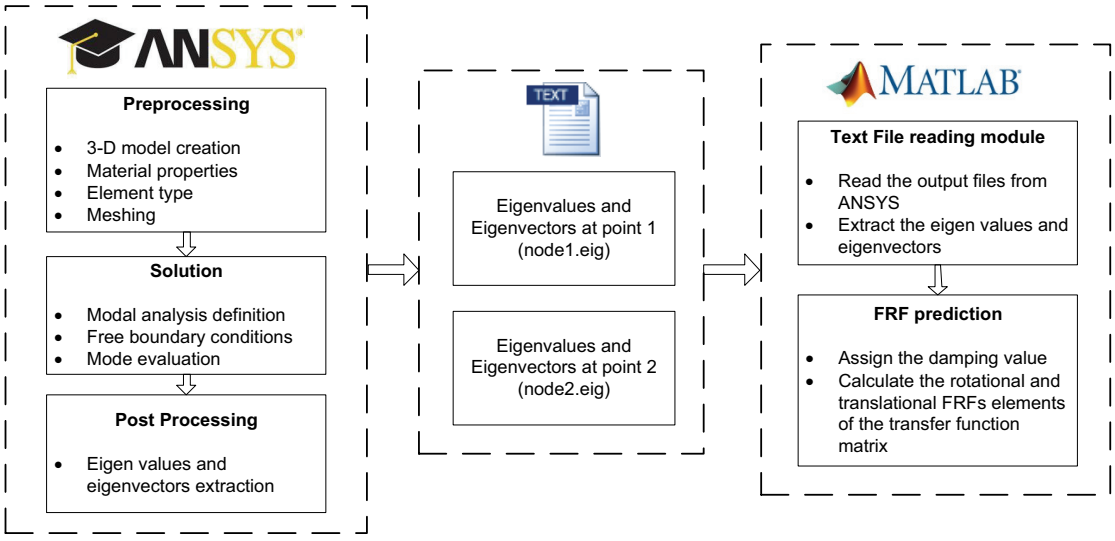

Figure 6.11: System for FRF prediction using ANSYS

ω_{nk} is the natural frequency of the k^{th} mode evaluated from ANSYS. The resulting FRFs are plotted in the form of Bode diagrams as shown in Figure 6.12a–Figure 6.12f and Figure 6.13a–Figure 6.13d

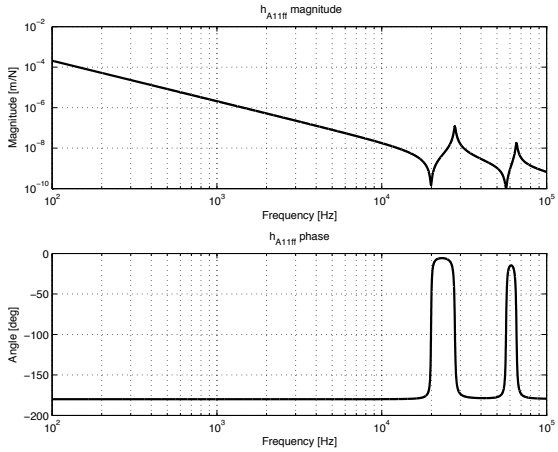

(a) Bode plot of h_{A11ff}

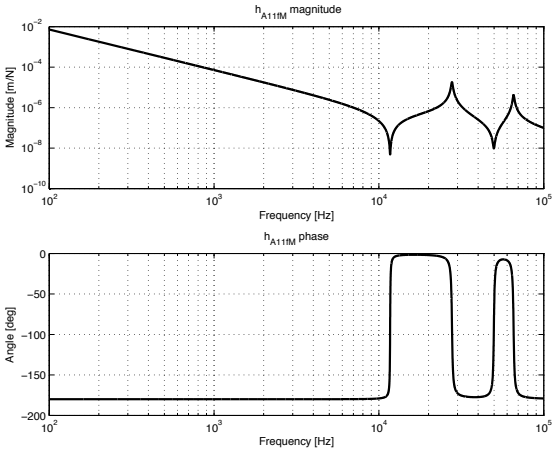

(b) Bode plot of h_{A11fM}

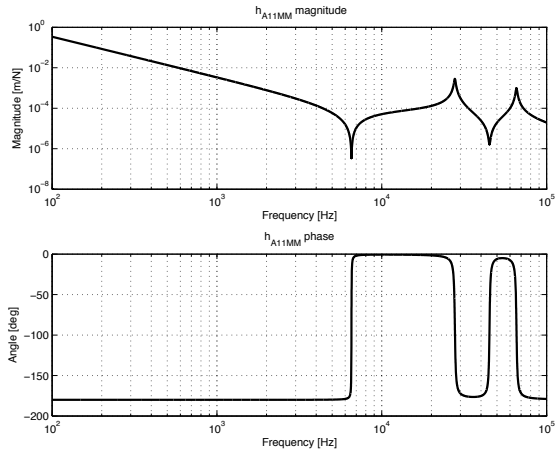

(c) Bode plot of h_{A11MM}

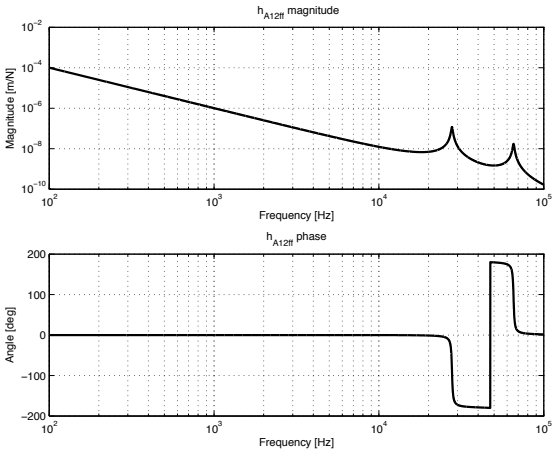

(d) Bode plot of h_{A12ff}

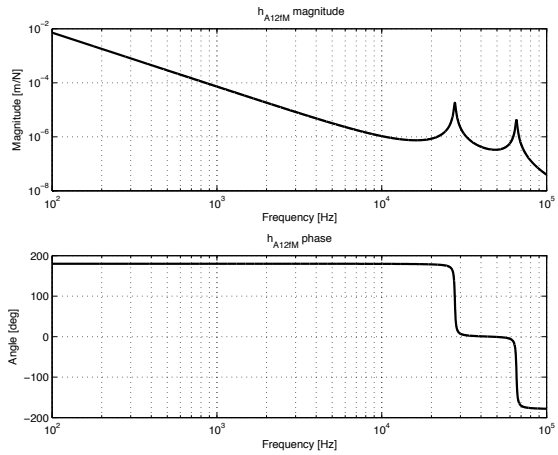

(e) Bode plot of h_{A12fM}

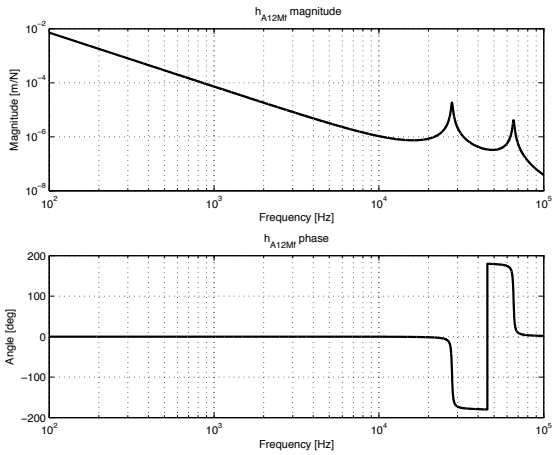

(f) Bode plot of h_{A12Mf}

Figure 6.12: Bode plots using ANSYS

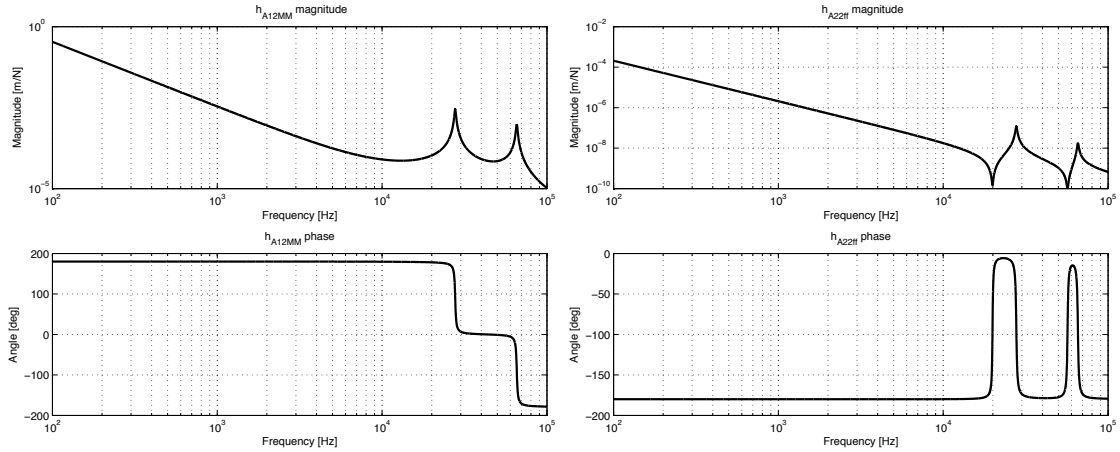

(a) Bode plot of h_{A12MM}

(b) Bode plot of h_{A22ff}

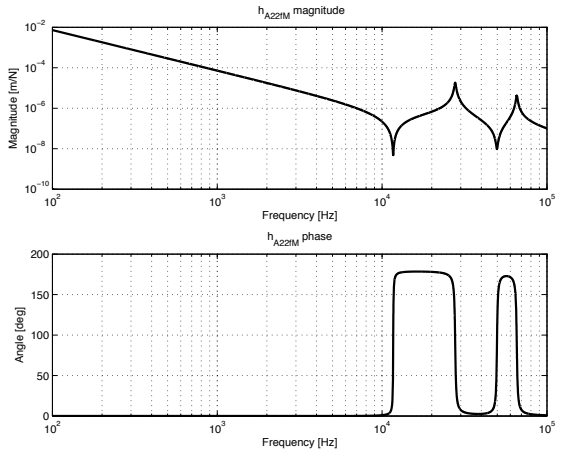

(c) Bode plot of h_{A22fM}

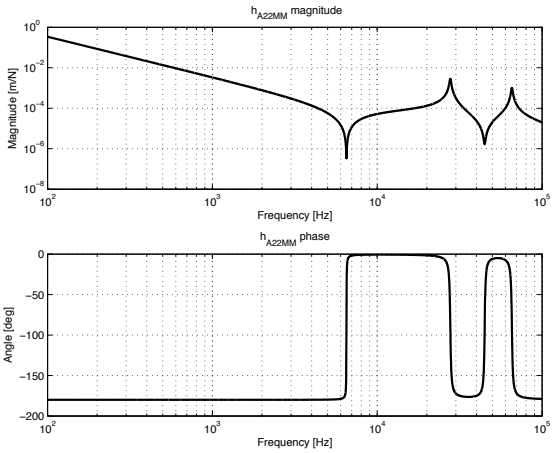

(d) Bode plot of h_{A22MM}

Figure 6.13: Bode plots using ANSYS

6.3.4 Comparison of Beam Theories

In this section the natural frequencies identified using beam theories and with FEM model are compared. The length of the beam (Table 6.1) is varied from 40mm-100mm and other parameters are kept the same. The natural frequency of each beam is identified with Euler–Bernoulli, Timoshenko beam theories and ANSYS. The comparison is presented in Table 6.3 and Figure 6.14. It is clear from that with increase in length of the beam (decreasing ratio of cross-sectional area to length) the difference between the results from ANSYS and beam theories decreases. There is also a decrease in the difference between the Timoshenko theory and Euler–Bernoulli theory. It is concluded from the comparison analysis that Timoshenko beam theory is more accurate than Euler–Bernoulli theory and produces similar results to ANSYS.

Table 6.3: Comparison of natural frequencies

L_{beam} (mm)	Natural Frequency (Hz)			Error	
	ANSYS	Timoshenko	Euler–Bernoulli	Timoshenko	Euler–Bernoulli
40	31000	32530	35490	4.94	14.48
50	20636	21420	22710	3.80	10.05
60	14694	15120	15770	2.90	7.32
70	10972	11220	11590	2.26	5.63
80	8490	8650	8873	1.88	4.51
90	6756	6866	7011	1.63	3.77
100	5502	5578	5679	1.38	3.22

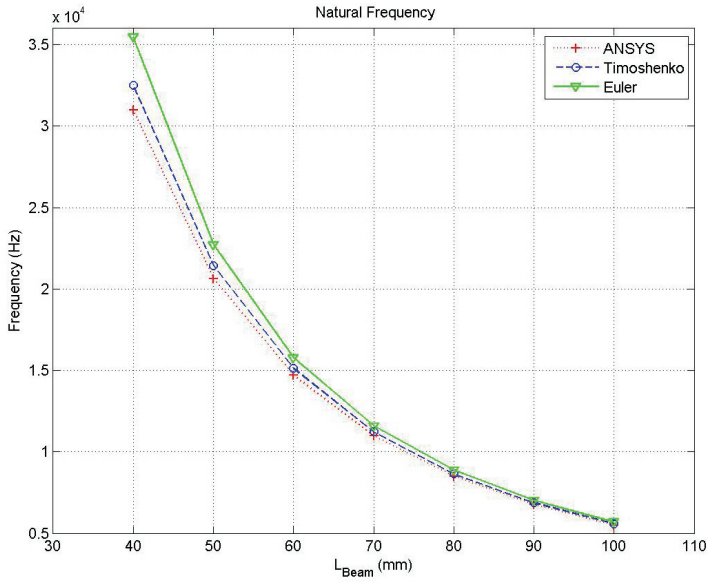

Figure 6.14: Comparison of natural frequencies

6.3.5 Modeling of Fluted End Mill

In order to predict FRF of spindle/tool holder/cutting tool system with an end mill, the dynamics of the end mill are predicted as explained in Section 6.3. Diameter of the beam will be different from the end mill diameter in order to incorporate the effect of the fluted portion (Cheng, 2007). Area section properties for fluted end mills are presented in Table 6.4 and the equivalent diameter of the beam is calculated.

Table 6.4: Area section properties for fluted end mills

N	A_{fluted}/A_{shank}	I_{fluted}/I_{shank}
2	38.27%	44.04%
3	35.66%	33.49%
4	35.88%	35.94%

A_{fluted} is the cross-section area of the fluted portion, A_{shank} is the cross-section area of the shank, I_{fluted} is the moment of inertia of the fluted portion and I_{shank} is the moment of inertia of the shank. The end mill dynamics are computed with beam receptance by incorporating the effect of the fluted portion.

The cutting tool tip FRF of spindle/tool holder/end mill system is calculated with Equation 6.11 from FRFs for subsystem A (equivalent diameter beam) and subsystem B. .

6.4 Implementation and Experimental Validation

In this section the complete procedure for FRF prediction at the cutting tool tip of the spindle/-tool holder/end mill system is presented. The procedure consists of two sub-steps which are explained as follows:

1. In the first step, the constant rotational degrees of freedom FRFs ($h_{B22fM}(= h_{B22Mf})$ and h_{B22MM}) of the spindle/tool holder subsystem are found by the inverse receptance coupling technique (as presented in Section 6.2.1) which is as follows:

   (a) Direct FRFs (h_{B22ff}) are measured at joint location 2 as shown in Figure 6.3. In the present work, a 20mm diameter blank tool is used for experimental purposes. The FRFs (h_{B22ff}) are measured on two different machine tool systems. The measurement setup for direct FRF at joint location 2 is presented in Figure 6.15a.

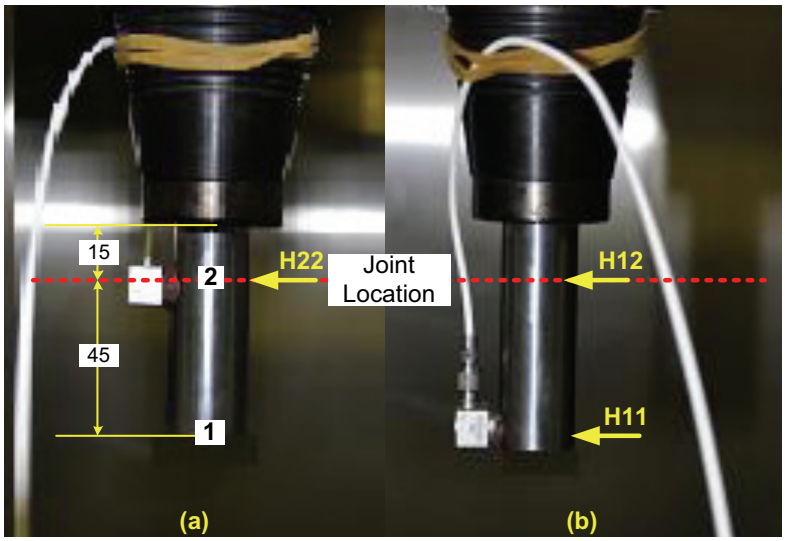

Figure 6.15: Experimental setup for measurement of FRFs

   (b) Direct (H_{11}) and cross (H_{12}) FRFs of spindle/tool holder/blank tool system at location 1 are measured as shown in Figure 6.15b. H_{22} is measured at the joint location with the same blank tool which is used for H_{12} and H_{11} measurement. All the

measured FRFs on the corresponding machine tools are presented in Figure 6.16a and Figure 6.16b .

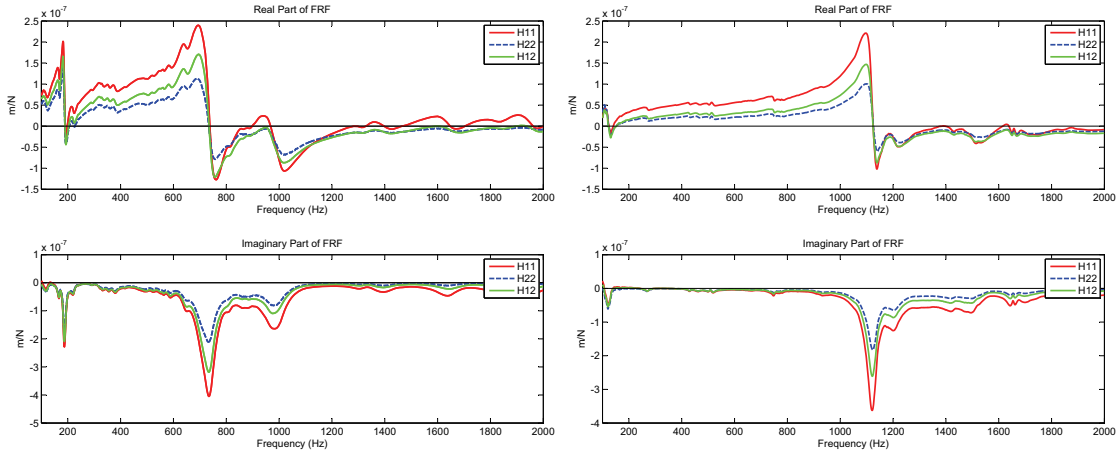

(a) Measured FRFs on machine tool system 1

(b) Measured FRFs on machine tool system 2

Figure 6.16: Measured FRFs for inverse RC

(c) the dynamics of the portion of a long blank are calculated using beam receptance modeling as detailed in Section 6.3.

(d) From the measured FRFs of subsystem B and computed FRFs of subsystem A, measured and modeled FRFs of subsystem A and subsystem B, rotational degrees of freedom (RDOF) FRFs for spindle/tool holder (subsystem B) are calculated from inverse receptance coupling (Equation 6.18). These RDOF are a constant property of the spindle/tool holder subsystems and will be used for the prediction of tool tip FRFs for different end mills.

2. In the second step, the equivalent beam (fluted end mill) is modeled using beam receptance (Section 6.3) by taking into account the effect of the fluted portion. Area section properties of the fluted end mill are given in Table 6.4. In order to predict the tool tip FRFs for new end mill, Equation 6.11 is used with the various FRFs of subsystem A (by beam receptance modeling for fluted end mill) and subsystem B (identified FRFs in step one).

The experimental details for predicted and measured FRFs for different end mills are presented in Figure 6.17. An end mill with diameter 16mm and 2 flutes is used with machine tool system 1 and an end mill with diameter 20mm and 2 flutes is tested with machine tool system 2.

The FRFs are predicted for both end mills by using the receptance coupling procedure. The FRFs are also measured directly at the tool tip with direct hammer testing. The predicted and measured FRFs for the 16mm end mill are presented in Figure 6.18a and the corresponding FRFs for the 20mm end mill are presented in Figure 6.18b.

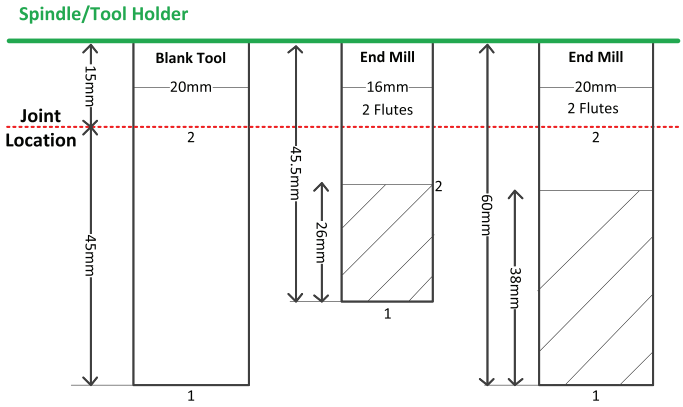

Figure 6.17: Experimental details for predicted and measured FRFs

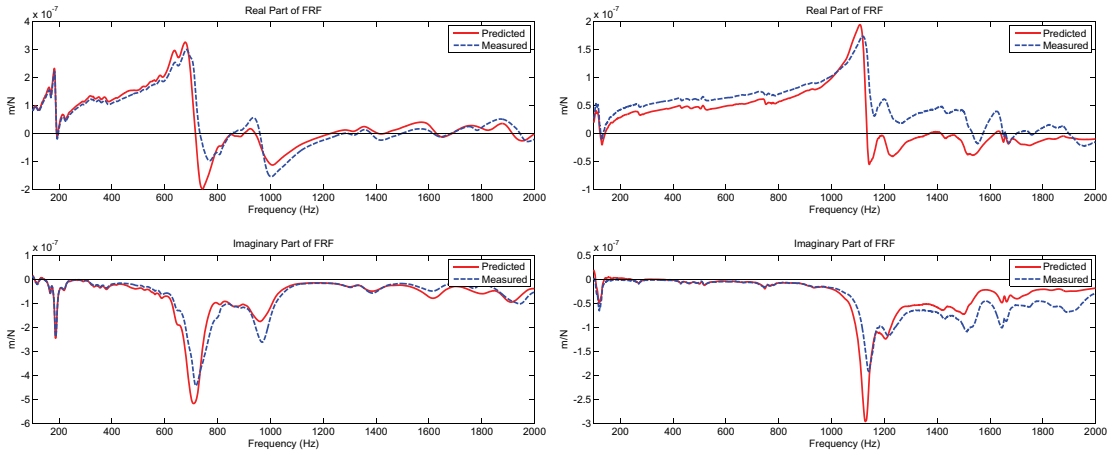

(a) Predicted and measured FRFs for end mill with 16mm diameter

(b) Predicted and measured FRFs for end mill with 20mm diameter

Figure 6.18: Predicted and measured FRFs for end mills

It is clear from Figure 6.18 that the predicted FRFs are quite accurate in comparison to their measured counterparts. The small difference can be because of the assumed properties of the fluted portion. It is concluded from the imaginary part of FRFs that the predicted FRFs are more flexible than the measured FRFs. The resulting SLDs from predicted and measured FRFs for the 16mm end mill are presented in Figure 6.19a and for the 20mm end mill are shown in Figure 6.19b. The SLDs are generated for full immersion with following inputs: $K_{tc} = 681 N/mm^2$, $K_{rc} = 86 N/mm^2$ and N=2. Conservative stability limits are developed from the predicted FRFs.

Based on the requirement and applications, one has to make a compromise between the accurate values of permissible limits of stable depths of cut with direct measurement of FRFs with hammer testing for different end mills or conservative values of permissible depths of cut

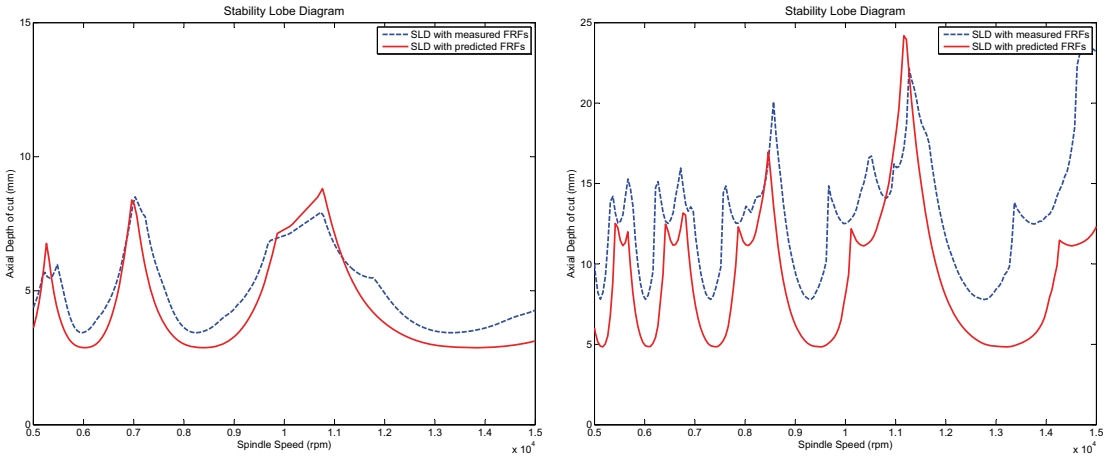

(a) SLDs for end mill with 16mm diameter

(b) SLDs for end mill with 20mm diameter

Figure 6.19: Resulting SLD for predicted and measured FRFs for end mills

with predicted FRFs while saving time in hammer testing each end mill.

6.5 Conclusion

A procedure is developed for the prediction of FRFs of the spindle/tool holder/end mill system for different end mills. The procedure includes the implementation of the receptance coupling technique by considering the rotational and translational degrees of freedom of both spindle/tool holder and end mill. The translational degree of freedom FRFs of the spindle/tool holder are measured directly with hammer testing. The rotational degrees of freedom FRFs of the spindle/tool holder are then identified by inverse receptance coupling. The FRFs of end mills are predicted with beam receptance considering the effect of the fluted portion. Different beam receptance models are presented and compared for the FRF computation of subsystem A. The FRFs of the machine tool system with different end mills are predicted with the developed procedure. The predicted FRFs are compared with the measured FRFs by direct hammer testing. The predicted FRFs are quite accurate in comparison to their measured counterparts.

In future, it would be interesting to compute the FRFs of end mills by finite element analysis of 3D models of fluted end mill. Better compliance is expected between predicted and measured FRFs.

7 Online Chatter Detection and Control

7.1 Introduction

In the developed optimization system (OptMill), the stability lobe diagrams are generated for selection of stable cutting conditions. Though the mathematical models predict accurately the chatter free cutting conditions their implementation on production floors has yet not been achieved due to the absence of technical expertise and experimental resources. Chatter vibrations are often encountered in industrial practice. There is still a practical need to bring to production floors an inexpensive, easy to use and computationally fast system that can automatically detect chatter during milling and thereafter propose a control strategy. This will be a considerable step towards fulfilling the goal of smart machining.

The objective of the present work is to develop an automatic online system which should be able to detect accurately the existence of chatter vibrations for whole range of spindle speeds. The system should be able to detect the evolution of the chatter vibrations and dominant chatter frequencies along the cutting toolpath. The developed system must be easy to implement for industrial application and should not hamper the normal working of the machining process. The chatter detection and control system should be computationally fast in order to be implemented for real time industrial applications. In the case of unstable milling the system should guide the machine tool user for corrective actions to control the chatter vibrations.

7.2 Chatter Detection and Control System

The overall architecture of the developed chatter detection and control system is presented in Figure 7.1. Cutting sound signals are measured with the help of a microphone. The real time values of spindle speed are collected directly from the machine controller. The user defined value of number of flutes of the cutting tool is also extracted from the machine controller. The data acquisition platform is developed in (MATLAB, 2011). The online chatter detection and control system is developed in (MATLAB, 2011). The measured cutting sound signal is

processed using frequency domain analysis.

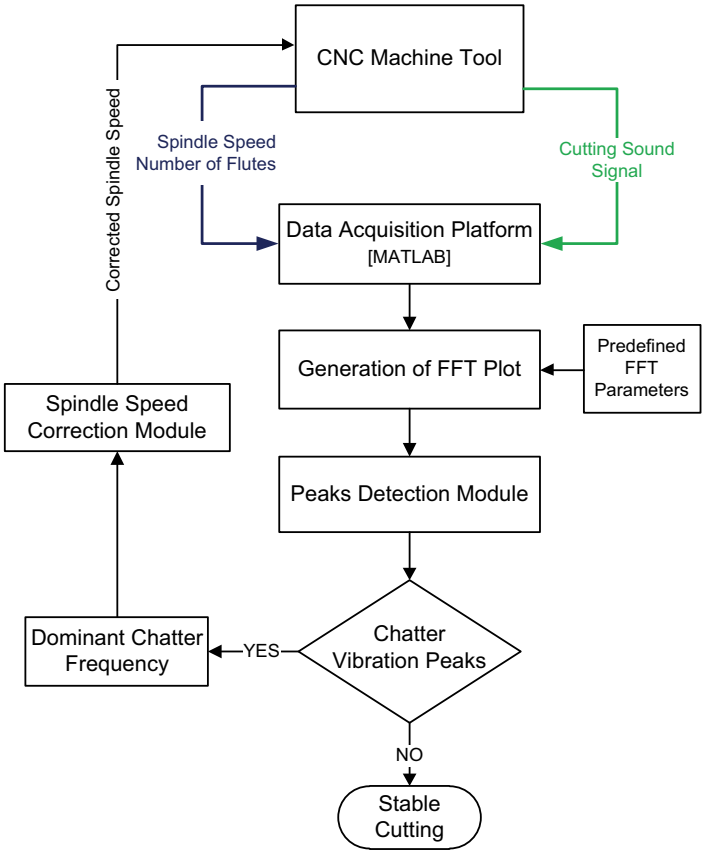

Figure 7.1: Overall architecture of chatter detection and control system

7.2.1 Frequency Domain Analysis of Cutting Sound Signal

The cutting sound signal in the time domain can be converted to its counterpart in the frequency domain by means of a Fourier Transform (FT). The signal must be sampled at discrete time by an A/D converter before it can be analyzed by a computer. Discrete Fourier Transform (DFT) is used to convert the discrete signal in the time domain to a discrete signal in the frequency domain (Lyons, 2011).

Given a sequence of N sample points of the sound signal, $X(n)$, indexed by $n = 0,1,2...N-1$, the discrete Fourier transform is defined as, $x(k)$, where $k = 0,1,2...N-1$.

$$x(k) = \sum_{n=0}^{N-1} X(n) e^{-j2\pi \frac{k}{N} n} \tag{7.1}$$

here,
x: Frequency domain representation of the sound signal in the time domain, X . The formula yields a complex number $x(k)$ for every k, the $x(k)$'s are called 'Fourier coefficients' or 'har-

monics'
k: k^{th} frequency component; $k = 0, 1, 2...N-1$
N: Total number of samples in sound signal X
n: n^{th} sample of the sound signal in time domain

Fast Fourier transform (FFT) is an efficient and fast algorithm to compute the discrete Fourier transform. In this section we will discuss the important parameters which significantly influence the frequency domain solution and thus affect the performance and accuracy of the chatter detection and control system.

Sampling Rate

Sampling rate dictates the highest frequency which can be detected from the sound signal. Chatter vibrations vary from 100Hz (because of heavy structures like the machine tool itself or the machine table etc.) to 5000Hz (because of flexible cutting tool or flexible workpiece) (Delio et al., 1992). In order to detect the highest possible chatter vibration in the sound signal the sampling rate must be selected accordingly. The sampling rate defines the number of samples per unit of time (usually seconds) taken from a continuous sound signal to make a discrete signal. In order to avoid the aliasing effect the sampling rate is selected according to the Nyquist theorem which states that *"sampling rate should be at least twice the highest frequency contained in the signal"*

$$F_s > 2\max(F_c) \tag{7.2}$$

Here F_s is the sampling rate. F_c is the chatter frequency. For the current work sampling rate is selected as 22050Hz. With 22050Hz sampling rate, we will be able to detect frequencies ranging from 0–11025Hz. It is important to mention here is that higher sampling rates also increase the computational cost involved during acquisition and analysis.

The typical syntax for computing the FFT of any discrete signal in MATLAB is presented as:

$$FFT_{signal} = FFT(X(n), NFFT) \quad \text{for} \quad NFFT \geq length(X) \tag{7.3}$$

$X(n)$ is the sound signal in time domain. $NFFT$ is the number of points in the FFT spectrum, $length(X)$ is the sample size of the sound signal which is defined as:

$$length(X) = F_s T \tag{7.4}$$

Here T is the recorded time in seconds.

Sample Size

The selection of sample size dictates the original frequency resolution that can be achieved in FFT spectrum.

$$FR_{original} = \frac{F_s}{length(X)} \tag{7.5}$$

In order to detect two frequencies in the sound signal which differ by aHz, the sample size must be:

$$length(X) \geq \frac{Fs}{a} \quad \text{or} \quad T \geq \frac{1}{a} \tag{7.6}$$

For the present work $FR_{original}$ is selected as 1Hz ($length(X) = F_s$ or $T = 1$s). From this part onwards $length(X) = F_s$.

NFFT

The basic FFT plot is presented in Figure 7.2. The obtained frequency resolution is defined as:

$$FR = \frac{F_s}{NFFT} \tag{7.7}$$

It is concluded from the FFT plot that the frequency spectrum is symmetrical about $\frac{F_s}{2}$. We will be able to detect the frequencies and their corresponding amplitude (also called power) up to $\frac{F_s}{2}$ depending upon the frequency resolution.

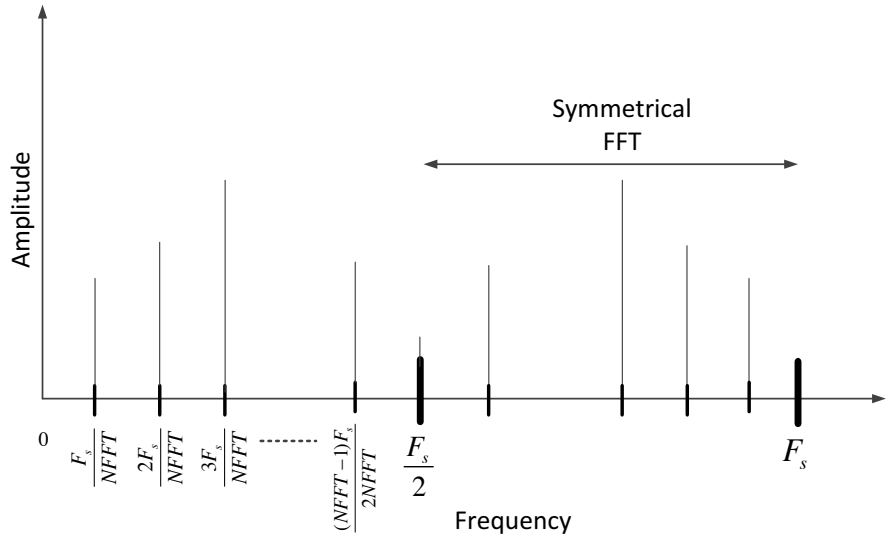

Figure 7.2: Concept of FFT plot

When $NFFT = length(X)$, the frequency resolution (FR) will be equal to 1Hz. The FFT spectral lines will be separated by 1Hz and will be indexed as $0, 1, 2...11025$Hz. In this case, the frequency peaks (for example 770Hz and 771Hz in the sound signal) will correspond exactly to FFT spectral lines and they will be detected with correct frequency value and correct power.

In the case of 770Hz and 773.5Hz, the frequency peak of 770Hz will be identified with correct power but instead of 773.5Hz frequency there will be two spectral lines at 773Hz and 774Hz. Moreover the power of the 773.5Hz frequency will be shared by 773Hz and 774Hz spectral lines. This effect is called “Picket Fence" which smears the peak or even makes it undetectable. One way to reduce the picket fence effect is to decrease further the original frequency resolution (increase $length(X)$). We are interested in detecting the chatter in a short sample size of sound to study the development of dominant chatter peaks along the cutting path so this option is ruled out.

Another way of reducing the picket fence effect is by increasing the NFFT without changing $length(X)$. When $NFFT > length(X)$, zeros are added at the end of the sample while keeping the original sound sample intact. This technique is called “Zero padding". This will change the location of FFT spectral lines and reduce the interval between these lines. In this way the spectral lines originally hidden in FFT plot ($NFFT = length(X)$) can be shifted to peaks where they can be detected. With this approach the frequency peak at 773.5Hz can be detected with correct power. Zero padding does not improve the original frequency resolution although it does provide more spectral lines via interpolation. Once the original frequency resolution is respected the zero padding is useful to locate accurately the frequency and power of the peaks present in the sound sample. It is important to mention here is that increase in NFFT value significantly increase the computational time. For the developed chatter detection system, $NFFT = 4length(X)$ is selected, frequency resolution of 0.25Hz, by considering the best compromise of computational cost and accuracy. With this the FFT spectral lines will be separated by 0.25Hz and will be indexed as $0, 0.25, 0.5...11025$Hz.

7.2.2 Chatter Detection System

The system is developed in a generic way so that it can be applied directly to detect chatter for different values of spindle speeds and other cutting conditions. In this section, the main steps involved in the development are explained as:

1. Real values of spindle speed are acquired directly from the machine controller. The number of flutes of the cutting tool is also extracted. Cutting sound is measured with the microphone with a sampling rate of 22050Hz. Input data for one second of recorded time is presented in Figure 7.3.

2. For a given input of cutting sound signal, the ‘Hann’ function is used as an anti-aliasing filter. FFT points are generated using predefined FFT parameters. The defined FFT parameters ensure the accurate calculation of frequencies and their corresponding

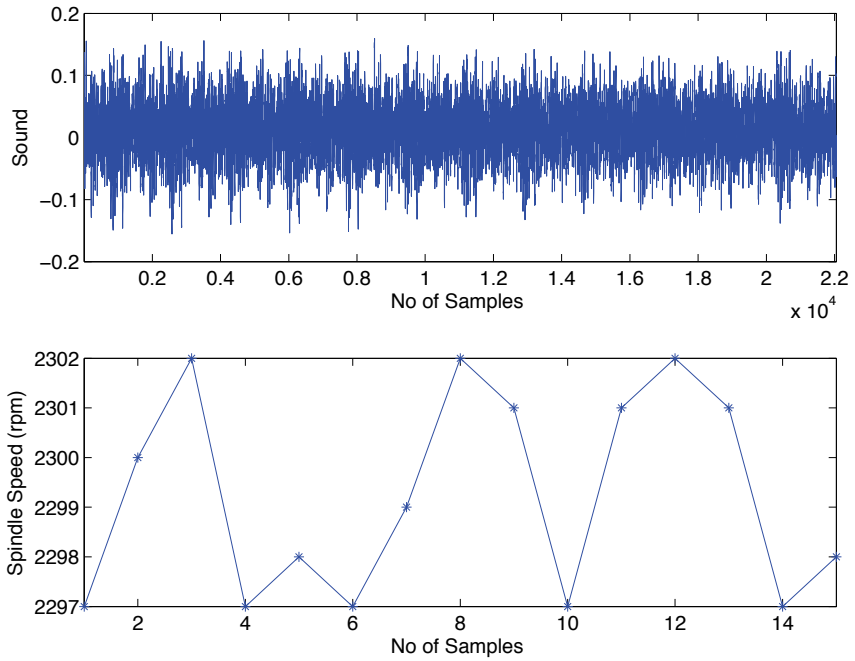

Figure 7.3: Cutting sound signal and spindle speed signal

power in the FFT spectrum. Power of the signal in the frequency domain is calculated as:

$$Power_{signal} = \frac{[abs(FFT_{signal})]^2}{length(X)} \tag{7.8}$$

It is clear from Figure 7.3 that spindle speed is not a constant value. For a given input of spindle speed signal, the average value of the spindle speed is used for calculating spindle frequency (SF), tooth passing frequency (TPF) and their corresponding harmonics. The spindle frequency and its harmonics (HSF) are given by:

$$\text{SF} = \frac{n}{60} \quad \text{and} \quad \text{HSF} = i\text{SF} \quad \text{where} \quad i = 1,2,3... \tag{7.9}$$

Tooth passing frequency (TPF) and its harmonics (HTPF) are given by:

$$\text{TPF} = \frac{Nn}{60} \quad \text{and} \quad \text{HTPF} = i\text{TPF} \quad \text{where} \quad i = 1,2,3... \tag{7.10}$$

Here n is the spindle speed in rpm and N is the number of flutes of the cutting tool. The resulting FFT spectrum along with spindle frequency, tooth passing frequency and their harmonic lines are presented in Figure 7.4. With 22050Hz of sampling rate and defined FFT parameters, frequencies up to 11025Hz can be detected with a resolution of 0.25Hz. The FFT spectrum from 100-1000Hz is presented in Figure 7.5. The frequency peaks present in the sound signal and their corresponding power can be identified from the

FFT spectrum plot.

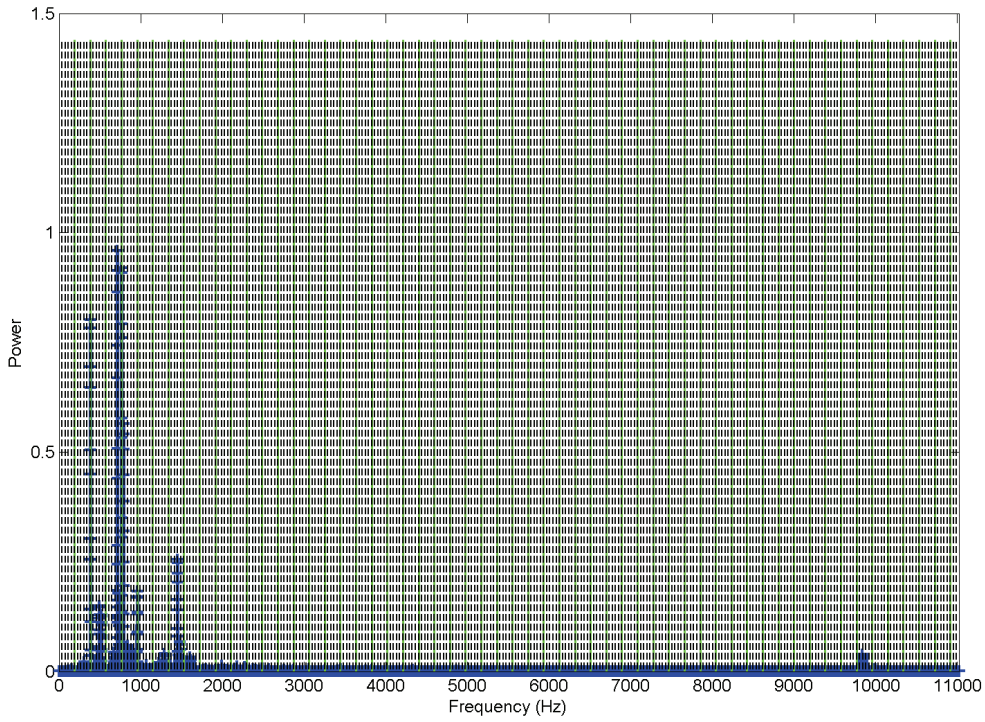

Figure 7.4: Complete FFT spectrum

3. For an automatic chatter detection system, the frequency of the peaks with high power must be selected automatically from the complete FFT spectrum. Mathematical peak detection methods (local maximum method, window search method, first derivative method etc.) can be implemented to detect the peaks and their corresponding frequencies. Local maximum method and window search methods are not very suitable and computationally effective for our objectives. Selecting the proper window size and its location for FFT spectrum points is a tedious task for the whole range of spindle speeds. For the present work, the first derivative method is used. The basic idea of the first derivative method is as follows:

   - A positive peak center is located in a position x_c where the first derivative at $x_c - 1$ is positive while the first derivative at $x_c + 1$ is negative.
   - A negative peak center is located in a position x_c where the first derivative at $x_c - 1$ is negative while the first derivative at $x_c + 1$ is positive.

   With the first derivative method all the peaks in the FFT spectrum are detected. Peaks with power higher than 5% of $[\max(Power_{signal}) - \min(Power_{signal})]$ are detected as high power peaks and will be used for later analysis. Here the 5% value is not a threshold level. It is used to reduce the computational time by targeting only the peaks of interest. Moreover, the selection of high power peaks is independent of the cutting conditions in

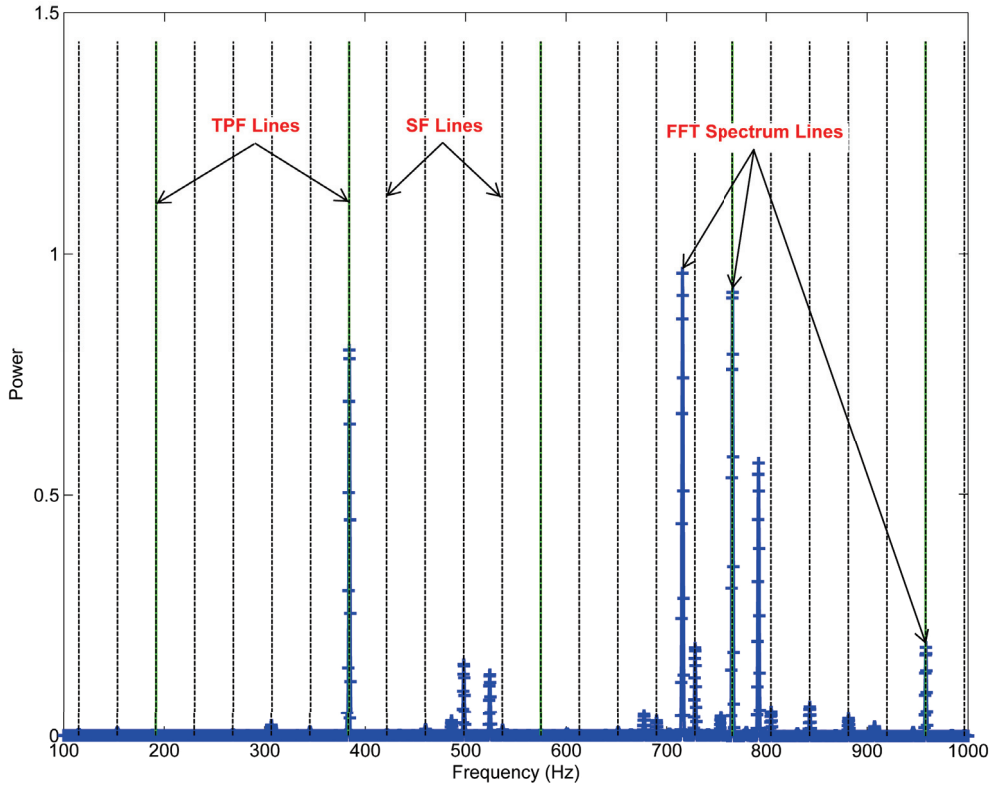

Figure 7.5: FFT spectrum for 100-1000Hz

the peak detection module. The resulting FFT spectrum plot with detected high power peaks is presented in Figure 7.6.

4. Once frequency and power of all the high peaks present in the sound signal are detected from the FFT spectrum plot, the dominant chatter peak is automatically detected (in the case of chatter).

    - During stable milling only the peaks of spindle frequency, tooth passing frequency and their harmonics are present in the FFT spectrum of the sound signal
    - In the case of unstable milling there a significance presence of chatter frequency peaks in addition to the peaks of spindle frequency, tooth passing frequency and their harmonics.

    A search algorithm is used for the detection of peaks of spindle frequency, tooth passing frequency and their harmonics as they are not exactly the same as FFT spectral lines. All other peaks are defined as chatter peaks and the dominant chatter peak is identified automatically. The resulting dominant peak in the FFT spectrum plot is presented in Figure 7.7. The dominant chatter frequency (f_c) is used for chatter control by suggesting a corrected spindle speed.

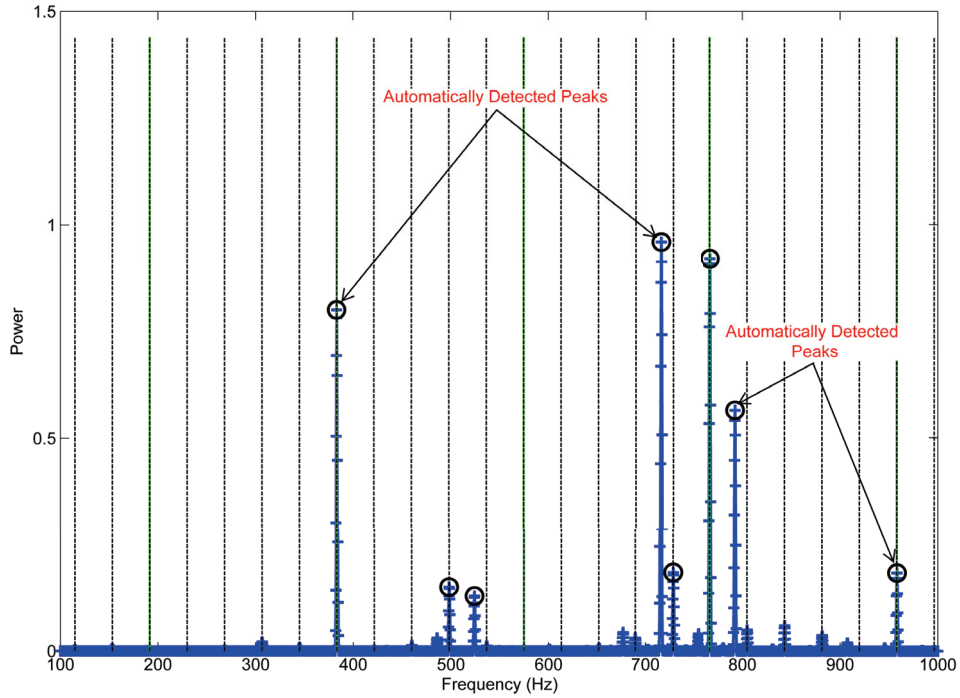

Figure 7.6: Approach for automatic peak detection

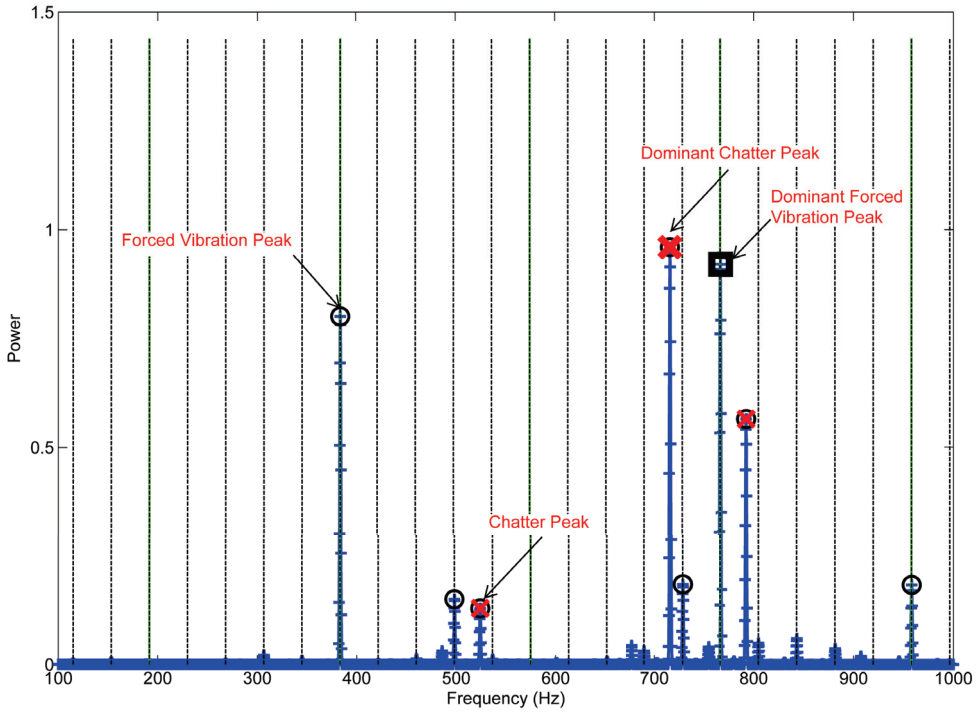

Figure 7.7: Approach for dominant chatter peak detection

It is important to mention that in the developed chatter detection system, the frequencies and corresponding power of dominant peaks (chatter or stable) are identified automatically and accurately. For a given cutting test, chatter is detected from the power of chatter peaks (in the case of chatter) in comparison to the power of stable peaks. Chatter detection during a cutting test with one set of cutting condition is independent of the cutting test conducted with different cutting conditions. The developed system does not require any prior cutting tests to define the threshold power limits of the dominant peaks and detect the existence of chatter.

7.2.3 Chatter Control System

As presented in Figure 2.5, If the relative phase (φ) is 0°, the dynamic chip thickness is also zero and leads to stable cutting cutting. From the developed chatter detection system (Section 7.2.2) in the case of unstable milling, the dominant chatter frequency is identified. For chatter control, new spindle speeds are chosen such that the dominant chatter frequency (f_c) coincides with the new tooth passing frequency (TPF) or its higher harmonics ($HTPF$). The chatter frequency is related to the phase difference between two subsequent waves (Altintas, 2000):

$$\varphi + s = \frac{60 f_c}{n(s) N} \tag{7.11}$$

Where s is the integer number of full vibration waves imprinted on the surface of the workpiece and φ is the phase different between the wavy surface left by the previous tooth and the current cutting tool vibration, $n(s)$ is the spindle speed in rpm.

For stable milling conditions as presented in Figure 2.5, φ in Equation 7.11 must be 0°. The corrected spindle speeds are calculated as:

$$n(s) = \frac{60 f_c}{N s} \tag{7.12}$$

7.3 Experimental Results and Discussion

The developed chatter detection system has been verified experimentally with different machine tools, cutting tools and workpiece materials as presented in Table 7.1. Although many cutting tests were conducted during development, implementation and verification of the developed system only the important results are presented which demonstrate the accuracy and scope of the chatter detection system. The different cutting conditions are presented in Table 7.2.

Table 7.1: Details of experiments for validation of chatter detection and control system

Cutting Tool	Diameter (mm)	No. of Flutes	Workpiece Material	Machine Used
Face Mill	40	5	Steel (CK 45)	Mikron 800 HPM
End Mill	20	2	Aluminium (EN AW-6082)	Mikron 800 HPM
End Mill	16/20	2	Al-7075/Certal	CB Ferrari A152

Table 7.2: Cutting conditions selected for experiments

Cutting Tool	Spindle Speed (n) (rpm)	Axial DOC (A_p) (mm)	Radial DOC (A_e) (mm)	Feed Rate (f_t) (mm/min)
Face Mill	2300	1.3	25	920
	2300	1.4	25	920
	2300	1.7	25	920
	2300	1.5	25	920
End Mill	6000	8	20	960
	6000	12	20	960
	6000	10	20	960
	6000	9.5	20	960
End Mill	19500	7.5	20	3900
	24000	5	16	7200

7.3.1 Results with Face Mill

Partial immersion tests were performed with face milling tools and steel as workpiece material. The main objectives of these tests were to verify the chatter detection system. For cutting test (A_p=1.3mm), the results of the analysis of cutting sound measured along cutting tool movement are presented in Figure 7.8. Every plot shows the FFT of cutting sound sampled during each second along the cutting tool movement. The plots contain only the forced frequencies with dominant frequency at 383Hz. It is concluded that this case is stable as there is no chatter vibration peak in the power spectrum of the cutting sound signal.

For the cutting test (A_p=1.4mm), the results of the simulation are presented in Figure 7.9. There are only forced frequency peaks in the plot. This cutting test is also a stable case as there is no presence of frequency peaks other than forced vibrations.

For the cutting test (A_p=1.7mm), the results of the simulation are presented in Figure 7.10. There is a significant presence of chatter peaks along with forced frequency peaks. It was detected that the power of the dominant chatter peaks (≈716Hz) was greater than the dominant forced vibration peaks. This is a clear case of high chatter vibration.

Cutting test (A_p=1.5mm) is also performed in order detect the transition of chatter peaks from cutting test (A_p=1.4mm) to cutting test (A_p=1.7mm) and moreover to confirm the ability of the developed system to detect the change in power of frequency peaks. The results of the simulation are presented in Figure 7.11. It is interesting to notice that there is a significant

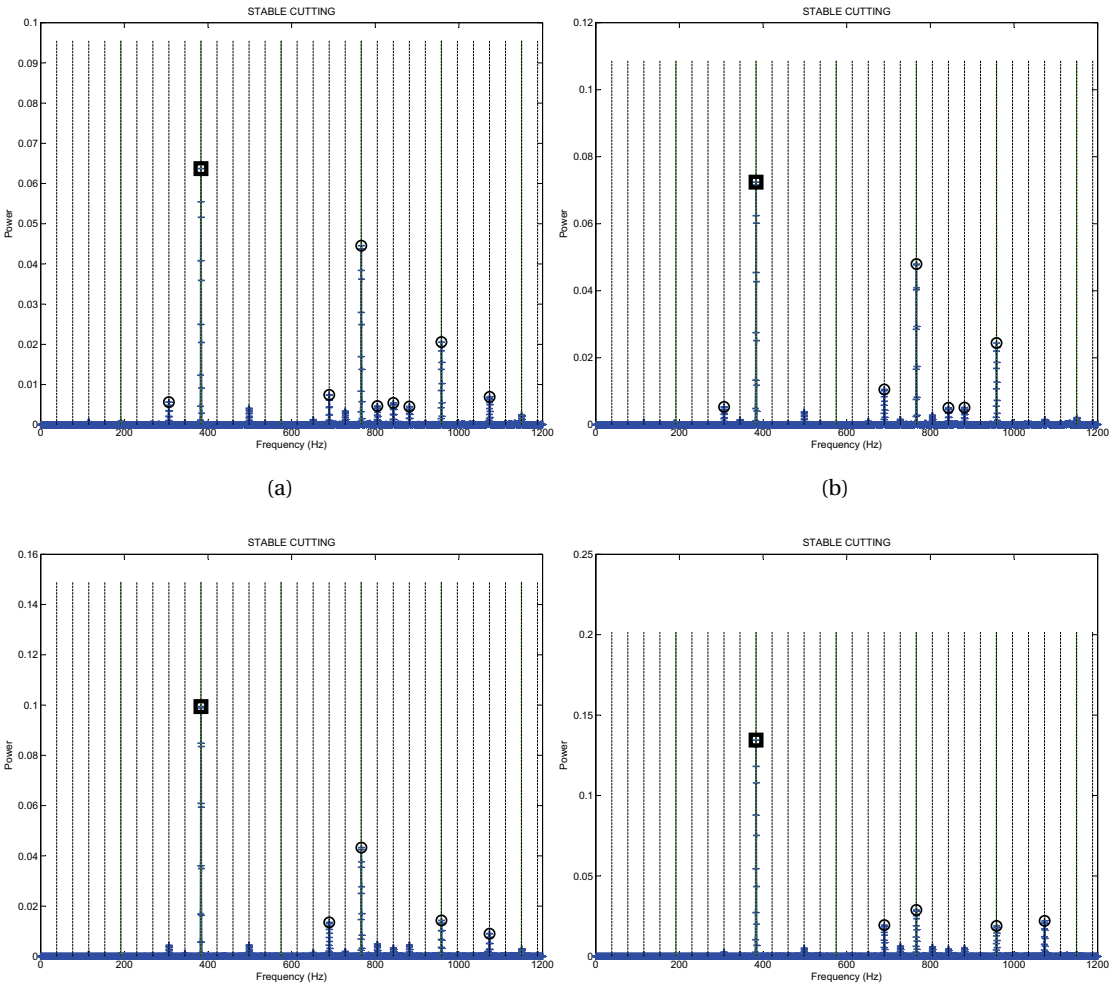

Figure 7.8: Results of cutting test (A_p=1.3mm), stable milling

presence of chatter peaks along with the forced vibrations. It is also a clear case of chatter. The power of dominant chatter peaks is comparatively smaller than the forced vibrations peaks. It is concluded from the plots shown Figure 7.10 and Figure 7.11 that the cutting test (A_p=1.7mm) is more unstable than cutting test (A_p=1.5mm).

The developed chatter detection system is capable of detecting chatter accurately. This is evident from the corresponding power spectra of different cutting tests. Depending on the applications of the developed system, it can even be used to detect chatter at an early stage so the high chatter cases can be avoided.

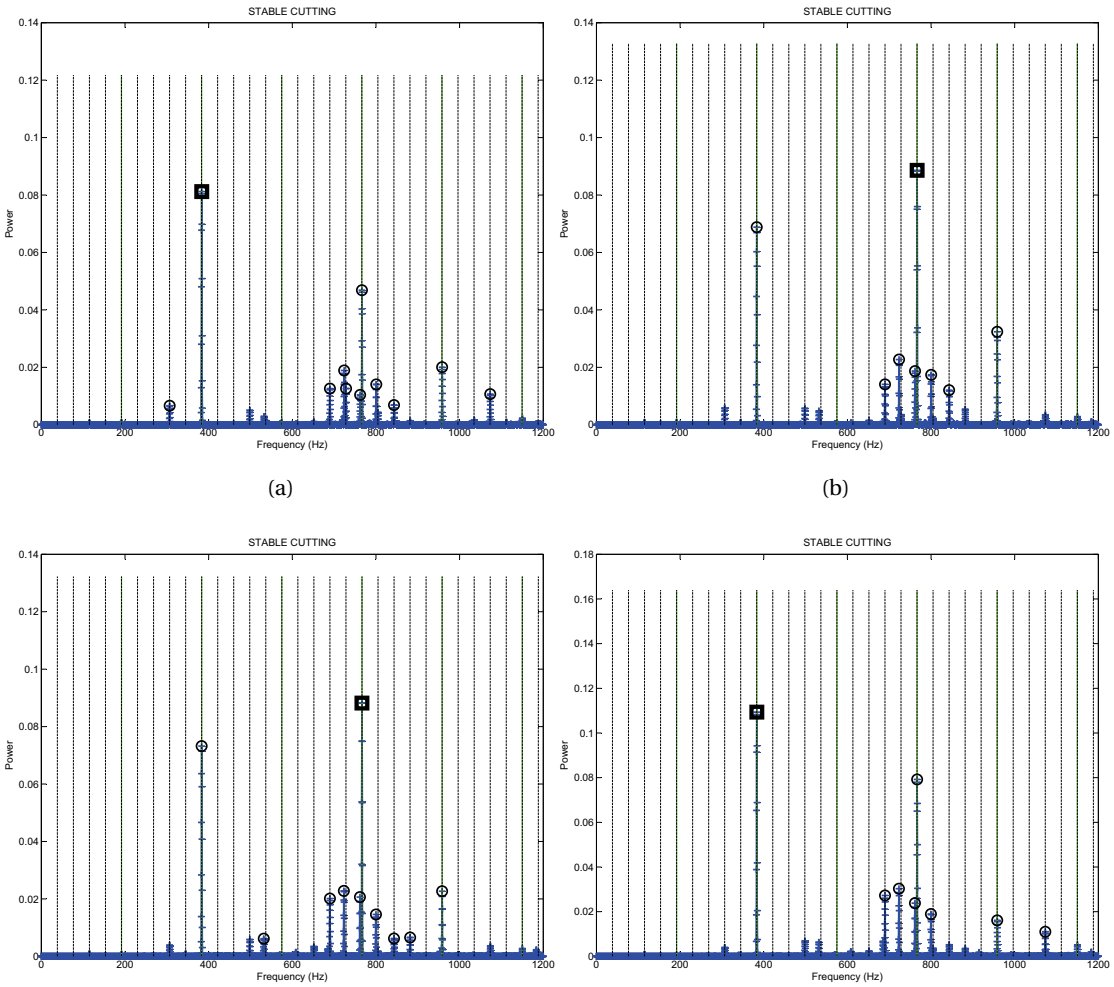

Figure 7.9: Results of cutting test (A_p=1.4mm), stable milling

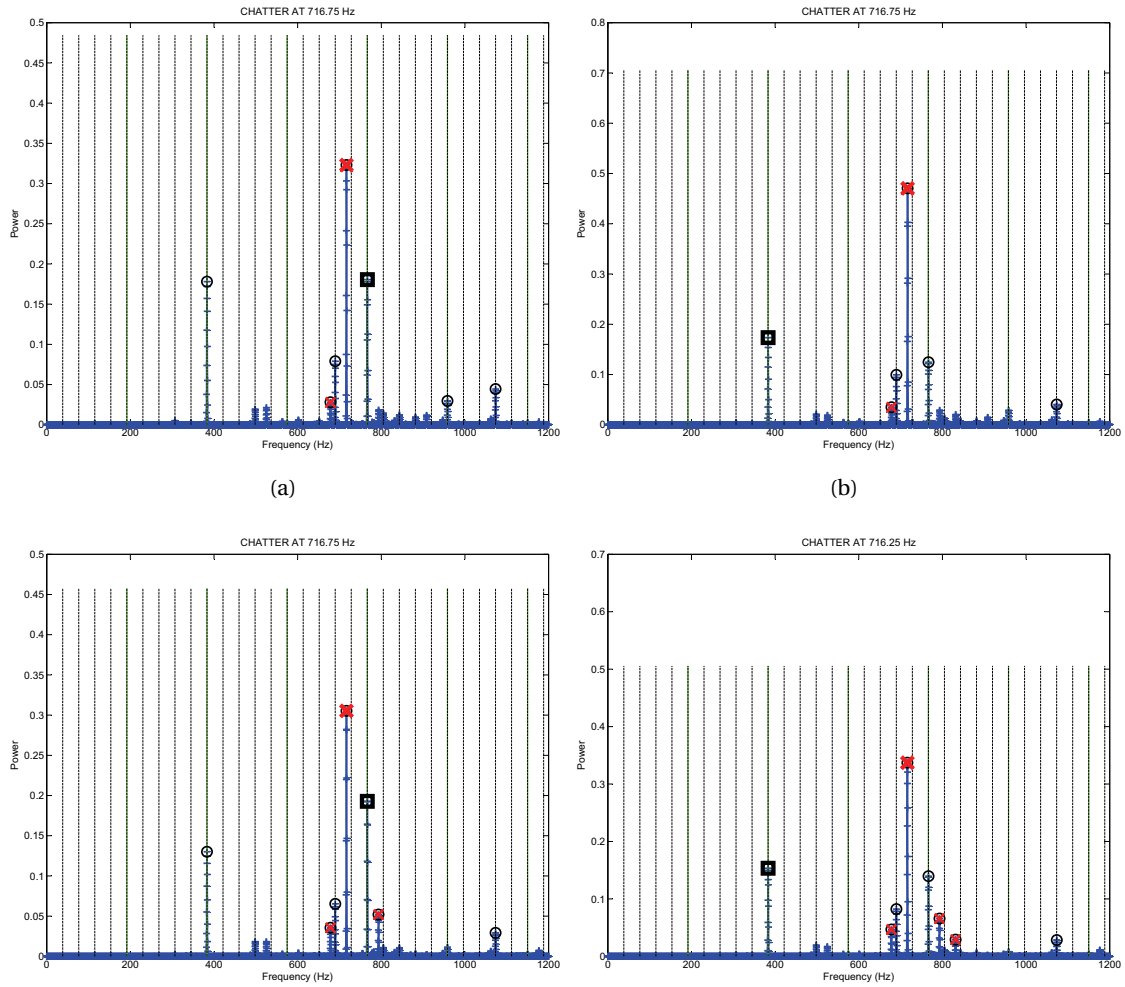

Figure 7.10: Results of cutting test (A_p=1.7mm), chatter

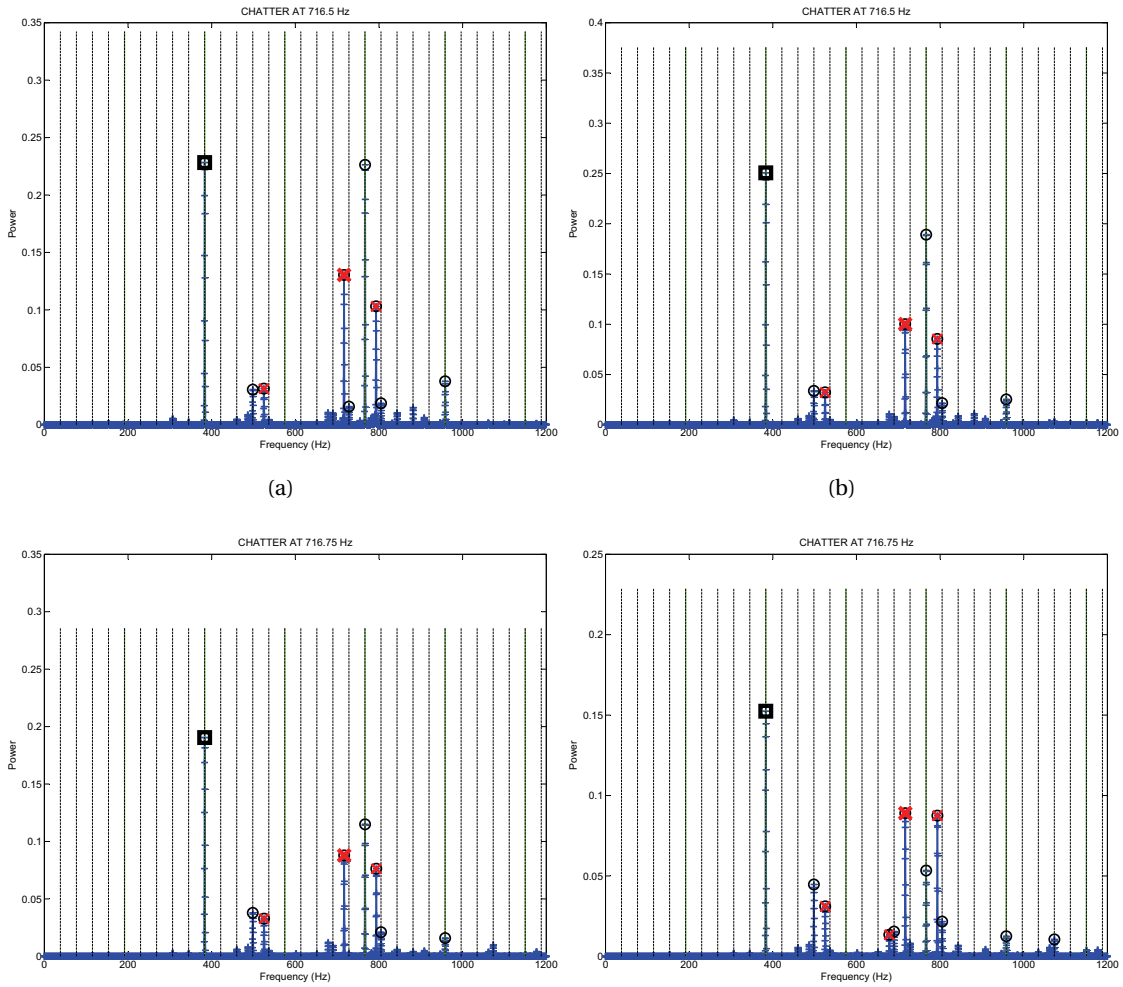

Figure 7.11: Results of cutting test (A_p=1.5mm), chatter

7.3.2 Results with End Mill

Although separate experiments were not performed at high spindle speed measured cutting sound during the experiments performed on CB Ferrari A152 was used for verification of the developed chatter detection system. These experiments were performed for the validation of optimal cutting conditions (Chapter 4). Spindle speed and number of flutes were entered manually during the simulation of the developed system. The results of simulation for cutting tests (end mill of 20mm, A_p=7.5mm and n=19500mm) and (end mill of 16mm, A_p=5mm and n=24000mm) are presented in Figure 7.12 and Figure 7.13 respectively. It is concluded from the plots that the cutting tests are stable.

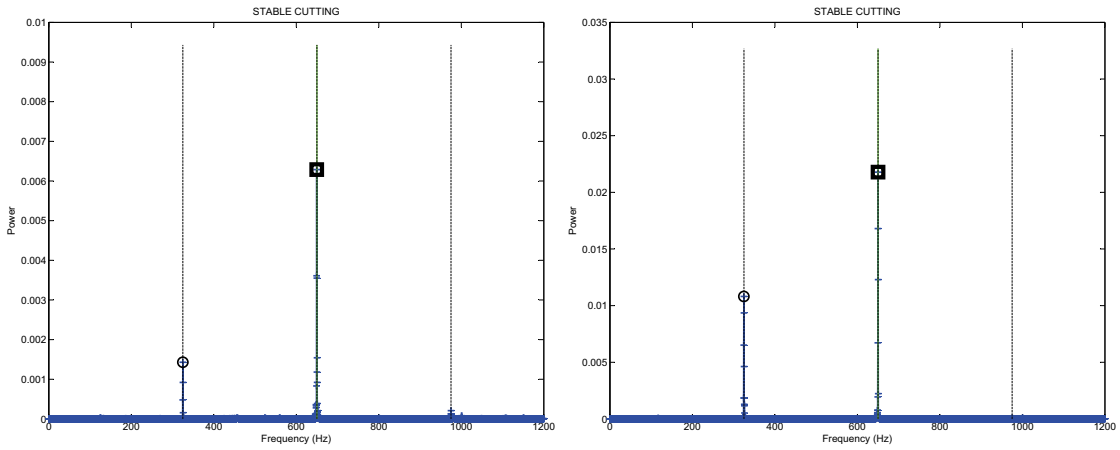

(a) (b)

Figure 7.12: Results of cutting test (A_p=1.5mm and n=19500rpm), stable milling

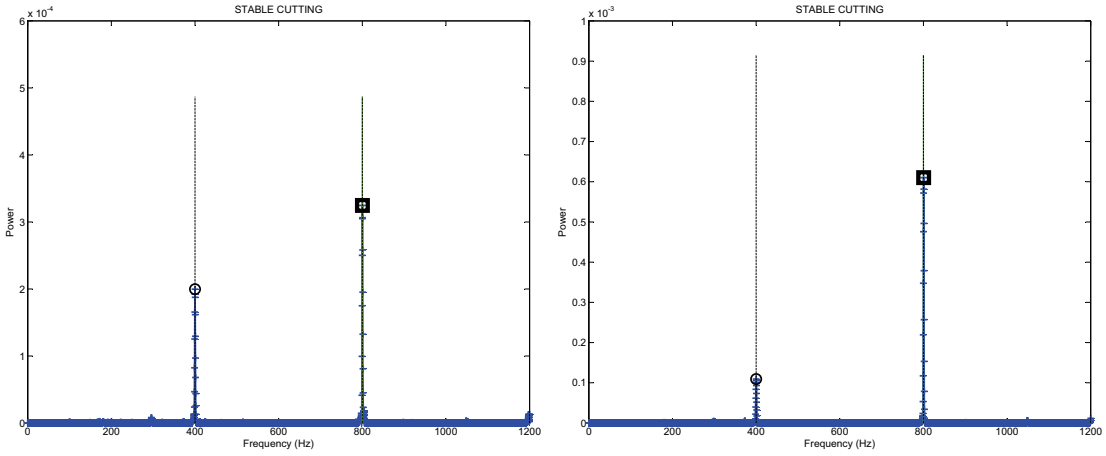

(a) (b)

Figure 7.13: Results of cutting test (A_p=1.5mm and n=24000rpm), stable milling

The developed chatter detection and control system was specially tested with an end mill (20mm) and aluminium workpiece (EN AW-6082) on a Mikron 800 HPM. Details of the slot cutting tests are presented in Table 7.2. The simulation results[1] of cutting test (A_p=8mm) are presented in Figure 7.14. The plots contain only forced vibration peaks (tooth passing frequency=200Hz). This is a clear case of stable milling.

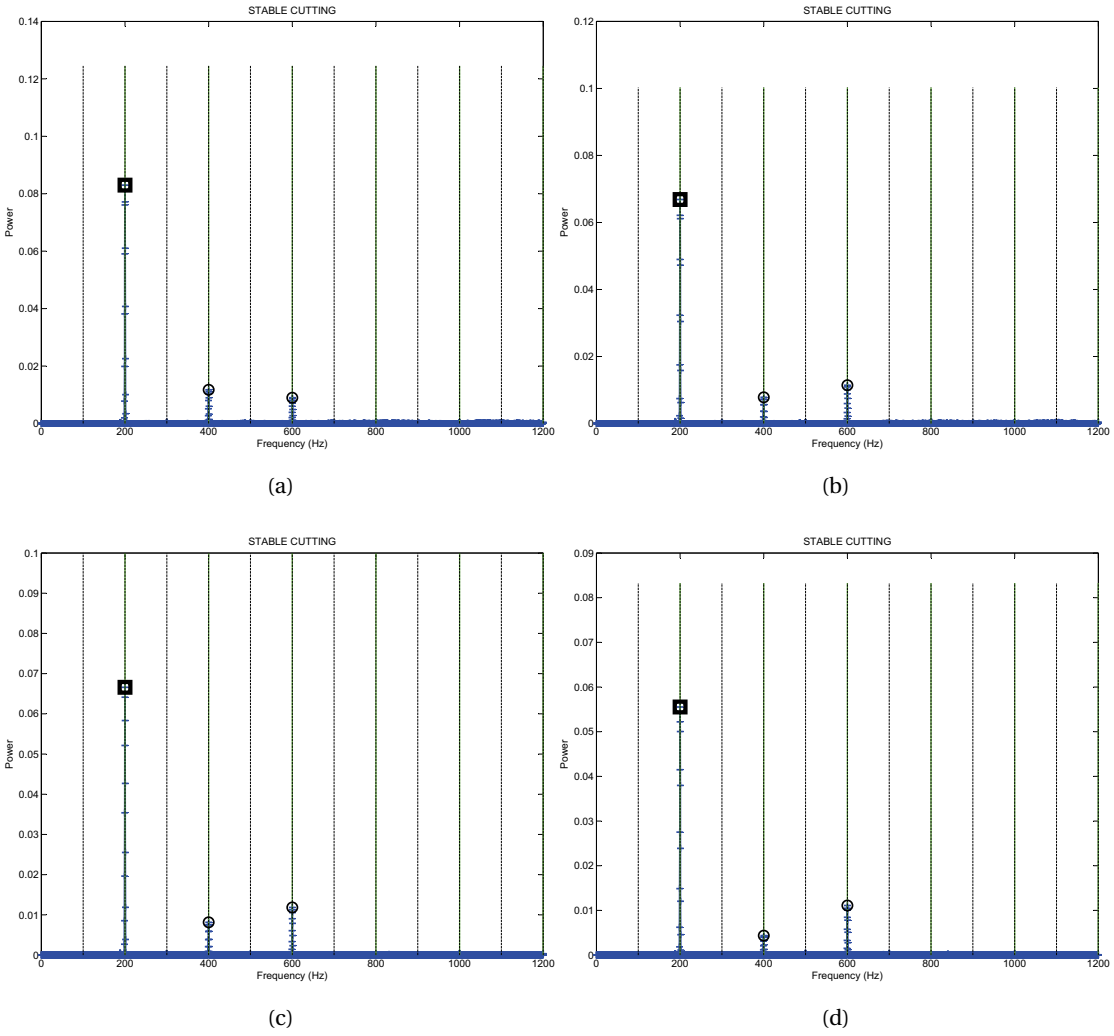

Figure 7.14: Results of cutting test (A_p=8mm), stable milling

For the cutting test (A_p=10mm and n=6000rpm), the results of the simulation are presented in Figure 7.15. There is a significant presence of chatter peaks along with forced frequency peaks. The power of dominant chatter peaks is greater than the dominant forced vibration peaks. This is a clear case of high chatter. The machined surface is shown in Figure 7.16a. It is noticed that there is a shift in the dominant chatter frequency along the cutting tool movement. This

[1] Every plot shows the FFT of cutting sound sampled during each second along the cutting tool movement

is due to the fact that different modes of a machine tool system can be excited during high chatter vibrations.

Chatter may grow/reduce or its dominant chatter frequency may change along the cutting toolpath because of the complex dynamic behavior of the machine tool system. The dynamic properties of a given machine tool system (spindle/tool holder/cutting tool) change at different locations and directions in the machine axes (Smith et al., 2000). The dynamic properties of the machine tool system, at a fixed location and direction, also changes at different spindle speeds (Schmitz et al., 2004). The developed chatter detection system can be used to investigate these changes in chatter peaks (both their power and frequency) along the toolpath.

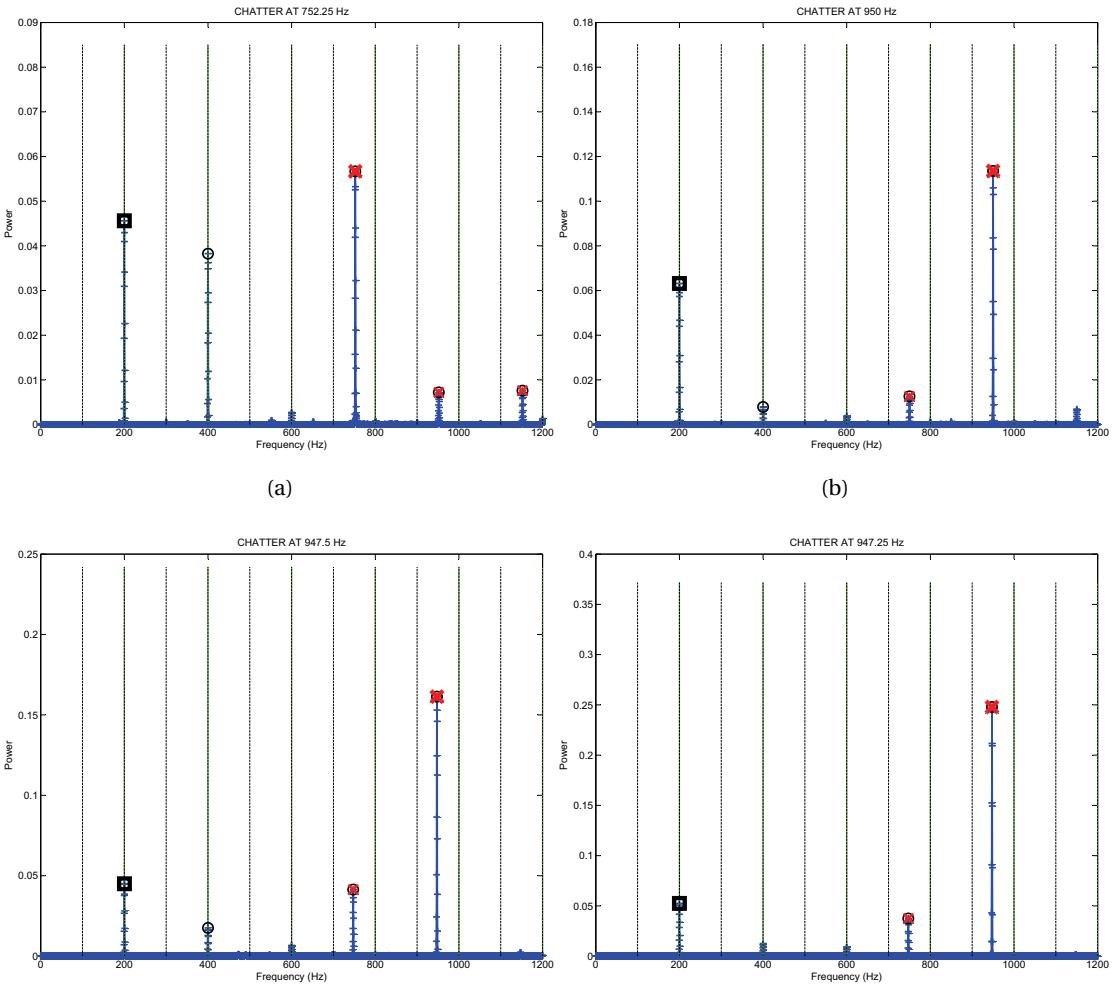

Figure 7.15: Results of cutting test (A_p=10mm), chatter

A cutting test (A_p=9.5mm) was performed to observe the development of chatter peaks in the sound signal. The results of the simulation are presented in Figure 7.17. The power

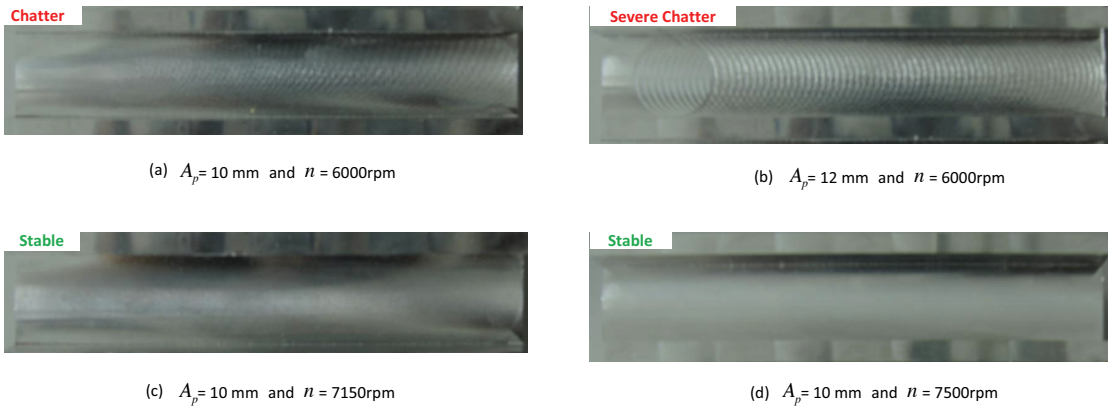

Figure 7.16: Finished surface of the workpiece

of dominant chatter peaks is comparatively smaller than the forced vibrations peaks. It is concluded from the plots shown in Figure 7.15 and Figure 7.17 that cutting test (A_p=10mm) is more unstable than cutting test (A_p=9.5mm). The developed chatter detection system is capable of detecting the changes in dominant chatter peaks with increase in axial depths of cut. With the developed system, the transition from stable (A_p=8mm) to unstable (A_p=9.5mm) cutting conditions can be clearly investigated.

Though we detected chatter at cutting test (A_p=10mm), as shown in Figure 7.15, cutting test (A_p=12mm) was performed in order to study the changes in power spectrum at high chatter. The results of the simulation are presented in Figure 7.18. It is quite interesting to observe that the power of the chatter peaks is significantly high and that the forced vibrations are even unnoticeable. This is a clear case of severe chatter. The machined surface of the workpiece with chatter marks is shown in Figure 7.16b.

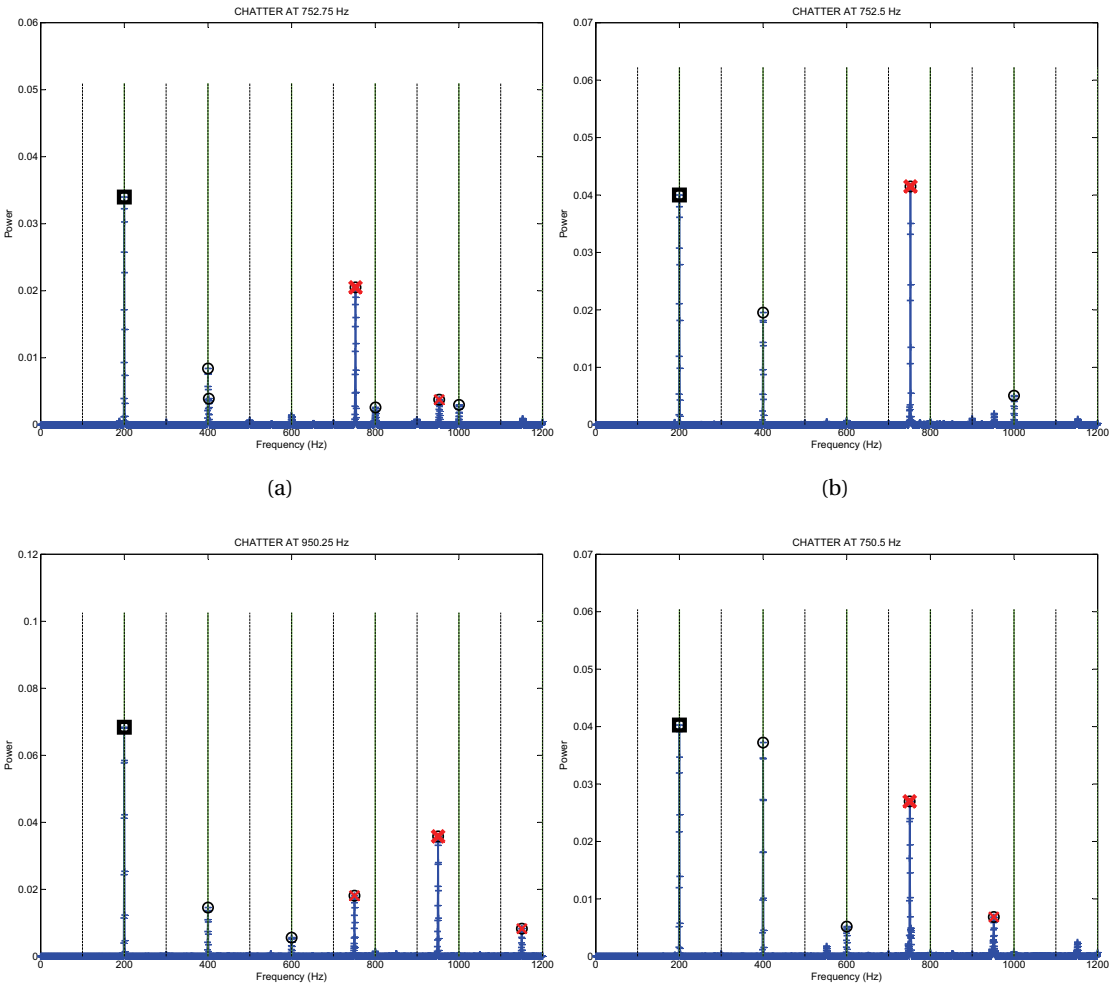

(a) (b)

(c) (d)

Figure 7.17: Results of cutting test (A_p=9.5mm), chatter

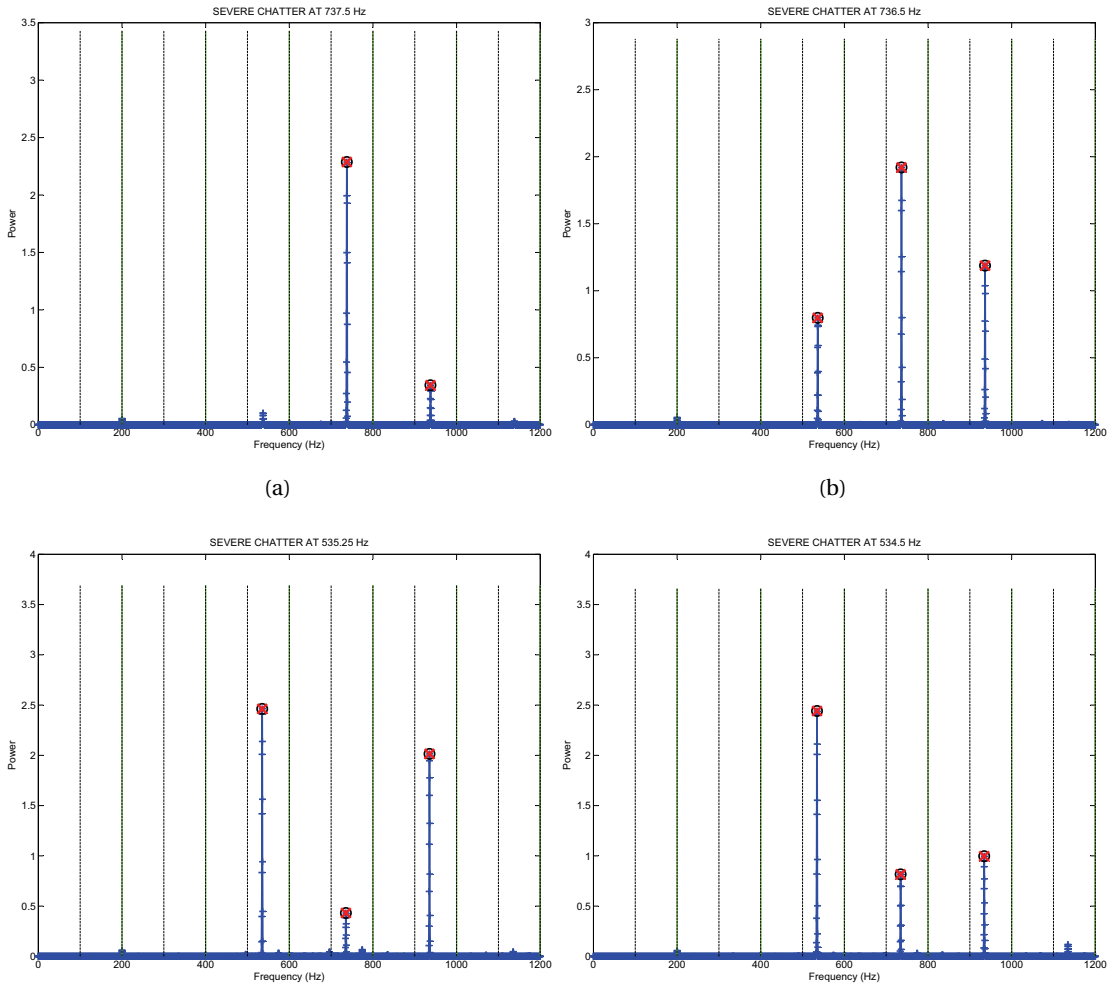

(a) (b)

(c) (d)

Figure 7.18: Results of cutting test (A_p=12mm), severe chatter

7.3.3 Verification of Corrected Spindle Speed

From the simulation results for cutting test (A_p=10mm), as shown in Figure 7.15, the detected dominant chatter peaks are 752Hz and 947Hz. From these dominant chatter frequency peaks the corrected values for spindle speeds are calculated as discussed in Section 7.2.3. The corrected values of spindle speeds for dominant chatter peaks at 752Hz and 947Hz are calculated as 7520rpm (s=3) and 7125rpm (s=4) respectively.

These spindle speeds were also verified experimentally. The results of the simulation for cutting test (A_p=10mm and n=7150rpm) and cutting test (A_p=10mm and n=7500rpm) are presented in Figure 7.19 and Figure 7.20 respectively. The corresponding machined surfaces are shown in Figure 7.16c and Figure 7.16d. From the FFT plots and machined surface, it is concluded that the suggested spindle speeds are stable.

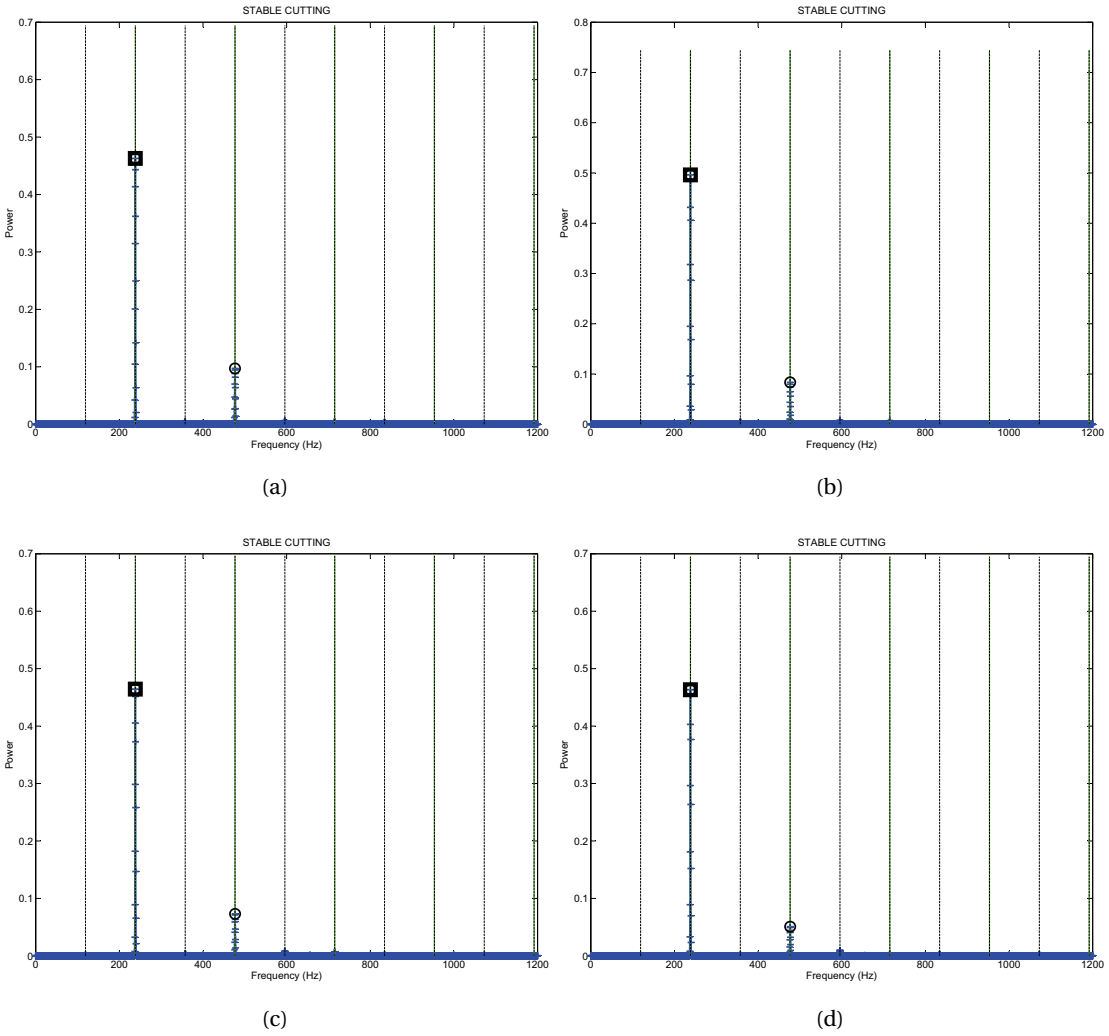

Figure 7.19: Results of cutting test (A_p=10mm and n=7150rpm), stable milling

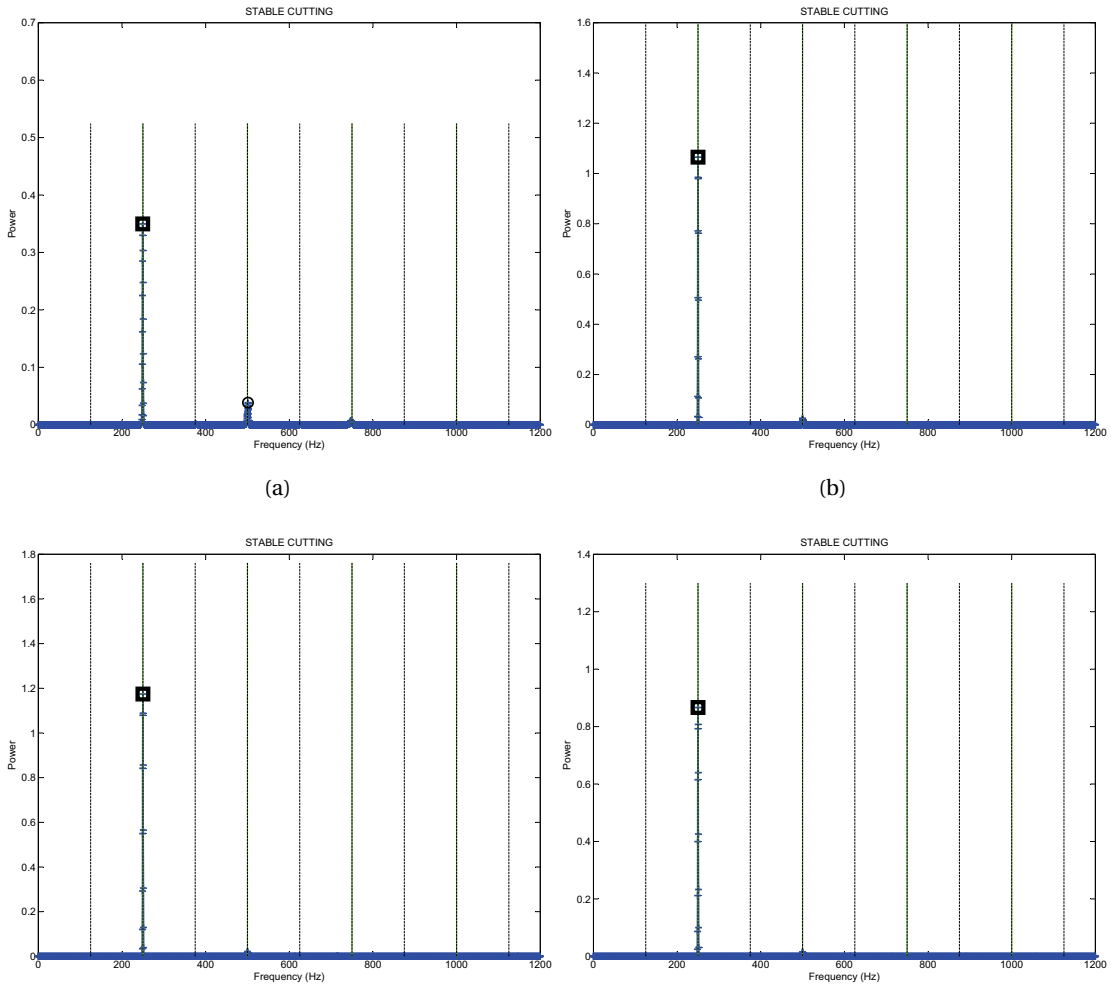

Figure 7.20: Results of cutting test (A_p=10mm and n=7500rpm), stable milling

7.4 Conclusion

The following conclusions are drawn from the development of chatter detection and control system:

- An online chatter detection system was developed to detect the existence of chatter in the case of unstable milling processes. The developed chatter control system propose the corrected spindle speed to avoid chatter.
- The influence of various parameters of the frequency domain analysis is presented in detail. The selected parameters ensure accurate identification of the frequencies and their corresponding power in the FFT spectrum and thus ensure accurate detection of the dominant chatter frequency.
- The system is capable of detecting accurately and automatically the existence of chatter at different spindle speeds and different cutting conditions. The developed system does not require any prior experiments to define the threshold limits for stable cutting. Experimental validation confirms the accuracy of the developed chatter detection and control system.
- The developed chatter detection system facilitates the investigation of the evolution of the chatter vibrations along the cutting toolpath. Moreover, the developed system helps study the change in power of chatter frequencies during milling with different axial depths of cut.
- The chatter detection and control system is computationally fast, which facilitates its industrial implementation for real time applications. Considerable steps for its implementation have already been taken with industrial end-users under the framework of our CTI Project- ChatFree[2].

[2]ChatFree: Part programming to realize chatter-free and efficient pocket milling (CTI-Projet no.10008.1 PFES-ES)

8 Conclusion

8.1 Summary of the Research Work

High speed milling of prismatic parts (2.5D) plays a vital role in the manufacturing of automotive and aerospace parts, as well as the, die and mold industry. The overall productivity of the milling process depends on the performance of part programs which is directly related to the selection of cutting conditions and toolpaths. Their wrong selection often causes chatter vibrations, high fluctuation of cutting forces, and/or violation of available limits of power and torque of a machine tool. Current part programs are prepared with long preparation time and lower machining performance. Moreover, due to the conservative selection of cutting conditions, the capabilities of modern high speed machine tools are not fully utilized. Current CAD/CAM systems and modern CNC machine tools do not provide any guidance for the selection of cutting conditions. Milling software (CutPro, 2008; MetalMax, 2008) developed by research groups suggests cutting conditions to avoid the above mentioned problems but the selection of cutting conditions and toolpath in this way does not ensure their optimal values for a given machine tool/spindle/tool holder/cutting tool/workpiece system.

In this PhD thesis, a genetic algorithm based optimization system is developed for optimal selection of cutting conditions and/or toolpath at the part programming stage. The operational constraints of the machine tool, such as available cutting power and torque, chatter vibration[1] limits due to the dynamic interaction between cutting tool and workpiece, acceptable limits of bending stress and deflection of the cutting tool and clamping load limits of the workpiece system are embedded in the optimization system. The developed system is a significant step toward narrowing the gap between virtual machining on CAD/CAM systems and actual machining on CNC machine tools.

The contributions of the developed optimization system in terms of definition of practical search space, encoded GA optimization variables and operators, targeted cutting conditions and embedded constraints are demonstrated with the development of three different opti-

[1] Amplitude of the cutting tool tip vibrations due to the regenerative effect

mization use cases. The different modules of the optimization system are developed in a generic way so that the overall system can satisfy different optimization use cases and user requirements. Each optimization use case represents a different optimization problem of a milling system.

Optimization System for Pocket Milling with One-Way Toolpath: For given pocket dimensions, material and machine tool/spindle/tool holder/cutting tool system, pocket milling time is minimized for a one-way toolpath with the optimal selection of spindle speed, feed rate, axial and radial depth of cut while respecting various constraints.

- The developed optimization use case[2] is compared with other studies available in the literature (Shunmugam et al., 2000; Dereli et al., 2001; Tandon et al., 2002; Tekeli and Budak, 2005), and it demonstrates contributions in terms of optimized cutting conditions and important practical constraints considered in the developed optimization model.

The developed optimization use case is implemented with real data of machine tool and workpiece system for the optimal selection of cutting conditions for different pocket sizes. The optimal cutting conditions are verified with dedicated experiments. The experimental verification confirms the accuracy of the developed optimization use case.

Moreover, the analysis of this optimization use case can also be performed while keeping one of the cutting conditions constant as per user requirements.

Optimization System for Prismatic Part: For a given multi-feature prismatic part and machine tool/spindle/tool holder/cutting tool system, machining time is minimized by optimal selection of spindle speed, feed rate and axial depth of cut while respecting various constraints.

- The developed optimization use case contributes as compared to (Heo et al., 2010; Rai et al., 2009) by considering the limiting values of radial depth of cut due to variation of engagement angle along the toolpath, and important constraints.
- The developed optimization system takes into account the toolpath geometry generated from the CAD/CAM system. The effect of change in stable depths of cut along different machine tool axes due to their different dynamic characteristics is also modeled in the developed optimization model.

The developed optimization use case is also implemented for the optimal selection of cutting conditions for a given prismatic part. The optimal cutting conditions during prismatic part milling are verified experimentally. The experimental verification concludes the accuracy of the developed optimization use case.

[2]Aggarwal, S. and Xirouchakis, P. (2012)., Selection of optimal cutting conditions for pocket milling using genetic algorithm. *The International Journal of Advanced Manufacturing Technology*, DOI: 10.1007/s00170-012-4472-x

For the case presented in Section 4.2, **47.6%** reduction in machining time is achieved with the optimal cutting conditions selected with developed optimization use case in comparison to the cutting conditions chosen by an experienced user based on the catalogue guidelines. Similarly, in the case of milling of deep pocket(Section 4.6.1), the optimal cutting conditions result in **48.96%** reduction in machining time and **18.04%** saving in total energy consumed during milling.

Optimization System for Pocket Milling with Smooth and Constant Engagement Toolpaths: For a given machine tool/spindle/tool holder/cutting tool system and a convex pocket, the machining time is minimized. There is no available study which simultaneously considers cutting conditions and toolpath geometry for high speed milling in their optimization system.

- This optimization use case contributes significantly in the optimal selection of spindle speed, feed rate, axial and radial depths of cut and corresponding smooth and constant engagement toolpath while respecting all embedded constraints.

The developed optimization use case[3] is implemented with real data of a machine tool and workpiece system for the optimal selection of cutting conditions and corresponding smooth and constant engagement toolpath for a given convex pocket. The optimal cutting conditions and toolpath are verified with experiments. The experimental verification demonstrates the accuracy of the developed optimization use case. The constant engagement toolpath is also compared with a conventional toolpath with experimental measurements.

This novel approach is a significant contribution towards achieving the highest overall productivity for pocket milling.

In order to expand the scope of industrial implementation of OptMill, the following developments were executed during the course of this research work:

(1) **Indirect Identification of Tangential Force Coefficients**: An enhanced methodology[4] is developed for the identification of the tangential force coefficients from the spindle motor current. The methodology includes the implementation of a spindle power model which takes into account all the mechanical and electrical power losses in a spindle motor for high speed milling. Further, an empirical model for cutting torque prediction has been developed from the results of air cutting and slot cutting experiments at different spindle speeds. It has been demonstrated that the model predicts the spindle power losses accurately as compared to (Dunwoody, 2010). Predicted values of the cutting torque by using the developed empirical model are additionally validated by the simultaneous direct

[3] Aggarwal, S., Dhanik, S. and Xirouchakis, P., High speed pocket milling optimisation, WO Patent 2012/107594/A1

[4] Aggarwal, S., Nešić, N. and Xirouchakis, P., Cutting torque and tangential cutting force coefficient identification from spindle motor current. *The International Journal of Advanced Manufacturing Technology*, DOI: 10.1007/s00170-012-4152-x

measurement of cutting torque from a cutting torque dynamometer. The results have demonstrated good compliance of the predicted cutting torque with the one obtained in the direct measurement, thus proving the accurate identification of tangential force coefficients.

(2) **FRF Prediction**: A procedure is developed for the prediction of FRFs of spindle/tool holder/end mill system for different end mills. The procedure includes the implementation of the receptance coupling technique. The rotational degree of freedom FRFs of the spindle/-tool holder subsystem are identified by inverse receptance coupling. The FRFs of the end mill subsystem are predicted with beam receptance considering the effect of the fluted portion. The FRFs of the machine tool system with different end mills are predicted with the developed procedure. The predicted FRFs are compared with the measured FRFs by direct hammer testing. The predicted FRFs are quite accurate in comparison to their measured counterparts.

Online Chatter Detection and Control: Chatter is detected during milling by frequency domain analysis of cutting sound recorded with a microphone. The dependency of various parameters of the Fourier transform is investigated for the accuracy of the chatter detection system.

- The chatter detection approach is developed to detect chatter from the relative power of the dominant peaks in the frequency spectrum rather than pre-defined threshold value of the dominant peaks from prior experiments as presented by (Smith, 1987; Harmonizer, 2008). Moreover the developed system contribute significantly to detect automatically and accurately the existence of chatter vibrations at any spindle speed and different cutting conditions.

Various cutting experiments were performed for the development, implementation and validation of the chatter detection and control system with an industrial end-user partner under the framework of the CTI project (ChatFree, 2011)[5]. The experimental results confirm the accuracy of the developed chatter detection and control system. The system is even able to detect the evolution of the chatter and dominant chatter frequencies along the cutting toolpath. The chatter detection and control system is computationally fast which facilitates its industrial implementation for real time applications. Considerable steps for its implementation have already been taken with industrial end-users.

Stability Analysis of Flexible Workpiece: Apart from the many developments discussed above, the stability analysis of a flexible workpiece was also performed. A flexible workpiece exhibits different dynamic characteristics at different contact points of the cutting tool with the workpiece. A finite element modeling based procedure is proposed to predict the stable conditions

[5]ChatFree: Part programming to realize chatter-free and efficient pocket milling (CTI-Project No.10008.1 PFES-ES)

at the part programming stage. It was demonstrated that the workpiece dynamics change significantly with material removal which explicate the need of new stability analysis at different stages of milling of a flexible workpiece.

Industrial Implementation: The developed system is very appealing for industrial application by direct integration with existing CAD/CAM systems and/or modern machine tools. Its industrial implementation is already in progress with industrial partners under the framework of a CTI project (ChatFree, 2011). Increase in overall productivity is ensured by optimal selection of cutting conditions and/or toolpath and also by simultaneous avoidance of repercussions due to their wrong selection.

8.1.1 Main Contributions of the Research Work

The main contributions of the present research work are:

1 A genetic algorithm based optimization model is developed for the minimization of machining time with the optimal selection of cutting conditions and/or toolpath with the following contributions:

   - Considering all the cutting conditions as optimization variables while respecting important constraints like cutting power and torque, chatter, bending stress and deflection of the cutting tool and clamping load limits.
   - Consideration of toolpath geometry for prismatic parts by taking into account the change in radial engagement and difference in dynamic characteristics along different machine tool axes.
   - Consolidation of smooth and constant engagement toolpaths for high speed pocket milling.

2 An enhanced methodology is developed for the indirect identification of tangential force coefficients from spindle motor current.

3 An online chatter detection and control system is developed with the following contributions:

   - Development of an approach for automatic and accurate identification of frequencies and corresponding power of the dominant peaks in the power spectrum.
   - Chatter detection approach is developed to detect chatter from the relative power of the dominant peaks in the frequency spectrum.

8.2 Recommendations for Future Work

There are the following recommendations for future work:

(i) The optimization system can be further developed for the minimization of energy consumed for milling of prismatic parts. It will require the following developments:

- Development of a mathematical model to predict the power consumption for milling of prismatic parts with selected cutting conditions and toolpath.
- Development of a mathematical model for the accurate calculation of machining time by considering the geometry of the toolpath and effect of acceleration/deceleration of the machine tool.
- Implementation of the developed power model and machining time model in the genetic algorithm based optimization system for the minimization of energy.

(ii) Effect of the change in machine tool system dynamics at higher spindle speeds should be taken in to account for the development of stability lobe diagrams. This would allow exploitation of the full dynamic capabilities of modern machine tools.

(iii) The optimization system can be improved for the minimization of machining time for milling of thin-walled workpieces. The change in dynamics along the workpiece should be considered for the selection of optimal cutting conditions. The deflection of the cutting tool should be modeled accurately. This approach will also allow the optimization system to be implemented for finishing operations.

(iv) Online chatter detection and control system can be extended for real time industrial application by the following developments:

- Development of a pre-processing module to identify no cutting, air cutting or material cutting scenarios so that the developed chatter detection system is simulated with cutting sound.
- The developed algorithms should be customized for high computational efficiency.

Bibliography

Adetoro, O., Sim, W., and Wen, P. (2010). An improved prediction of stability lobes using nonlinear thin wall dynamics. *Journal of Materials Processing Technology*, 210(6-7):969–979.

Agba, E. I., Ishee, D., and Berry, J. T. (1999). High speed machining of unsupported thin-walled structures. *Technical Paper - Society of Manufacturing Engineers. MR*, 204:1–10.

Aggarwal, S., Dhanik, S., and Xirouchakis, P. (2012a). High speed pocket milling optimisation. WO Patent 2012/107594 A1.

Aggarwal, S., Nešić, N., and Xirouchakis, P. (2012b). Cutting torque and tangential cutting force coefficient identification from spindle motor current. *The International Journal of Advanced Manufacturing Technology*, DOI: 10.1007/s00170-012-4152-x.

Aggarwal, S. and Xirouchakis, P. (2012). Selection of optimal cutting conditions for pocket milling using genetic algorithm. *The International Journal of Advanced Manufacturing Technology*, DOI: 10.1007/s00170-012-4472-x.

Altintas, Y. (2000). *Manufacturing automation: Metal cutting mechanics, machine tool vibrations, and CNC design*. Cambridge University Press.

Altintas, Y. and Budak, E. (1995). Analytical prediction of stability lobes in milling. *CIRP Annals - Manufacturing Technology*, 44:357–362.

Altintas, Y. and Chan, P. K. (1992). In-process detection and suppression of chatter in milling. *International Journal of Machine Tools & Manufacture*, 32(3):329–347.

Altintas, Y. and Weck, M. (2004). Chatter stability of metal cutting and grinding. *CIRP Annals-Manufacturing Technology*, 53:619–642.

Avram, I. O. (2010). *Machine tool use phase: Modeling and analysis with environmental considerations*. Phd thesis, Swiss Federal Institute of Technology Lausanne (EPFL), Switzerland.

Balachandran, B. (2001). Nonlinear dynamics of milling processes. *Philosophical Transactions of the Royal Society of London Series A-Mathematical Physical and Engineering Sciences*, 359(1781):793–819.

Bravo, U., Altuzarra, O., Lacalle, L. N. L., Sanchez, J. A., and Campa, F. J. (2005). Stability limits of milling considering the flexibility of the workpiece and the machine. *International Journal of Machine Tools & Manufacture*, 45:1669–1680.

Budak, E. (2006a). Analytical models for high performance milling part i: Cutting forces, structural deformations and tolerance integrity. *International Journal of Machine Tools and Manufacture*, 46:1478–1488.

Budak, E. (2006b). Analytical models for high performance milling part ii: Process dynamics and stability. *International Journal of Machine Tools and Manufacture*, 46:1489–1499.

Budak, E. and Altintas, Y. (1994). Peripheral milling conditions for improved dimensional accuracy. *International Journal of Machine Tools & Manufacture*, 34:907–918.

Budak, E. and Altintas, Y. (1998). Analytical prediction of chatter stability in milling - part i: General formulation. *Journal of Dynamic Systems Measurement and Control-Transactions of the ASME*, 120:22–30.

Budak, E., Altintas, Y., and Armarego, E. J. A. (1996). Prediction of milling force coefficients from orthogonal cutting data. *Journal of Manufacturing Science and Engineering-Transactions of the ASME*, 118:216–224.

Byrne, G., Dornfeld, D., Inasaki, I., Ketteler, G., Konig, W., and Teti, R. (1995). Tool condition monitoring (TCM) - the status of research and industrial application. *CIRP Annals - Manufacturing Technology*, 44(2):541–567.

Cao, Y. and Altintas, Y. (2004). A general method for the modeling of spindle-bearing systems. *Journal of Mechanical Design*, 126:1089–1104.

CATIA V5 (2010). Computer Aided Three-dimensional Interactive Application developed by Dassault Systemes.

ChatFree (2011). Part programming to realize chatter-free and efficient pocket milling (cti-projet no. 10008.1 pfes-es).

Cheng, C. H. (2007). *Improved prediction of spindle-holder-tool frequency response functions*. PhD thesis, University of Florida.

CutPro (2008). PC based milling simulation, V8.0.

Davies, M. A. and Balachandran, B. (2000). Impact dynamics in milling of thin-walled structures. *Nonlinear Dynamics*, 22:375–392.

Delio, T., Tlusty, J., and Smith, S. (1992). Use of audio signals for chatter detection and control. *Journal of Engineering for Industry-Transactions of the ASME*, 114(2):146–157.

Dereli, T., Filiz, I. H., and Baykasoglu, A. (2001). Optimizing cutting parameters in process planning of prismatic parts by using genetic algorithms. *International Journal of Production Research*, 39:3303–3328.

Dhanik, S. (2009). *NC tool path evaluator and generator for high speed milling*. PhD thesis, Swiss Federal Institute of Technology Lausanne (EPFL), Switzerland.

Dijck, K. (2008). Identification machine dynamics in high-speed milling. Technical report, Technical University Eindhoven.

Dijk, N. J. M., Doppenberg, E. J. J., Faassen, R. P. H., Wouw, N., Oosterling, J. A. J., and Nijmeijer, H. (2010). Automatic in-process chatter avoidance in the high-speed milling process. *Journal of Dynamic Systems Measurement and Control-Transactions of the ASME*, 132(3):1–14.

Dunwoody, K. (2010). Automated identification of cutting force coefficients and tool dynamics on CNC machines. Master's thesis, University of British Columbia, Vancouver.

Engin, S. and Altintas, Y. (2001). Mechanics and dynamics of general milling cutters.: Part i: Helical end mills. *International Journal of Machine Tools and Manufacture*, 41:2195–2212.

Ewins, D. (1999). *Modal Testing: Theory, Practice and Applications*. John Wiley & Sons.

Faassen, R. P. H. (2007). *Chatter prediction and control for high-speed milling: Modelling and experiments*. PhD thesis, Eindhoven University of Technology.

Faassen, R. P. H., Wouw, N., Oosterling, J. A. J., and Nijmeijer, H. (2003). Prediction of regenerative chatter by modelling and analysis of high-speed milling. *International Journal of Machine Tools and Manufacture*, 43:1437–1446.

Fraisa (2007). Catalogue for carbide end mills, http://www.fraisa.com.

Gagnol, V., Bouzgarrou, B. C., Ray, P., and Barra, C. (2007). Model-based chatter stability prediction for high-speed spindles. *International Journal of Machine Tools & Manufacture*, 47:1176–1186.

Harmonizer (2008). Selection of optimum spindle speed range for machining process.

Hatna, A., Grieve, R. J., and Broomhead, P. (1998). Automatic CNC milling of pockets: Geometric and technological issues. *Computer Integrated Manufacturing Systems*, 11:309–330.

Held, M. (1991a). A geometry-based investigation of the tool path generation for zigzag pocket machining. *The Visual Computer*, 7:296–308.

Held, M. (1991b). *On the computational geometry of pocket machining*. Springer-Verlag.

Hendriks, F. (2005). Chatter detection in high-speed milling. Technical report, TU Eindhoven.

Heo, E., Merdol, D., and Altintas, Y. (2010). High speed pocketing strategy. *CIRP Journal of Manufacturing Science and Technology*, 3(1):1–7.

Hutchinson, J. R. (2001). Shear coefficients for timoshenko beam theory. *Journal of Applied Mechanics-Transactions of the ASME*, 68(1):87–92. 414QU Times Cited:45 Cited References Count:15.

Kim, B. and Choi, B. (2002). Machining efficiency comparison direction-parallel tool path with contour-parallel tool path. *Computer-Aided Design*, 34:89–95.

Kistler (2010). *Instruction manuals (Type 9255B, 9722A500, 8776A50)*.

Ko, J. and Shaw, K. (2009). Chatter prediction based on frequency domain solution in cnc pocket milling. *International Journal of Precision Engineering and Manufacturing*, 10(4):19–25.

Kramer, T. (1992). Pocket milling with tool engagement detection. *Journal of Manufacturing Systems*, 11(2):114–123.

Kuljanic, E., Sortino, M., and Totis, G. (2008). Multisensor approaches for chatter detection in milling. *Journal of Sound and Vibration*, 312(4-5):672–693.

Kuljanic, E., Totis, G., and Sortino, M. (2009). Development of an intelligent multisensor chatter detection system in milling. *Mechanical Systems and Signal Processing*, 23:1704–1718.

Lambregts, C., Delbressine, F., De Vries, W., and Van der Wolf, A. (1996). An efficient automatic tool path generator for 2.5D free-form pockets. *Computers in Industry*, 29(3):151–157.

Le Lan, J. V., Marty, A., and Debongnie, J. F. (2007). Providing stability maps for milling operations. *International Journal of Machine Tools & Manufacture*, 47:1493–1496.

Lee, Y. and Chang, T. (1995). Application of computational geometry in optimizing 2.5D and 3D NC surface machining. *Computers in Industry*, 26(1):41–59.

LoadControls (2010). *Power Cell PPC-3 datasheet, Load Controls Inc., www.loadcontrols.com*.

Lopez, L., Lamikiz, A., Sanchez, J., and de Bustos, I. F. (2006). Recording of real cutting forces along the milling of complex parts. *Mechatronics*, 16(1):21 – 32.

Lyons, R. G. (2011). *Understanding digital signal processing*. Prentice Hall, third edition.

Mackerle, J. (1998). Finite-element analysis and simulation of machining: A bibliography (1976–1996). *Journal of Materials Processing Technology*, 86(1):17–44.

Mackerle, J. (2003). Finite element analysis and simulation of machining: An addendum: A bibliography (1996-2002). *International Journal of Machine Tools and Manufacture*, 43(1):103–114.

Mane, I., Gagnol, V., Bouzgarrou, B. C., and Ray, P. (2008). Stability-based spindle speed control during flexible workpiece high-speed milling. *International Journal of Machine Tools & Manufacture*, 48:184–194.

MATLAB (2011). User guide for data analysis, data aquisition toolbox.

Merritt, H. (1965). Theory of self-excited machine tool chatter. *Journal of Engineering for Industry*, 87:447–454.

MetalMax (2008). The complete package for machine-tool dynamic characterization.

Morgan, G., Cheng, R. Q., Altintas, Y., and Ridgway, K. (2007). An expert troubleshooting system for the milling process. *International Journal of Machine Tools & Manufacture*, 47(9):1417–1425.

Nešić, N. (2012). *Modeling and simulation of energy efficient milling process plans for prismatic parts*. PhD thesis, Swiss Federal Institute of Technology Lausanne (EPFL), Switzerland.

Palanisamy, P., Rajendran, I., and Shanmugasundaram, S. (2007). Optimization of machining parameters using genetic algorithm and experimental validation for end-milling operations. *International Journal of Advanced Manufacturing Technology*, 32:644–655.

Park, S. S., Altintas, Y., and Movahhedy, M. (2003). Receptance coupling for end mills. *International Journal of Machine Tools & Manufacture*, 43(9):889–896.

Quintana, G. (2009). *Stability lobes diagram indentification and surface roughness monitoring in milling processes*. PhD thesis, Universitat de Girona, Spain.

Quintana, G. and Ciurana, J. (2011). Chatter in machining processes: A review. *International Journal of Machine Tools and Manufacture*, 51(5):363–376.

Quintana, G., Ciurana, J., Ferrer, I., and Rodríguez, C. A. (2009). Sound mapping for identification of stability lobe diagrams in milling processes. *International Journal of Machine Tools and Manufacture*, 49(3-4):203–211.

Quintana, G., Ciurana, J., and Teixidor, D. (2008). A new experimental methodology for identification of stability lobes diagram in milling operations. *International Journal of Machine Tools and Manufacture*, 48(15):1637–1645.

Rai, J. (2008). *FEM-MILL: A finite element based 3D transient milling simulation environment for process plan verification and optimization*. PhD thesis, Swiss Federal Institute of Technology Lausanne (EPFL), Switzerland.

Rai, J., Brand, D., Slama, M., and Xirouchakis, P. (2009). Optimal selection of cutting parameters in multi-tool milling operations using genetic algorithm. *International Journal of Production Research*.

Riviére, E., Stalon, V., Abeele, O. V. d., Fillipi, E., and Dehombreux, P. (2006). Chatter detection techniques using microphone. Accessed on 5th May, 2008: http://www.geniemeca.fpms.ac.be/Recherche/Articles/riviere2006c.pdf.

Schmitz, T. L. (2000). Predicting high-speed machining dynamics by substructure analysis. *CIRP Annals - Manufacturing Technology*, 49(1):303–308.

Schmitz, T. L. and Burns, T. J. (2003). Receptance coupling for high-speed machining dynamics prediction. In *IMAC-XXI: Conference & Exposition on Structural Dynamics*, Kissimmee, FL.

Schmitz, T. L., Davies, M. A., and Kennedy, M. D. (2001). Tool point frequency response prediction for high-speed machining by RCSA. *Journal of Manufacturing Science and Engineering-Transactions of the ASME*, 123:700–707.

Schmitz, T. L. and Duncan, G. S. (2005). Three-component receptance coupling substructure analysis for tool point dynamics prediction. *Journal of Manufacturing Science and Engineering-Transactions of the ASME*, 127(4):781–790.

Schmitz, T. L., Medicus, K., and Dutterer, B. (2002). Exploring once-per-revolution audio signal variance as a chatter indicator. *Machining Science and Technology*, 6(2):215–233.

Schmitz, T. L. and Smith, S. (2009). *Machining Dynamics*. Springer.

Schmitz, T. L., Ziegert, J. C., and Stanislaus, C. (2004). A method for predicting chatter stability for systems with speed-dependent spindle dynamics. In *Transactions of the North American Manufacturing Research Institution of SME*.

Schulz, H. and Moriwaki, T. (1992). High-speed machining. *CIRP Annals - Manufacturing Technology*, 41(2):637 – 643.

Shunmugam, M. S., Bhaskara Reddy, S. V., and Narendran, T. T. (2000). Selection of optimal conditions in multi-pass face-milling using a genetic algorithm. *International Journal of Machine Tools and Manufacture*, 40:401–414.

Shure (2010). *Shure PG81 mircophone, data sheet*.

Smith, S. (1987). *Automatic selection of optimum spindle speed in high speed milling*. PhD thesis, University of Florida.

Smith, S. and Tlusty, J. (1997). Current trends in high-speed machining. *Journal of Manufacturing Science and Engineering-Transactions of the ASME*, 119:664–666.

Smith, S., Winfough, W. R., Young, K., and Halley, J. (2000). The effect of dynamic consistency in spindles on cutting performance. *American Society of Mechanical Engineers, Manufacturing Engineering Division, MED*, 11:927–930.

Soliman, E. and Ismail, F. (1996). Statistical evaluation of different signals for chatter detection. In *CSME Forum*, pages 148–153.

Soliman, E. and Ismail, F. (1997). Chatter suppression by adaptive speed modulation. *International Journal of Machine Tools & Manufacture*, 37(3):355–369.

Solis, E., Peres, C. R., Jimenez, J. E., Alique, J. R., and Monje, J. C. (2004). A new analytical-experimental method for the identification of stability lobes in high-speed milling. *International Journal of Machine Tools & Manufacture*, 44:1591–1597.

Stroud, I. (2006). *Boundary representation modelling techniques*. Springer.

Stroud, I. and Nagy, H. (2011). *Solid modelling and CAD systems: How to survive a CAD system*. Springer.

Tandon, V., El-Mounayri, H., and Kishawy, H. (2002). NC end milling optimization using evolutionary computation. *International Journal of Machine Tools and Manufacture*, 42:595–605.

Tarng, Y. S. and Chen, M. C. (1994). An intelligent sensor for detection of milling chatter. *Journal of Intelligent Manufacturing*, 5(3):193–200.

Tatar, K. and Gren, P. (2008). Measurement of milling tool vibrations during cutting using laser vibrometry. *International Journal of Machine Tools & Manufacture*, 48(3-4):380–387.

Tekeli, A. and Budak, E. (2005). Maximization of chatter-free material removal rate in end milling using analytical methods. *Machining Science and Technology*, 9:147–167.

Thevenot, V., Arnaud, L., Dessein, G., and Cazenave-Larroche, G. (2006a). Influence of material removal on the dynamic behavior of thin-walled structures in peripheral milling. *Machining Science and Technology*, 10:275–287.

Thevenot, V., Arnaud, L., Dessein, G., and Cazenave-Larroche, G. (2006b). Integration of dynamic behaviour variations in the stability lobes method: 3D lobes construction and application to thin-walled structure milling. *International Journal of Advanced Manufacturing Technology*, 27:638–644.

Tlusty, J. and Andrews, G. C. (1983). Critical review of sensors for unmanned machining. *CIRP Annals - Manufacturing Technology*, 32:563–572.

Tlusty, J. and Polacek, M. (1963). The stability of machine tools against self-excited vibrations in machining. In *ASME International Research in Production Engineering*, pages 456–474.

Tobias, S. and Fishwick, W. (1958). A theory of regenerative chatter. *The Engineer*.

Toh, C. (2005). Design, evaluation and optimisation of cutter path strategies when high speed machining hardened mould and die materials. *Materials & Design*, 26(6):517 – 533.

Totis, G. (2009). RCPM–A new method for robust chatter prediction in milling. *International Journal of Machine Tools and Manufacture*, 49:273–284.

Tsai, N. C., Chen, D. C., and Lee, R. M. (2009). Chatter prevention for milling process by acoustic signal feedback. *International Journal of Advanced Manufacturing Technology*, pages 1–9.

Tsai, N.-C., Chen, D.-C., Lee, R.-M., and Wang, B.-L. (2010). Milling chatter prevention by adaptive spindle speed tuning. *World Academy of Science, Engineering and Technology*, 62.

Urbanski, J., Koshy, P., Dewes, R., and Aspinwall, D. (2000). High speed machining of moulds and dies for net shape manufacture. *Materials & Design*, 21(4):395 – 402.

Wang, H., Qin, X., Ren, C., and Wang, Q. (2012). Prediction of cutting forces in helical milling process. *The International Journal of Advanced Manufacturing Technology*, pages 1–11.

Wang, Z. G., Wong, Y. S., and Rahman, M. (2004). Optimisation of multi-pass milling using genetic algorithm and genetic simulated annealing. *International Journal of Advanced Manufacturing Technology*, 24:727–732.

Weaver, W., Timoshenko, S. P., and Young, D. H. (1990). *Vibration problems in engineering*. John Wiley and Sons.

Weck, M., Altintas, Y., and Beer, C. (1994). CAD assisted chatter-free NC tool path generation in milling. *International Journal of Machine Tools and Manufacture*, 34:879–891.

Weingaertner, W. L., Schroeter, R. B., Polli, M. L., and Gomes, J. D. (2006). Evaluation of high-speed end-milling dynamic stability through audio signal measurements. *Journal of Materials Processing Technology*, 179(1-3):133–138.

Wiercigroch, M. and Budak, E. (2001). Sources of nonlinearities, chatter generation and suppression in metal cutting. *Philosophical Transactions of the Royal Society of London Series A-Mathematical Physical and Engineering Sciences*, 359:663–693.

Yokoyama, T. (1990). Vibrations of a hanging timoshenko beam under gravity. *Journal of Sound and Vibration*, 141(2):245–258.

Zhang, J., Schmitz, T., Zhao, W. H., and Lu, B. H. (2011). Receptance coupling for tool point dynamics prediction on machine tools. *Chinese Journal of Mechanical Engineering*, 24(3):340–345.

Zhang, Y. and Li, Z. (2012). Stability and online monitoring of cutting chatter: A review. *Applied Mechanics and Materials*, 121-126:377–381.

A Cutting Force Modeling

For the present work an analytical force model developed by Altintas and Budak is implemented (Budak and Altintas, 1994; Altintas, 2000). This study assumes that during milling the cutting tooth traces a circular path. The geometry of chip formation is shown in Figure 3.10.

A.1 Analytical Modeling of Milling Force

For the analytical modeling of the milling forces the axial depth of cut and immersion angle is divided into small intervals (Δa) and ($\Delta\phi$) respectively. The bottom edge of one flute is assigned as the reference immersion angle ϕ, i.e flute $j = 0$ (the reference flute) is aligned at $\phi = 0$; where $j = 0, 1, 2 \ldots (N-1)$. The instantaneous angle of immersion (ϕ) is measured in clockwise direction measured from the normal to feed Y direction. The bottom end points of the remaining flutes are at angles $\phi_j(0) = \phi + j\phi_p$ where $\phi_p = 2\pi/N$, is the pitch angle. At an axial depth of cut z, the lag angle is given by $\psi = k_\beta z$ where $k_\beta = 2\tan\beta/D$. The immersion angle for flute j at axial depth of cut z is calculated by:

$$\phi_j(z) = \phi + j\phi_p - k_\beta z \tag{A.1}$$

If $\phi_{\text{st}} \leq \phi_j(z) \leq \phi_{\text{ex}}$, then the tangential ($dF_{t,j}$), radial ($dF_{r,j}$) and axial ($dF_{a,j}$) cutting forces on the differential element with height Δa of the j^{th} flute is quantified as:

$$\begin{aligned} dF_{t,j}(\phi, z) &= [K_{tc} h_j(\phi_j(z)) + K_{te}]\Delta a \\ dF_{r,j}(\phi, z) &= [K_{rc} h_j(\phi_j(z)) + K_{re}]\Delta a \\ dF_{a,j}(\phi, z) &= [K_{ac} h_j(\phi_j(z)) + K_{ae}]\Delta a \end{aligned} \tag{A.2}$$

where K_{tc}, K_{rc} and K_{ac} are the cutting force coefficients contributed by shearing action and K_{te}, K_{re} and K_{ae} are the edge force coefficients in tangential, radial and axial directions respectively, . ϕ_{st} and ϕ_{ex} are the start and exit angles for the cutting zone respectively. In milling the chip thickness is a periodic function of the varying immersion angle ϕ. Due to

the assumption of a circular tooth path, the chip thickness associated with the j^{th} flute is approximated as:

$$h_j(\phi, z) = f_t \sin\phi_j(z) \tag{A.3}$$

where f_t denotes the feed rate in *mm/rev-flute*.

The elemental milling forces on flute j in the feed (X), normal to feed (Y) and axial (Z) directions are calculated by resolving the differential cutting forces using Equation A.4:

$$\begin{aligned} dF_{x,j}(\phi_j(z)) &= -dF_{t,j}\cos\phi_j(z) - dF_{r,j}\sin\phi_j(z) \\ dF_{y,j}(\phi_j(z)) &= dF_{t,j}\sin\phi_j(z) - dF_{r,j}\cos\phi_j(z) \\ dF_{z,j}(\phi_j(z)) &= dF_{a,j} \end{aligned} \tag{A.4}$$

Substituting the differential forces (Equation A.2) and the chip thickness (Equation A.3) into Equation A.4 leads to:

$$\begin{aligned} dF_{x,j}(\phi_j(z)) &= \frac{f_t}{2}\left[-K_{tc}\sin 2\phi_j(z) - K_{rc}(1-\cos 2\phi_j(z))\right]dz \\ &\quad + \left[-K_{te}\cos\phi_j(z) - K_{re}\sin\phi_j(z)\right]dz \\ dF_{y,j}(\phi_j(z)) &= \frac{f_t}{2}\left[K_{tc}(1-\cos 2\phi_j(z)) - K_{rc}\sin 2\phi_j(z)\right]dz \\ &\quad + \left[K_{te}\sin\phi_j(z) - K_{re}\cos\phi_j(z)\right]dz \\ dF_{z,j}(\phi_j(z)) &= \left[K_{ac} f_t \sin\phi_j(z) + K_{ae}\right]dz \end{aligned} \tag{A.5}$$

The total cutting force for the j th flute is calculated by integrating the differential cutting forces along the cutting zone of the j th flute:

$$F_w(\phi_j(z)) = \int_{z_{j,1}}^{z_{j,2}} dF_w(\phi_j(z))dz, \qquad w = x, y, z \tag{A.6}$$

where $z_{j,1}(\phi_j(z))$ and $z_{j,2}(\phi_j(z))$ are the lower and upper axial engagement limits of the cutting zone of the flute j. The total instantaneous force on the cutter at immersion angle ϕ is summed up from the differential cutting forces from all slices and all flutes and is given by Equation A.7:

$$\begin{aligned} F_x(\phi) &= \sum_{j=0}^{N-1} F_{x_j} \\ F_y(\phi) &= \sum_{j=0}^{N-1} F_{y_j} \\ F_z(\phi) &= \sum_{j=0}^{N-1} F_{z_j} \end{aligned} \tag{A.7}$$

Table A.1: Input parameters for validation of cutting force modeling

D	N	β	K_{tc}	K_{te}	K_{rc}	K_{re}	K_{ac}	K_{ae}	f_t	A_p	A_e
19.05	4	30	1698	24.7	438	42.9	591	5.5	0.05	5.08	9.525

The resultant of cutting forces acting on the milling cutter is expressed as

$$F(\phi) = \sqrt{F_x(\phi)^2 + F_y(\phi)^2 + F_z(\phi)^2} \tag{A.8}$$

The accuracy of the model depends on the selected integration intervals, (Δa) and ($\Delta\phi$).

A.1.1 Validation of the Prediction Model

The program is written in MATLAB 2009a. For validating the programmed analytical prediction model the input data is taken from (Budak et al., 1996). All required inputs for the up milling case are given in Table A.1.

ϕ_{st} and ϕ_{ex} are calculated from the radial depth of cut (A_e) depending upon the mode of milling (up milling, down milling or slot milling).

Results are shown in Figure A.1. It is clear from Figure A.1b and Figure A.1a that the programmed model fits well with the results from (Budak et al., 1996).

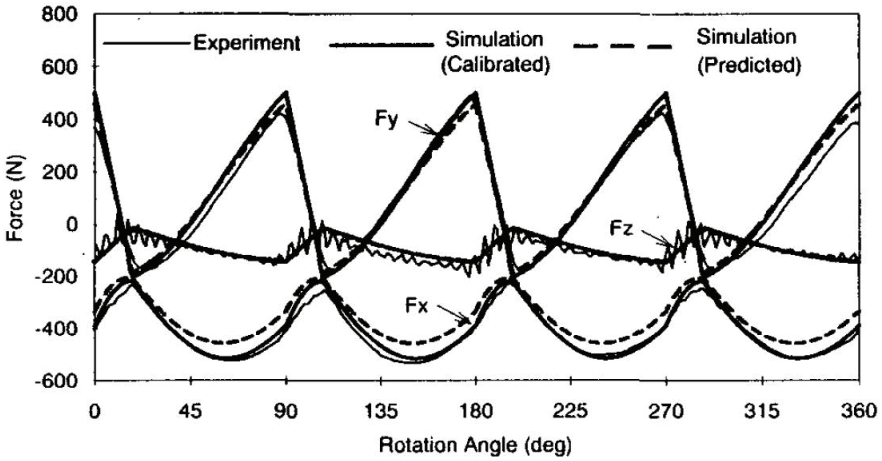

(a) Milling force results from (Budak et al., 1996)

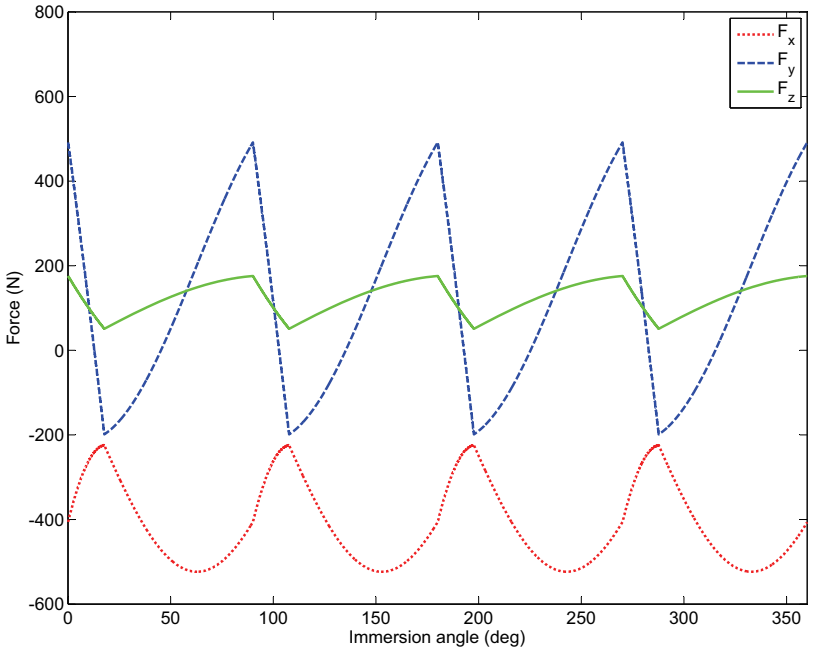

(b) Modeled milling force

Figure A.1: Validation of milling forces

B Force Coefficients Identification

This chapter presents the identification of cutting force coefficients for a given material and cutting tool.

B.1 Experimental Details

The work piece material is Al-7075 which belongs to the hardened aluminium alloy class. A set of slot milling experiments were performed at different feed rate values for the identification of the cutting force coefficients. The details of the slot milling experiments conducted for C15273610[1] are presented in Table B.1. Cutting forces in feed (X), normal to feed (Y) and axial (Z) directions were measured during each slot milling pass with the help of a cutting force dynamometer. The dynamometer system consists of the dynamometer, multi-channel charge amplifier and the connection cable. Spindle speed[2] (n) and axial depth of cut (A_p) is a stable combination.

Table B.1: Slot milling experiments

Experiment No	f_t $(mm/flute)$	n (rpm)	A_p (mm)
1	0.04	10000	4
2	0.06	10000	4
3	0.08	10000	4
4	0.10	10000	4
5	0.12	10000	4
6	0.14	10000	4
7	0.16	10000	4
8	0.18	10000	4
9	0.20	10000	4

[1] Cutting tool from Fraisa (Fraisa, 2007)

[2] Spindle speed is selected by performing the dynamic calibration of dynamometer in order to avoid the tooth passing frequency to fall in the range of resonance of dynamometer setup.

Dynamic Calibration of Dynamometer

A Kistler 9255B dynamometer that, because of its size (260x260 mm) and force range (-20 to 20 kN in X and Y, -10 to 40 kN in Z), is the most appropriate of measuring forces in milling and has a natural frequency of 1.7 kHz in the X and Y axes and 2 kHz in the Z axis. The natural frequency of the system decreases below 1 kHz because of a certain weight mounted on the dynamometer. Kistler does not provide the entire calibration response chart (they provide only the sensitivity values and the linearity of the response) (Lopez et al., 2006). For accurate measurement of the cutting forces it is vital to know the response of the dynamometer/work piece system so the measurement of cutting force should not be influenced by the resonance of the dynamometer/work piece system. The dynamometer is calibrated using hammer testing. The experimental setup to perform the dynamic calibration of the dynamometer is presented in Figure B.1.

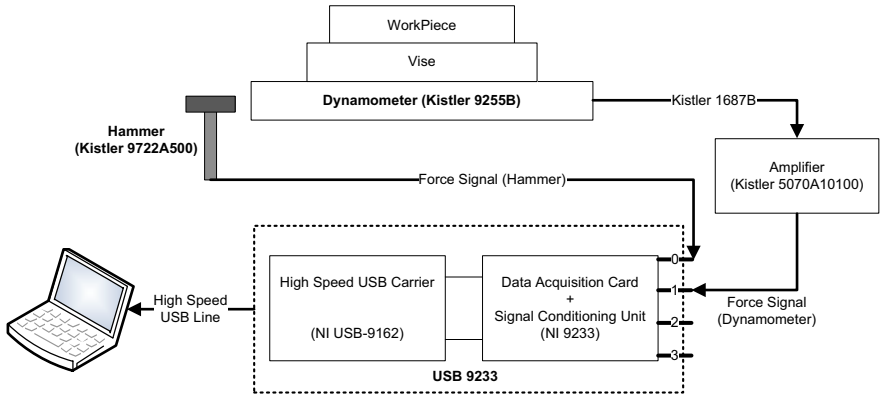

Figure B.1: Setup for dynamic calibration of dynamometer

Results of Dynamic Calibration

The dynamometer is impacted five times to reduce the errors in the measurement. The dynamic response of the dynamometer/work piece system was measured using CutPro 2008 (CutPro, 2008). The phase and magnitude of the dynamic response are presented in Figure B.2. It is clear from the dynamic response of the dynamometer/work piece system that the resonance peaks of the dynamometer and work piece setup are around ~200 Hz and ~1175 Hz. Tooth passing frequency ($nN/60$, n is number of flutes and N is the spindle speed) should not match these frequencies of the dynamometer/work piece system for accurate measurement of the cutting forces.

B.2 Force Coefficients Results

Spindle speed is selected as 10000 rpm. Tooth passing frequency ($Nn/60$) for two flute cutting tool (C15273610) is 333.3 Hz which is the safe zone as per dynamic response of the dynamome-

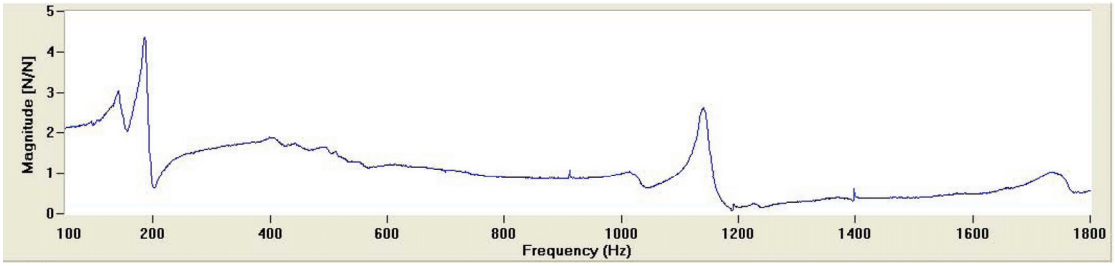

Figure B.2: Magnitude and phase of the dynamic response

ter/work piece system. The cutting tests were conducted and cutting force components were recorded. LabVIEW 8.5 was used as a platform to record the cutting force components. The text files of cutting forces are exported from LabVIEW and the data is analyzed in MATLAB 2010a. To avoid the influence of run out on the measurements, average cutting force components per spindle revolution at each feed rate were calculated. Average cutting forces for the cutting tool (C15723610) are presented with markers in Figure B.3. For each cutting force component the slope and intercept of the line (average force vs feed rate) is estimated by linear regression. Dotted lines in Figure B.3 represent the fitted lines. Cutting force coefficients are calculated using Equations 2.7. Identified cutting force coefficients are presented in Table B.2.

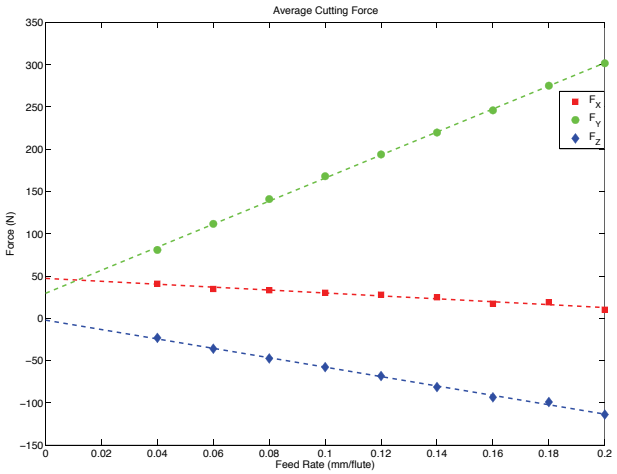

Figure B.3: Average cutting forces

Table B.2: Cutting force coefficients

Index	K_{tc} (N/mm^2)	K_{rc} (N/mm^2)	K_{ac} (N/mm^2)	K_{te} (N/mm)	K_{re} (N/mm)	K_{ae} (N/mm)
Fraisa C15723610	681	86	218	12	19	2

C FRF Measurement

The experimental setup for the FRF measurement (CutPro, 2008) is presented in Figure C.1. The setup consists of impact hammer, an accelerometer and data acquisition unit.

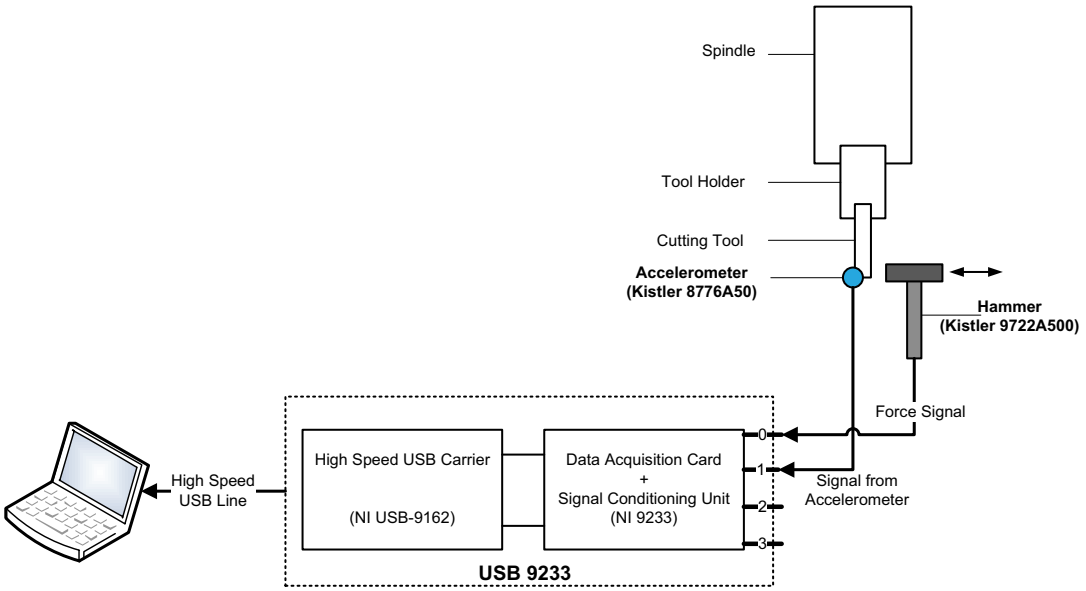

Figure C.1: Details of experimental setup for FRF measurement

The hardware setup is explained briefly as follows:

- Connect the hammer to the first channel (channel 0) of USB-9233 by a cable (type 1511)
- Connect the accelerometer to the second channel (channel 1) of the USB-9233 by a cable (type 1761B2)
- Connect the USB-9233 system with the computer by a high speed USB cable
- Clean the surface of the cutting tool in order to make the proper attachment of the accelerometer at the tool tip.

The main parts of the FRF measurement system are explained as follows:

Data Acquisition Unit

The National Instrument USB-9233 is a four-channel dynamic signal acquisition module for making high-accuracy audio frequency measurement integrated electronic piezoelectric (IEPE) sensors. The NI USB-9233 incorporates IEPE signal conditioning for accelerometer and microphones.

Hammer

A hammer is most commonly used in impact testing. The equipment consists of an impactor, usually with a set of different tips and heads which serve to extend the frequency and force level ranges for testing. In order to increase the frequency range it is necessary to induce a shorter pulse length. This is related to the stiffness of the contacting surfaces and the mass of the impactor head. The stiffer the materials, the shorter will be the duration of the pulse and the higher will be the frequency range covered by the impact. Similarly the lighter the impactor mass the higher the effective frequency range

Accelerometer

In an accelerometer, transduction is indirect and is achieved using an auxiliary mass. When the accelerometer vibrates, an internal mass in the assembly applies a force to the crystal element which is proportional to the acceleration. This relationship is simply Newton's Law: force equals mass times acceleration. In general, the optimum accelerometer has high sensitivity, wide frequency range and small mass.

D Stability Limit Modeling

For the present work the study from (Altintas and Budak, 1995; Budak and Altintas, 1998) has been used. The study considered the milling system as a two orthogonal degree of freedom (2-DOF) system as shown in Figure D.1. The main step in developing the predicted stable limits is to find the transfer function (in the frequency domain, this is the ratio of displacement response to input force) at the tool tip for a given set of machine tool/spindle/tool holder/ tool. Transfer functions are processed further to develop the stability lobe diagrams.

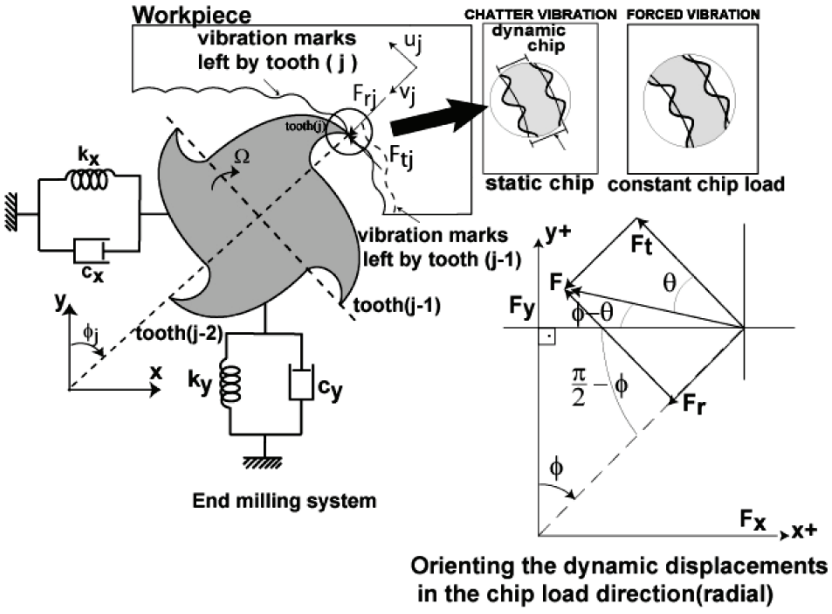

Figure D.1: Flexible machine tool system (Altintas and Weck, 2004)

In Figure D.1, the X axis represents the cutting feed direction (cutting direction) and the Y axis represents the normal to feed direction. The cutter has N number of flutes. The milling system develops the dynamic displacements x and y as the cutting forces excite the system in the feed and normal directions respectively. ϕ_j is the instantaneous angular immersion of tooth

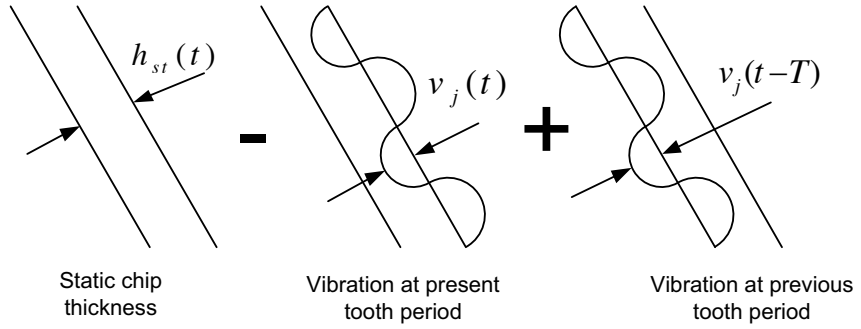

Figure D.2: Dynamic chip thickness

j measured clockwise from the normal Y axis. $\phi_j(t) = \Omega t$, here Ω(in rad/s) is the angular speed of the spindle. Chip thickness is composed of two parts, the static part ($f_t \sin\phi_j$) due to the rigid body motion of the cutter and the dynamic part due to the cutter vibrations during the present and previous tooth periods. Chip thickness is measured in the radial direction (v_j). The total chip load is given by

$$h(\phi_j) = \left[f_t \sin\phi_j + (v_{j,0} - v_j) \right] g(\phi_j) \tag{D.1}$$

f_t denotes the feed rate per flute and ($v_{j,0}, v_j$) denotes the dynamic displacements of the cutter at the previous and present tooth periods respectively. $g(\phi_j)$, a unit step function, determines whether the cutter flute is in or out of the cut. $g(\phi_j)$ is defined by

$$g(\phi_j) = \left\{ \begin{array}{ll} 1, & \phi_{st} \le \phi_j \le \phi_{ex} \\ 0, & \phi_j < \phi_{st} \text{ or } \phi_j > \phi_{ex} \end{array} \right\} \tag{D.2}$$

where ϕ_{st} and ϕ_{ex} are the start and exit immersion angles of the cutter to and from the cutting zone. The static part of the chip thickness ($f_t \sin\phi_j$) does not contribute to the dynamic chip load regeneration mechanism and consequently is dropped from the expression. Equation D.1 becomes:

$$h(\phi_j) = \left[\Delta x \sin\phi_j + \Delta y \cos\phi_j \right] g(\phi_j) \tag{D.3}$$

where $\Delta x = x - x_0$ and $\Delta y = y - y_0$. Here (x, y) and $x_0 = x(t-T), y_0 = y(t-T)$ denote the dynamic displacements of the cutter structure at the present and previous tooth periods respectively. Here T is the tooth period and is given by $\frac{2\pi}{\omega}$. (ω)is the tooth passing frequency. The tangential cutting force, $F_{tj} = K_{tc} A_p h(\phi_j)$ and radial cutting force, $F_{rj} = K_r F_{tj}$ are proportional to the axial depth of cut A_p and chip thickness h. $\left(K_r = \frac{K_{rc}}{K_{tc}} \right)$, where K_{tc} and K_{rc} are the tangential and radial cutting force coefficients due to the shearing action. The cutting forces

are expressed in the feed X and normal to the feed direction Y by the following equations:

$$\begin{aligned} F_{xj} &= -F_{tj}\cos\phi_j - F_{rj}\sin\phi_j \\ F_{yj} &= +F_{tj}\sin\phi_j - F_{rj}\cos\phi_j \end{aligned} \tag{D.4}$$

The total cutting forces can be expressed by substituting the chip thickness (Equation D.3) and tooth forces (tangential and radial cutting forces) in Equation D.4. This will lead to the following equations:

$$\begin{Bmatrix} F_x \\ F_y \end{Bmatrix} = \frac{1}{2} A_p K_t \begin{bmatrix} \alpha_{xx} & \alpha_{xy} \\ \alpha_{yx} & \alpha_{yy} \end{bmatrix} \times \begin{Bmatrix} \Delta x \\ \Delta y \end{Bmatrix} \tag{D.5}$$

here α_{xx}, α_{xy}, α_{yx} and α_{yy} are the time-varying directional dynamic milling force coefficients.

$$\begin{aligned} \alpha_{xx} &= \sum_{j=0}^{N-1} -g_j[\sin 2\phi_j + K_r(1-\cos 2\phi_j)] \\ \alpha_{xy} &= \sum_{j=0}^{N-1} -g_j[(1+\cos 2\phi_j) + K_r \sin 2\phi_j] \\ \alpha_{yx} &= \sum_{j=0}^{N-1} g_j[(1-\cos 2\phi_j) - K_r \sin 2\phi_j] \\ \alpha_{yy} &= \sum_{j=0}^{N-1} g_j[\sin 2\phi_j - K_r(1+\cos 2\phi_j)] \end{aligned} \tag{D.6}$$

Equation D.5 can be expressed in the time domain as the angular position of the parameters change with time and angular velocity.

$$F(t) = \frac{1}{2} A_p K_t [A(t)] \Delta t \tag{D.7}$$

where

$$[A(t)] = \begin{bmatrix} \alpha_{xx} & \alpha_{xy} \\ \alpha_{yx} & \alpha_{yy} \end{bmatrix} \tag{D.8}$$

Due to the rotation of the cutting tool, the directional factors vary with time. Like the milling forces, $[A(t)]$ is periodic at tooth passing frequency. Thus it can be expanded into a Fourier series:

$$\begin{aligned} [A(t)] &= \sum_{r=-\infty}^{\infty} [A_r] e^{irwt} \\ [A_r] &= \frac{1}{T} \int_0^T [A(t)] e^{-irwt} dt \end{aligned} \tag{D.9}$$

r is the number of harmonics of the tooth passing frequency (ω) to be considered for an accurate reproduction of $[A(t)]$: this depends upon the immersion conditions and on the number of teeth in the cutting zone. In most practical cases of milling, Fourier series expansion with $r = 0$ is considered:

$$[A_0] = \frac{1}{T}\int_0^T [A(t)]\,dt \tag{D.10}$$

$[A_0]$ is valid between the entry (ϕ_{st}) and the exit (ϕ_{ex}) angle of the cutting zone and becomes equal to the average value of $[A(t)]$ at cutter pitch angle $\phi_p = 2\pi/N$

$$[A(0)] = \frac{1}{\phi_p}\int_{\phi_{st}}^{\phi_{ex}} [A(\phi)]\,d\phi = \frac{N}{2\pi}\begin{bmatrix}\alpha_{xx} & \alpha_{xy}\\ \alpha_{yx} & \alpha_{yy}\end{bmatrix} \tag{D.11}$$

Where the integrated functions of directional dynamic milling force coefficients are given by:

$$\begin{aligned}
\alpha_{xx} &= \frac{1}{2}\left[\cos 2\phi - 2K_{\mathrm{r}}\phi + K_{\mathrm{r}}\sin 2\phi\right]_{\phi_{st}}^{\phi_{ex}}\\
\alpha_{xy} &= \frac{1}{2}\left[-\sin 2\phi - 2\phi + K_{\mathrm{r}}\cos 2\phi\right]_{\phi_{st}}^{\phi_{ex}}\\
\alpha_{yx} &= \frac{1}{2}\left[-\sin 2\phi + 2\phi + K_{\mathrm{r}}\cos 2\phi\right]_{\phi_{st}}^{\phi_{ex}}\\
\alpha_{yy} &= \frac{1}{2}\left[-\cos 2\phi - 2K_{\mathrm{r}}\phi - K_{\mathrm{r}}\sin 2\phi\right]_{\phi_{st}}^{\phi_{ex}}
\end{aligned} \tag{D.12}$$

The directional factors are dependent on the radial cutting force coefficients (K_r) and the entry and exit angles. The dynamic milling expression as presented in Equation D.7 is reduced to:

$$F(t) = \frac{1}{2}A_p K_t [A_0]\Delta t \tag{D.13}$$

$[A_0]$ is the time-invariant but immersion dependent directional cutting coefficient matrix.

D.1 Chatter Stability Theory

The transfer function matrix $[\Phi(i\omega)]$ for the machine tool/spindle/tool holder/tool system-workpiece contact zone is given by:

$$[\Phi(i\omega)] = \begin{bmatrix}\Phi_{\mathrm{xx}}(i\omega) & \Phi_{\mathrm{xy}}(i\omega)\\ \Phi_{\mathrm{yx}}(i\omega) & \Phi_{\mathrm{yy}}(i\omega)\end{bmatrix} \tag{D.14}$$

where Φ_{xx} and Φ_{yy} are the direct transfer functions in the feed X and normal to feed Y directions. Φ_{xy} and Φ_{yx} are the cross transfer functions in the feed X and normal to feed Y directions. The vibrations at the present time (t) and previous tooth period ($t - T$) are defined

as:

$$\begin{aligned} \{r\} &= \{x(t)\, y(t)\}^T \\ \{r_0\} &= \{x(t-T)\, y(t-T)\}^T \end{aligned} \tag{D.15}$$

The displacements due to vibrations at the chatter frequency ω_c in the frequency domain using harmonic functions are expressed as:

$$\begin{aligned} \{r(i\omega_c)\} &= [\Phi(i\omega)]\{F\}e^{i\omega_c t} \\ \{r_0(i\omega_c)\} &= e^{-i\omega_c T}\{r(i\omega_c)\} \end{aligned} \tag{D.16}$$

and substituting $\{\Delta\} = \{(x-x_0)(y-y_0)\}^T$ gives

$$\{\Delta(i\omega_c)\} = \{r(i\omega_c)\} - \{r_0(i\omega_c)\} = [1-e^{i\omega_c T}]e^{i\omega_c t}[\Phi(i\omega_c)]\{F\} \tag{D.17}$$

$\omega_c T$ is the phase delay between the vibrations at successive tooth periods T. Substituting $\{\Delta(i\omega_c)\}$ in Equation D.13 leads to:

$$\{F\} = \frac{1}{2}A_p K_t[1-e^{-i\omega_c T}][A_0][\Phi(i\omega_c)]\{F\}e^{i\omega_c t} \tag{D.18}$$

This has a nontrivial solution if its determinant is zero.

$$det\left[[I] - \frac{1}{2}K_t A_p\left(1-e^{-i\omega_c T}[A_0][\Phi(i\omega_c)]\right)\right] = 0 \tag{D.19}$$

This is the characteristic equation of the closed loop dynamic milling system. It is simplified further by defining the oriented transfer functions matrix by:

$$[\Phi_0(i\omega_c)] = \begin{bmatrix} \Phi_{xx}(i\omega_c)\alpha_{xx} + \Phi_{yx}(i\omega_c)\alpha_{xy} & \Phi_{xy}(i\omega_c)\alpha_{xx} + \Phi_{yy}(i\omega_c)\alpha_{xy} \\ \Phi_{xx}(i\omega_c)\alpha_{yx} + \Phi_{yx}(i\omega_c)\alpha_{yy} & \Phi_{xy}(i\omega_c)\alpha_{yx} + \Phi_{yy}(i\omega_c)\alpha_{yy} \end{bmatrix} \tag{D.20}$$

and the eigenvalue of the characteristic equation is given by:

$$\Lambda = -\frac{N}{4\pi}\, A_p K_t\left(1-e^{-i\omega_c T}\right) \tag{D.21}$$

The resulting characteristic equation is given by:

$$\det\left[[I] + \Lambda[\Phi_0(i\omega_c)]\right] = 0 \tag{D.22}$$

The characteristic equation becomes a quadratic function if two orthogonal degrees of freedom in the feed X and normal to feed Y directions are considered ($\Phi_{xy} = \Phi_{yx} = 0$):

$$a_0\Lambda^2 + a_1\Lambda + 1 = 0 \tag{D.23}$$

then

$$\Lambda = -\frac{1}{2a_0}\left(a_1 \pm \sqrt{a_1^2 - 4a_0}\right) \tag{D.24}$$

where

$$\begin{aligned} a_0 &= \Phi_{\mathrm{xx}}(i\omega_c)\Phi_{\mathrm{yy}}(i\omega_c)(\alpha_{xx}\alpha_{yy} - \alpha_{xy}\alpha_{yx}) \\ a_1 &= \alpha_{xx}\Phi_{\mathrm{xx}}(i\omega_c) + \alpha_{yy}\Phi_{\mathrm{yy}}(i\omega_c) \end{aligned} \tag{D.25}$$

The eigenvalue has real and imaginary parts as the transfer functions are complex functions.

$$\Lambda = \Lambda_{\mathrm{R}} + i\Lambda_{\mathrm{I}} \tag{D.26}$$

Substituting eigenvalues and $e^{-i\omega_c T} = \cos\omega_c T - i\sin\omega_c T$ in Equation D.21 gives:

$$A_{plim} = -\frac{2\pi}{NK_t}\left[\frac{\Lambda_R(1-\cos\omega_c T) + \Lambda_I \sin\omega_c T}{(1-\cos\omega_c T)} + i\frac{\Lambda_I(1-\cos\omega_c T) - \Lambda_R \sin\omega_c T}{(1-\cos\omega_c T)}\right] \tag{D.27}$$

A_{plim} is a real number so the imaginary part should be zero:

$$\Lambda_I(1-\cos\omega_c T) - \Lambda_R \sin\omega_c T = 0 \tag{D.28}$$

By using

$$\kappa = \frac{\sin\omega_c T}{1-\cos\omega T} \tag{D.29}$$

into the real part of Equation D.27, the chatter free axial depth of cut is found as:

$$A_{plim} = -\frac{2\pi\Lambda_{\mathrm{R}}}{NK_{\mathrm{t}}}\left(1+\kappa^2\right) \tag{D.30}$$

Equation D.29 can also be written as:

$$\kappa = \frac{\cos(\omega_c T/2)}{\sin(\omega T/2)} = \tan\psi = \tan[\pi/2 - (\omega T/2)] \tag{D.31}$$

this leads to

$$\omega_c T = \pi - 2\psi + 2s\pi, \quad \text{where} \quad s = 0, 1, 2... \tag{D.32}$$

and by defining

$$\epsilon = \pi - 2\psi \quad \text{and} \quad \psi = \tan^{-1}\kappa \tag{D.33}$$

ϵ represents the phase shift (portion of the full wave) between the inner and outer modulation

(present and previous vibration mark). It can lie between $(0-2\pi)$. So the value of the ψ will vary from $\left(\frac{\pi}{2}:\frac{-\pi}{2}\right)$. In MATLAB 2009a, the $atan$ function is used which produces the inverse tan value in the range of $\left(\frac{\pi}{2}:\frac{-\pi}{2}\right)$. s is the integer number of lobes (full vibration waves) imprinted on the surface of workpiece. The spindle speed is given by

$$n = \frac{60\,\omega_c}{N(\epsilon + 2s\pi)} \tag{D.34}$$

E Improvements in Toolpath Generation Algorithm

To detect the intersection between “(Boundary_Conforming_Pass)” and “(Current_Pass)”, Case 1 (as shown in Figure E.1) is implemented in the algorithm to generate constant step over and smooth toolpaths.

- In the present research work, for a given pocket boundary, toolpaths are generated at different values of step over. There may be existence of Case 2 at some step over values as shown in Figure E.1. Case 2 is now implemented in the developed algorithm for toolpath generation.
- Depending upon the shape of the pocket boundary, there may not be any interaction between “(Boundary_Conforming_Pass)” and “(Current_Pass)” as presented in Case 3 in Figure E.1. Case 3 is now implemented in the developed algorithm for toolpath generation.

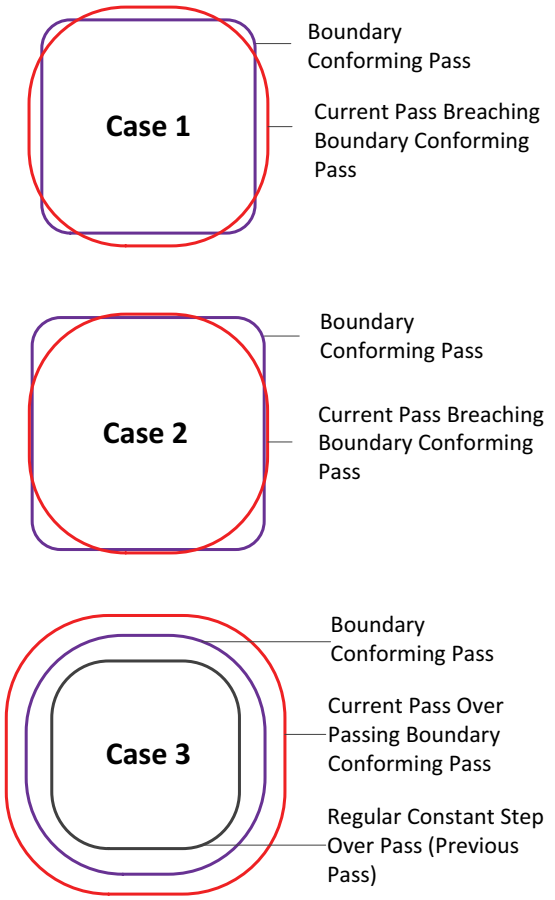

Figure E.1: Different cases to detect intersection in toolpath generation algorithm

F Detailed Literature Review: Online Chatter Detection

F.1 Introduction

In a highly competitive machining industry, there is an immense need for automatic and unmanned machine tools or intelligent machining systems in order to reduce the production cost and increase the overall productivity. Machine tool systems should be able to detect and prevent collisions, monitor the cutting tool condition, control high fluctuations of cutting forces, detect and control of chatter vibrations, select optimized cutting conditions.

(Tlusty and Andrews, 1983) reviewed various studies for sensors used in order to achieve unmanned machining. They presented various monitoring and controlling systems for geometrical corrections, cutting tool wear, cutting tool breakage comprising dimensional and proximity sensors, cutting force sensors, spindle torque and power sensors and acoustic emission sensors. (Byrne et al., 1995) presented a state-of-the-art study for the available sensors for cutting tool condition monitoring (TCM) and chatter detection. The study reviewed the various sensors used in monitoring systems, developments in their signal processing methods, decision making capabilities and their implementation in industrial applications.

Most machine shops have adopted computerized numerical control (CNC) high speed machining (HSM) to achieve high productivity. Many of the above mentioned sensors have been implemented in CNC machines for various purposes. High speed machining is widely used in the aerospace and automobile industries to achieve high material removal rates due to high efficiency and reliability. The goal of achieving high material removal rates is hampered by the instability in the milling process. This unstable phenomenon is called chatter and is the most undesirable and complex phenomenon during the machining process. Chatter vibrations are characterized by chaotic relative motions between the cutting tool and workpiece and by high fluctuations of cutting forces. As a consequence, chatter vibrations reduce the surface quality of the workpiece, reduce the machine tool spindle and cutting tool working life and thus significantly lower the overall productivity of the machining process. Since the late 1950s, several studies/methods have been developed for chatter detection, prevention, reduction, suppression or control. In the present work, we will focus on chatter detection methods in the

milling process.

F.1.1 Requirement for Chatter Detection Sensors

The chatter phenomenon may result from vibrations of the workpiece system, cutting tool, spindle and the machine tool structure. During a milling process, the occurrence of chatter can be detected from cutting force, cutting sound, displacement of cutting tool tip, spindle power, spindle torque or spindle current signals. All these signals are measured with the help of various available sensors. Sensor selection is one of the most critical aspects for designing the detection and control system for chatter vibrations. The accuracy and effectiveness of the chatter detection and control system depends on the various sensor characteristics like frequency response, accuracy, reliability, robustness.

In the milling processes, face mills vibrate with lower frequencies whereas the end mills vibrate with high frequencies. Chatter vibrations may typically range in frequencies from 100 Hz, due to vibrations from the machine table or machine structure, to as high as 5000 Hz, when the cutting tool or flexible thin-walled workpiece is used. Frequency bandwidth of the sensor must be sufficient to detect the possible frequency range of the chatter vibrations (Delio et al., 1992).

The sensor location is another important aspect for the sensor selection. Generally, the closer the sensor the more reliable are the measurements. Direct placement of the sensor at or very near the cutting zone, either on the cutting tool or on the workpiece, allows direct measurement of the desired signal. Often the type of sensor and machine tool system configuration dictate the sensor location. For example in the case of a table type dynamometer (cutting force sensor) the dynamometer is located on the machine tool table and beneath the workpiece.

Sensor durability, performance and accuracy are also greatly influenced by the cutting process, cutting chips and coolant fluids.

In addition, the requirements of the sensors for chatter detection in industrial implementation are summarized as follows (Kuljanic et al., 2008)

- The sensor should not change the dynamics properties (modal parameters) of the machine tool system particularly it should not reduce the stiffness of the machine tool system.
- The sensor should not put any additional constraints on the selection of cutting conditions and on any other machining conditions like cutting tool dimensions, workpiece dimensions, and others.
- The functioning of the chatter detection system should not rely on the knowledge of actual cutting process or any prior knowledge of the machining tool system dynamic characteristics.

- The sensor must be practical to use and easy to implement. It should not restrict the normal working of the machining process.

F.2 Literature Review of Chatter Detection Sensors

Various studies have been performed for chatter detection with different sensors and using different signal processing techniques. (Tlusty and Andrews, 1983) presented a review study of various sensors and their capabilities for unmanned machining. They classified cutting forces and spindle motor sensors as the primary sensors necessary for chatter detection and control. (Byrne et al., 1995) reviewed the state-of-the-art studies for cutting tool monitoring, chatter detection and prevention in the milling process. (Altintas and Chan, 1992) implemented various sensors (dynamometer for cutting forces, proximity sensor for displacements and microphone for sound signals) for the in-process detection and suppression of chatter in milling. (Tarng and Chen, 1994) developed a real-time sensor chatter detection system by analyzing the cutting forces in end milling operations. They verified the developed chatter detection system experimentally with spindle speeds up to 1500 rpm. (Soliman and Ismail, 1997) developed a system to detect chatter with the spindle drive current signal of a vertical milling machine. They stated that current sensors meet many requirements of a good sensor like low cost, reliable, durable and remote from the cutting zone. They experimentally verified the chatter detection system for low speed machining (up to 800 rpm). They concluded that the narrow bandwidth of the current sensors imposes a serious restriction on their implementation for detection of milling chatter which usually develops at high frequencies.

Recently (Kuljanic et al., 2008) presented a multisensory approach for online chatter detection in face milling operations. Comparison of various sensors (rotating dynamometer, accelerometer, acoustic emission and electric power sensors) is demonstrated along with various signal processing techniques for chatter detection. Their experimental system is shown in Figure F.1. They concluded that axial cutting force, cutting torque and acceleration signals can be successfully applied for chatter detection in face milling operations. An electric power sensor is not useful for chatter indication as the frequency spectrum of the power signal is poor and is limited to very low frequencies (less than 100 Hz). They concluded from the time domain and frequency domain analysis of power signals that this sensor may only be applied for very low spindle speeds. Chatter identification with acoustic emission (AE) signal is less reliable as its signal characteristics do not change during unstable milling. It is important to mention here that acoustic emission is not related to sound signals. Acoustic emission is a high frequency oscillation, or stress wave, occurring spontaneously within metals (and other materials) when they are deformed, fractured or undergo phase changes. It is caused by the release of strain energy as the material's micro-structure is being rearranged and the oscillations can easily be detected at the surface of the workpiece using piezoelectric transducers (Tlusty and Andrews, 1983). (Kuljanic et al., 2009) then developed an intelligent chatter detection system based on neural networks consisting of accelerometer and axial force sensors and by implementing advanced signal processing techniques.

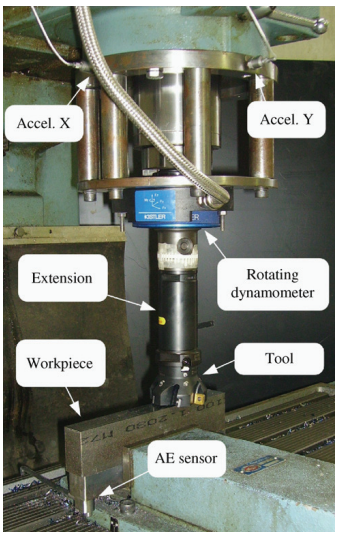

Figure F.1: Setup for chatter detection (Kuljanic et al., 2008)

(Faassen, 2007) and (Dijk et al., 2010) presented an in-process chatter detection technique which detects chatter in the premature stage from an acceleration signal in the time domain. They also presented online control strategies to avoid chatter by changing the spindle speed.

The use of laser Doppler vibrometery (LDV) for chatter detection is used by (Tatar and Gren, 2008). In order to measure the signal accurately, a cylindrical casing with high optically smooth surface was manufactured and mounted on the cutting tool. The laser vibrometer signal contains information on cutting tool vibrations, radial misalignments and eccentricity errors. It was shown that cutting vibration information can be extracted by proper subtraction of the non-cutting part of the laser vibrometer signal from the cutting part of the recording. The main advantage of the LDV is that it is possible to perform remote non-contact measurement on a rotating cutting tool. The method can be used for high frequency machine tool vibrations as well.

(Soliman and Ismail, 1996) presented a detailed comparison of the cutting force signal using dynamometer, vibration signal measured by accelerometer, sound signal using a microphone and current signal of spindle drive for chatter detection in the milling process. They concluded that the microphone signal was found to be very reliable and the acceleration signal to be the least reliable for chatter detection. (Hendriks, 2005) presented a detailed comparison of microphone and accelerometer for chatter detection in high speed machining. With the help of dedicated experiments the microphone was shown to be the best sensor to detect chatter in high speed milling applications. Recently (Quintana and Ciurana, 2011) reviewed various studies in the field of chatter vibrations also considering the chatter detection approaches. They demonstrated that a microphone is an excellent sensor for chatter detection as compared to other available sensors like force dynamometer, displacement probes and accelerometer.

F.2.1 Limitations of the Sensors

From the literature, it is clear that various sensors have been used successfully in different conditions based on the objective of the proposed studies. In order to select the sensor which is most suitable for the developed chatter detection system it is important to present the main drawbacks of the available sensors. The main limitations of the sensors are discussed in following sections.

Table Type Dynamometer

The maximum frequency range of table type dynamometer is about 1 kHz which is reduced significantly when the workpiece is attached to the dynamometer. The frequency response of table type dynamometer degrades considerably above 300 Hz. The chatter detection results will not be reliable for higher spindle speeds. (Delio et al., 1992)investigated the table type force dynamometer for chatter detection. The table type dynamometer is massive and has quite low frequency response. The transfer functions (TF) of the dynamometer, without any workpiece attached to it, for the feed (X) and normal to feed (Y) directions are shown in Figure F.4. It is evident from the transfer functions that vibrations encountered above 1000 Hz are difficult to detect as the response of the dynamometer is reduced significantly. The dynamometer possesses its own natural modes even below 1000Hz. When a workpiece is attached to the dynamometer the frequency bandwidth will be further degraded. This makes chatter detection difficult and not reliable for higher spindle speeds.

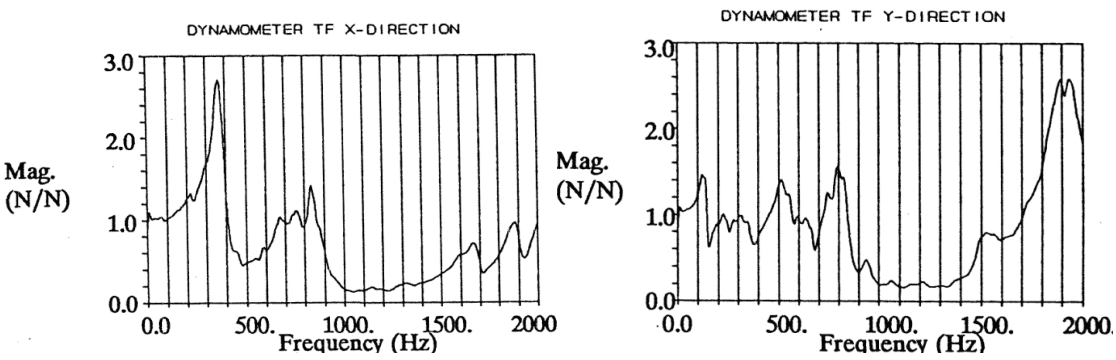

(a) TF in feed direction (X)

(b) TF in normal to feed direction (Y)

Figure F.2: Transfer function of the table type dynamometer (Delio et al., 1992)

Another limitation of table type dynamometers lies in their capability to detect chatter during low immersion milling. Low immersion cuts produce cutting forces for very short durations during cutting tool rotation. These low cutting forces may not provide adequate signals to recognize the existence of chatter.

Moreover, table type dynamometers also provide constraints on the size of the workpiece which can be fitted on them. Table type dynamometers are quite expensive and experimental

set up is not very easy to implement for industrial applications.

Rotating Type Dynamometer

The rotating type of dynamometer is used to measure the axial cutting force and cutting torque. The main drawback with rotating type dynamometers is also the low frequency bandwidth. Rotating type dynamometers can only be used to detect chatter at lower spindle speeds. The rotating type of dynamometer reduces the stiffness of the machine tool system significantly and thus affects the stability limits. They also put additional constraints on the selection of cutting conditions. Usually the rotating type dynamometer is designed to run up to a particular spindle speed. Moreover rotating dynamometers are not compatible with cutting tool changers (Kuljanic et al., 2008). The rotating type dynamometer is also expensive and not practical for industrial applications.

Accelerometer and Displacement Sensors

In comparison to the cutting force signals (less than 1 kHz) measured by the force dynamometer, the acceleration signals have wider frequency spectra (about 5 kHz), therefore they are suitable for a wider range of applications. Mostly the accelerometer is mounted on the spindle housing which is the closest to the cutting tool. Accurate detection of chatter with an accelerometer lies in the proper selection of its mounting location. It is conceivable that the accelerometer might be located near a nodal point of the chatter mode of vibration. Also, reduction in sensitivity results when chatter arise from flexibility of the workpiece. If a chatter frequency is not located near to a natural mode present in the cutting tool/sensor transfer function, sensitivity to the vibrations is reduced. Additionally, as the machine configuration changes (feed direction, tooling etc.); the nodal point of chatter mode will also change and may coincide with the sensor location (Delio et al., 1992).

In general, placement of transducers (accelerometers, displacement, and velocity transducers) on an active point for all expected chatter modes is a difficult task. It requires prior knowledge of the dynamic behavior over the expected range of the machine operation. Different attachments and cutting tools, varying geometry of workpieces produce numerous chattering mode shapes and frequencies and thus make placement of the accelerometer or other transducer a difficult task.

A non-contact displacement sensor like a laser Doppler vibrometer (LDV) is not practical for industrial implementation due to its high cost and laborious experimental setup.

Microphone

Though many studies presented in the literature concluded that a microphone is an excellent sensor for chatter detection there are also some restrictions associated with its use for chatter

detection. The environmental noise originating from other sources can influence the chatter detection capability. To overcome this problem, some sound isolation and filter techniques can be used depending upon the application.

Remaining Sensors

Current sensors and spindle power have been tested for very low spindle speeds in the literature. These sensors are not useful for high speed milling as they have really low (less than 100Hz) frequency bandwidth. Studies have also proven that acoustic emission sensors do not produce reliable results for chatter detection (Kuljanic et al., 2008).

F.3 Literature Review of Chatter Recognition Techniques

Once the required signal is acquired with the use of sensors, it is processed mathematically to recognize the existence of chatter vibrations. The sensor signal can be expressed as the sum of periodic and aperiodic components (Kuljanic et al., 2008):

$$S(t) = S_p(t) + S_a(t) \tag{F.1}$$

where $S_p(t)$ is the τ-periodic component and $S_a(t)$ is the aperiodic component. τ is the spindle revolution period. It is noted that the reference period τ is also for the cutting tools with multiple teeth due to the run-out in the machine tools. The periodic component of the signal contains the harmonics of the spindle frequency (SF), while all the other components are treated in the aperiodic term. During the stable milling process, only the periodic component is present in the signal whereas during unstable milling there is a significance presence of aperiodic components in the measured signal along with periodic components.

There are some studies in the literature which demonstrate the signal processing technique which help recognize chatter.

F.3.1 Threshold Level

The amplitude of the sensor signal is usually low during stable milling but it changes drastically during unstable milling. The first technique is to detect chatter by fixing a threshold level of the amplitude of the sensor signal (Altintas and Chan, 1992) and (Delio et al., 1992). Two kinds of method are used in literature to recognize chatter by defining a threshold. In the first method the threshold level of the signal value is defined by conducting some experiments in stable conditions. Then, the amplitude of the sensor signal is compared with this predefined threshold level during stable milling. If the signal value exceeds the threshold level chatter is detected.

In the second method, the threshold level of the amplitude (or power) of the dominant peak

in the frequency spectrum is defined by conducting a series of experiments in stable cutting conditions. If the amplitude of the dominant peak in the frequency spectrum of the measured signal exceeds the predefined threshold level the occurrence of chatter is detected. Figure F.3 presents two frequency spectrums shown from two similar cutting processes (Morgan et al., 2007). The amplitude of the dominant peak concerned changes very little between these two cases. According to the predefined threshold level, the outcome of first case will be unstable and other case is stable but both the cases are unstable because of the presence of a dominant peak other than the spindle frequency, tooth passing frequency and their harmonics (discussed in Section F.3.3).

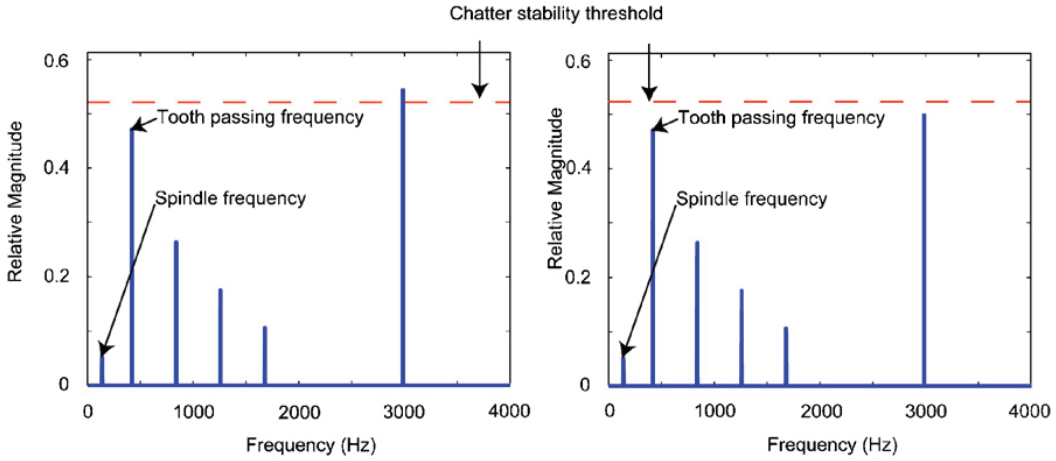

Figure F.3: Threshold method to determine stability (Morgan et al., 2007)

Defined threshold values are dependent on the cutting conditions and other machining setups like workpiece material, cutting tool etc. A series of experiments is needed to fix the threshold value for each machining setup. Threshold techniques can only detect the occurrence of chatter vibrations but does not provide any information for the control of chatter.

F.3.2 Statistical Detection

(Schmitz et al., 2002) proposed a technique using a statistical method to detect chatter in the sensor signal. They proposed a method comprising measurement of the sensor signal at a once per revolution rate and computing the variance of the sampled signal. If the variance exceeds a predefined value of threshold level, chatter is detected. During stable machining, the cutting tool moves with the same frequency as the spindle frequency. Its position is the same for each rotation (as shown in Figure F.4a). In the unstable case, the frequency of the chatter vibration is different and the cutting tool tends to have an elliptical movement (as shown in Figure F.4b).

The variance of the sampled sensor signal per revolution of spindle is calculated. The variance

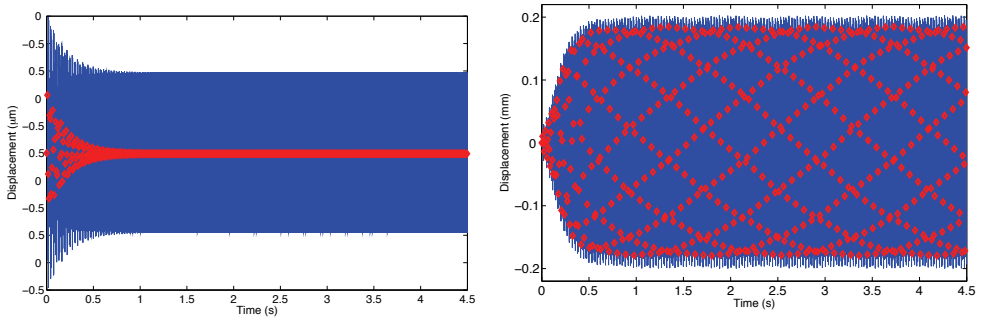

(a) Stable machining

(b) Unstable machining

Figure F.4: Chatter detection using statistical method (Riviére et al., 2006)

is calculated as:

$$\sigma^2 = \frac{\sum_{i=1}^{P} (x_i^2 - x_m^2)}{P-1} \tag{F.2}$$

Where P is the size of sampled signal, x_i are the signal data points and x_m is the mean which is given by:

$$x_m = \frac{\sum_{i=1}^{P} (x_i)}{P} \tag{F.3}$$

This technique is computationally fast and requires low sampling rate of sensor signal. This technique is good for real time chatter detection but the technique only produces reliable results with acceleration or displacement signals. Also this technique also can only detect the occurrence of chatter vibrations but does not provide any information for their control.

F.3.3 Frequency Domain Analysis

In this technique, the time domain signal is converted in the frequency domain using a discrete Fourier transform. The frequency content of the sensor signal is different for stable and unstable milling. During stable cutting, the frequency spectrum is composed of spindle frequency, tooth passing frequency and their harmonics. An unstable cutting signal also contains frequencies close to the dominant Eigen frequency of the machine tool system which is called the chatter frequency. This method requires additional information about the cutting process namely spindle speed and number of flutes. This technique is computationally costlier than threshold level and statistical detection. The main advantage of this technique is that the dominant chatter frequency can be identified from the frequency spectrum and this can be a useful input for the chatter control system.

G Stability Analysis of Flexible Workpiece

G.1 Introduction

Monolithic parts are widely used as structural components in the aeronautical industry due to their homogeneity and excellent strength to weight ratio. In current manufacturing practice, the monolithic parts are milled starting from the blank and removing up to 95% of the initial weight. The goal of achieving high material removal rate is hampered by chatter vibrations due to the high flexibility of the thin-walled workpiece. In these specific milling applications, the workpiece system dynamics are quite significant and the workpiece system cannot be treated as rigid.

FRFs of the workpiece system are required for the stability analysis. FRFs of the workpiece system can be measured directly with hammer testing or can be computed by numerical methods. Due to the non-existence of the final workpiece at the part programming stage, FRF measurement with hammer testing is not feasible. Finite element analysis is used for computation of the FRF of the flexible workpiece. The dynamic characteristics of the flexible workpiece are different at different positions of the cutting tool along the workpiece. Moreover, the dynamics change significantly due to the material removal of the workpiece. To predict the stability of a flexible workpiece system it is very important to consider the change in dynamics due to the material removal along the toolpath as well as at different contact points of the cutting tool with the workpiece.

In this chapter, an enhanced procedure is presented for the stability analysis of milling process considering the coupled dynamics of workpiece and machine tool system. The complete procedure consists of two main steps:

1. Computation of stability limits for one milling pass along the thin-wall

2. Investigation of the change in stability limits at different milling passes (further stages with material removal)

Table G.1: Material properties of the workpiece

Young's Modulus (N/m^2)	Poisson Ratio	Density (Kg/m^3)
$70e^9$	0.33	2700

G.2 Stability Analysis during Single Milling Pass

The complete procedure is explained with the help of a thin-walled workpiece as follows:

- The dimensions of the thin-walled flexible workpiece chosen for the stability analysis are presented in Figure G.1a. A 3D model of the workpiece is created in ANSYS 13.0.

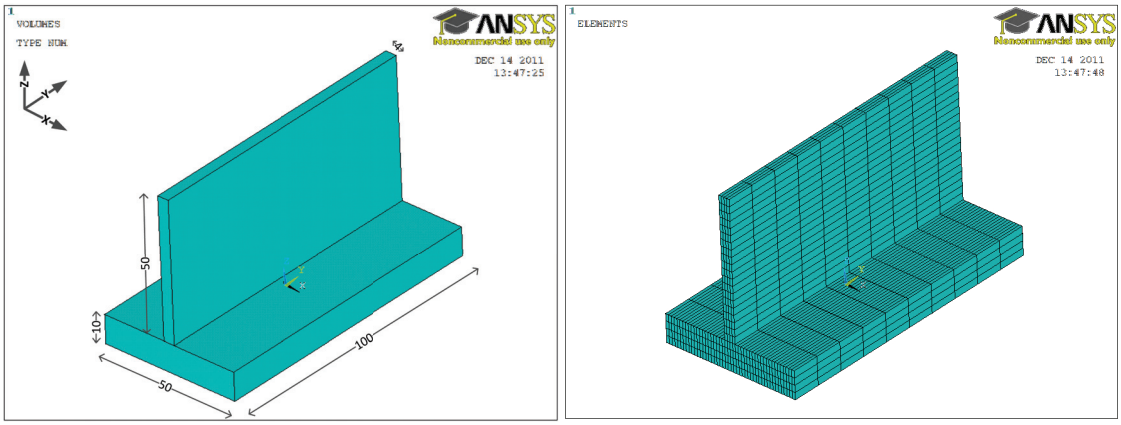

(a) Dimensions of the flexible workpiece

(b) Meshed workpiece

Figure G.1: Finite element modeling of flexible workpiece

- The workpiece material is AS7 aluminium alloy. The material properties of the workpiece are defined in Table G.1. The material properties are taken from (Mane et al., 2008).
- Solid185 is used as an element type for 3D modeling of the solid structure. It is defined by eight nodes having three degrees of freedom at each node: translations in the nodal x,y and z directions.
- A brick shaped mapped meshing is performed. This type of meshing is done in order to control precisely the impact and response points during FRF computation. The meshed workpiece is presented in Figure G.1b.
- The boundary conditions are applied by fixing the nodes of the workpiece base (this can be seen in Figure G.3a). This configuration will allow the thin wall to vibrate freely under real machining conditions.
- Modal analysis is performed with the Block Lanczos method. Modal analysis is performed to identify the natural frequencies of the dominant modes of the flexible work-

piece. The range of frequency is selected from the modal analysis results which will be used later to perform the harmonic analysis for FRFs computation. The first three modes are identified at 1375Hz, 2056Hz and 5032Hz. The corresponding first two mode shapes are presented in Figure G.2. The frequency range for FRF analysis is selected as 0–2500Hz.

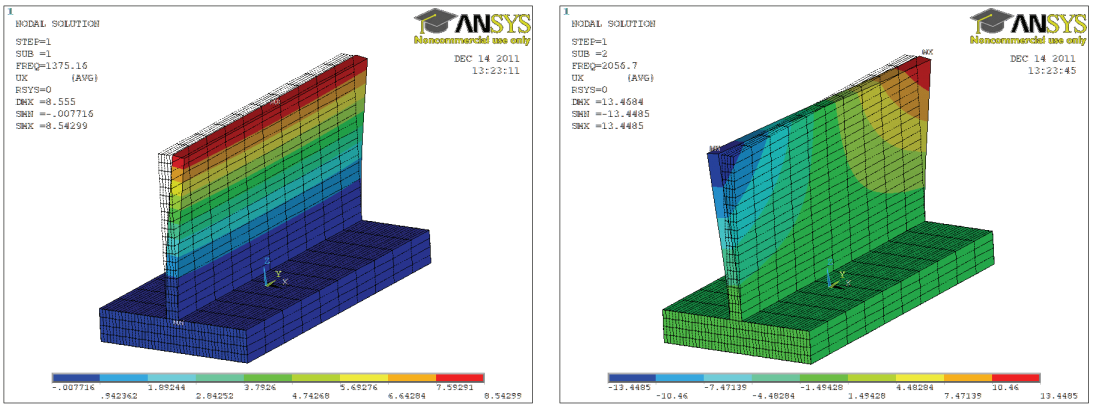

Figure G.2: Mode shapes of the flexible workpiece

- Harmonic analysis is performed within the selected range of frequencies (0–2500Hz). Direct FRFs are computed with harmonic analysis at different contact points which are termed “P” in Figure G.3b. Only FRFs of P1–P6 need to be computed due to symmetry. The damping value is considered as 0.02.

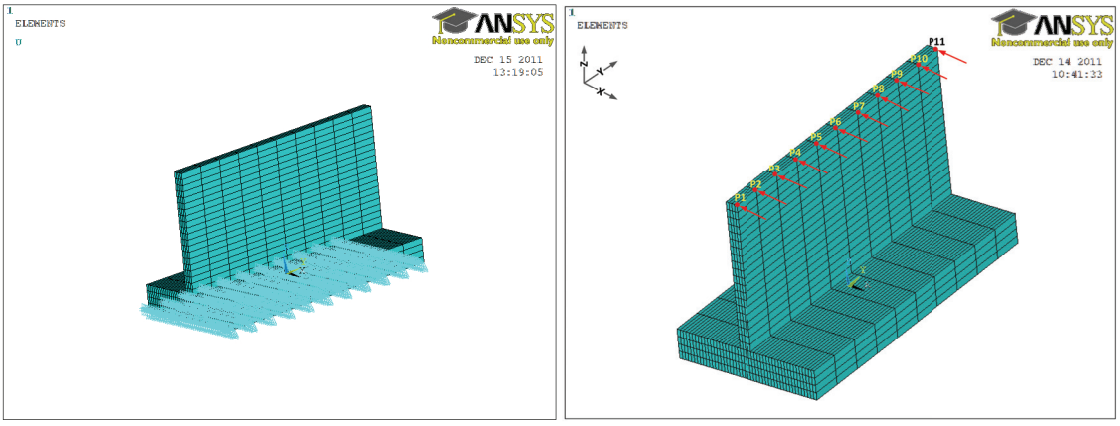

(a) Boundary condition for modal analysis and FRF computation

(b) Different contact points for FRF measurement

Figure G.3: FRF computation by FEM

- The real and imaginary parts of the computed FRFs at points P1–P6 are presented in Figure G.4. For the first mode, the response at different contact points is the same which

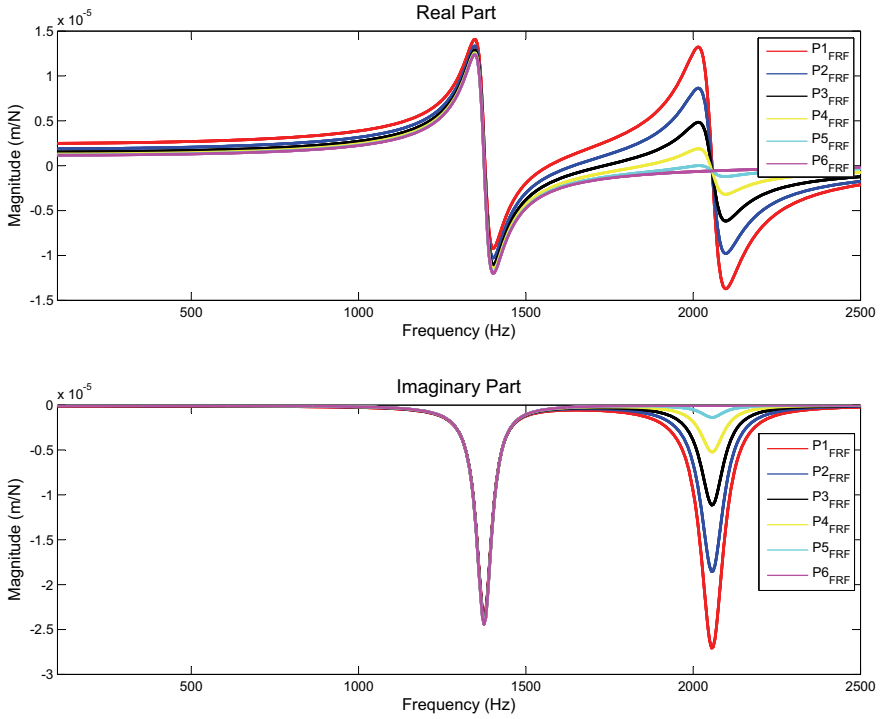

Figure G.4: FRFs at different contact points (P1–P6)

is understood from its mode shape (Figure G.2a). For the second mode, P1 (also P11) are the most dominant points. The magnitude of FRFs at all points (P1–P11) are represented in three dimensions as shown in Figure G.5.

- FRFs of the machine tool system (with 20mm diameter end mill with 2 flutes) are coupled with FRFs of the workpiece system. As presented in Section 2.4.3, (Bravo et al., 2005) has developed a methodology to identify coupled FRF by presenting the relationship of cutting tool/thin-wall interaction in both up and down milling. In the coupled system, the relative displacement between cutting tool and workpiece is due to the sum of their individual displacements. In the present work SLDs are generated from the FRFs of coupled system. The coupled FRF at P1 is presented in Figure G.6.

- The real and imaginary part of FRFs of the coupled system computed at different points (P1–P6) are presented in Figure G.7.

- The FRFs of the coupled system are used for the development of stability lobe diagrams. The following cutting conditions are used for SLD generation (D=20mm, N=2, $K_{tc} = 711N/mm^2$, $K_{rc} = 86N/mm^2$ and A_e = 1mm for down milling). The resulting 3D SLD is presented in Figure G.8.

- SLDs of the coupled system at different contact points (P1–P6) are plotted as shown in Figure G.9a. A study from (Mane et al., 2008) has proposed a strategy of having different spindle speeds between the points along a single milling pass. This strategy

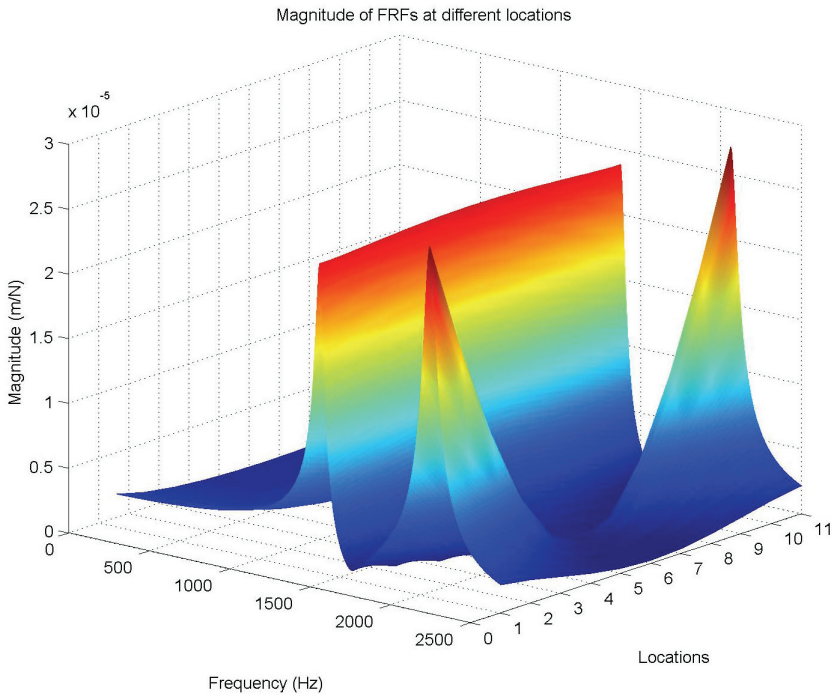

Figure G.5: 3D representation of FRFs at different contact points

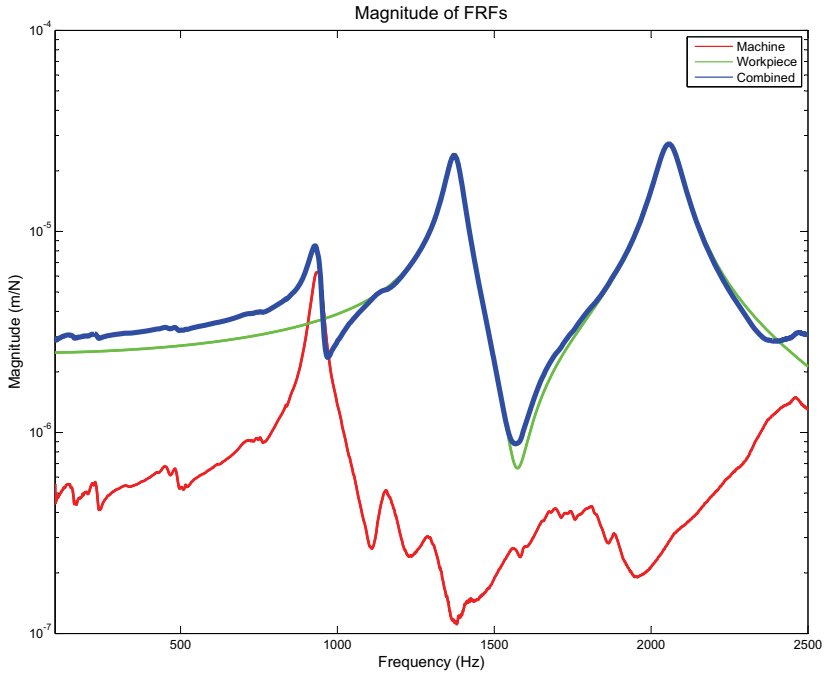

Figure G.6: Comparison of FRFs of machine tool, workpiece and coupled system

is not feasible in practical conditions as it is preferred to have the same spindle speed along the milling pass. Moreover, change in spindle speed values along a single milling

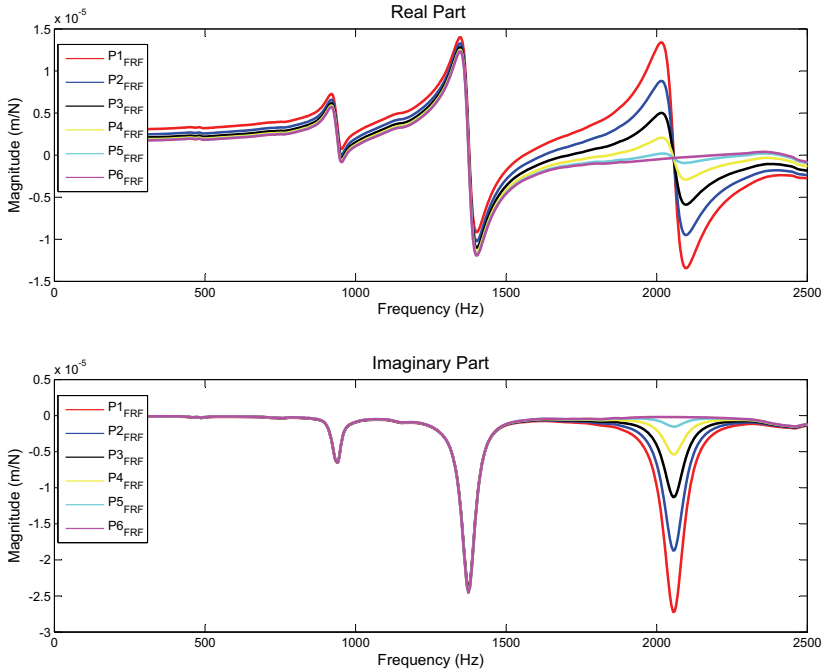

Figure G.7: FRFs of the coupled system at different contact points

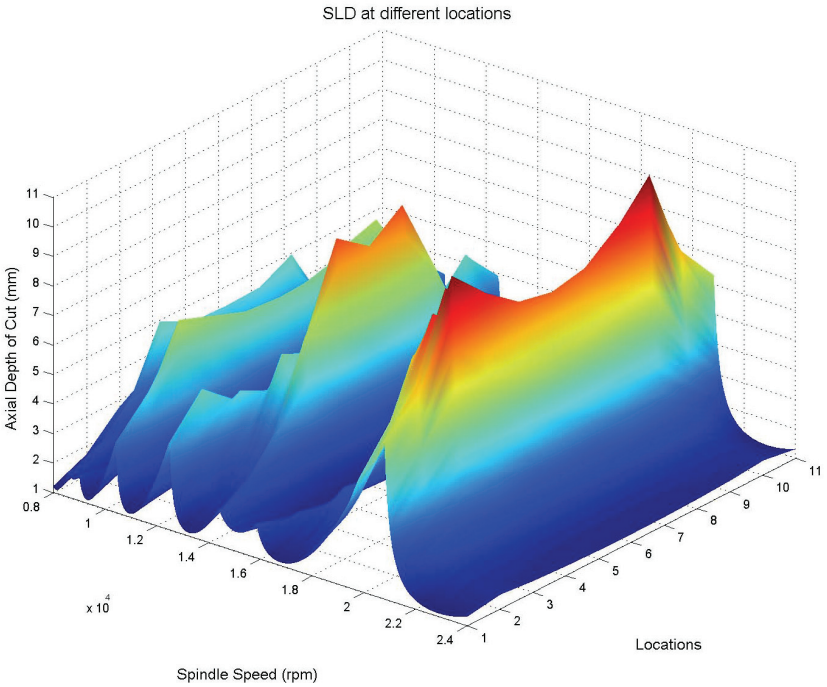

Figure G.8: 3D stability lobe diagram

pass leaves marks on the machined surface. In the present work, from the computed SLDs, a minimum SLD is selected as presented in Figure G.9b. The cutting conditions

Table G.2: Natural frequencies of modes of different cases

Case No	Mode1	Mode2	Mode3
Case1	1375	2056	5032
Case2	1633	2263	5107
Case3	1760	2244	4801
Case4	1514	1872	4827

are selected from the SLD (Figure G.9b) which will ensure stable milling. In this way the same spindle speed is maintained along the milling pass.

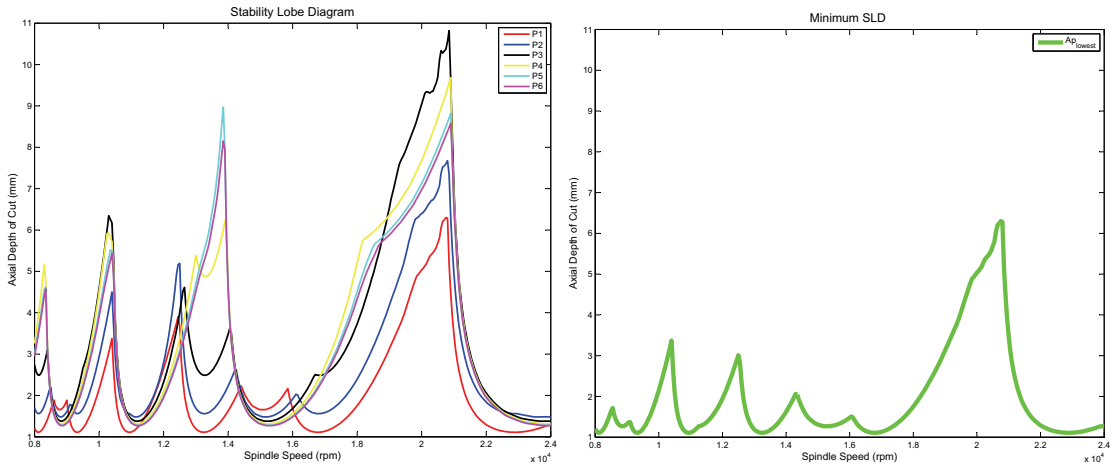

(a) Stability lobe diagrams at different contact points (P1–P6)

(b) Corresponding minimum stability lobe diagram

Figure G.9: Stability lobe diagram for coupled system

G.3 Change in the Dynamics of Thin-Walled Workpiece

The effect of change in dynamics is presented by considering various cases as shown in Figure G.10. The corresponding contact points are also presented. Each case represents the machined workpiece after a few number of single milling passes. Every milling pass consists of 1mm of radial immersion with defined stable depth of cut. The main objective of this subsection is to demonstrate the change in dynamics and corresponding stable depths of cut due to material removal.

Modal analysis is performed for different cases in order to find the natural frequencies of the dominant modes. The natural frequencies of the first three modes of different cases are presented in Table G.2.

For every case, FRFs are computed at different points (contact points of cutting tool with workpiece) with the same procedure as defined in Section G.2. The computed FRFs (magnitude) of

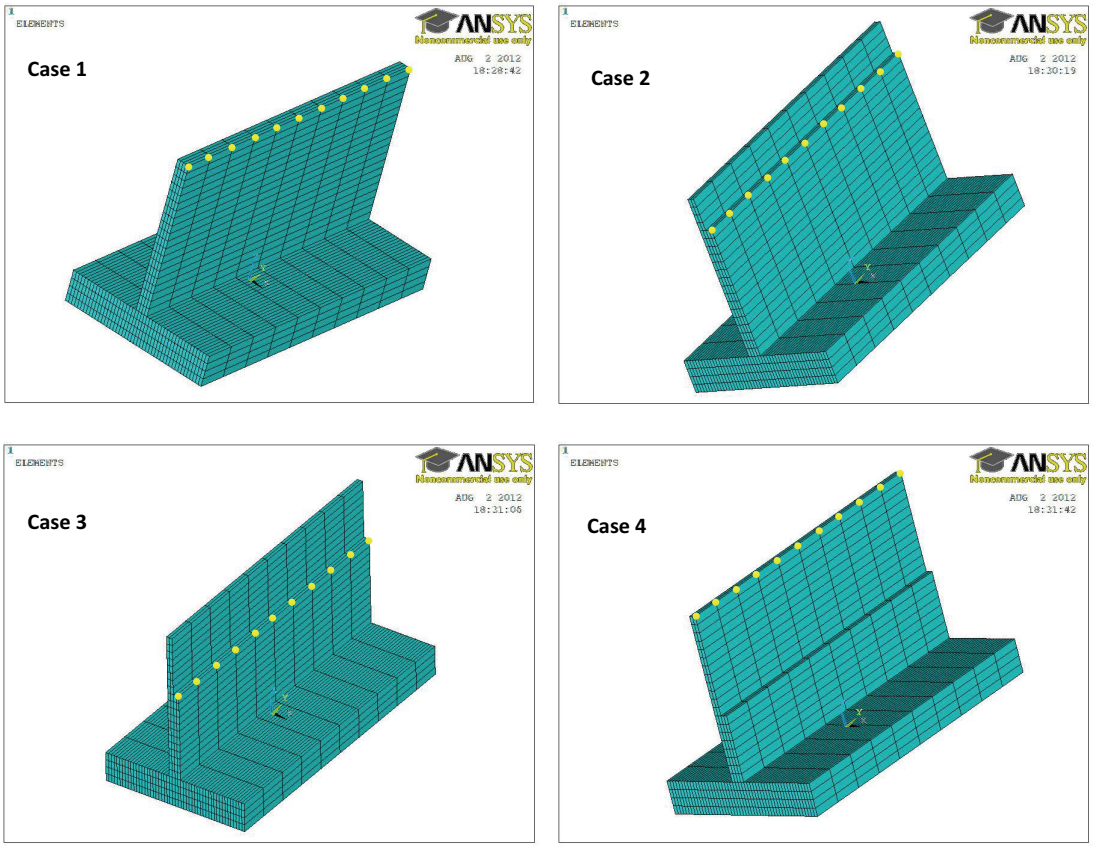

Figure G.10: Different stages of milling of flexible workpiece

the workpiece system for different cases are presented in Figure G.11. It is clear from the FRFs that there is a significant change in the dynamics of the workpiece system due to material removal. Case4 is the most flexible among all cases. Locations of computation of FRFs for case1 and case4 are the same. The higher flexibility of case4 as compared to the others is because of its thinnest wall. Case3 is the stiffest case as FRFs are computed closer to the base of the workpiece which provided the stiffness.

Workpiece FRFs at different points are coupled with the machine tool system FRF. It is assumed that the machine tool system FRFs do not change at different locations. With predefined inputs, stability lobes are computed at different points and minimum stable depths of cut are identified for a milling pass as presented in Section G.2. The corresponding resulting minimum stability lobe diagrams are presented in Figure G.12.

It is clear from the minimum stability lobe diagrams that there is a significant change in the stable depths of cut for different cases. The allowable stable axial depths of cut in case4 reduce significantly as compared to case1 due to change in dynamic characteristics caused by material removal. Due to the high stiffness for case3 deeper axial depths of cut can be achieved. This is also interesting to show that there is also a change in stable spindle speeds

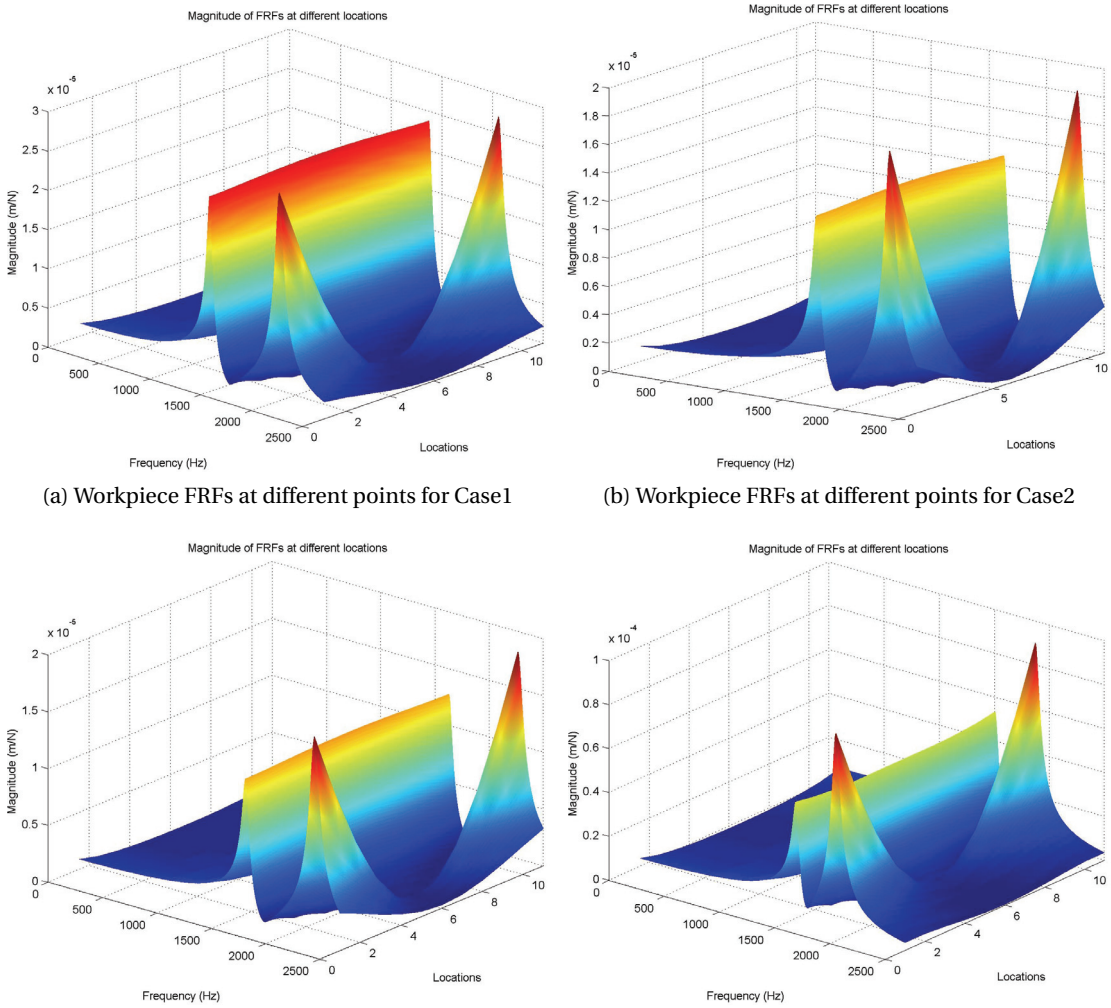

(a) Workpiece FRFs at different points for Case1

(b) Workpiece FRFs at different points for Case2

(c) Workpiece FRFs at different points for Case3

(d) Workpiece FRFs at different points for Case4

Figure G.11: Change in workpiece dynamics

for different cases. This is because of the fact that there is a change in the natural frequencies of dominant modes of the workpiece system.

G.4 Conclusion

Stability analysis of the flexible workpiece is performed. A flexible workpiece exhibits different dynamic characteristics at different contact points of the cutting tool with the workpiece.

Finite element modeling is used to compute the FRFs at different contact points by harmonic analysis. The workpiece FRFs are then coupled with the machine tool system.

Stable limits are predicted by stability analysis of coupled FRFs at different contact points.

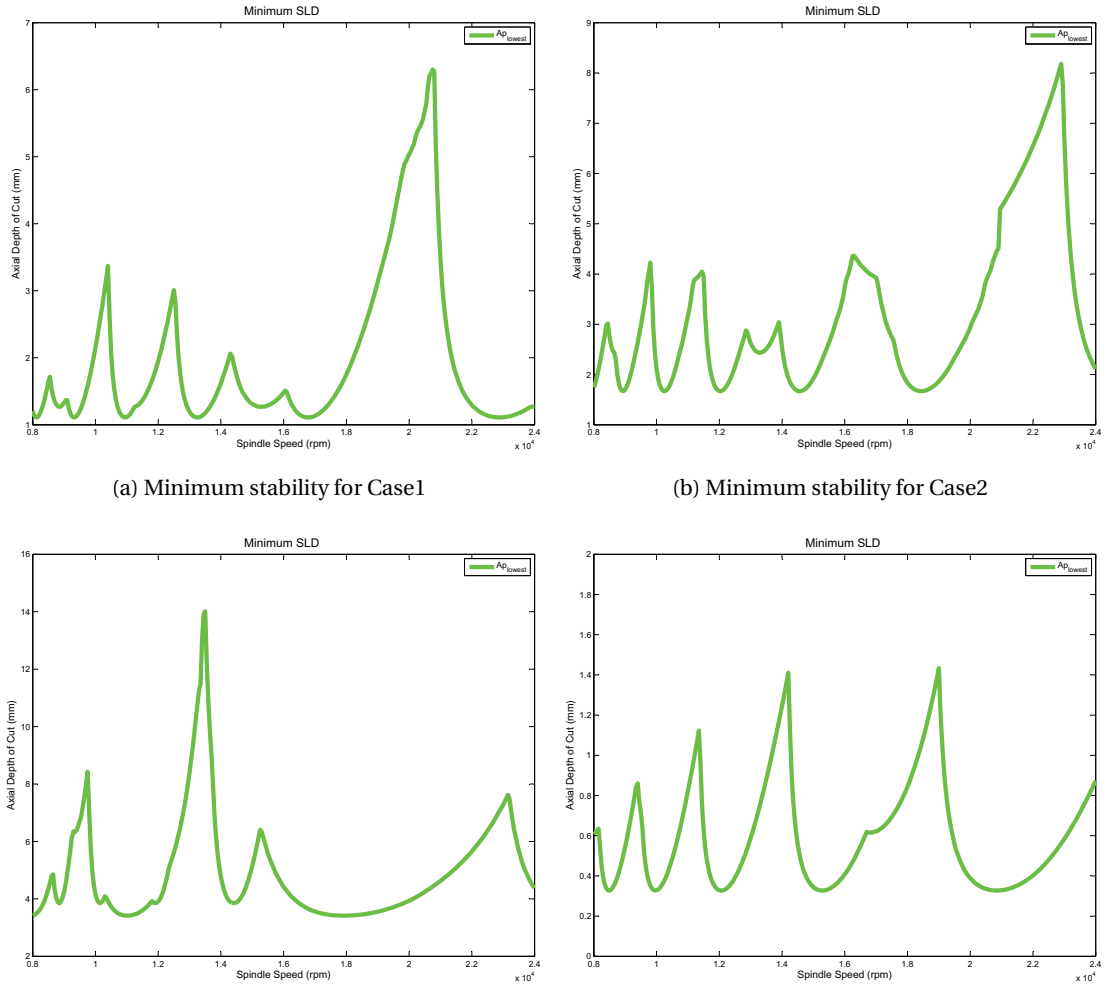

(a) Minimum stability for Case1

(b) Minimum stability for Case2

(c) Minimum stability for Case3

(d) Minimum stability for Case4

Figure G.12: Change in stable limits due to change in dynamics

Stable cutting conditions along one milling pass are selected from the minimum SLD from computed SLDs at different contact points.

It is demonstrated that the workpiece dynamics change significantly with material removal which explains the need for new stability analysis at different stages of milling of flexible workpieces.

Saurabh AGGARWAL

Date of Birth: 9th June, 1983
Nationality: Indian
saggarwal.1983@gmail.com

PROFILE

Five years plus experience in **computer-aided design, engineering and manufacturing**. My **technical expertise, international education and experience** motivate challenging and competitive assignments in a multinational environment

PROFESSIONAL EXPERIENCE

PROJECT RESPONSIBLE — Since Feb 2011

Laboratory of CAD/CAM, Swiss Federal Institute of Technology Lausanne (EPFL), Switzerland
Industrial Partners: Mikron Agie Charmilles AG and Calcom ESI

- Development of a system for the optimal selection of cutting conditions for **high speed milling**
- Development of an **online chatter detection and control** systems during milling operations

DOCTORAL ASSISTANT — Since Apr 2008

Laboratory of CAD/CAM, Swiss Federal Institute of Technology Lausanne (EPFL), Switzerland

- Development of systems for **milling process modeling and optimization**
- Teaching assistantship in simulation of multi-body dynamics and mentoring of semester projects
- Proposal writing for Swiss and European industrial manufacturing projects
- Underwent advanced training for modeling, simulation and experimentation of milling operations at *University of British Columbia Vancouver, Canada*

DEPUTY MANAGER — Aug 2007-Mar 2008

Ashok Leyland Limited, Product Development Division, Chennai, India

- Designing, modeling and prototyping of packaging system for air brakes of 49 ton future truck "UNITRUCK 4921"
- Responsible for collaboration between future development team and computer-aided analysis team

TRAINEE

Schenck Rotec GmbH (The DÜRR Group), Darmstadt, Germany — May 2007

- Development and implementation of computational algorithms for balancing of rotors

Guru Gobind Singh Super Thermal Plant (1260 MW), Ropar, India — July-Dec 2004

- Detailed study of boiler, turbine, air conditioning, coal handling and air compressors units

Swaraz Madza Limited, Nawanshahr, India — July 2003

- Detailed study of assembly, paint, and engine testing shops

EDUCATION

PhD — Since Apr 2008

Laboratory of CAD/CAM (LICP), Swiss Federal Institute of Technology Lausanne (EPFL), Switzerland

Thesis: Part Programming to Realize Chatter Free and Efficient High Speed Milling

Key Area: High Speed Milling Optimization, Computer-Aided Design and Manufacturing, Machine Dynamics, Finite Element Analysis, Milling Processes Modeling and Simulation

Achievement: Nomination for thesis prize for industrial impact

MASTER OF TECHNOLOGY (M.Tech) THESIS Sep 2006-May 2007

Laboratory for System Reliability and Machine Acoustics, Technical University Darmstadt (TUD), Germany

Thesis: Failure and Lifetime Assessment of Welded Stainless Steel Structures via Finite Element Modeling and Variance Based Sensitivity Analysis Methods

Key Area: Modeling of Welded Joints, Finite Element Analysis, Sensitivity Analysis

MASTER OF TECHNOLOGY (M.Tech) 2005-2007

Industrial Safety and Hazards Management

Indian Institute of Technology (IIT), Roorkee, India

Achievement: 1st in the class (CGPA 9.77/10)

BACHELOR OF TECHNOLOGY (B.Tech) 2001-2005

Mechanical Engineering

Punjab Technical University (PTU), India

Achievement: **1st in the class (82.24%)**

CREDENTIALS & AWARDS

- Awarded **Deutscher Akademischer Austausch Dienst (DAAD) scholarship,** TUD Germany, 2006-2007
- Received **Ministry of Human Resource Development scholarship**, IIT Roorkee, 2005-2007
- Awarded **Gold Medal** for meritorious performance in B.Tech among 500 mechanical engineers
- Inclusion in merit list (top 0.4%) of Punjab School Education Board at senior secondary school level, 2001
- Won awards in quizzes, speeches and debates at inter-school competitions

ORGANISATIONAL RESPOSIBILITIES

- Member of delegation from EPFL for **World Model United Nations, Singapore**, Mar 2011
- Member of delegation from EPFL for **Harvard National Model United Nations, Boston, USA**, 2010
- Responsible for development and maintenance of LICP, EPFL website, 2010 onwards
- Represented Cossonay cricket club for Swiss National Cricket League, 2009
- Co-Coordinator of the organizing committee to organize Ganga Bhawan Day in IIT Roorkee, 2006
- Member of JAGRITI (non-profit organization) in IIT Roorkee, 2005-2006
- Player of Ropar district cricket team for **Punjab State Championship**, 1999

COMPUTER SKILLS

- CAD/CAE/CAM: CutPro, ADAMS, MATLAB, CATIA V5, ANSYS 13.0
- Proficient in MS Office, LATEX and Adobe Photoshop CS5

LANGUAGES

English (Fluent), Hindi (Native), Punjabi (Native), French (A2/B1), German (A1)

PATENT & PUBLICATIONS

Aggarwal S, Dhanik S, Xirouchakis P, High Speed Pocket Milling Optimization, **WO Patent** 2012 107594/A1

Aggarwal S, Xirouchakis P (2012), *Selection of Optimal Cutting Conditions for Pocket Milling Using Genetic Algorithm*, Int J Adv Manuf Tech, DOI: 10.1007/s00170-012-4472-x

Aggarwal S, Nesic N, Xirouchakis P (2012), *Cutting Torque and Tangential Cutting Force Coefficient Identification from Spindle Motor Current*, Int J Adv Manuf Tech, DOI: 10.1007/s00170-012-4152-x

Aggarwal S, Ian S, Xirouchakis P, *Minimization of Machining Time for Milling of Prismatic Parts* (preparing)

Aggarwal S, Dhanik S, Xirouchakis P, *Optimization of High Speed Pocket Milling with Optimal Selection of Cutting Conditions and Constant Engagement Toolpath* (preparing)

OTHER INTERESTS

- 10km Running, 10m Air Pistol, Tennis, Badminton, Cooking, Travelling, Cuban Salsa